UNCLASSIFIED

AD NUMBER

ADB008985

LIMITATION CHANGES

TO:

Approved for public release; distribution is unlimited.

FROM:

Distribution authorized to U.S. Gov't. agencies only; Test and Evaluation; JAN 1976. Other requests shall be referred to Arnold Engineering Development Center, Arnold AFB, TN 37389.

AUTHORITY

AEDC ltr dtd 9 Aug 1978

THIS PAGE IS UNCLASSIFIED

AEDC-TR-76-13

cy.1

ARCHIVE COPY
DO NOT LOAN

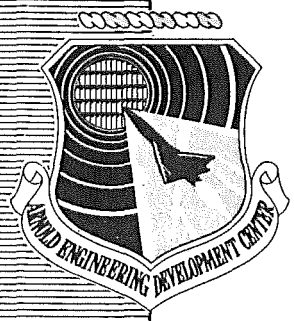

CALIBRATION OF THE AEDC-PWT 16-FT TRANSONIC TUNNEL AT TEST SECTION WALL POROSITIES OF TWO, FOUR, AND SIX PERCENT

PROPULSION WIND TUNNEL FACILITY
ARNOLD ENGINEERING DEVELOPMENT CENTER
AIR FORCE SYSTEMS COMMAND
ARNOLD AIR FORCE STATION, TENNESSEE 37389

January 1976

Final Report for Period October 1972 — June 1973

Distribution limited to U.S. Government agencies only; this report contains information on test and evaluation of military hardware; January 1976; other requests for this document must be referred to Arnold Engineering Development Center (DYFS), Arnold Air Force Station, Tennessee 37389.

This document has been approved for public release
its distribution is unlimited.
DOS letter 8-9-78

Property of U. S. Air Force
AEDC LIBRARY
F40600-75-C-0001

Prepared for

DIRECTORATE OF TECHNOLOGY (DY)
ARNOLD ENGINEERING DEVELOPMENT CENTER
ARNOLD AIR FORCE STATION, TENNESSEE 37389

AEDC TECHNICAL LIBRARY
5 0720 00033 9269

NOTICES

When U. S. Government drawings specifications, or other data are used for any purpose other than a definitely related Government procurement operation, the Government thereby incurs no responsibility nor any obligation whatsoever, and the fact that the Government may have formulated, furnished, or in any way supplied the said drawings, specifications, or other data, is not to be regarded by implication or otherwise, or in any manner licensing the holder or any other person or corporation, or conveying any rights or permission to manufacture, use, or sell any patented invention that may in any way be related thereto.

Qualified users may obtain copies of this report from the Defense Documentation Center.

References to named commercial products in this report are not to be considered in any sense as an endorsement of the product by the United States Air Force or the Government.

APPROVAL STATEMENT

This technical report has been reviewed and is approved for publication.

FOR THE COMMANDER

Elton R. Thompson

ELTON R. THOMPSON
Research & Development
Division
Directorate of Technology

Robert O. Dietz

ROBERT O. DIETZ
Director of Technology

REPORT DOCUMENTATION PAGE		READ INSTRUCTIONS BEFORE COMPLETING FORM
1. REPORT NUMBER AEDC-TR-76-13	2. GOVT ACCESSION NO.	3. RECIPIENT'S CATALOG NUMBER
4. TITLE (and Subtitle) CALIBRATION OF THE AEDC-PWT 16-FT TRANSONIC TUNNEL AT TEST SECTION WALL POROSITIES OF TWO, FOUR, AND SIX PERCENT		5. TYPE OF REPORT & PERIOD COVERED Final Report- October 1972 - June 1973 6. PERFORMING ORG. REPORT NUMBER
7. AUTHOR(s) F. M. Jackson, ARO, Inc.		8. CONTRACT OR GRANT NUMBER(s)
9. PERFORMING ORGANIZATION NAME AND ADDRESS Arnold Engineering Development Center (DY) Arnold Air Force Station, Tennessee 37389		10. PROGRAM ELEMENT, PROJECT, TASK AREA & WORK UNIT NUMBERS Program Element 65807F
11. CONTROLLING OFFICE NAME AND ADDRESS Arnold Engineering Development Center (DYFS) Arnold Air Force Station, Tennessee 37389		12. REPORT DATE January 1976 13. NUMBER OF PAGES 167
14. MONITORING AGENCY NAME & ADDRESS(if different from Controlling Office)		15. SECURITY CLASS. (of this report) UNCLASSIFIED 15a. DECLASSIFICATION DOWNGRADING SCHEDULE N/A

16. DISTRIBUTION STATEMENT (of this Report)

Distribution limited to U.S. Government agencies only; this report contains information on test and evaluation of military hardware; January 1976; other requests for this document must be referred to Arnold Engineering Development Center (DYFS), Arnold Air Force Station, Tennessee 37389.

17. DISTRIBUTION STATEMENT (of the abstract entered in Block 20, if different from Report)

1. Transonic wind tunnels -- PWT
2 " " -- Calibration

18. SUPPLEMENTARY NOTES

Available in DDC

19. KEY WORDS (Continue on reverse side if necessary and identify by block number)

calibration	test facility
AEDC-PWT 16-Ft	porosity (wall)
transonic	Mach numbers
wind tunnel	

20. ABSTRACT (Continue on reverse side if necessary and identify by block number)

Tests were conducted in the AEDC Propulsion Wind Tunnel (16T) to determine the centerline Mach number distributions and the tunnel calibration at test section wall porosities of two, four, and six percent. The calibration was conducted over the Mach number range from 0.2 to 1.6. A quantitative evaluation of the effects of Mach number, tunnel pressure ratio, test section wall angle, and test section wall porosity upon the centerline Mach

DD FORM 1 JAN 73 1473 EDITION OF 1 NOV 65 IS OBSOLETE

20. ABSTRACT (Continued)

number distributions was determined by analysis of the local Mach number deviations. Limited data were also obtained to provide an indication of the effect of Reynolds number upon the calibration. The results indicate that Mach number distributions of good flow quality are obtained at porosities of two, four, and six percent for test section wall angles which vary from 0 to 0.50 deg. Variation of test section wall porosity, as well as wall angle, significantly affects the Tunnel 16T calibration. Comparison of this calibration with a previous calibration, however, indicates that no new tunnel calibration is required for operation at a porosity of six percent with either a zero or optimum wall angle schedule.

AFSC
Arnold AFS Tenn

PREFACE

The work reported herein was conducted by the Arnold Engineering Development Center (AEDC), Air Force Systems Command (AFSC), at the request of the AEDC/DYR in support of the AEDC/AFFDL AGARD Nozzle Afterbody Study under Program Element 65807F. The results of the test were obtained by ARO, Inc. (a subsidiary of Sverdrup & Parcel and Associates, Inc.), contract operator of AEDC, AFSC, Arnold Air Force Station, Tennessee. The work was done under ARO Project No. PF230. The author of this report was F. M. Jackson, ARO, Inc. The data analysis was completed (under ARO Project No. P32P-11A) in September 1974, and the manuscript (ARO Control No. ARO-PWT-TR-75-97) was submitted for publication on June 26, 1975.

CONTENTS

Page

1.0 INTRODUCTION 7
2.0 APPARATUS
2.1 Test Facility 7
2.2 Test Section Wall Configurations 8
2.3 Calibration Equipment 8
3.0 PROCEDURE
3.1 Calibration Discussion 9
3.2 Data Reduction 10
3.3 Data Precision 10
3.4 Flow Quality 11
4.0 RESULTS AND DISCUSSION
4.1 Centerline Mach Number Distributions 11
4.2 Tunnel Calibration 16
5.0 CONCLUSIONS 18
REFERENCES 19

ILLUSTRATIONS

Figure

1. Tunnel 16T Centerline Pipe Installation 21
2. Tunnel 16T Porous Wall Corking Setup 24
3. Variation of Tunnel Pressure Ratio 26
4. Variation of Test Section Wall Angle 27
5. Tunnel 16T Centerline Mach Number Distributions for τ = Six percent at $\lambda = \lambda_N$ and $\theta_w = 0$ 28
6. Effect of Mach Number upon the Mach Number Deviations for Six-percent porosity at $\lambda = \lambda_N$ and $\theta_w = 0$ 31
7. Tunnel 16T Centerline Mach Number Distributions for Various Test Section Wall Porosities with $\lambda = \lambda_N$ and $\theta_w = 0$ 33
8. Effect of Test Section Wall Porosity Variation upon the 2σ Mach Number Deviation for Tunnel Station 8.2 to 28.2 at $\lambda = \lambda_N$ and $\theta_w = 0$ 48
9. Effect of Test Section Wall Porosity Variation upon the 2σ Mach Number Deviations for Tunnel Station 1.2 to 20.2 at $\lambda = \lambda_N$ and $\theta_w = 0$ 51

Figure | Page

10. Tunnel 16T Centerline Mach Numbeı Distributions for Various Tunnel Pressure Ratios with Six-percent Porosity Walls and $\theta_w = 0$ 54
11. Tunnel 16T Centerline Mach Number Distributions for Various Tunnel Pressure Ratios with Four-percent Porosity Walls and $\theta_w = 0$ 62
12. Tunnel 16T Centerline Mach Number Distributions for Various Tunnel Pressure Ratios with Two-percent Porosity Walls and $\theta_w = 0$ 71
13. Effect of Tunnel Pressure Ratio Variation upon the 2σ Mach Number Deviations for Tunnel Stations 8.2 to 28.2 at $\theta_w = 0$ 80
14. Effect of Tunnel Pressure Ratio Variation upon the 2σ Mach Number Deviation for Tunnel Stations 1.2 to 20.2 at $\theta_w = 0$ 83
15. Tunnel 16T Centerline Mach Number Distributions for Various Test Section Wall Angles with Six-percent Porosity Walls and $\lambda \cong \lambda_N$ 86
16. Tunnel 16T Centerline Mach Number Distributions for Various Test Section Wall Angles with Four-percent Porosity Walls and $\lambda \cong \lambda_N$ 97
17. Tunnel 16T Centerline Mach Number Distributions for Various Test Section Wall Angles with Two-percent Porosity Walls and $\lambda \cong \lambda_N$ 109
18. Effect of Test Section Wall Angle Variation upon the 2σ Mach Number Deviations for Tunnel Station 8.2 to 28.2 at $\lambda = \lambda_N$ and M = 0.5 to 0.9 120
19. Effect of Test Section Wall Angle Variation upon the 2σ Mach Number Deviations for Tunnel Station 1.2 to 20.2 at $\lambda = \lambda_N$ and M = 0.5 to 0.9 123
20. Effect of Test Section Wall Angle Variation upon the 2σ Mach Number Deviations for Tunnel Station 8.2 to 28.2 at $\lambda = \lambda_N$ and M = 1.0 to 1.3 126
21. Effect of Test Section Wall Angle Variation upon the 2σ Mach Number Deviations for Tunnel Station 1.2 to 20.2 at $\lambda = \lambda_N$ and M = 1.0 to 1.3 129

Figure Page

22. Effect of Test Section Wall Angle Variation upon the 2σ Mach Number Deviations for Tunnel Station 8.2 to 28.2 at $\lambda = \lambda_N$ and M = 1.4 to 1.6 132
23. Effect of Test Section Wall Angle Variation upon the 2σ Mach Number Deviations for Tunnel Station 1.2 to 20.2 at $\lambda = \lambda_N$ and M = 1.4 to 1.6 135
24. Effect of Test Section Region upon the Tunnel 16T Mach Number Calibration at $\theta_w = 0$ 138
25. Tunnel 16T Mach Number Calibration at Various Test Section Porosities for $\theta_w = 0$ 140
26. Tunnel 16T Mach Number Calibration for Various Test Section Wall Angles at Wall Porosities of Two, Four, and Six percent 141

TABLES

1. Coefficients of the 16T Calibration Surface Fit for $\theta_w = 0$ and Variable Test Section Porosity 144
2. Coefficients of the 16T Calibration Curve Fit for $\tau = 6$ and $\theta_w = 0$ 145
3. Coefficients of the 16T Calibration Curve Fit for $\tau = 4$ and $\theta_w = 0$ 146
4. Coefficients of the 16T Calibration Curve for $\tau = 2$ and $\theta_w = 0$ 147
5. Coefficients of the 16T Calibration Surface Fit for $\tau = 6$ and Variable Test Section Wall Angle 148
6. Coefficients of the 16T Calibration Surface Fit for $\tau = 4$ and Variable Test Section Wall Angle 149
7. Coefficients of the 16T Calibration Surface Fit for $\tau = 2$ and Variable Test Section Wall Angle 150

APPENDIXES

A. PROCEDURES FOR OBTAINING VARIABLE WALL POROSITY IN 16T 151

B. EFFECT OF REYNOLDS NUMBER 153

NOMENCLATURE 167

1.0 INTRODUCTION

A comprehensive program, involving both testing and technology, has been conducted at the AEDC to support an overall AGARD program to investigate various aspects of problems associated with integrated nozzle/afterbody (NAB) testing. As a part of this program, it was desired to obtain test data in the AEDC Propulsion Wind Tunnel (16T), Propulsion Wind Tunnel Facility, at wall porosities of two, four, and six percent.

Tunnel 16T is equipped with six-percent perforated test section walls. These walls, however, were modified to obtain wall porosities other than six percent. Based on operating experience in the AEDC 4-ft and 1-ft Aerodynamic Wind Tunnels (4T and 1T), the tunnel calibration changes significantly with variation of wall porosity. Consequently, to support the AEDC Nozzle/Afterbody Study a special tunnel calibration was required.

Tests were conducted in the AEDC Propulsion Wind Tunnel (16T) to determine the tunnel calibration and centerline Mach number distributions at various test section wall porosities. During the calibration, centerline Mach number distributions were obtained for wall porosities of two, four, and six percent at Mach numbers from 0.2 to 1.6. The effects of Mach number, test section porosity, tunnel pressure ratio, and test section wall angle upon the centerline Mach number distributions were also determined. The results of this calibration are presented in this report.

2.0 APPARATUS

2.1 TEST FACILITY

The PWT 16-ft Transonic Wind Tunnel (Propulsion Wind Tunnel (16T)) is a continuous flow, closed-circuit tunnel which can be operated at Mach numbers from 0.2 to 1.6. The tunnel has a test section 40 ft long and 16 ft square with six-percent porosity walls. The test section sidewalls can be either converged or diverged 1 deg.

Tunnel 16T is a variable density tunnel which can be operated within a stagnation pressure range of 120 psfa to a maximum of 4,000 psfa, depending upon the Mach number. The stagnation temperature can be varied from a minimum of about 80°F, dependent upon available cooling water temperature, to a maximum of 160°F. The stagnation pressure and temperature can be held within ±5 psf and ±1°F, respectively.

The Tunnel 16T main compressor is a constant speed, three-stage, axial-flow compressor with variable stator blades. The compressor drive system consists of four motors with a power rating of 216,000 hp. To prevent tunnel choking in the transonic range, test section flow removal is accomplished with a plenum evacuation system (PES). The

PES consists of ten compressors which are driven by motors with a total power rating of 179,000 hp. The PES is also utilized for tunnel pressure level control.

Various Mach numbers in Tunnel 16T are established by regulation of compressor speed and pressure ratio, plenum pressure, and the contour of a flexible, two-dimensional Laval nozzle. Mach numbers below 0.55 are obtained by operating the compressor drive motors subsynchronously. Auxiliary flow removal is utilized at Mach numbers above 0.75 and supersonic nozzle contours are utilized at $M \geqslant 1.05$. Additional details with regard to Tunnel 16T and its capabilities are presented in Ref. 1.

2.2 TEST SECTION WALL CONFIGURATIONS

The calibration utilized the PWT test Cart 1; however, corks were utilized to modify the wall porosity from the normal six-percent configuration. The general arrangement of the test section and the normal six-percent perforated wall geometry is shown in Fig. 1. To obtain two-percent porosity, two-thirds of the holes were corked. To obtain four-percent porosity, one-half of these corks were removed. Between station -0.5 and 40, the rows of holes which were at 17 deg to the tunnel longitudinal centerline were corked. The starting point and an indication of the two-percent porosity pattern is shown in Fig. 2a. For the taper strips region (Sta -8.5 to -0.5), the holes which were in columns at 73 deg to the tunnel longitudinal centerline were corked (see Fig. 2b). Although each of the 2-ft-wide stabilizer plates were corked identically, the distribution of holes and an attempt to obtain a smooth porosity distribution from zero to two-percent or four-percent porosity created a complicated hole pattern. The detailed procedures used for obtaining variable wall porosity are provided in Appendix A.

2.3 CALIBRATION EQUIPMENT

A 6.5-in.-diam static pressure pipe was used to obtain the centerline static pressure distribution from tunnel station -5.8 to 48.2. Noting that the centerline pipe used in Ref. 3 was unsatisfactory at $M_\infty > 1$, a significant effort was made during the design of the centerline pipe and its supporting system to make the pipe satisfactory for acquisition of data at supersonic Mach numbers. Data presented in Ref. 2 were utilized in the pipe design.

The rear end of the calibration pipe protruded through a cone tip on the 16T scavenging scoop and was attached internally to a mechanism which provided a restoring moment to counteract the weight of the pipe. A total of four cables, swept rearward at 30 deg to the tunnel centerline and spaced to produce a moment to also aid in removing pipe sag, provided pipe support. The pipe, which encompassed an ogive tip, was subject to a tensile load through the use of a cable which extended far upstream into the tunnel nozzle and connected to a streamlined forebody and cable support system.

The centerline pipe included a total of 75 static orifices. The orifices were spaced at 1-ft intervals from tunnel station -5.8 to 0.2, 0.5-ft intervals from tunnel station 0.2 to 24.2, 1-ft intervals from tunnel station 24.2 to 40.2, and 2-ft intervals from tunnel station 40.2 to 48.2. A schematic and photographs of the pipe installation are shown in Fig. 1.

The pipe orifices were connected to differential pressure transducers which were referenced to the tunnel plenum chamber pressure. The tunnel plenum chamber pressure was determined by measurement from a self-balancing precision manometer. The tunnel stagnation pressure was determined by averaging measurements from two self-balancing precision manometers.

3.0 PROCEDURE

3.1 CALIBRATION DISCUSSION

The calibration was conducted over the Mach number range from 0.2 to 1.6, and data were obtained for wall porosities of two, four, and six percent. Primary emphasis was placed upon investigation at Mach numbers from 0.8 to 1.2 which was the principal range of interest of the AEDC NAB test.

The centerline Mach number distributions were defined for a tunnel stagnation pressure of 1,600 psf. The tunnel stagnation temperature was maintained at 110°F for Mach numbers of 0.5 and above and at 80°F for Mach numbers below 0.5. The effect of Reynolds number on the tunnel calibration was also investigated at Mach numbers of 0.6 and 0.8 by operation at 800 and 3,200 psf. Because only limited data were obtained, the results of Reynolds number variation are presented in Appendix B.

Based on data presented in Refs. 3 and 4 and some unpublished Tunnel 16T operations data, a nominal pressure ratio schedule was defined for utilization during variations of test section wall porosity and wall angle. This schedule, which is considered near the optimum pressure ratio schedule, is shown in Fig. 3. To determine the effects of pressure ratio upon the distribution, the pressure ratio was also varied from about 30 percent above and below the nominal schedule as shown in Fig. 3.

For the test, the test section wall angle was varied from 0.50 to -1.0 deg. The Tunnel 16T optimum wall angle schedule and the range of wall angles investigated during this test are shown in Fig. 4. The Tunnel 16T optimum wall angle schedule was defined from data presented in Ref. 5 for long slender bodies of revolution with a test section blockage of one percent. The optimum wall angle schedule was used during the AEDC NAB test.

3.2 DATA REDUCTION

The distribution of local Mach number in the test section was obtained from reduction of the centerline pipe pressure data to Mach number assuming isentropic flow through the nozzle. The average Mach number and the 2σ Mach number deviation for two test section regions were computed. These include tunnel station 8.2 to 28.2, which encompasses the region in which the AEDC NAB model was installed and tunnel station 1.2 to 20.2 which is a "standard" test region. The current tunnel calibration (Ref. 4) is defined for the latter test regions.

The statistical parameter, σ, the standard deviation, is approximately a root-mean-square quantity which is a measure of the deviation of the local Mach numbers from the average. Assuming a normal distribution, 95.4 percent of the local Mach numbers will fall within a distribution band of $\pm 2\sigma$.

The calibration of Tunnel 16T is based on the measured pressure differential across the test section walls at various operating conditions. As a matter of procedure, a plenum chamber Mach number equivalent was determined from plenum chamber and stagnation pressure measurments using the isentropic relationship. A calibration parameter is defined as the difference between the free-stream and plenum chamber Mach numbers. This parameter (M_∞-M_c) is utilized to express the tunnel calibration for various operating conditions. Analytical expressions of the Ref. 4 calibration were determined using a least-squares, multiple regression data fitting program.

3.3 DATA PRECISION

A Taylor series method of error propagation was utilized to estimate the precision in the data which could be attributed to instrumentation errors and data acquisition techniques. For a confidence level of 95.4 percent, the maximum errors are as follows:

$\Delta\lambda$	± 0.0003
$\Delta\theta_w$	± 0.030
$\Delta\tau$	± 0.15
ΔM_∞	± 0.0003
ΔM_c	± 0.0009
$\Delta(2\sigma)$	± 0.0002
$\Delta(M_\infty - M_c)$	± 0.0010

The precision in Mach number, M_∞, is not representative of the precision of free-stream Mach number for test operations. The precision given above is that associated with the average of about 40 local Mach numbers from the calibration pipe.

3.4 FLOW QUALITY

One of the primary objectives of a tunnel calibration is to ascertain that adequate flow quality exists for acquisition of test data for various locations of test models and various combinations of tunnel conditions. Tunnel flow quality encompasses several parameters, such as flow angularity and turbulence levels, which were not investigated during this calibration. For purposes of this report, flow quality will refer to the uniformity of the centerline Mach number distributions and to longitudinal pressure gradients.

A quantitative evaluation of the uniformity of a Mach number distribution and pressure gradients, if they exist, for a particular test section region can be provided by the 2σ Mach number deviation. This parameter does not distinguish between nonuniformity and gradients; however, this is easily ascertained by observation of the distributions. Past tunnel calibrations have illustrated that undesirable pressure gradients do not exist in Tunnel 16T for normal operating conditions. Typical values of Tunnel 16T Mach number gradients are presented in Ref. 3.

The author is unaware of any industry "standard" which exists for values of the 2σ Mach number deviation which indicate "good" flow quality. For purposes of this report, 2σ Mach number deviations of 0.005 M_∞ and 0.01 M_∞ for subsonic and supersonic Mach numbers, respectively, will be considered indicative of "good" flow quality.

The 2σ Mach number deviation can also be utilized to evaluate the effects of various test parameters upon the centerline Mach number distributions. The minimum Mach number deviation is, of course, indicative of the "best" distribution, and therefore flow quality, for a particular test section length and set of tunnel conditions. The 2σ parameter, however, is very sensitive to small changes in the distributions and to moderate changes in local conditions. To facilitate judgement with regard to the effects of various test parameters, a variation less than 0.001 in the 2σ Mach number deviation (or ten-percent of the nominal 2σ level if greater) will be considered insignificant.

4.0 RESULTS AND DISCUSSION

4.1 CENTERLINE MACH NUMBER DISTRIBUTIONS

4.1.1 General

Tunnel 16T centerline Mach number distributions were obtained at a variety of test conditions. Typical distributions obtained at Mach numbers from 0.2 to 1.6 are presented in Fig. 5. Specifically, the data presented in Fig. 5 were obtained at zero test section wall angle (θ_W) for the nominal pressure ratio schedule (λ_N) and a test section wall porosity (τ) of six percent.

The data in Figs. 5a and 5b indicate that the centerline pipe installation for this test provides a good measure of the subsonic Mach number distributions for the full Tunnel 16T test cart and testing region. The supersonic Mach number distributions shown in Fig. 5c are considered acceptable since some of the disturbances in the forward portion of the distributions are believed attributable to the pipe and its cable support system. Comparison of the data in Fig. 5c with distributions from previous calibrations (Refs. 4 and 6) lead to the conclusion that the centerline pipe installation used for this calibration provides a good measure of the Tunnel 16T supersonic Mach number distributions.

The variation of the 2σ Mach number deviation with Mach number for both the AEDC NAB test region and the "standard" test region is illustrated in Fig. 6. The data presented in Fig. 6a illustrate that, except for M = 1.6, the deviations for tunnel station 8.2 to 28.2 are less than that assumed for "good" flow quality. The data presented in Fig. 6b illustrate that the deviations for tunnel station 1.2 to 20.2 are lower at subsonic Mach numbers but higher at supersonic Mach numbers than those obtained in Ref. 4. It is noted that the Ref. 4 calibration was based on wall static pressure distributions. With the exception of M = 1.6, the deviations for the "standard" tunnel test region are considered indicative of "good" flow quality.

The Mach number deviations at M_∞ = 1.6, as well as other supersonic Mach numbers, are believed affected by disturbances which emanate from the calibration rig. This is partially substantiated by the fact that the supersonic Mach number deviations for station 1.2 to 20.2 are greater than those for station 8.2 to 28.2 (see Fig. 6). In addition, a review of the distribution obtained at M = 1.6 during the Ref. 6 calibration revealed that a similar disturbance, but of less magnitude, did exist in the forward portion of the cart. Disturbances which are attributable to the calibration rig are justifiably correctable, but such corrections are somewhat academic since the calibration rig is removed for tunnel operation. Because the distributions for the AEDC NAB model test region and Mach number range were considered very acceptable, no corrections for the centerline pipe disturbances were made.

4.1.2 Effects of Porosity

The centerline Mach number distributions for various test section wall porosities at Mach numbers from 0.2 to 1.6 for θ_W = 0 and the nominal pressure ratio schedule are presented in Fig. 7. The data presented in Fig. 7 indicate that except for $M > 1.3$, porosity variation has only a small effect on the Mach number distributions.

The effects of wall porosity upon the 2σ Mach number deviations for tunnel stations 8.2 to 28.2 and 1.2 to 20.2 are presented in Figs. 8 and 9, respectively. The data in Figs. 8 and 9 indicate that for $M_\infty \leq 1.1$ variation of porosity has an insignificant effect

upon the distributions. The best distributions, however, were obtained at either four- or six-percent porosity. For $M \geq 1.2$, the variation of porosity becomes more significant. Of particular interest are the trends at M = 1.5 and 1.6. As noted from Figs. 8c and 9c, opposite trends occur for the two tunnel lengths. It can be readily seen from Fig. 7o that the disturbances which exist in the forward portion of the cart are attenuated by a decrease of porosity to two percent but that two percent porosity provides the poorer distribution over the remainder of the cart. Some of the disturbances noted in the supersonic distributions are attributable to tunnel components such as wall joints and the porosity taper region. The data presented in Fig. 7o imply that a lengthening of the taper strip region could improve the supersonic distributions in Tunnel 16T. An adequate analysis of this possibility is beyond the scope of this report; however, future effort in this regard is recommended.

The data presented in Figs. 7 to 9 indicate that for $M_\infty \leq 1.3$, the Mach number distributions obtained at two- and four-percent porosity with $\theta_w = 0$ are of "good" flow quality. At $M_\infty \geq 1.3$, the distributions at $\tau = 4$ and $\theta_w = 0$ are considered marginal. For $\tau = 2$ and $\theta_w = 0$, the distributions at $M_\infty > 1.3$ are considered unacceptable, in spite of the fact that some improvement was obtained for M = 1.5 and 1.6 for the "standard" tunnel test region.

4.1.3 Effects of Tunnel Pressure Ratio

The centerline Mach number distributions for various tunnel pressure ratios at Mach numbers from 0.8 to 1.6 for $\theta_w = 0$ are presented in Figs. 10, 11, and 12 for wall porosities of six, four, and two percent, respectively. The data presented in Figs. 10 to 12 indicate that with some exceptions pressure ratio variation at $M < 1.3$ does not significantly affect the Mach number distributions upstream of tunnel station 32. The exceptions include the extremely low pressure ratios for four- and six-percent porosity and the lower pressure ratios for two-percent porosity. For these data, some significant effects of pressure ratio variation are noted as far forward as station 28.0. For $M \geq 1.3$, no effect of pressure ratio variation for the range investigated is evident.

The effects of pressure ratio variation upon the 2σ Mach number deviations are presented in Figs. 13 and 14. The nominal pressure ratios (see Fig. 3) and the optimum pressure ratios (λ_*) are also illustrated in Figs. 13 and 14. As noted from Figs. 10 to 12, the optimum pressure ratios are those associated with "flat" distributions in the rear end of the test section (Station 40). Such an operating condition usually corresponds to the lowest potential total power consumption; however, neither the main drive nor the plenum evacuation system power was recorded during this test. It is noted that for $M \geq 1.2$, the nominal pressure ratio schedule provided "flat" distributions to Station 40.

The data presented in Figs. 13 and 14 indicate that for both test section regions, variation of the pressure ratio over a wide range does not significantly affect the Mach number distributions except for $M \leq 0.9$ at $\tau = 2.0$. The data presented in Fig. 13c show that significantly decreasing the pressure ratio below the nominal schedule at subsonic Mach numbers for $\tau = 2.0$ percent can affect the distributions for tunnel station 8.2 to 28.2. It can be concluded, however, that for normal operating conditions the distributions are not affected by pressure ratio variation and that the nominal, as well as the optimum pressure ratio schedule, is acceptable for tunnel operation.

4.1.4 Effects of Wall Angle

The centerline Mach number distributions for various test section wall angles at Mach numbers from 0.5 to 1.6 are presented in Figs. 15, 16, and 17 for wall porosities of six, four, and two percent, respectively. The data presented in Figs. 15 through 17 illustrate that wall angle variation can have a significant effect upon the Mach number distributions. The effect is primarily associated with the rear end of the distributions; however, at supersonic Mach numbers the forward portion of the distributions are also affected. In general, the data presented in Figs. 15 through 17 indicate that for the nominal pressure ratio schedule (λ_N) the "flattest" distributions to station 40 were obtained with wall divergence (0.25 to 0.50 deg) at $M_\infty \leq 0.7$ and $M_\infty \geq 1.3$ with $\theta_w = 0$ for $M_\infty = 0.8$ and 1.2 and with wall convergence (-0.25 deg) at $0.9 \leq M_\infty \leq 1.1$.

The effects of wall angle variation upon the 2σ Mach number deviations are presented in Figs. 18 to 23. In general, the data presented in Figs. 18 to 23 indicate that as the wall angle is varied a 100-percent increase from the minimum to the maximum deviations is not uncommon.

Data at $M \leq 0.9$ are presented for tunnel stations 8.2 to 28.2 and 1.2 to 20.2 in Figs. 18 and 19, respectively. The data presented in Figs. 18 and 19 indicate that for all porosities and both test regions the effects of wall angle variation at M = 0.8 and 0.9 are not significant. The effects of wall angle variation at $M \leq 0.7$ are more pronounced. The data indicate that as the porosity is decreased, from six to two percent, the "best" distributions for $M_\infty \leq 0.7$ were obtained by increasing the wall angle from 0 to 0.50 deg.

The variation of the Mach number deviations for Mach numbers from 1.0 to 1.3 for the two test section regions of interest is presented in Figs. 20 and 21. The data presented in Figs. 20 and 21 illustrate that with the exception of M = 1.3 at $\tau = 2.0$, the "best" distributions for both test regions are obtained at $\theta_w = 0, \pm 0.25$ deg. At M = 1.3 and $\tau = 2.0$ percent, a disturbance at tunnel station 5 (see Fig. 17h) requires divergence of the wall to 0.50 deg for acceptable attenuation.

The effects of wall angle variation upon the 2σ Mach number deviations for $M \geqslant 1.4$ are presented in Figs. 22 and 23 for the AEDC NAB and "standard" tunnel test regions, respectively. The data presented in Figs. 22 and 23 indicate that, with the exception of $M = 1.4$ at $\tau = 6.0$, the "best" distributions for both test regions were obtained with either 0.25- or 0.50-deg wall divergence. In general, for $M > 1.4$, increased wall divergence was required with decreasing porosity. The data indicate that for $\tau = 4$ and $M \geqslant 1.5$ and for $\tau = 2$ and $M \geqslant 1.4$ wall divergence of more than 0.50 deg would further improve the distributions.

To summarize, the data presented in Figs. 18 to 23 indicate that at $M \leqslant 1.3$ for all porosities and both test regions, the distributions obtained at wall angles of 0 or 0.25 deg are considered to be of "good" flow quality. For $M_\infty > 1.3$ and $\tau = 6$, $\theta_w = 0$ or 0.25 deg provides acceptable distributions; however, wall divergence at $M = 1.6$ is considered desirable. At $\tau = 4$ for $M_\infty > 1.3$, acceptable distributions were obtained for the AEDC NAB test region at wall angles from 0 to 0.50 deg. For the "standard" test region (station 1.2 to 20.2), however, from 0.25- to 0.50-deg wall divergence is required for acceptable distributions at $\tau = 4$. For $M_\infty > 1.3$ and $\tau = 2$, from 0.25 to 0.50 deg, wall divergence is required to provide acceptable distributions for both tunnel test regions.

The test section wall angles associated with the optimum wall angle schedule, θ_w^*, (see Fig. 5) are also noted on Figs. 18 to 23 for $\tau = 6$. No optimum wall angle schedule has previously been defined for porosities other than six percent. Data presented herein and in Ref. 7, however, could be utilized to estimate such schedules. According to Ref. 7, decreasing wall porosity is equivalent to wall convergence, hence some wall divergence should be utilized as the porosity is decreased. In general, this is substantiated by the data presented herein.

The comparison of the optimum wall angle schedule with the wall angle which supplies the minimum Mach number deviation for $\tau = 6$ is considered excellent with the exception of data at $M = 1.1$. The Mach number deviation at $M = 1.1$ and θ_w^* is considered acceptable for the AEDC NAB test region but not for the tunnel region from station 1.2 to 20.2 (Fig. 21a). As pointed out in Ref. 5, the optimum wall angle schedule represented conditions which minimized test section interference with a particular model type and size. Although one would not expect the wall angle for "best" shock correlation on a cone-cylinder model to coincide with the wall angle for best "empty tunnel" distributions, one would expect better agreement than that shown for $M = 1.1$.

A review of Ref. 5 indicates that considerable judgement was utilized in defining the optimum wall angle schedule. In fact, no cone-cylinder pressure data were obtained specifically at the optimum wall angles for Mach numbers from $M = 1.05$ to 1.20. The

Ref. 5 data do indicate that wall convergence for that Mach number range did decrease the test section interference; however, the improvement over $\theta_w = 0$ was small.

As noted by Ref. 5, operation at highly converged wall angles requires a significant increase in tunnel power requirements as compared to operation at $\theta_w = 0$. Considering the nation's energy crisis and the results presented herein, a re-evaluation of the Tunnel 16T optimum wall angle schedule may be warranted.

4.2 TUNNEL CALIBRATION

4.2.1 General

As previously indicated in Section 3.2, a Mach number parameter (M_∞-M_c) is utilized to express the Tunnel 16T calibration. The effects of test section porosity and wall angle upon the calibration are presented herein. Since pressure ratio variation does not have a significant effect upon the Mach number distributions, it also does not affect the tunnel calibration.

To aid in the preparation of computer programs for Tunnel 16T tests utilizing variable porosity test section walls, analytic expressions of the Mach number calibration parameter were determined using a least-squares, multiple regression data fitting program. Several data fits were required to adequately specify the tunnel calibration at various porosities and wall angles. The analytical expression coefficients and accuracy for the various data fits are presented in Tables 1 through 7. Several sets of coefficients have been included herein so that computer programs could be prepared for specific applications as required.

A comparison of the Tunnel 16T calibration for the AEDC NAB test region and the "standard" tunnel test region at $\theta_w = 0$ is presented in Fig. 24. The data presented in Fig. 24 illustrate that the calibrations for the two test regions agree within ±0.003 at all conditions but within ±0.001 for most conditions. Such agreement is the same order of magnitude as the data precision. Considering such excellent agreement and the fact that this calibration was conducted in support of the AEDC NAB test program, the additional results presented herein are restricted to data for the test region from station 8.2 to 28.2.

Current Tunnel 16T calibration is based upon results from Ref. 4. The data from Ref. 4 are presented and compared to the $\tau = 6$ data in Fig. 24a. The data presented in Fig. 24a indicate that for both test regions the current Cart 1 centerline calibration and the Ref. 4 Cart 2 wall calibration agree within ±0.002. Such agreement is considered satisfactory and leads to the conclusion that no new Tunnel 16T calibration is required for operation at $\theta_w = 0$ and τ = six percent.

4.2.2 Effects of Porosity

The effects of test section wall porosity upon the Tunnel 16T calibration at $\theta_w = 0$ are shown in Fig. 25. The data presented in Fig. 25 indicate that the tunnel calibration varies significantly with porosity for $M_\infty > 0.8$. These data verify that new computational procedures are required for operation of Tunnel 16T at porosities other than six percent.

The coefficients associated with the surface fits of the data presented in Fig. 25 are presented in Table 1.* The curves shown in Fig. 25 depict the analytical results of the data fitting program. The best results were achieved by splitting the data into two or three ranges as shown in Tables 1 through 4. The maximum residual (the difference between the actual and computed value) which results from the surface fits vary from 0.0008 to 0.0032 for the three ranges. However, 95 percent of the data have residuals which are significantly smaller as shown in Table 1. As shown by Fig. 25 and Tables 1 through 4, some improvement can be obtained at higher Mach numbers by utilization of the curve fits. The surface fits however can be utilized for operation at porosities other than two and four percent.

4.2.3 Effects of Wall Angle

The effects of test section wall angle variation upon the Tunnel 16T calibration for various porosities are illustrated in Fig. 26. The data presented in Fig. 26 indicate that the calibration is significantly affected by wall angle variation. Calibration data fits are therefore required as a function of wall angle.

The Ref. 4 calibration data are also presented in Fig. 26a for $\tau = 6$ percent. The data presented in Fig. 26a indicate excellent agreement between the Ref. 4 and the current calibration at $\theta_w \geq 0$. For converged wall angles the comparison is not generally considered satisfactory. At the specific wall angles associated with the optimum wall angle schedule ($\theta_w{}^*$), however, the two calibrations agree within ± 0.002 which is satisfactory. Since converged wall angles other than those associated with the optimum schedule are rarely run in Tunnel 16T no new tunnel calibration is required for operation at $\tau = 6$ percent.

The coefficients associated with surface fits of the data with wall angle as a variable are presented in Tables 5, 6, and 7. Attempts to fit a hypersurface to the entire data set proved unsuccessful. The curves shown in Fig. 26 depict the analytic surface which corresponds to the best results of the data fitting program. The best results were achieved

*The coefficients associated with curve fits of the data for individual porosities are presented in Tables 2, 3, and 4 for $\tau = 6$, 4, and 2, respectively.

by splitting the data into either two or three regions as shown in Tables 5 through 7. The maximum residuals which result from the various data fits are presented in Tables 5 through 7. In general, the maximum residuals vary significantly with Mach number range and porosity. In addition, ignoring the worst five percent of the data fits, significantly lower residuals for the remaining 95 percent of the data are indicated. Considering the accuracy of porosity which results from porosity variation techniques such as that used during this calibration, the calibration data curve and surface fits are considered quite satisfactory.

5.0 CONCLUSIONS

Based on the results from this centerline calibration of Tunnel 16T, the following conclusions are made:

1. The centerline pipe installation used for this test provides a good measure of both subsonic and supersonic Mach number distributions in Tunnel 16T.

2. For $M_\infty \leqslant 1.1$, the Mach number distributions are not significantly affected by variation of wall porosity from six to two percent. At higher Mach numbers, porosity variation becomes significant.

3. Variation of pressure ratio over the normal operating range has an insignificant effect upon the centerline Mach number distributions. The nominal pressure ratio schedule used during this test is satisfactory for operation in Tunnel 16T.

4. In general, variation of the test section wall angle can have a significant effect upon the Mach number distributions.

5. For a porosity of six percent, Mach number distributions of "good" flow quality are obtained for $0.2 \leqslant M_\infty \leqslant 1.6$ for both $\theta_w = 0$ and 0.25 deg.

6. For a porosity of four percent and $\theta_w = 0$, the Mach number distributions are of "good" flow quality at $M_\infty \leqslant 1.3$ but are considered marginal at $M_\infty > 1.3$. Divergence of the test section wall angle to either 0.25 or 0.50 deg, however, provides acceptable distributions at $M_\infty > 1.3$.

7. For a porosity of two percent and $\theta_w = 0$, the Mach number distributions are of "good" flow quality at $M_\infty \leqslant 1.3$ but are considered unacceptable at $M_\infty > 1.3$. For $M_\infty > 1.3$, from 0.25- to 0.50-deg wall divergence is required to provide acceptable distributions.

8. Satisfactory Mach number distributions are obtained at the Tunnel 16T optimum wall angle schedule for the AEDC NAB test region.

9. Variation of test section wall porosity or wall angle significantly affects the Tunnel 16T calibration. Analytical expressions which adequately represent the tunnel calibration at various porosities and wall angles were developed.

10. Comparison of this calibration with the Ref. 4 calibration indicates that no new Tunnel 16T calibration is required for operation at six-percent porosity with either $\theta_w = 0$ or the optimum wall angle schedule ($\theta_w{}^*$).

REFERENCES

1. Test Facilities Handbook (Tenth Edition). "Propulsion Wind Tunnel Facility, Vol. 4." Arnold Engineering Development Center, Arnold Air Force Station, Tennessee, May 1974.

2. Dick, Richard S. "The Influence of Several Cable-Type Supports Upon the Static Pressures Along the Centerline Tube in a Transonic Wind Tunnel." AEDC-TN-54-26, January 1955.

3. Jackson, F. M. "Supplemental Calibration Results for the AEDC Propulsion Wind Tunnel (16T)." AEDC-TR-70-163 (AD872375), August 1970.

4. Gunn, J. A. "Check Calibration of the AEDC 16-Ft Transonic Tunnel." AEDC-TR-66-80 (AD633277), May 1966.

5. Nichols, James H. "Determination of Optimum Operating Parameters for the PWT 16-Ft Transonic Circuit Utilizing One-Percent Bodies of Revolution." AEDC-TN-59-100 (AD225362), September 1959.

6. Dick, R. S. "Calibration of the 16-ft Transonic Circuit of the Propulsion Wind Tunnel with an Aerodynamic Test Cart Having 6-Percent Open Inclined-Hole Walls." AEDC-TN-58-90 (AD204846), November 1958.

7. Jackson, F. M. "Calibration of the AEDC-PWT 1-ft Transonic Tunnel with Variable Porosity Test Section Walls." AEDC-TR-69-114, (AD853073), May 1969.

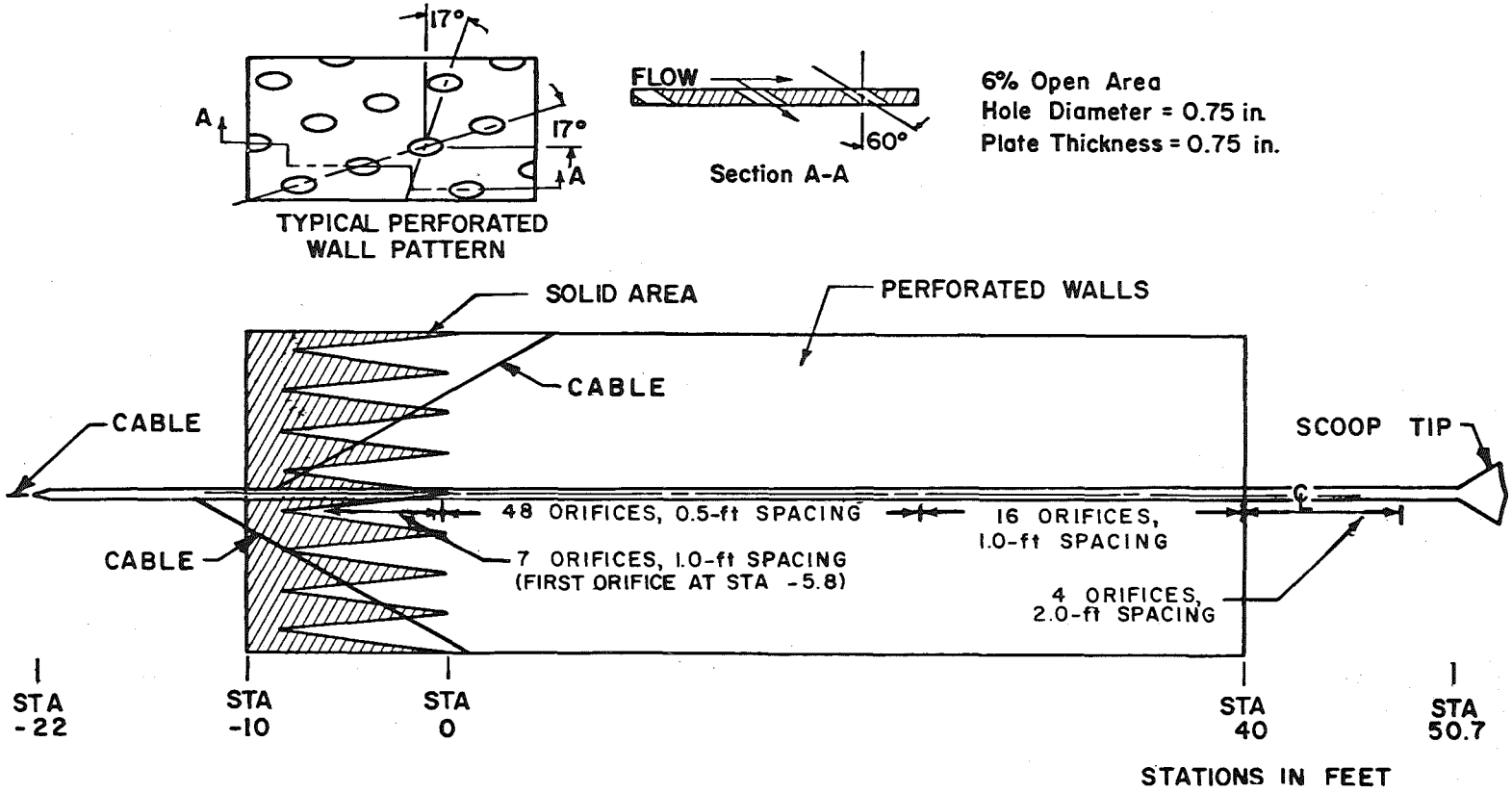

a. Schematic of the test installation

Figure 1. Tunnel 16T centerline pipe installation.

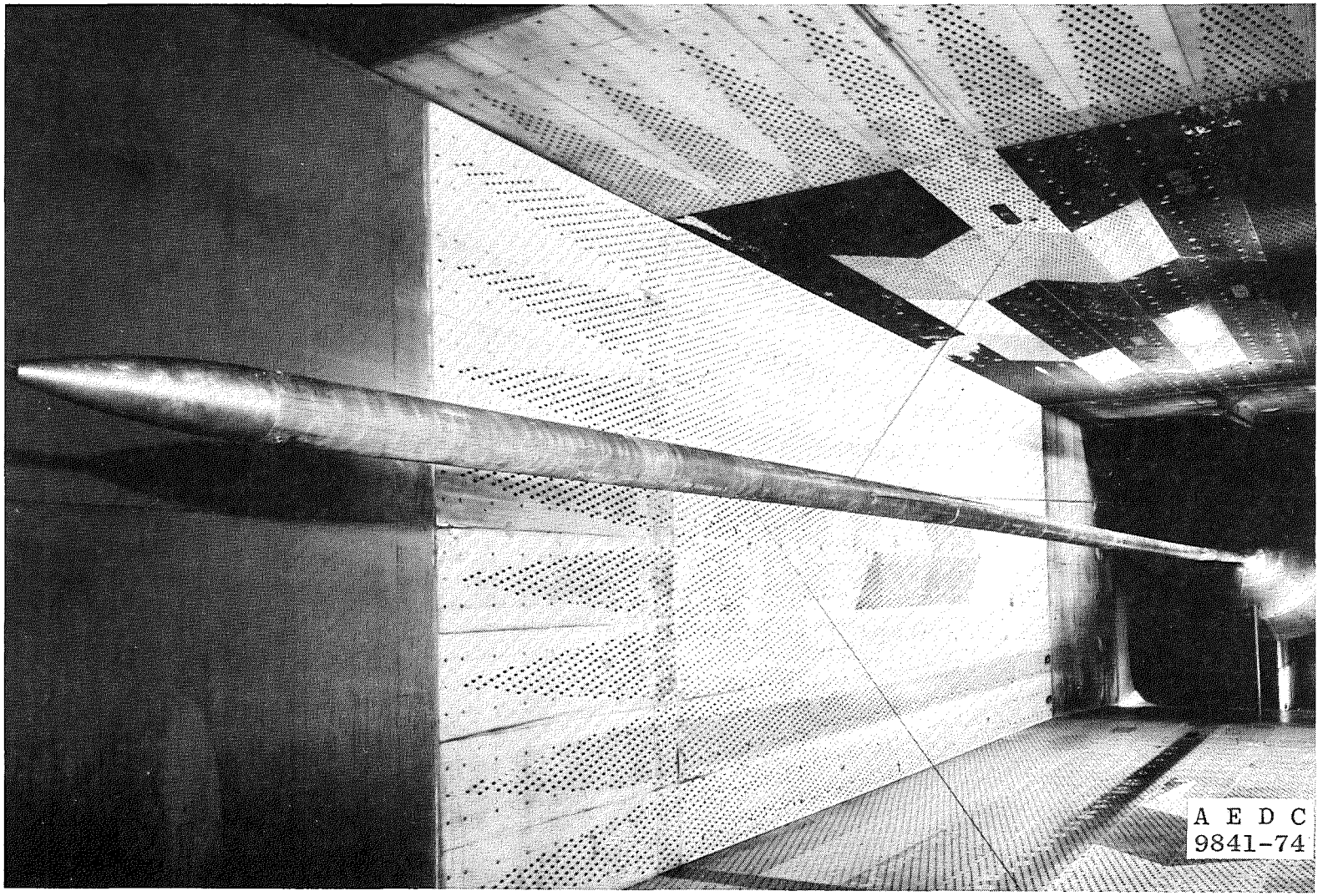

b. Pipe, main supporting cables, and rear mount
Figure 1. Continued.

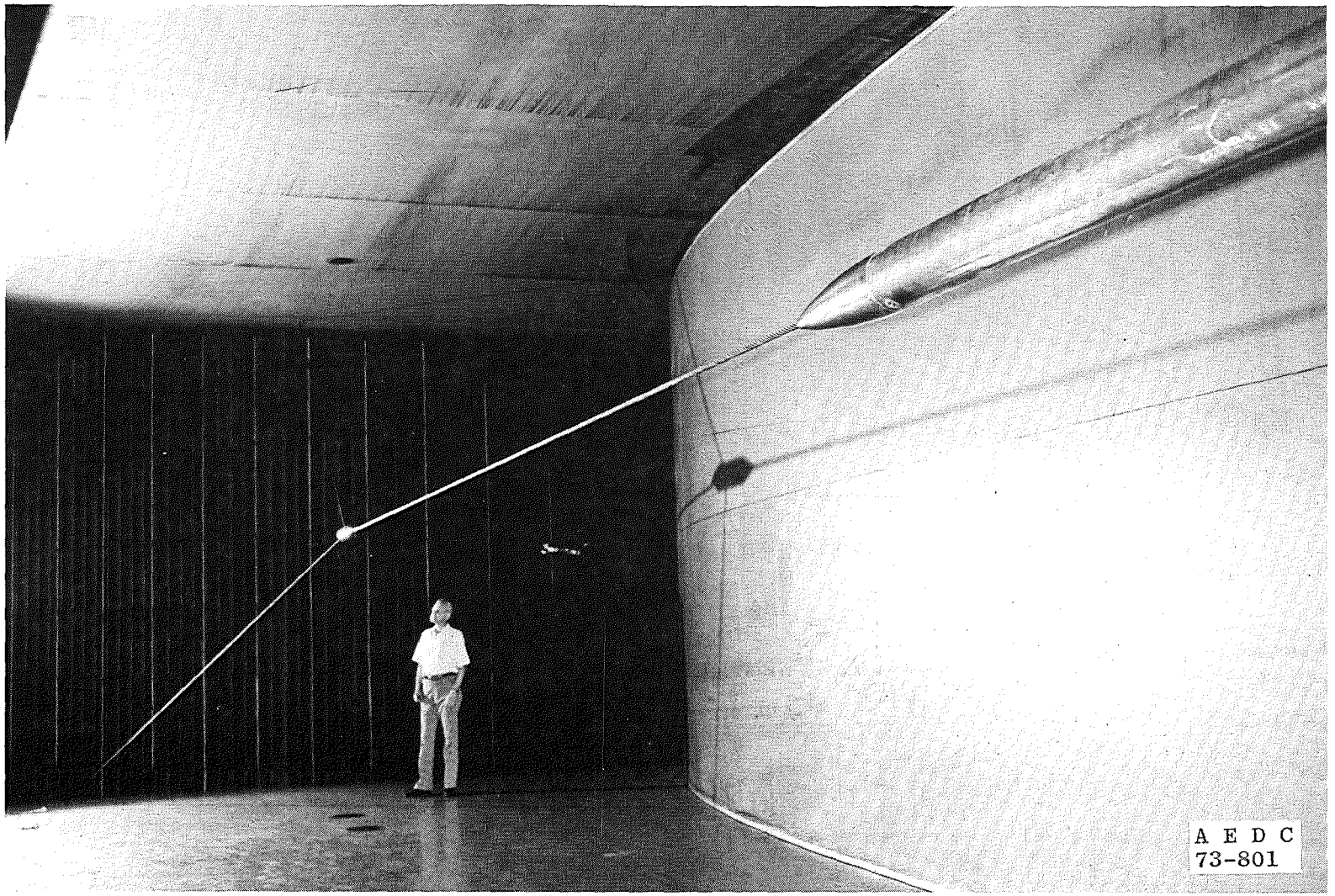

c. Pipe and forward cable system
Figure 1. Concluded.

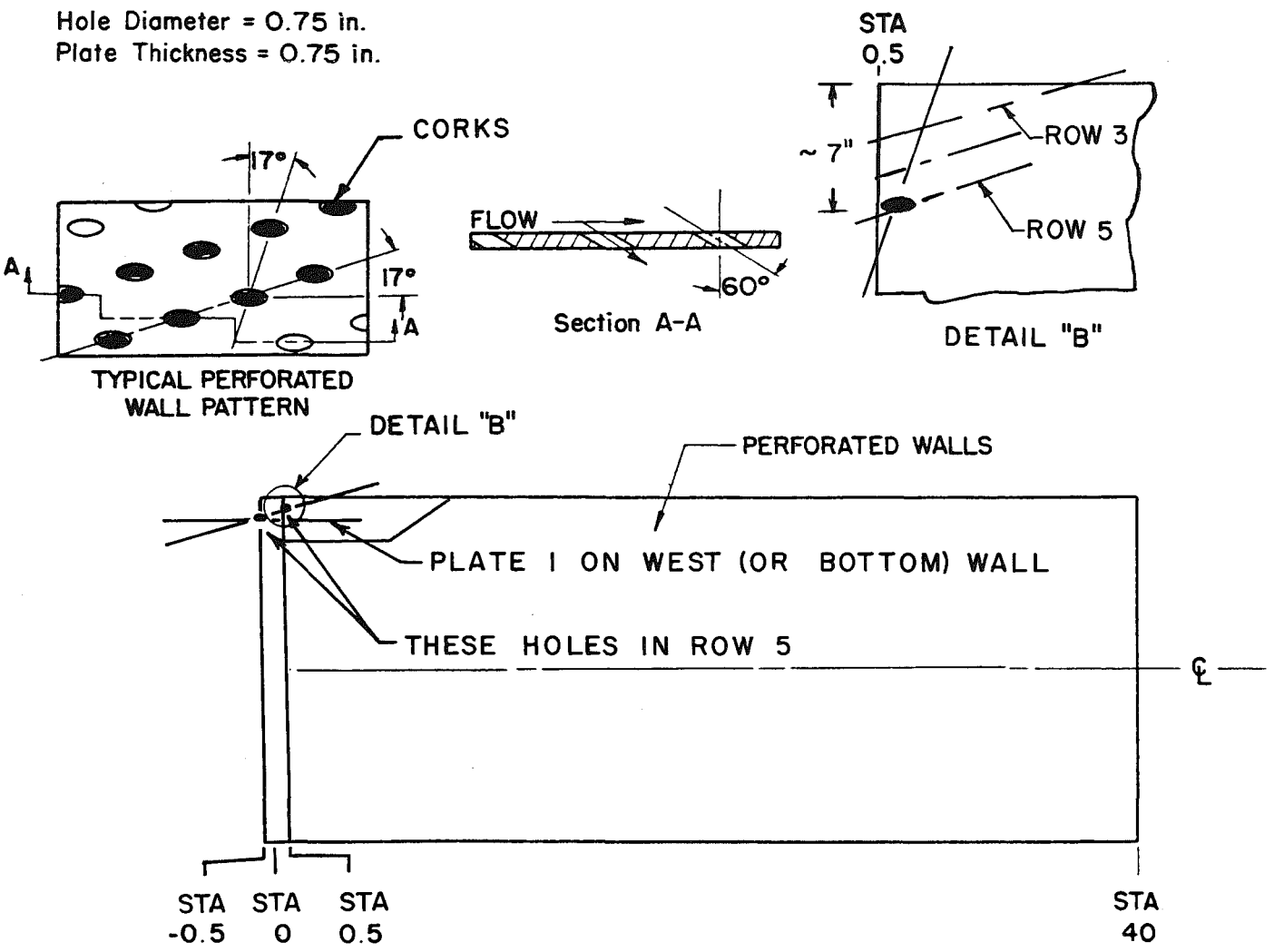

a. Station -0.5 to 40

Figure 2. Tunnel 16T porous wall corking setup.

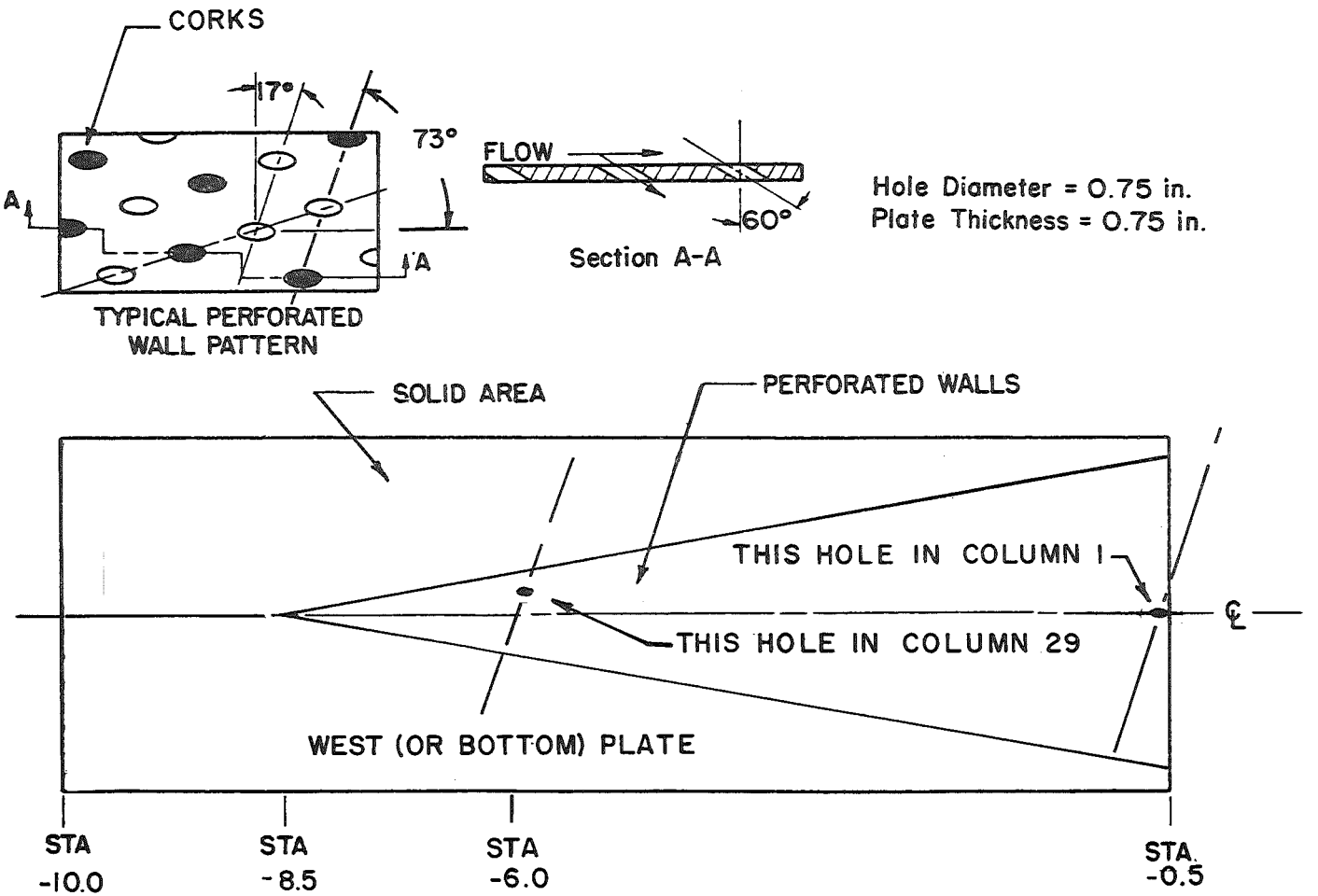

b. Station -8.5 to 0.5
Figure 2. Concluded.

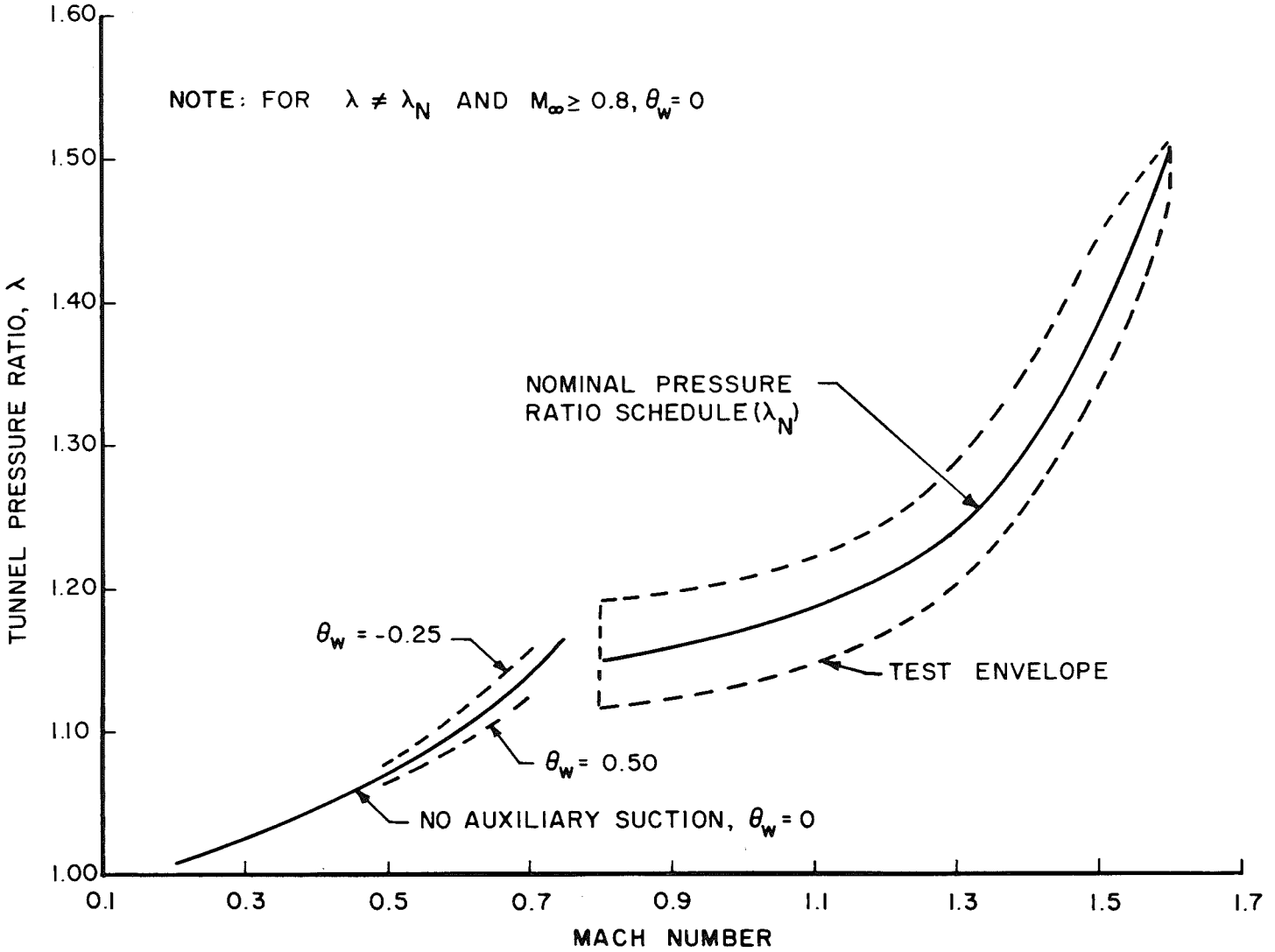

Figure 3. Variation of tunnel pressure ratio.

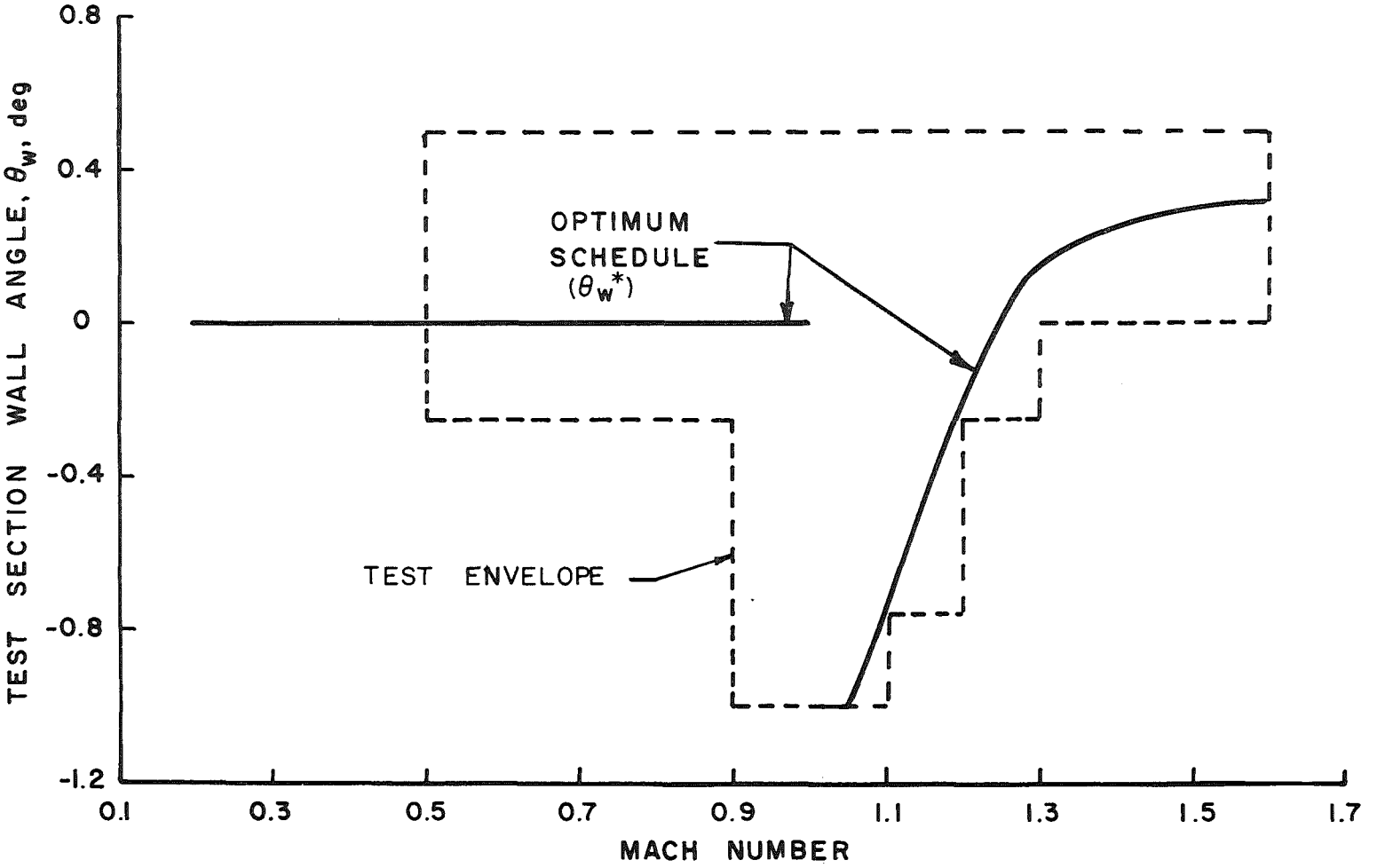

Figure 4. Variation of test section wall angle.

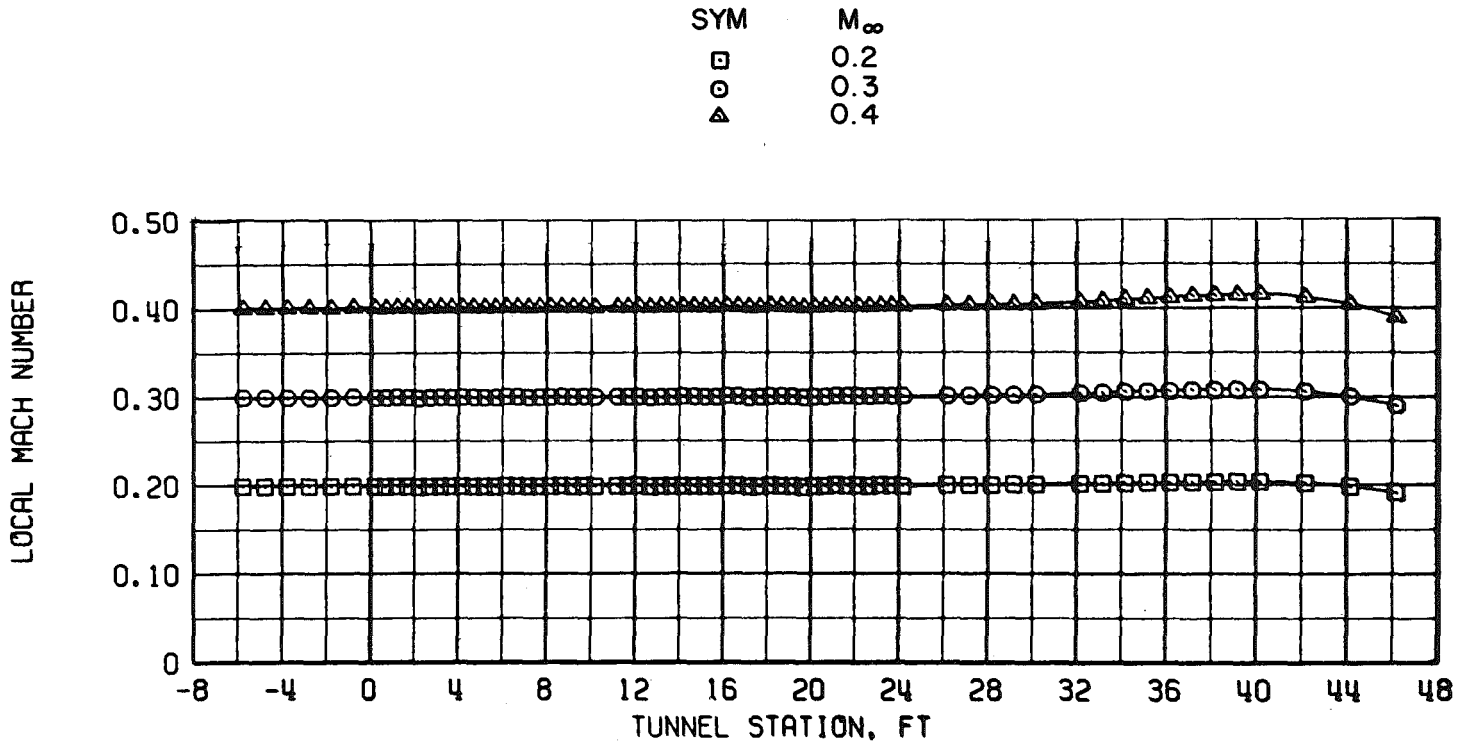

a. M_∞ = 0.2 to 0.4

Figure 5. Tunnel 16T centerline Mach number distributions for τ = six percent at $\lambda = \lambda_N$ and $\theta_w = 0$.

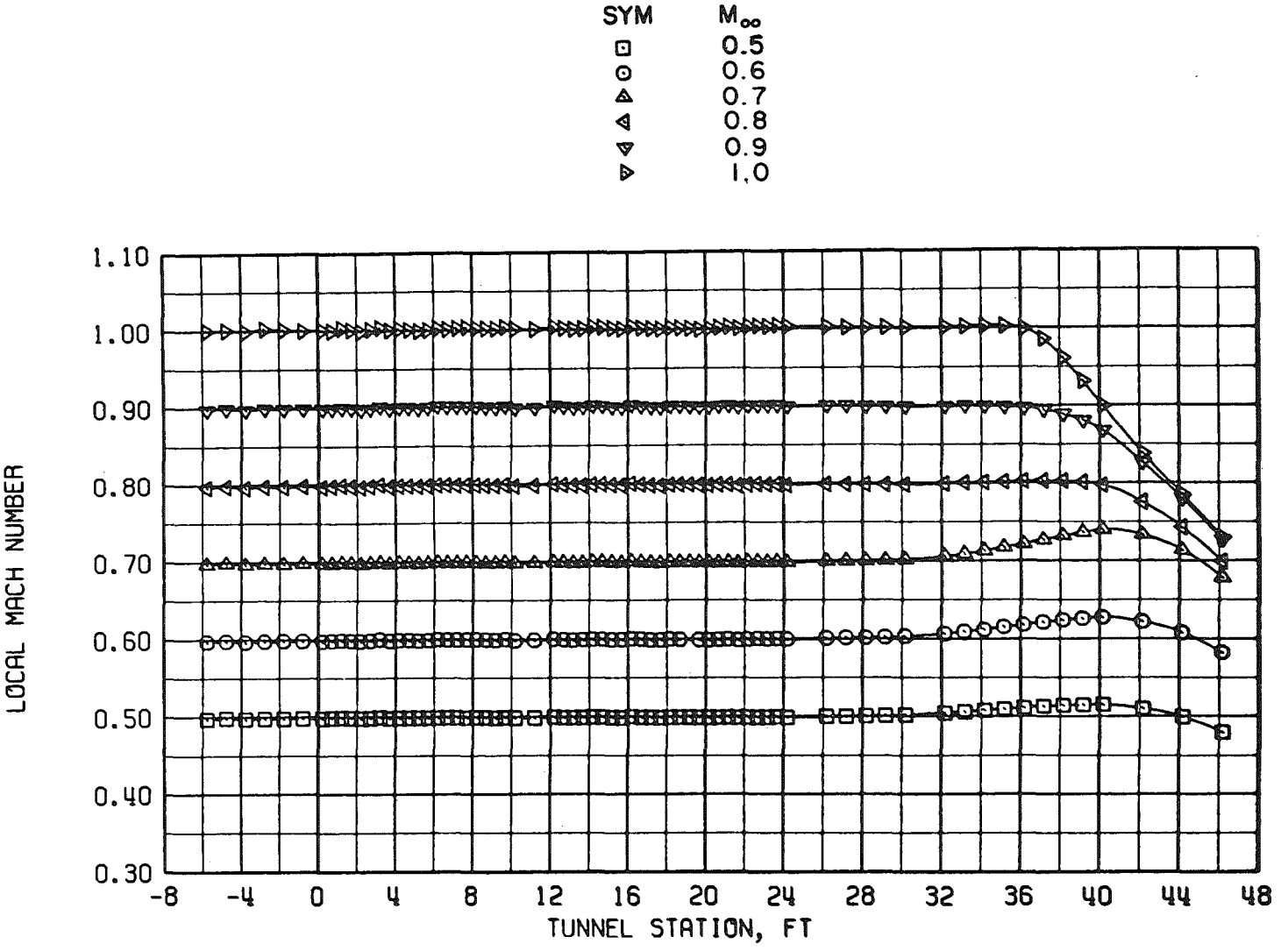

b. M_∞ = 0.5 to 1.0

Figure 5. Continued.

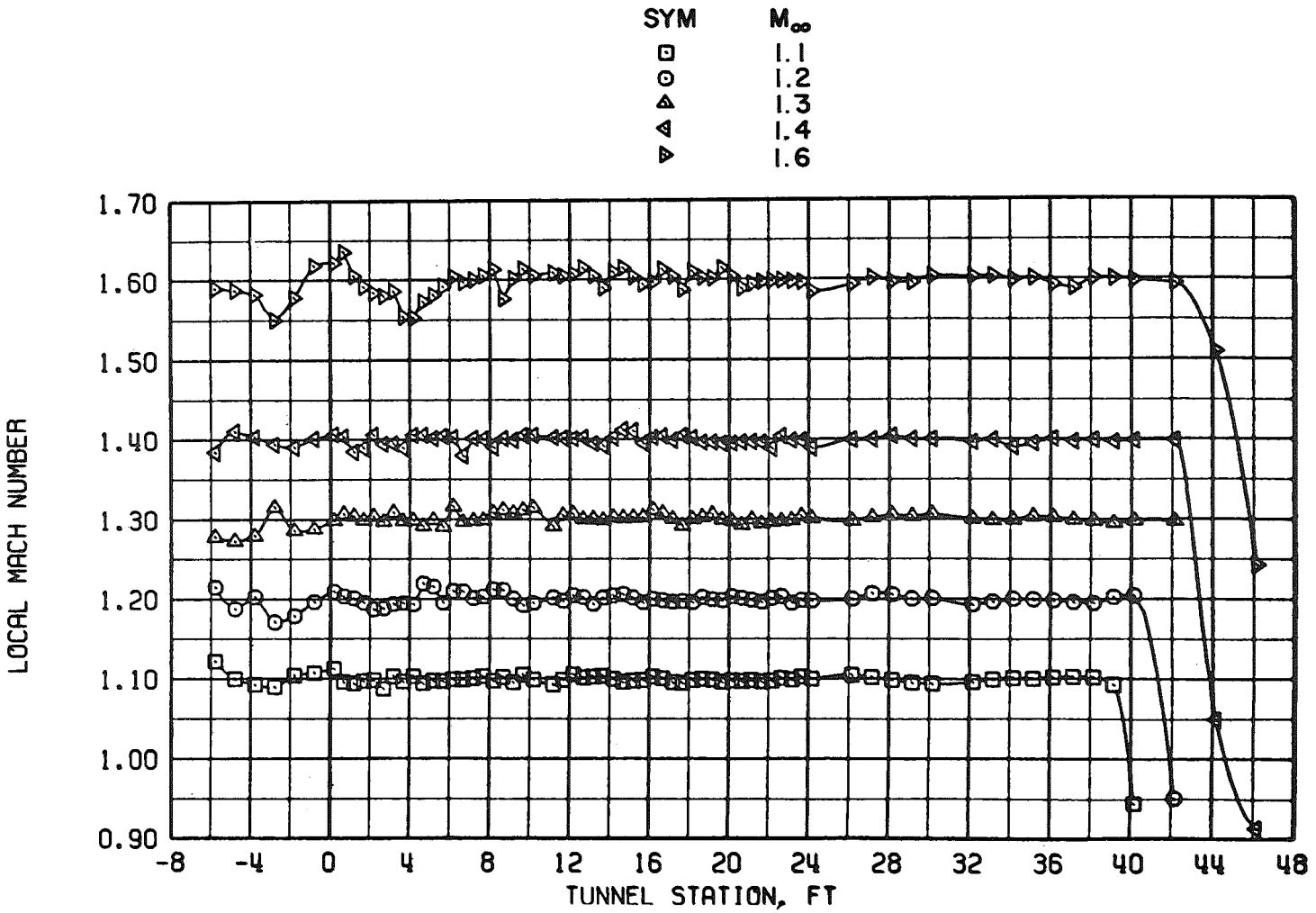

c. M_∞ = 1.1 to 1.6

Figure 5. Concluded.

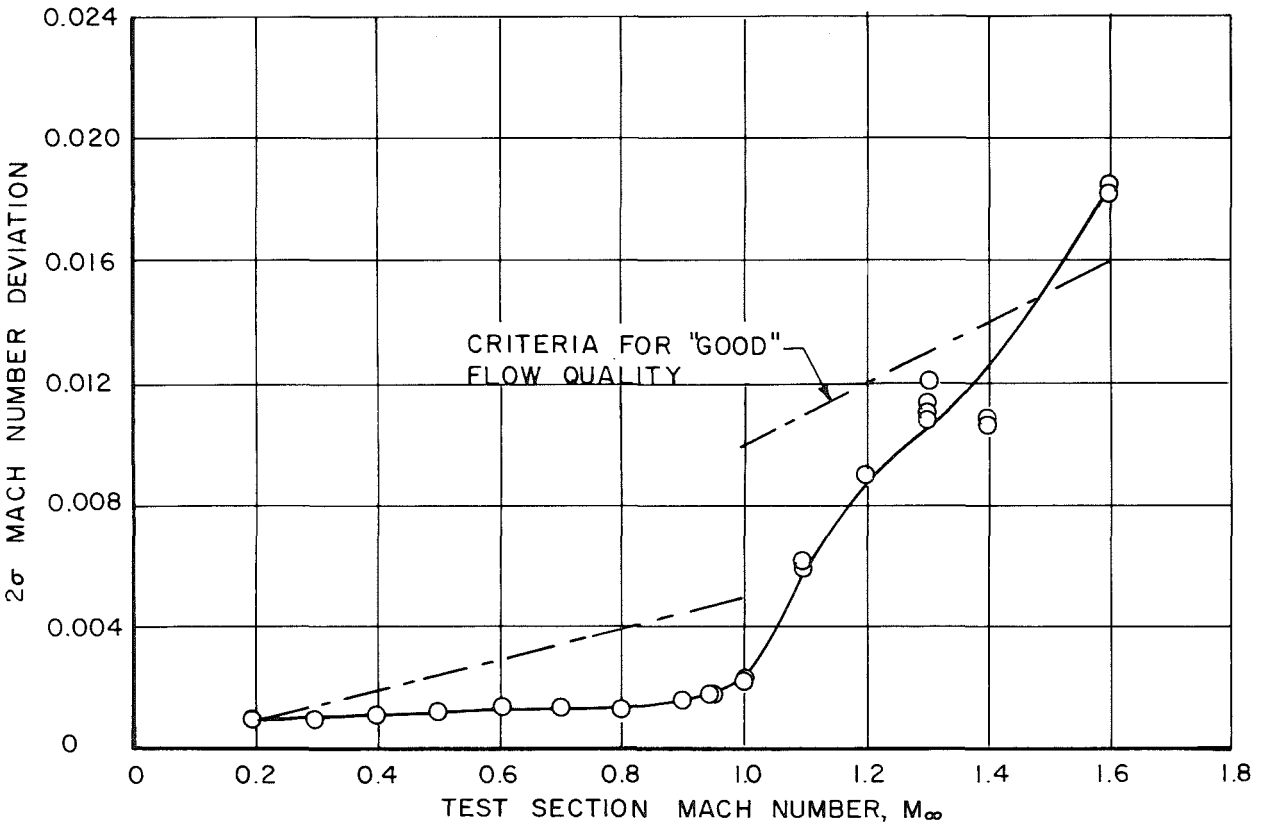

a. Tunnel station 8.2 to 28.2

Figure 6. Effect of Mach number upon the Mach number deviations for six-percent porosity at $\lambda = \lambda_N$ and $\theta_w = 0$.

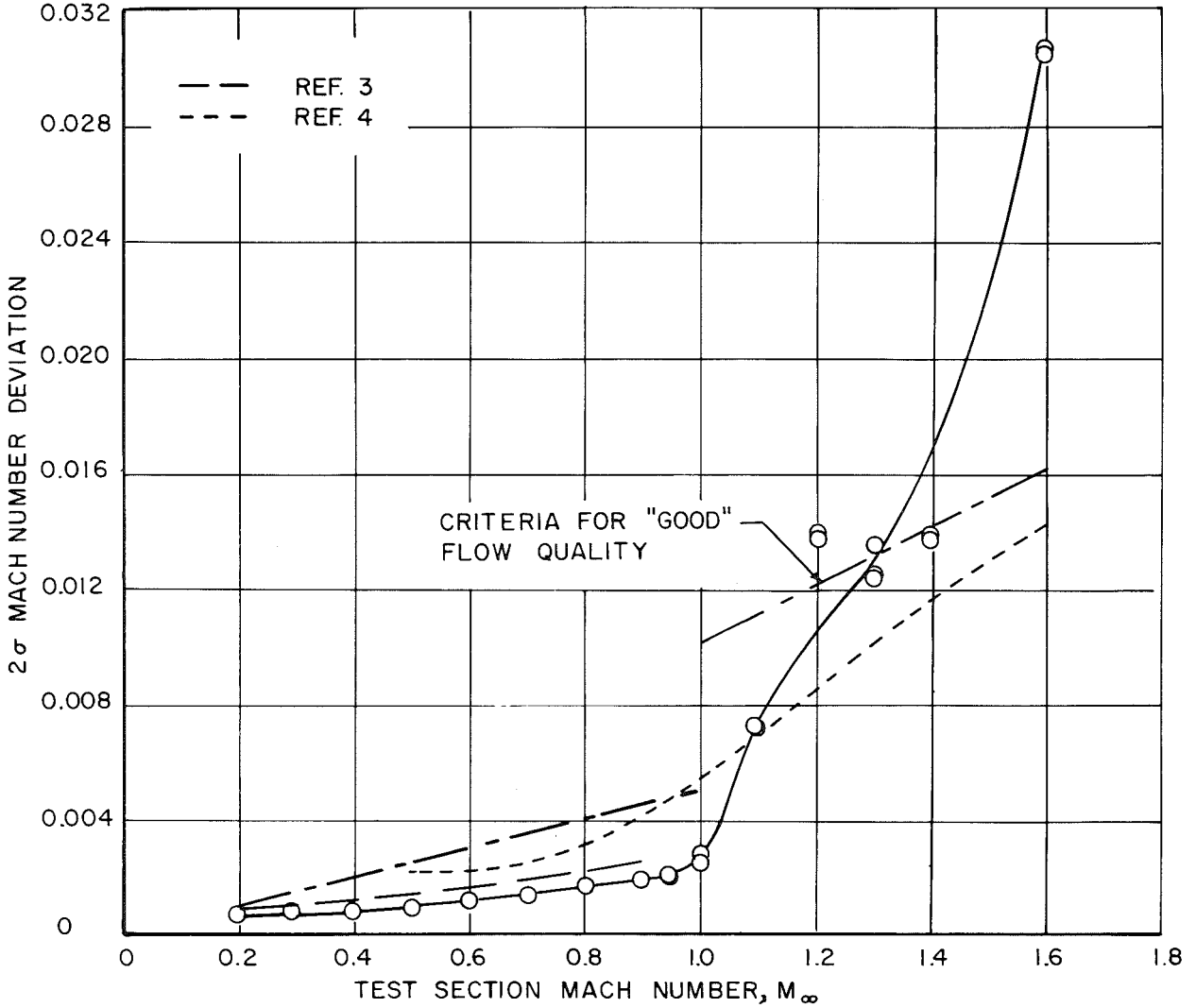

b. Tunnel station 1.2 to 20.2
Figure 6. Concluded.

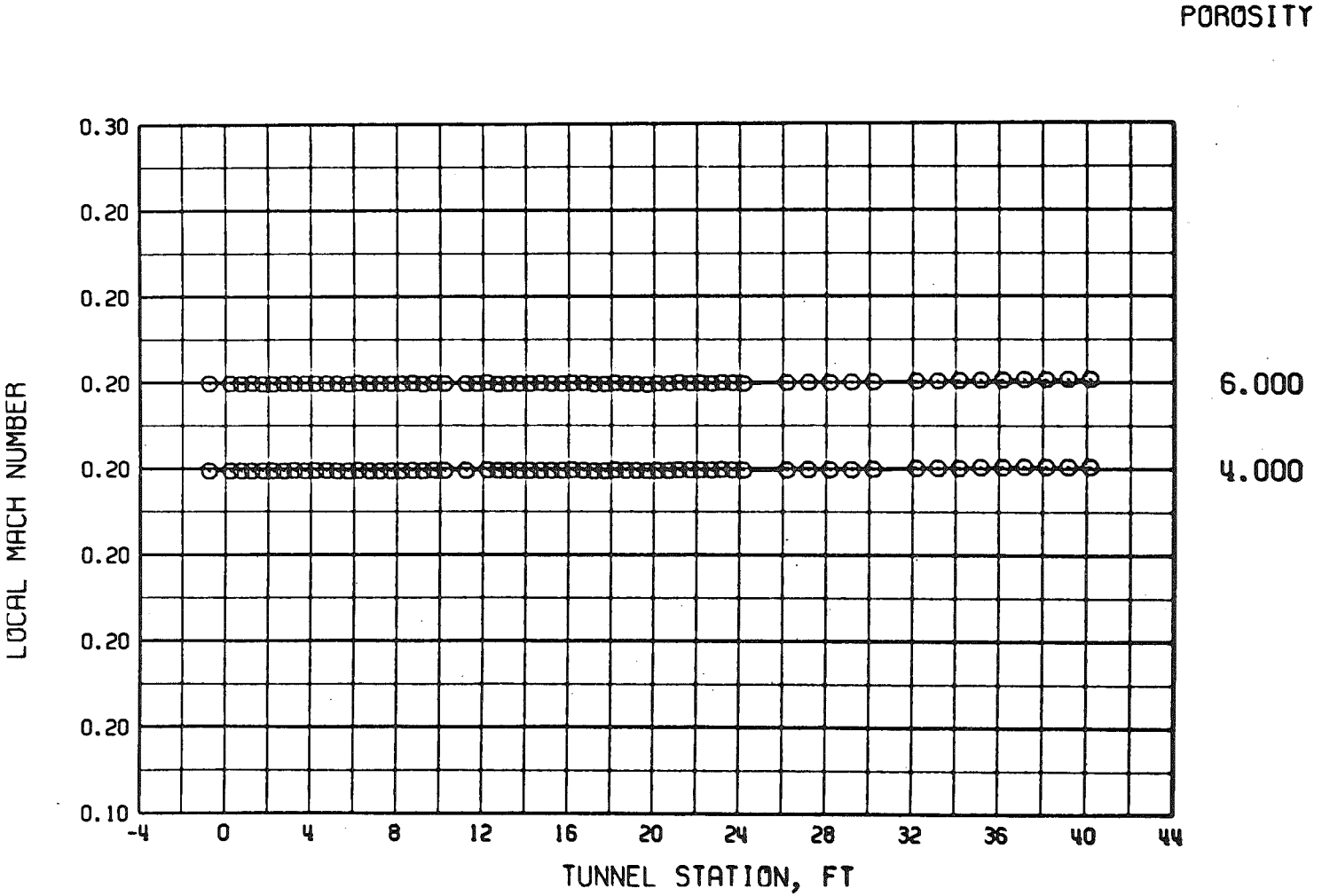

a. M = 0.2, θ_w = 0 and λ = 1.01

Figure 7. Tunnel 16T centerline Mach number distributions for various test section wall porosities with $\lambda = \lambda_N$ and $\theta_w = 0$.

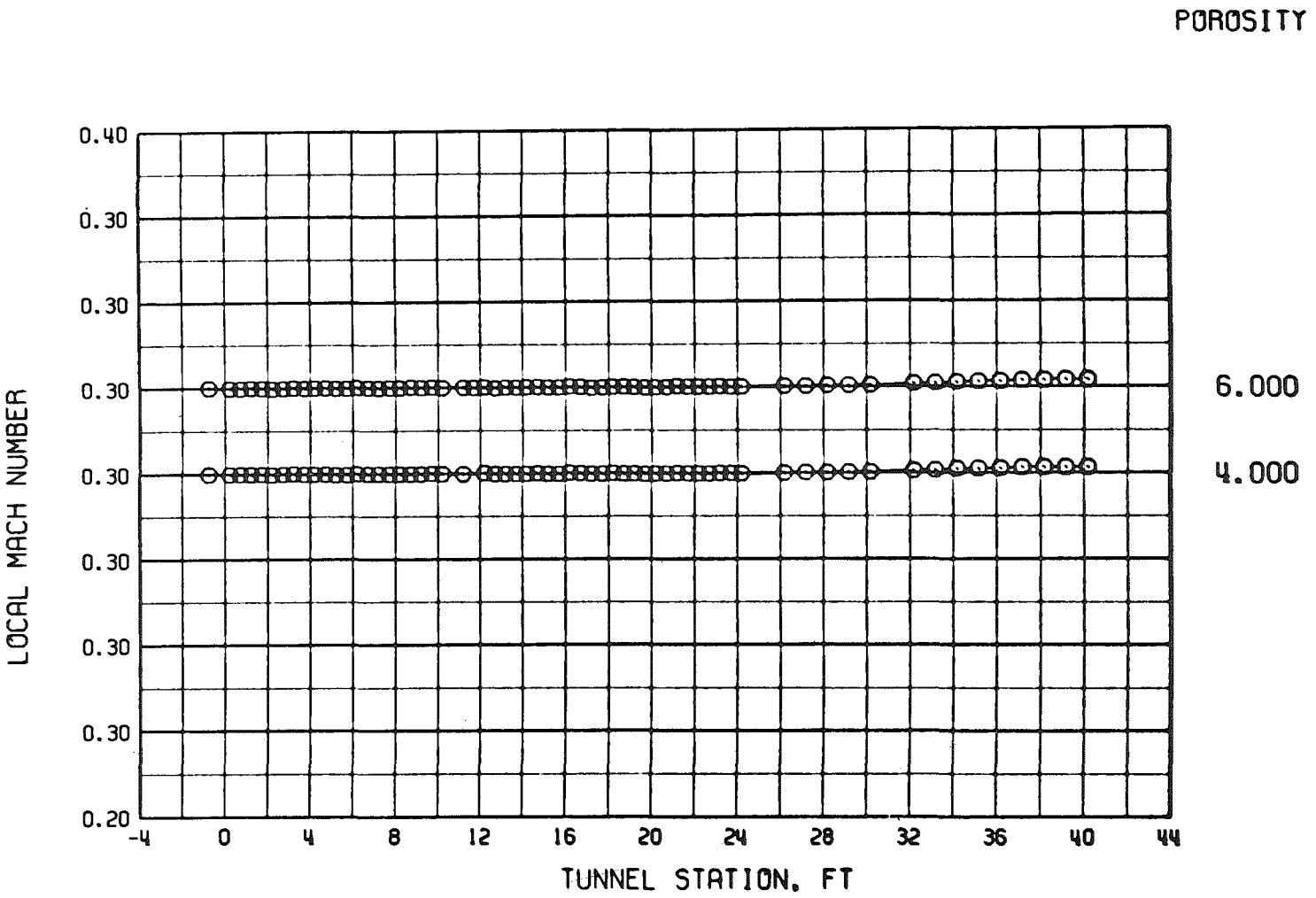

b. M = 0.3, θ_w = 0, and λ = 1.03

Figure 7. Continued.

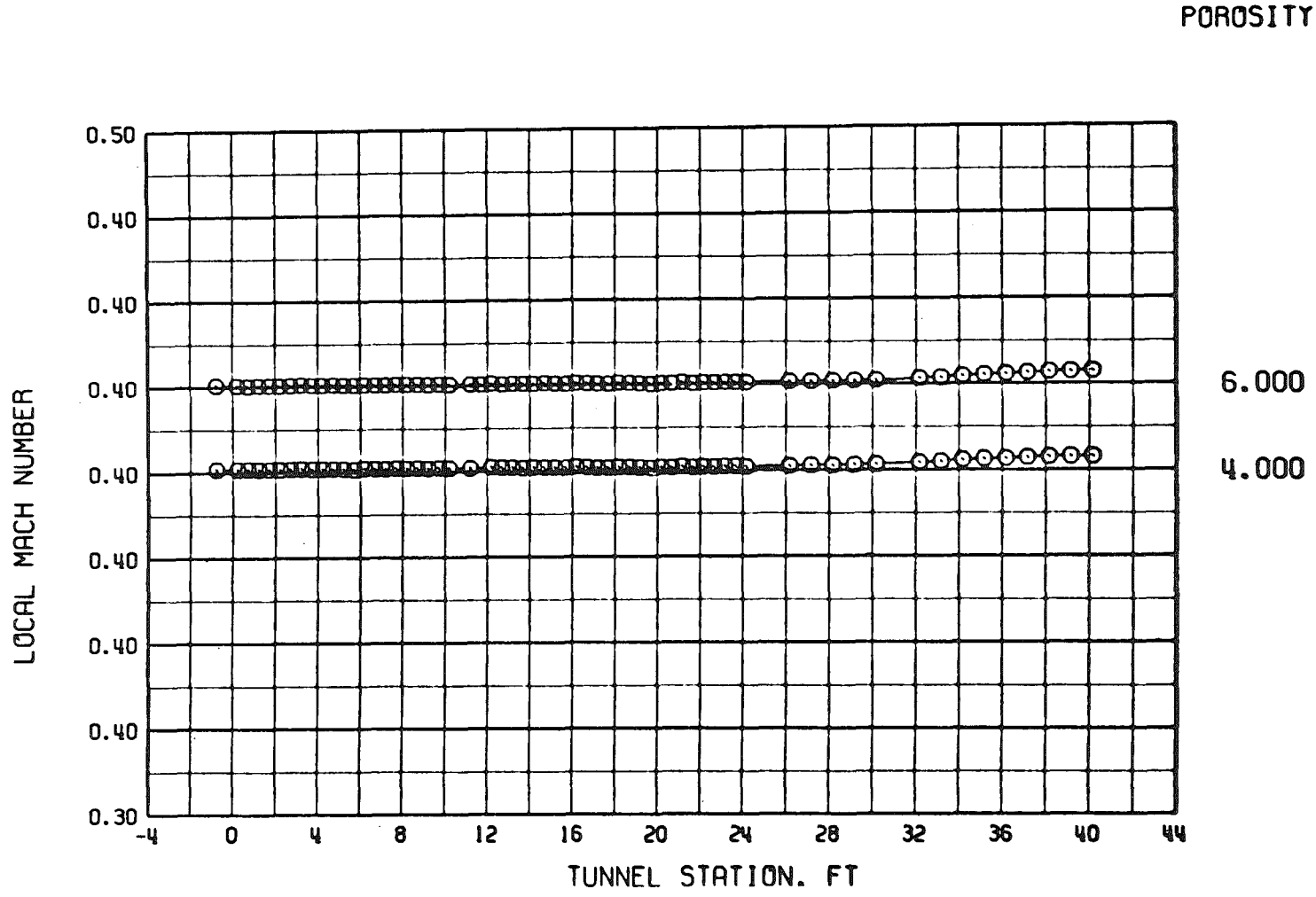

c. M = 0.4, θ_w = 0, and λ = 1.05

Figure 7. Continued.

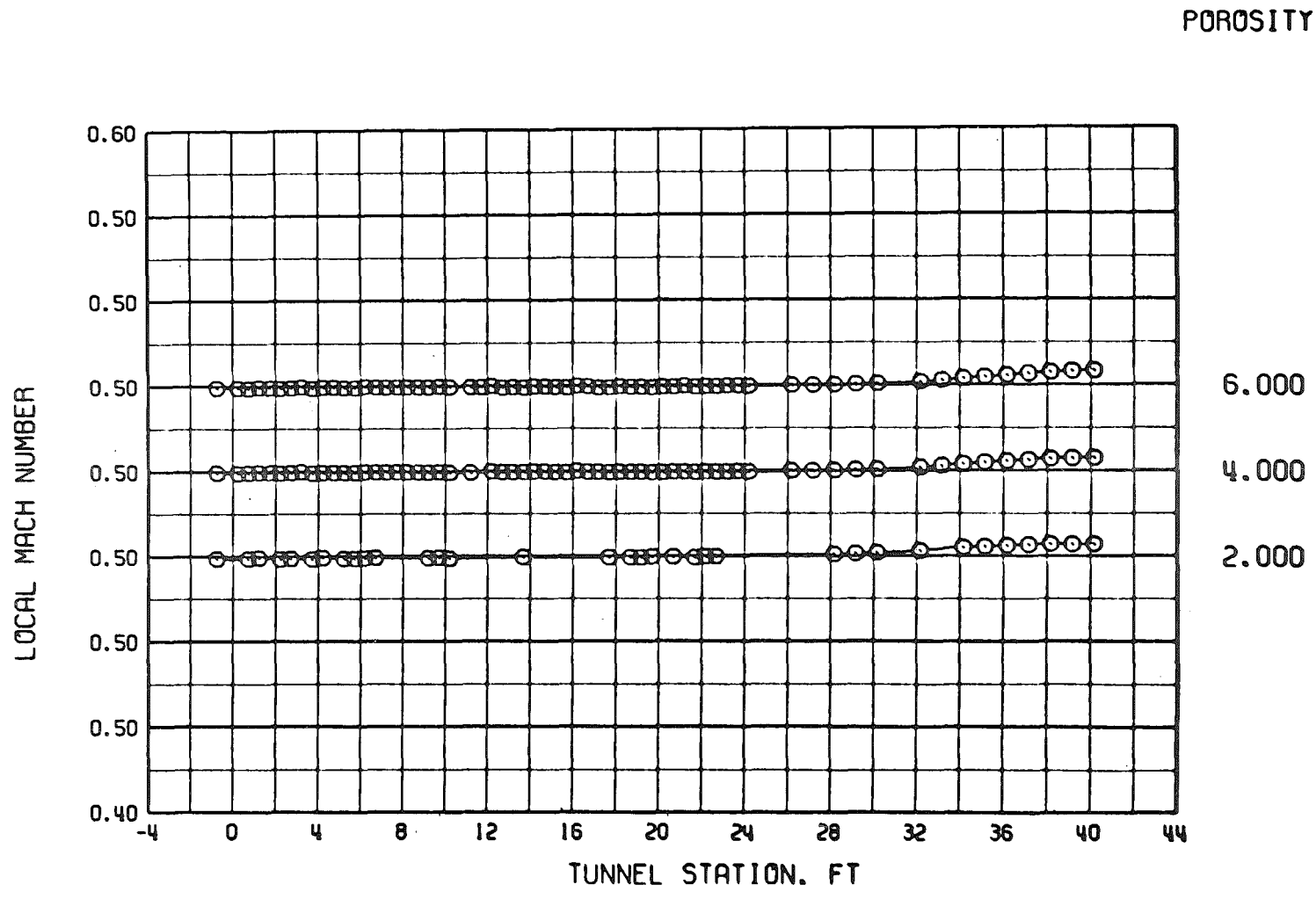

d. M = 0.5, θ_w = 0, and λ = 1.07

Figure 7. Continued.

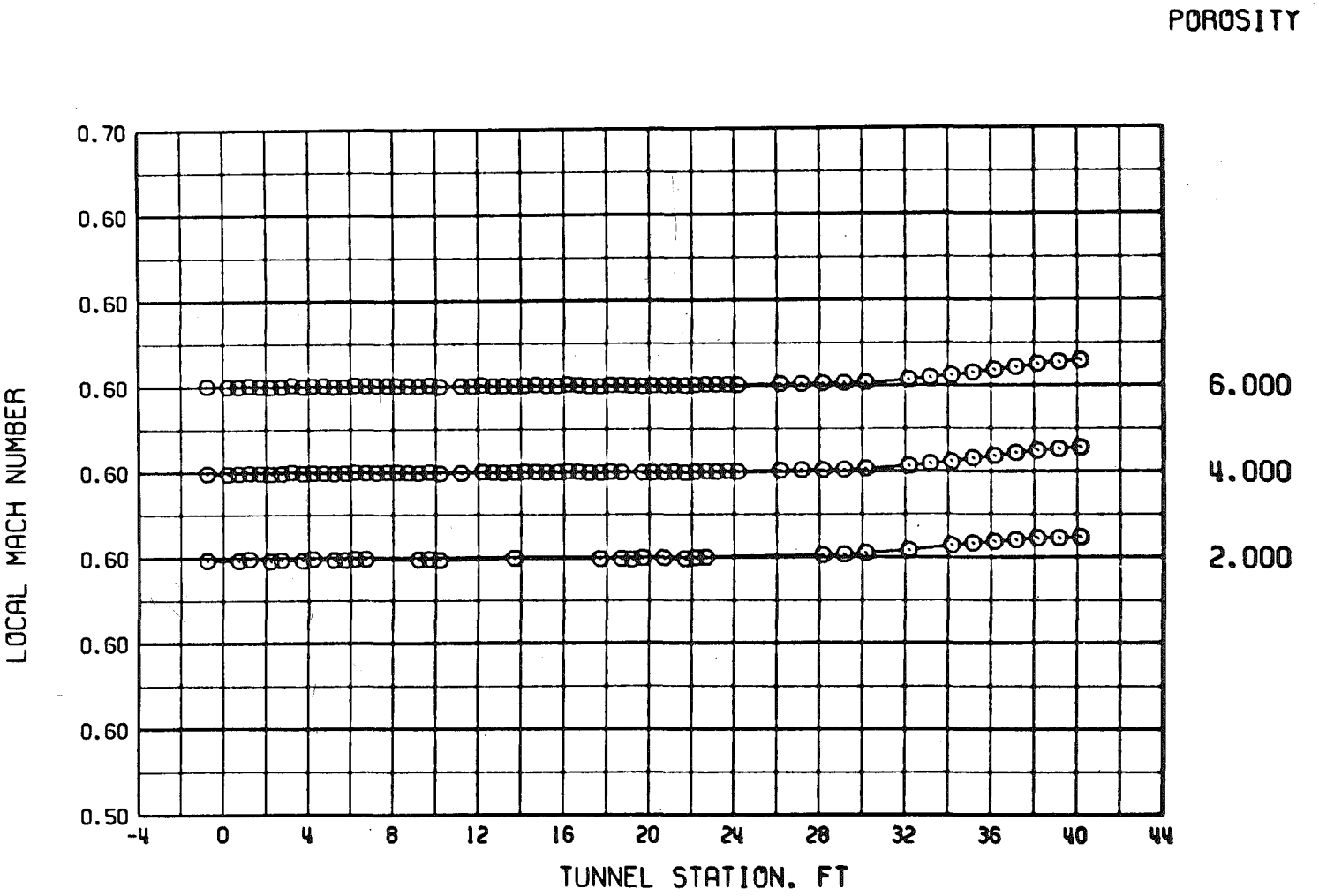

e. M = 0.6, θ_w = 0, and λ = 1.10

Figure 7. Continued.

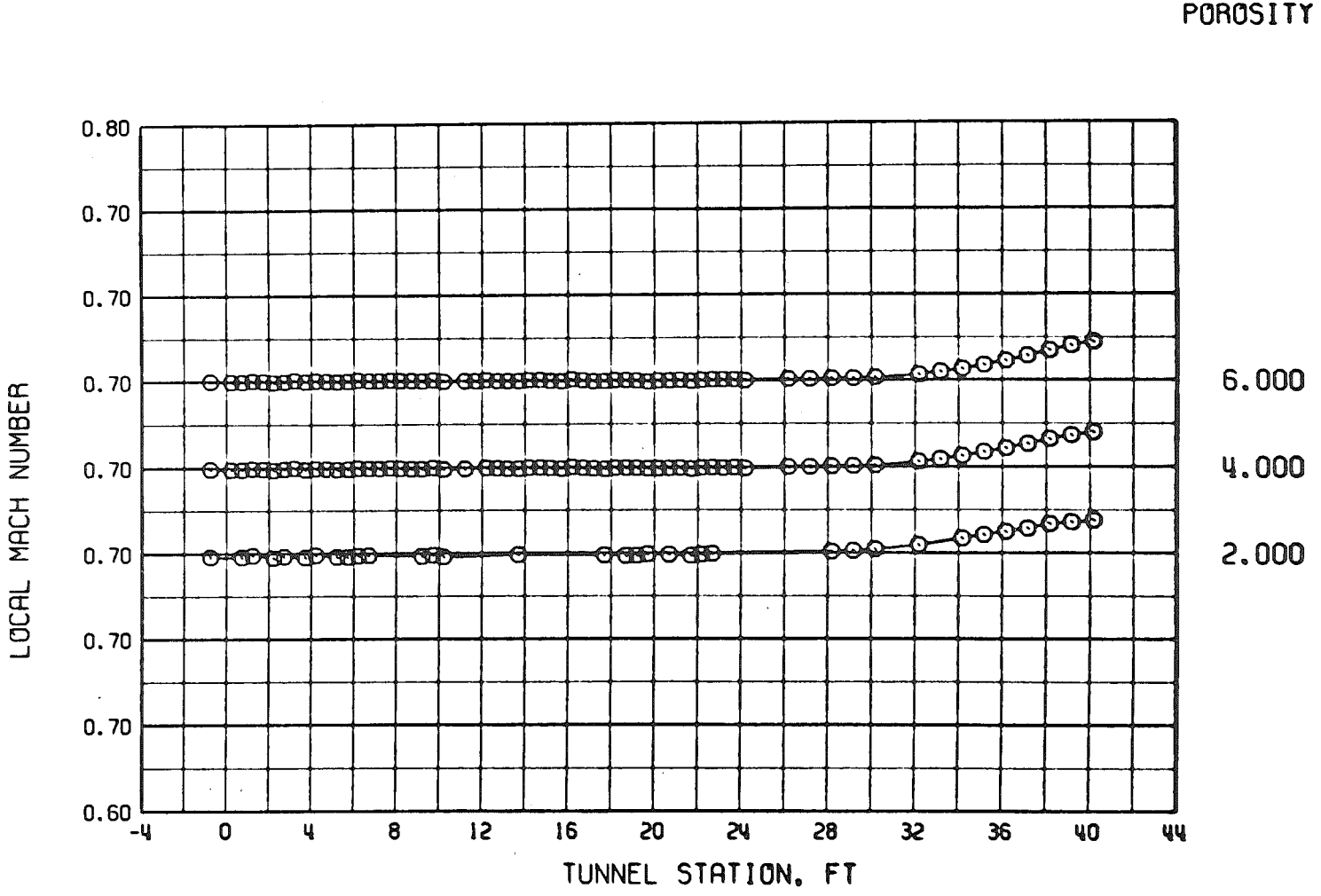

f. M = 0.7, θ_w = 0, and λ = 1.14

Figure 7. Continued.

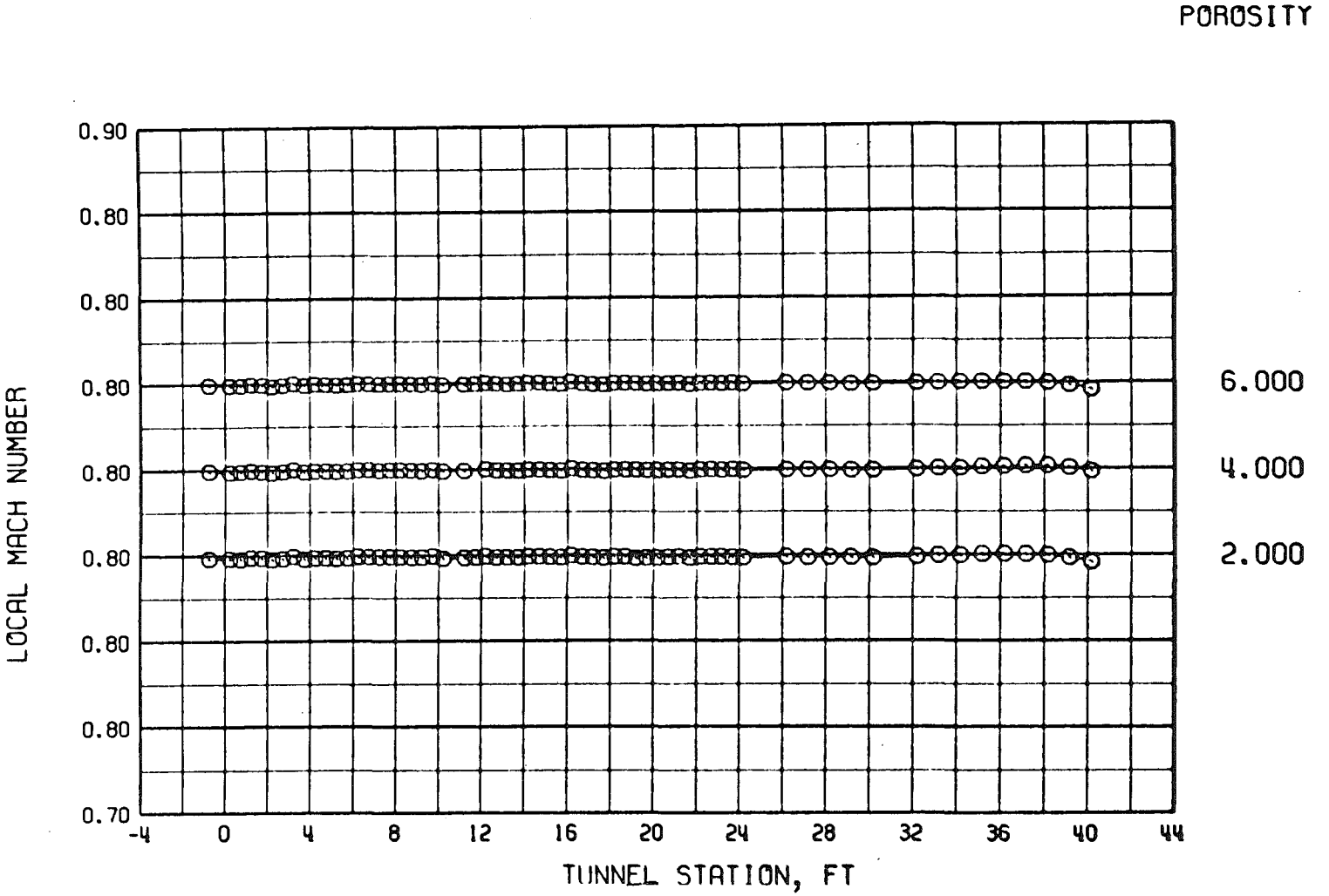

g. M = 0.8, θ_w = 0, and λ = 1.15

Figure 7. Continued.

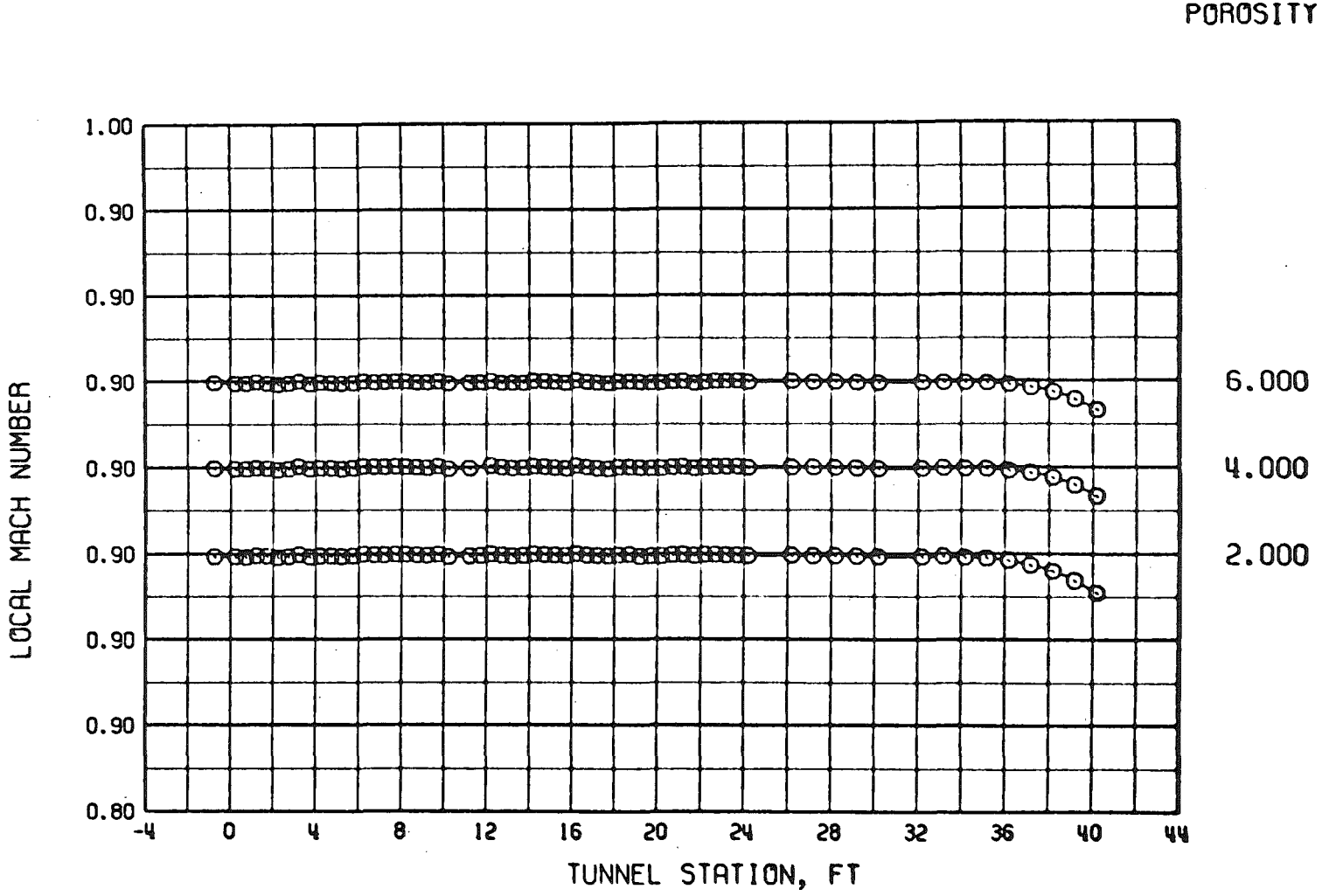

h. M = 0.9, θ_w = 0, and λ = 1.16

Figure 7. Continued.

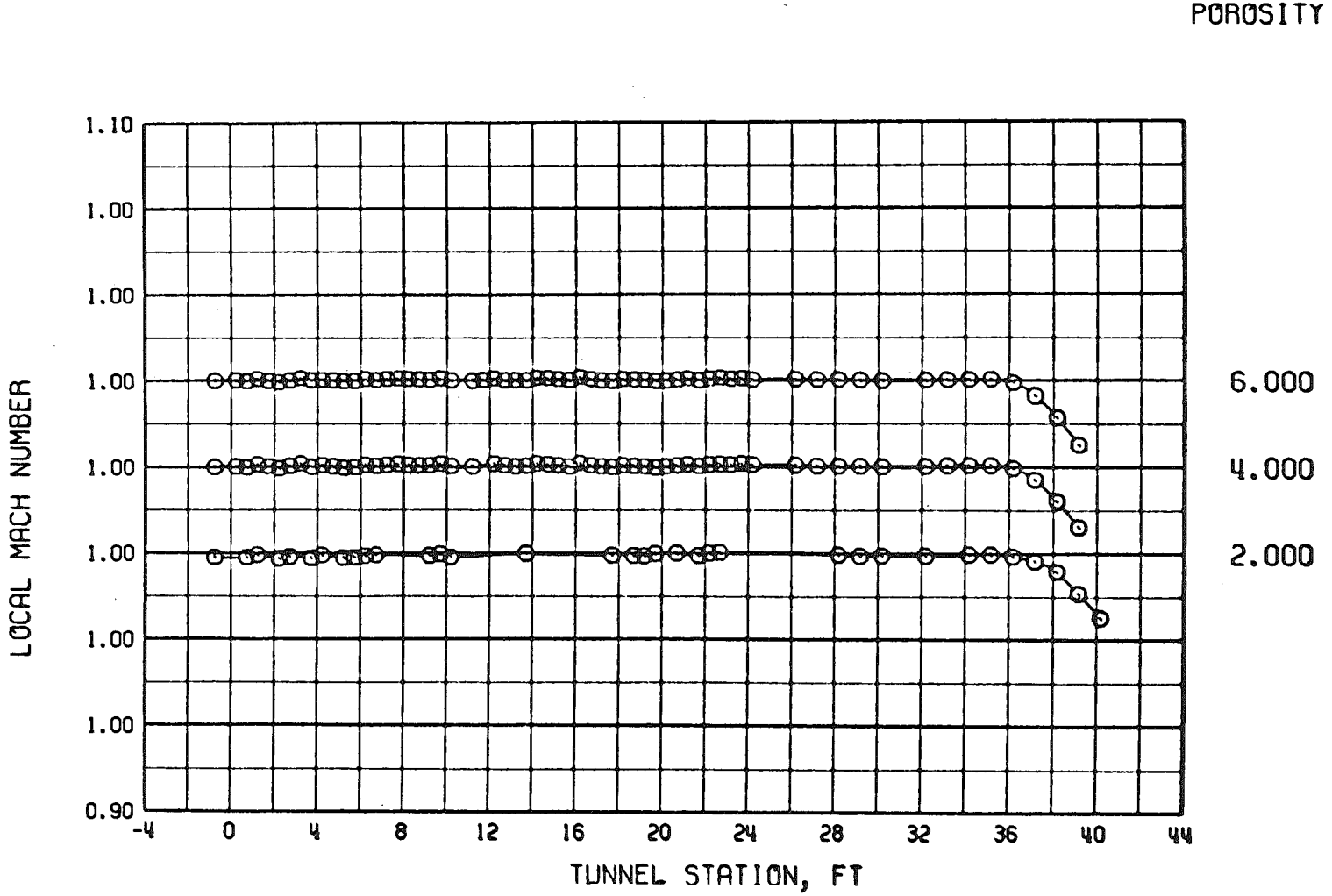

i. M = 1.0, θ_w = 0, and λ = 1.17

Figure 7. Continued.

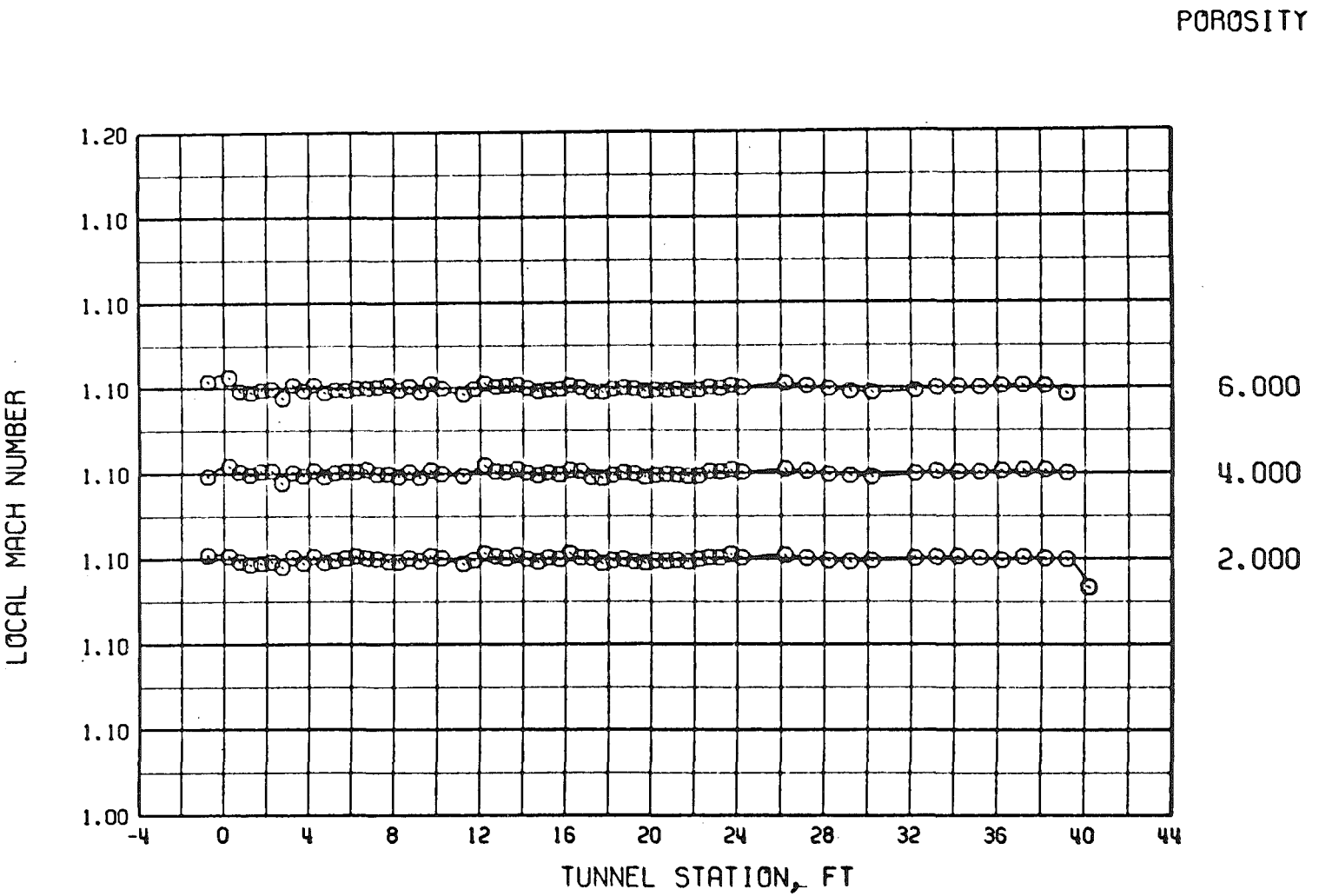

j. M = 1.1, θ_w = 0, and λ = 1.19

Figure 7. Continued.

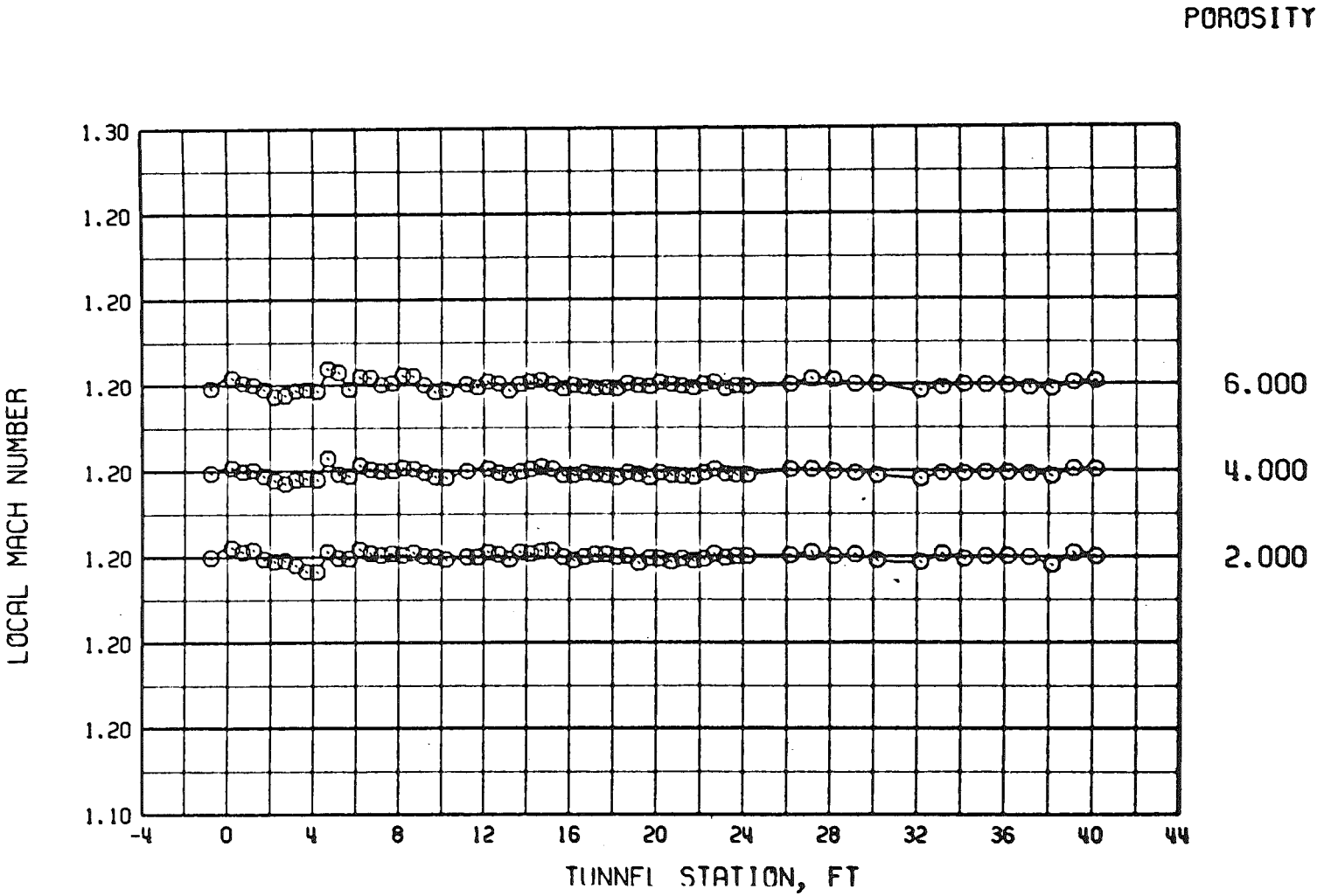

k. M = 1.2, θ_w = 0, and λ = 1.21

Figure 7. Continued.

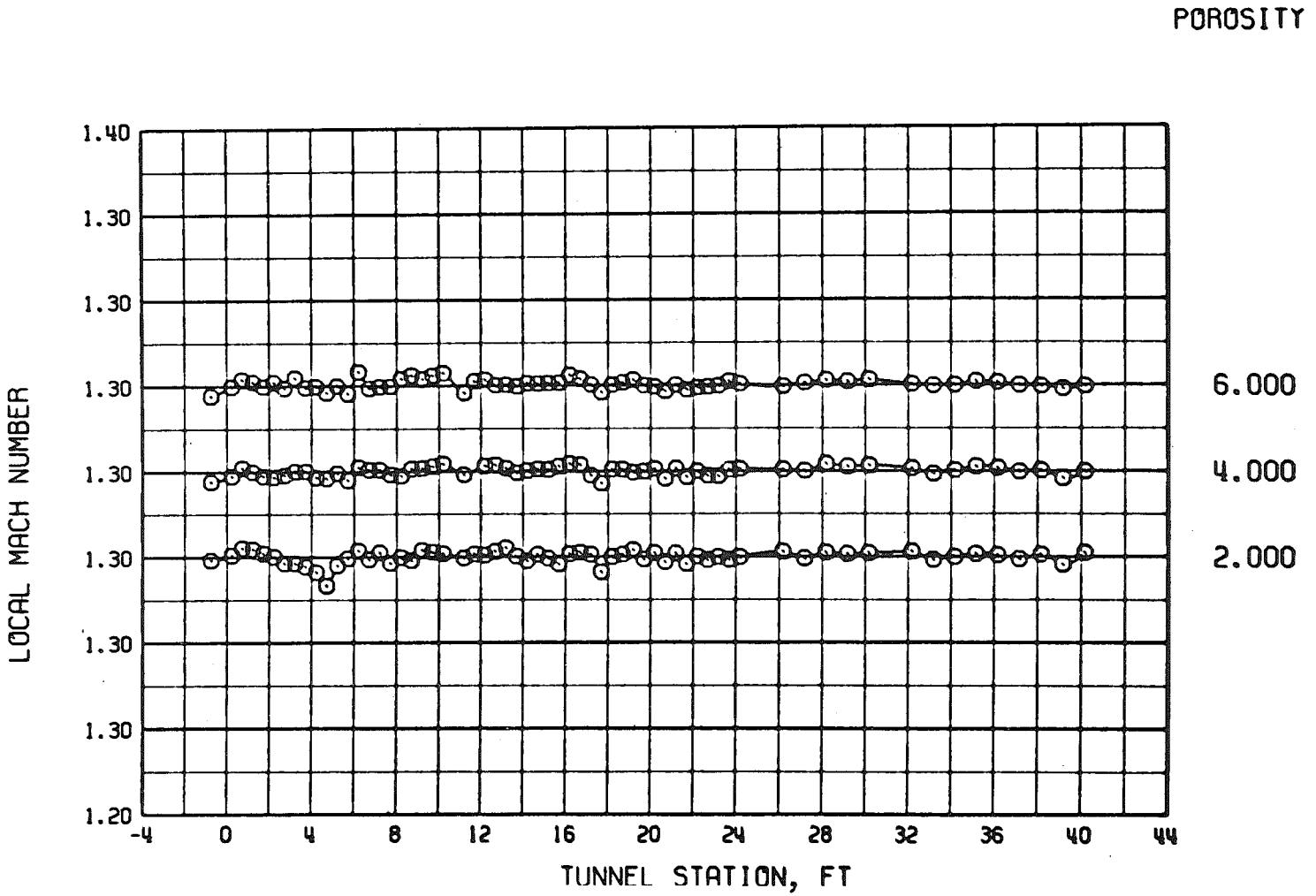

l. M = 1.3, θ_w = 0, and λ = 1.25

Figure 7. Continued.

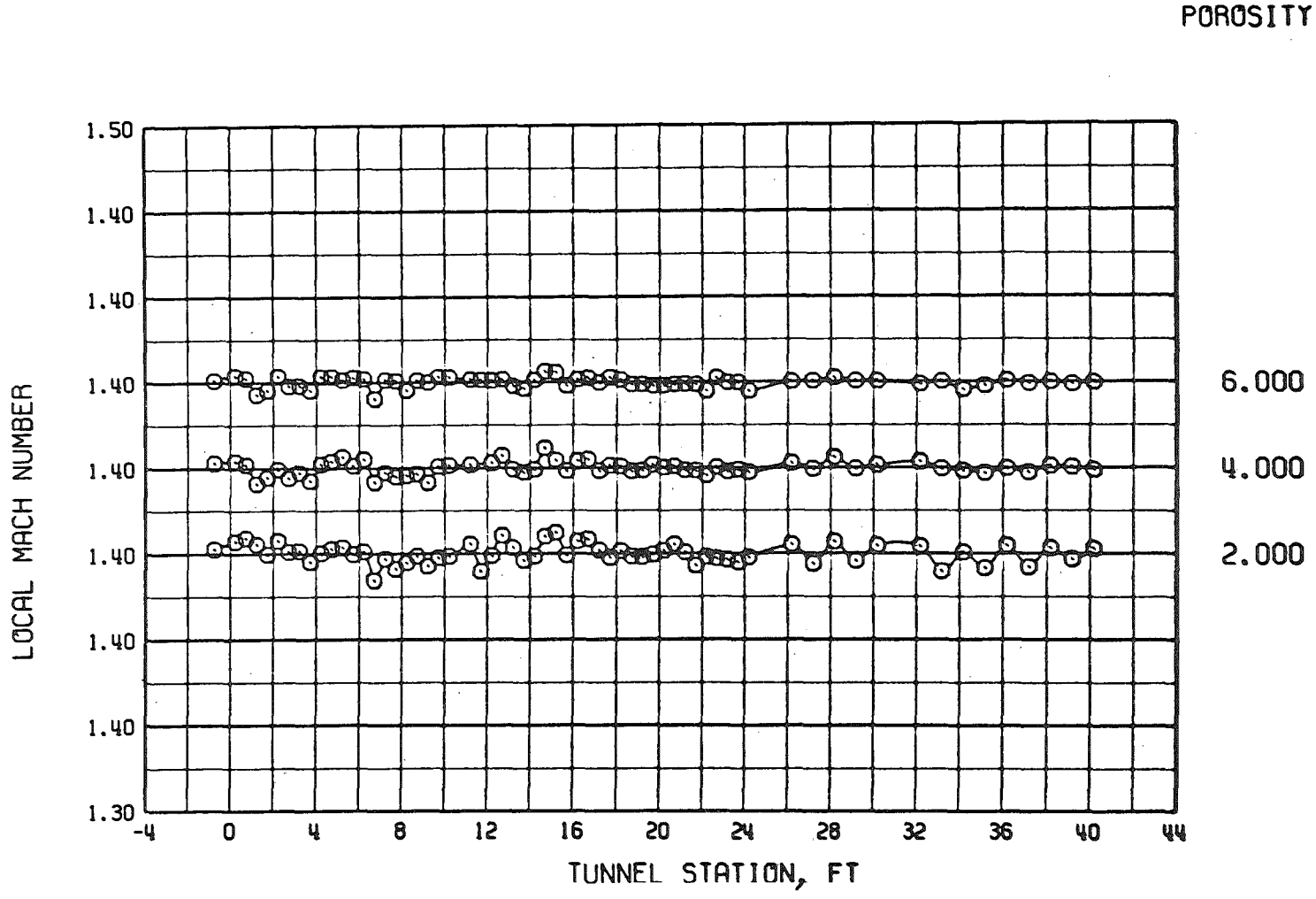

m. M = 1.4, θ_w = 0, and λ = 1.30

Figure 7. Continued.

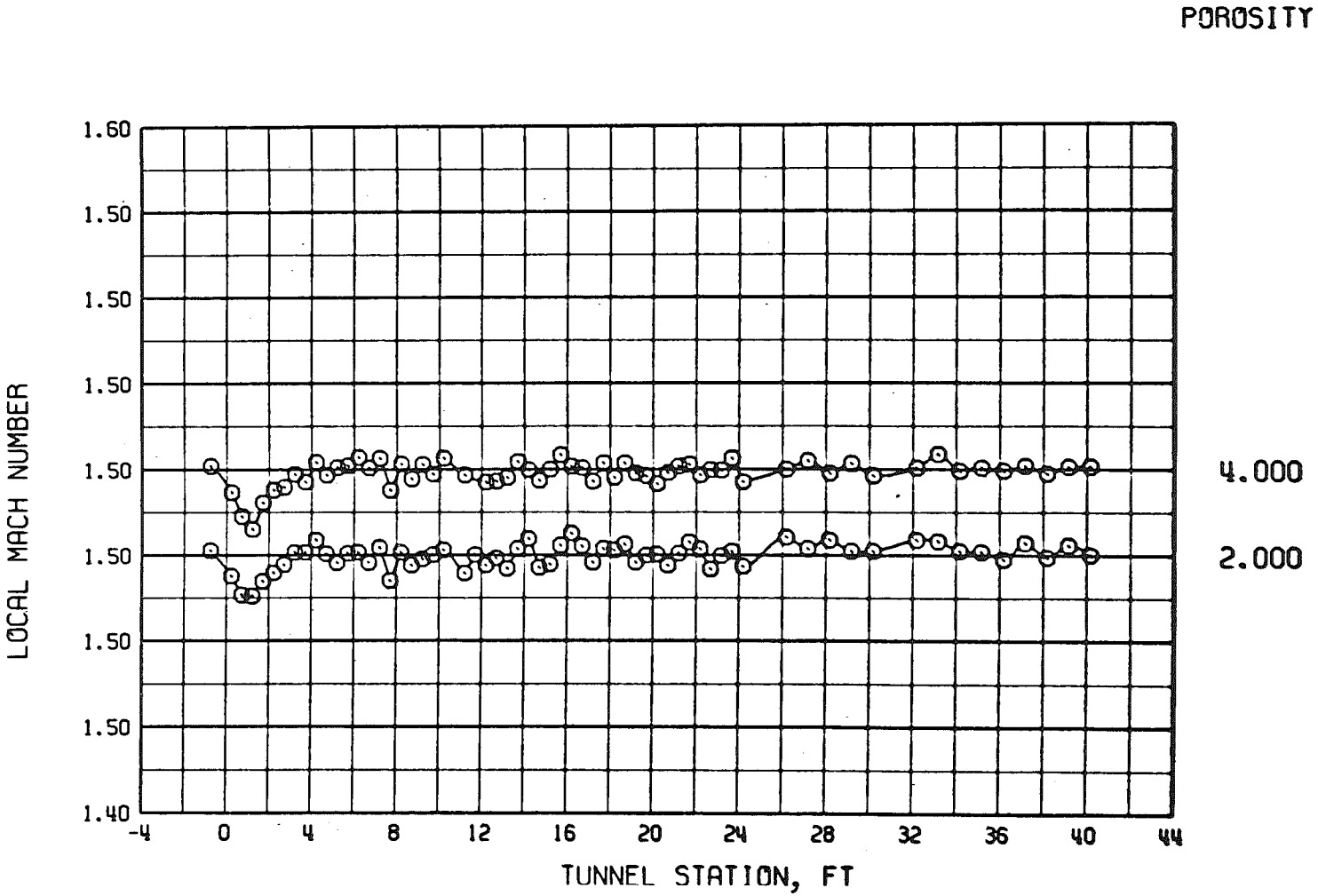

n. M = 1.5, θ_w = 0, and λ = 1.38

Figure 7. Continued.

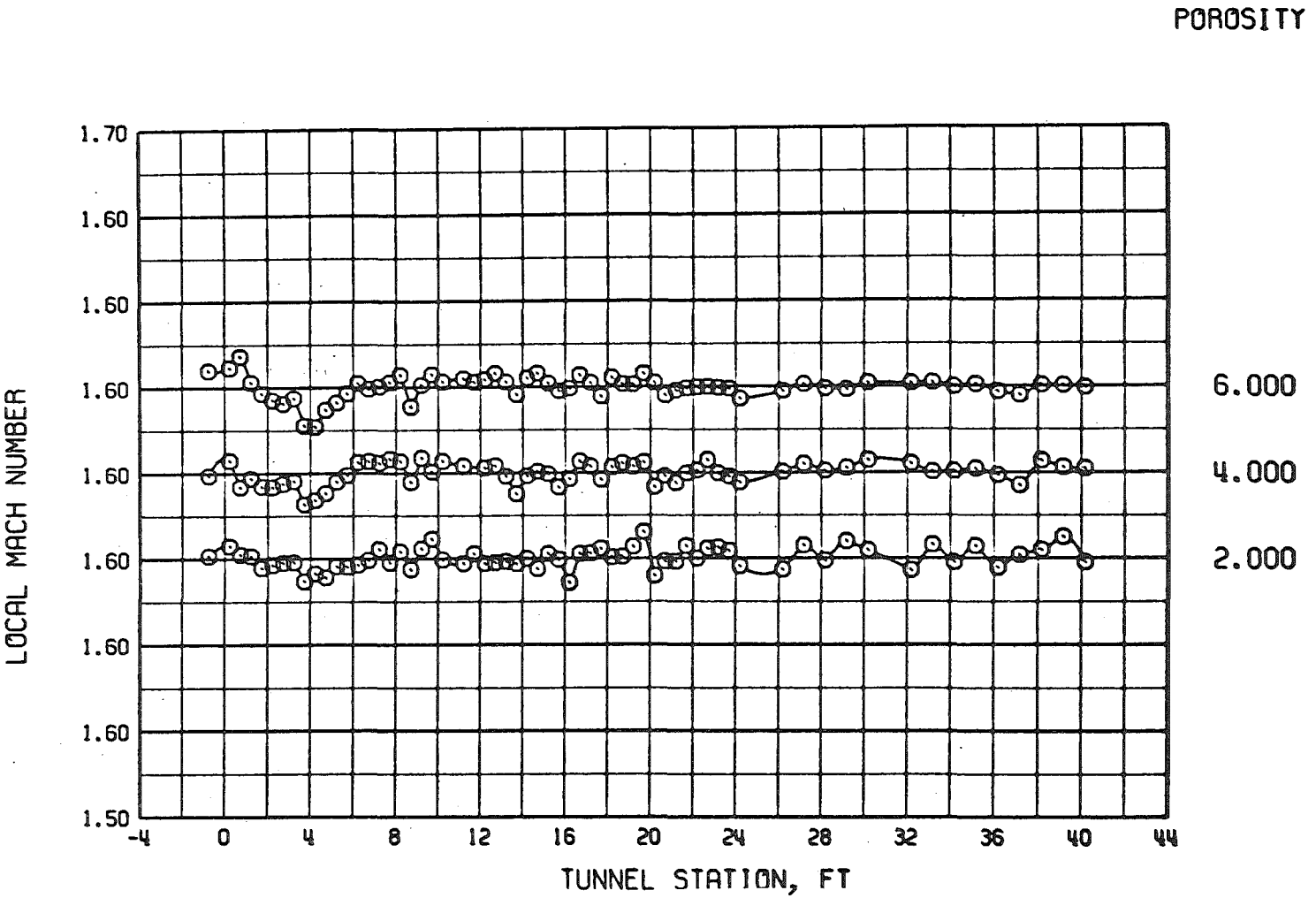

o. M = 1.6, θ_w = 0, and λ = 1.50

Figure 7. Concluded.

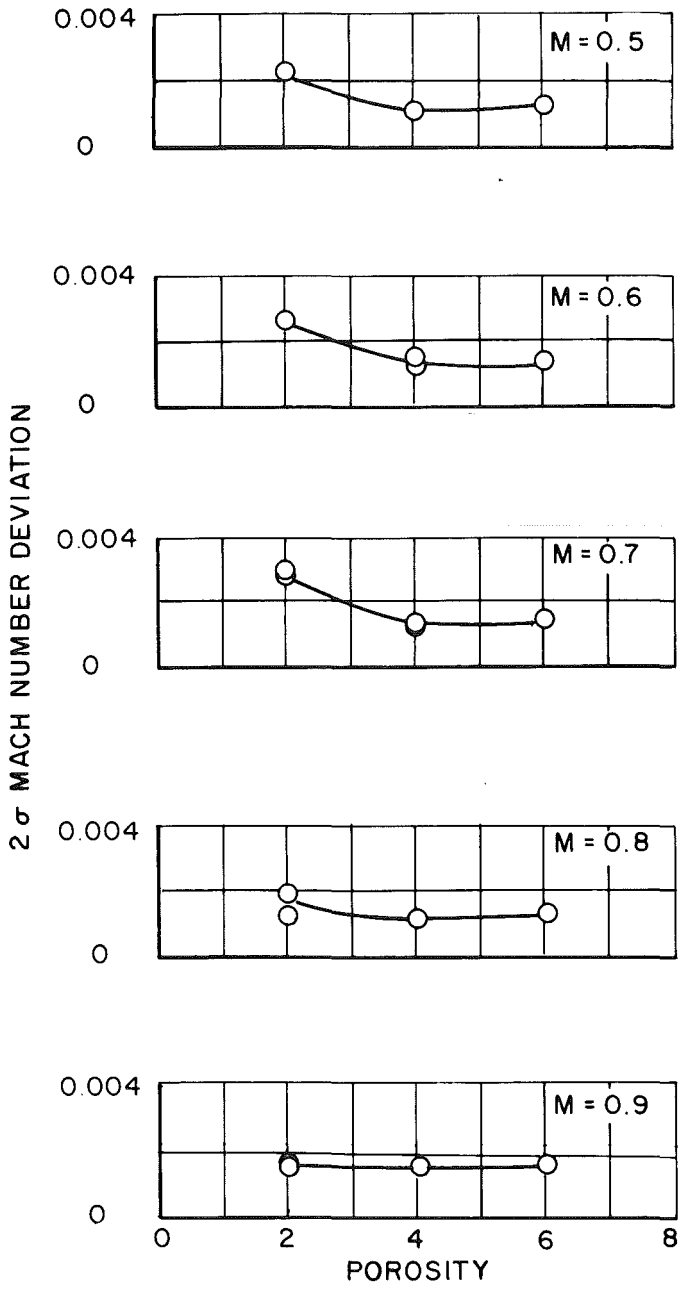

a. M = 0.5 to 0.9

Figure 8. Effect of test section wall porosity variation upon the 2σ Mach number deviation for tunnel station 8.2 to 28.2 at $\lambda = \lambda_N$ and $\theta_w = 0$.

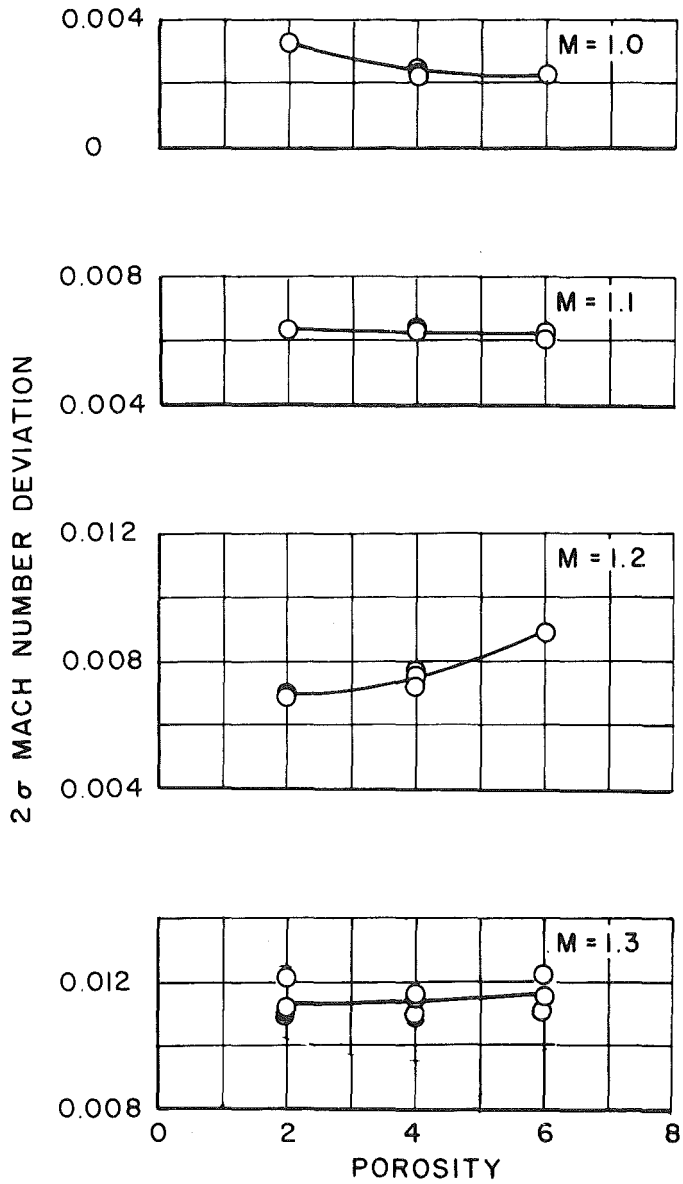

b. M = 1.0 to 1.3
Figure 8. Continued.

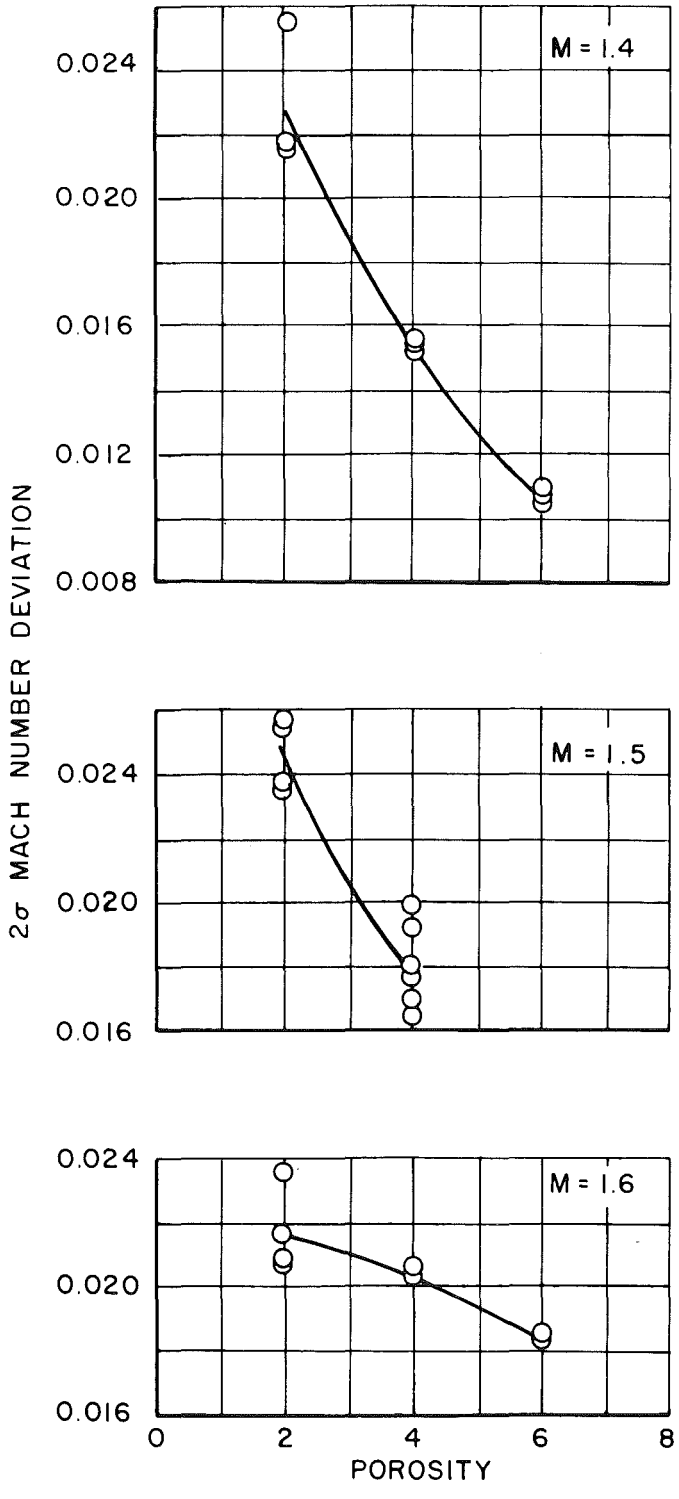

c. M = 1.4 to 1.6
Figure 8. Concluded.

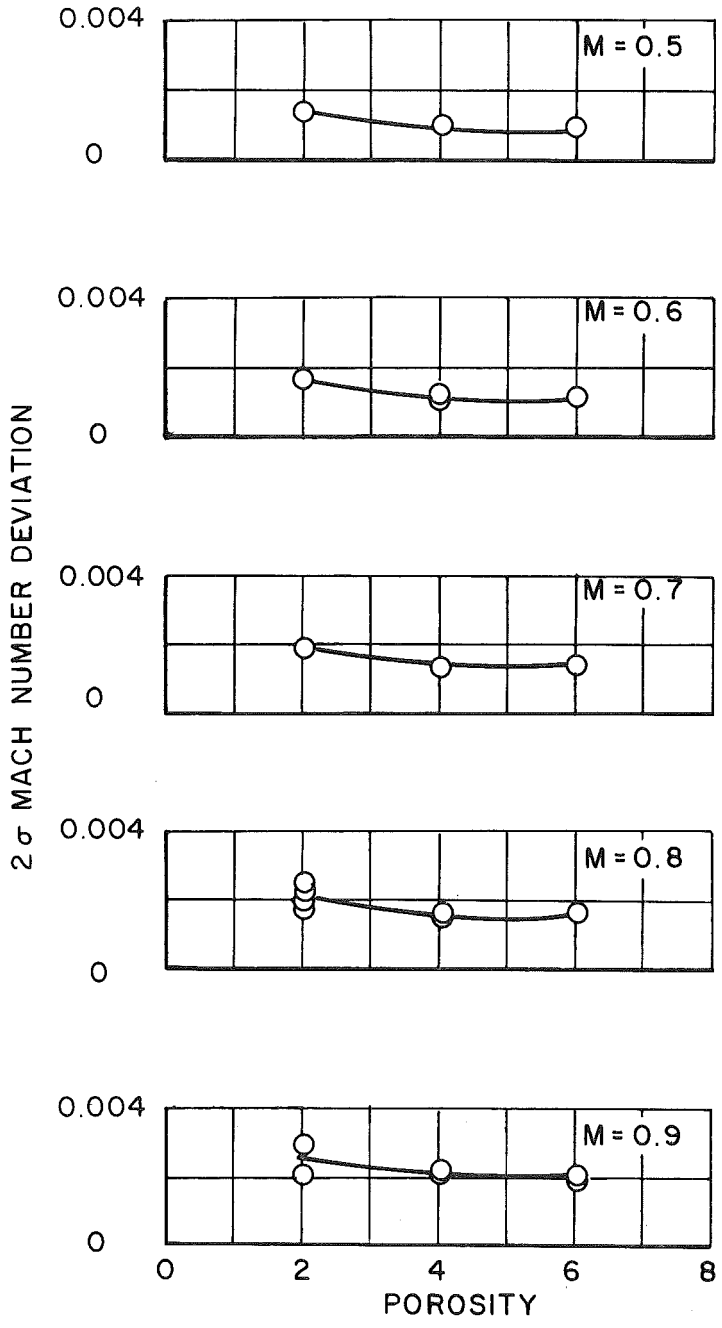

a. M = 0.5 to 0.9

Figure 9. Effect of test section wall porosity variation upon the 2σ Mach number deviations for tunnel station 1.2 to 20.2 at $\lambda = \lambda_N$ and $\theta_w = 0$.

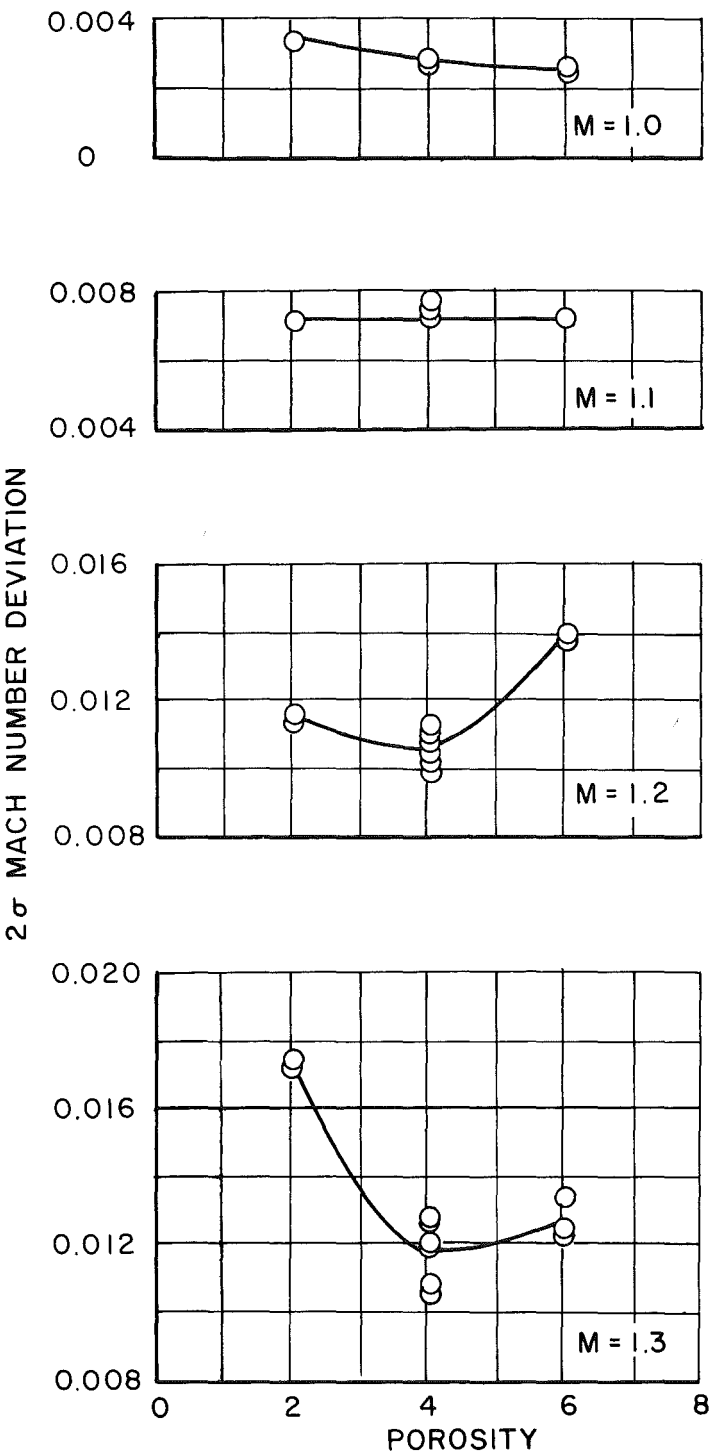

b. M = 1.0 to 1.3
Figure 9. Continued.

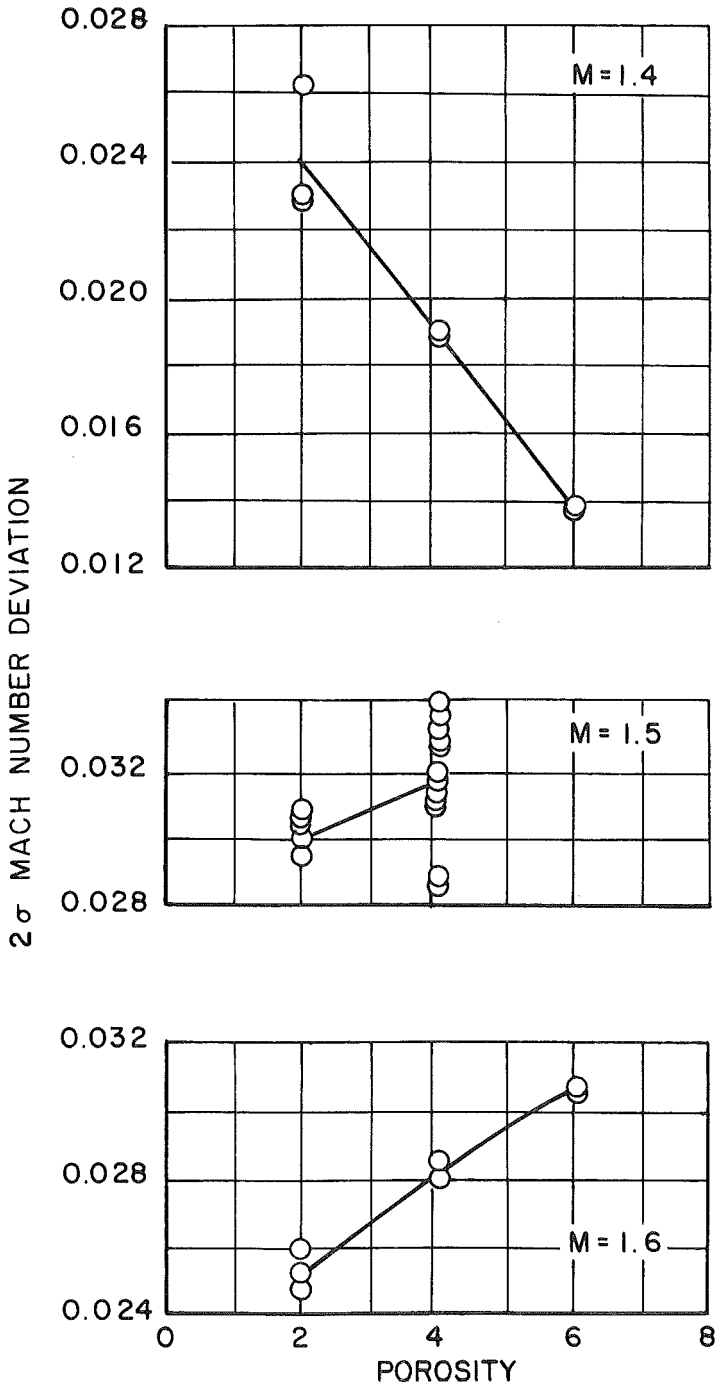

c. M = 1.4 to 1.6

Figure 9. Concluded.

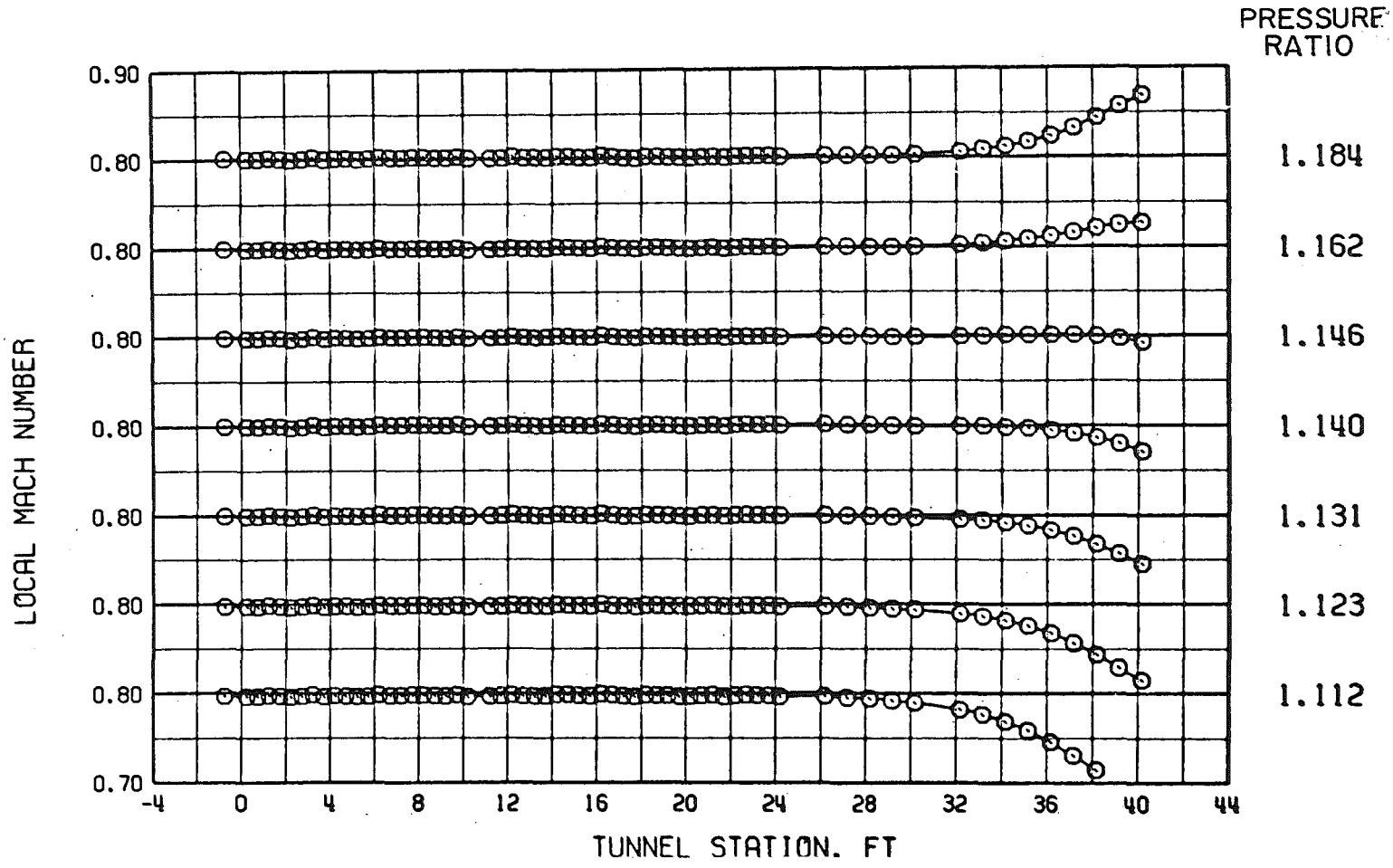

a. M = 0.8, θ_w = 0, and τ = 6

Figure 10. Tunnel 16T centerline Mach number distributions for various tunnel pressure ratios with six-percent porosity walls and θ_w = 0.

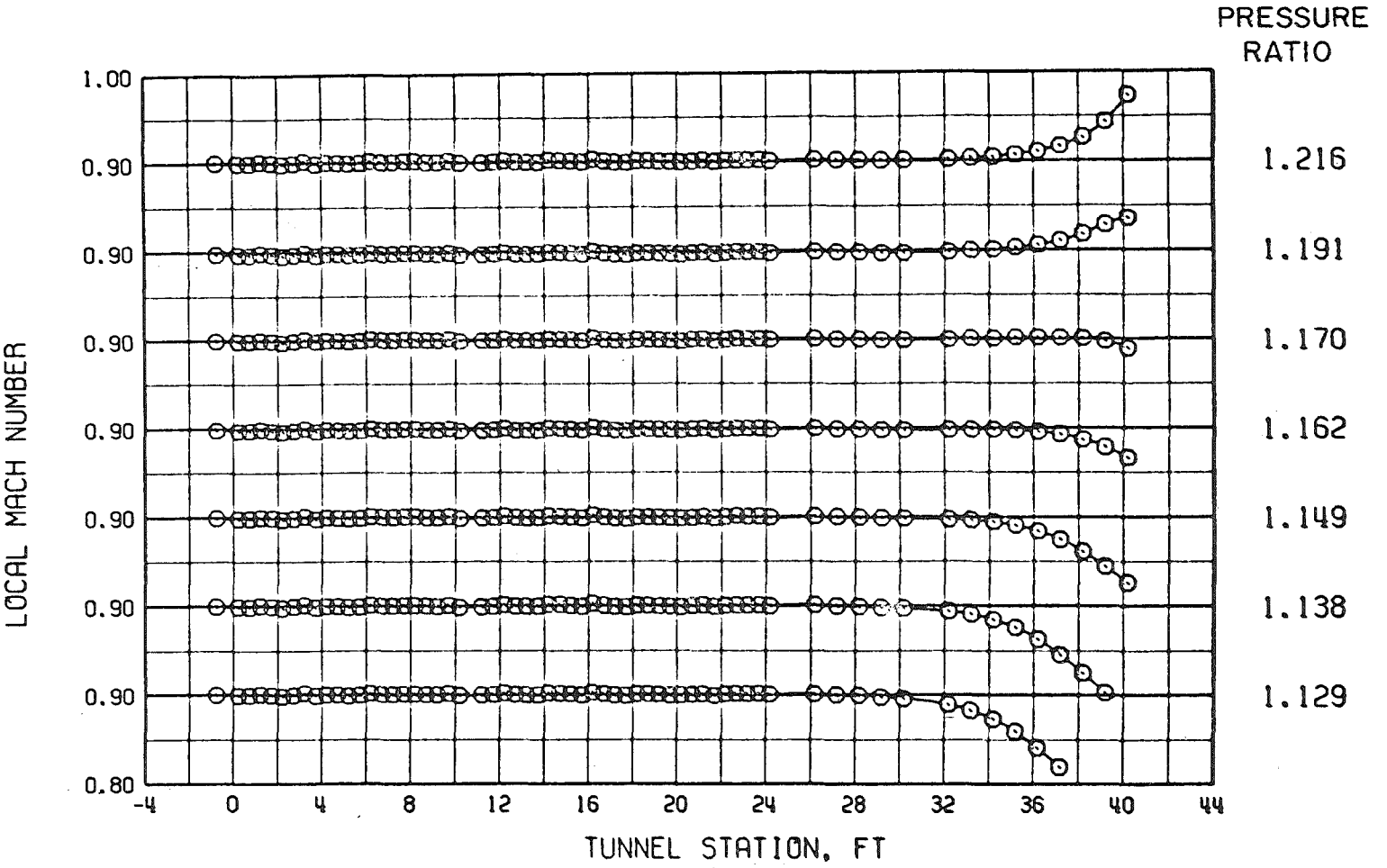

b. M = 0.9, θ_w = 0, and τ = 6

Figure 10. Continued.

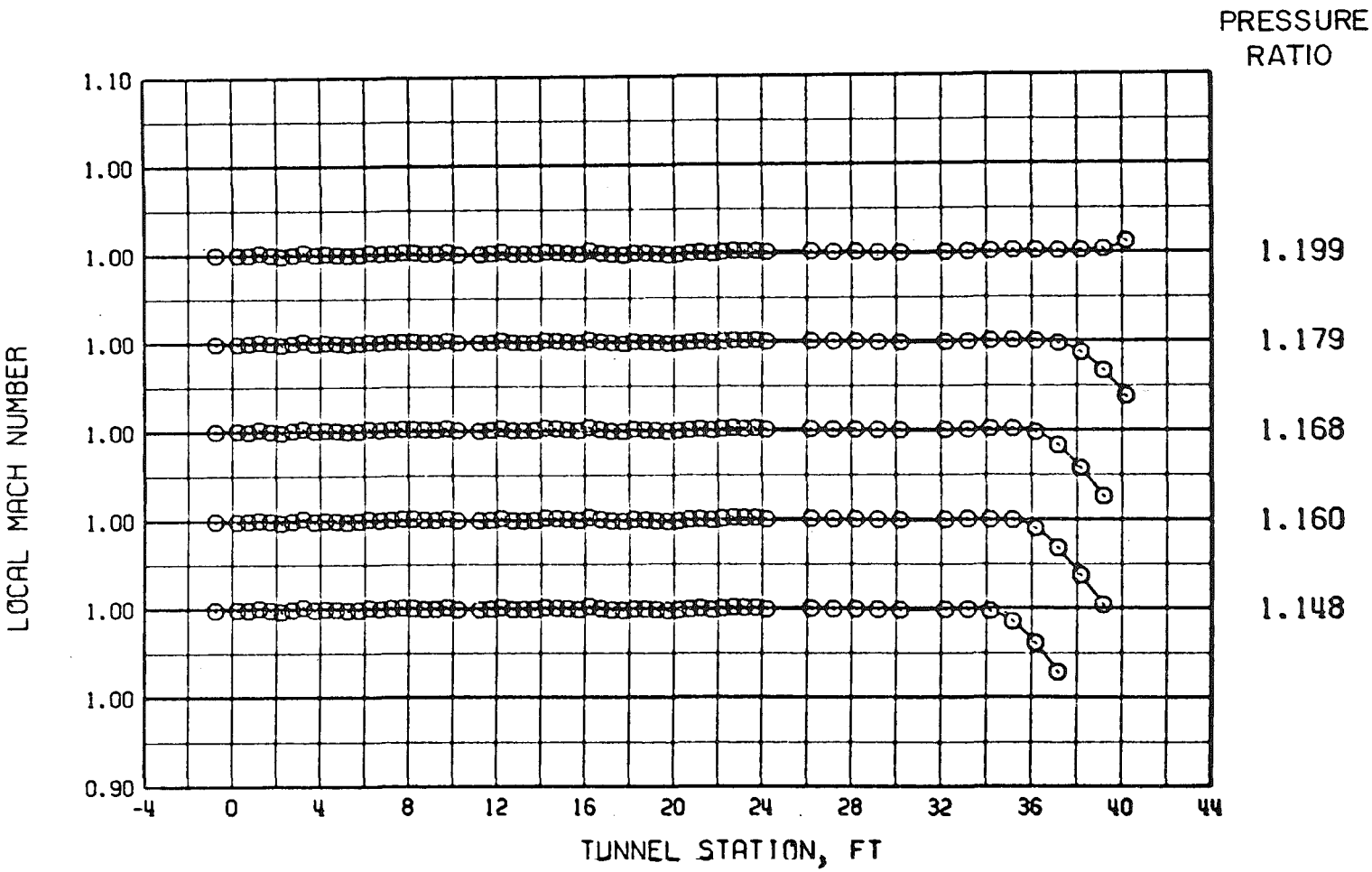

c. M = 1.0, θ_w = 0, and τ = 6
Figure 10. Continued.

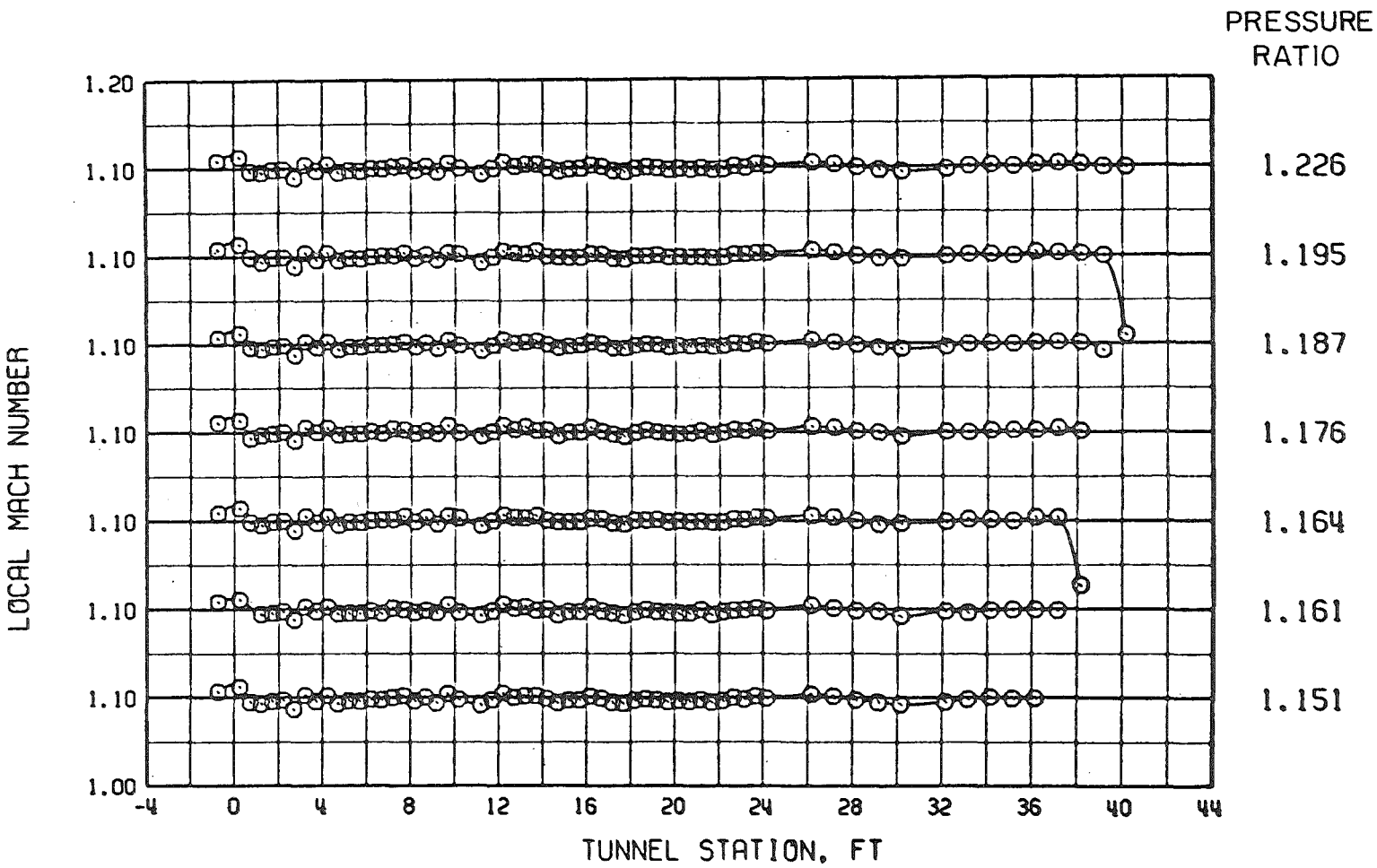

d. M = 1.1, θ_w = 0, and τ = 6

Figure 10. Continued.

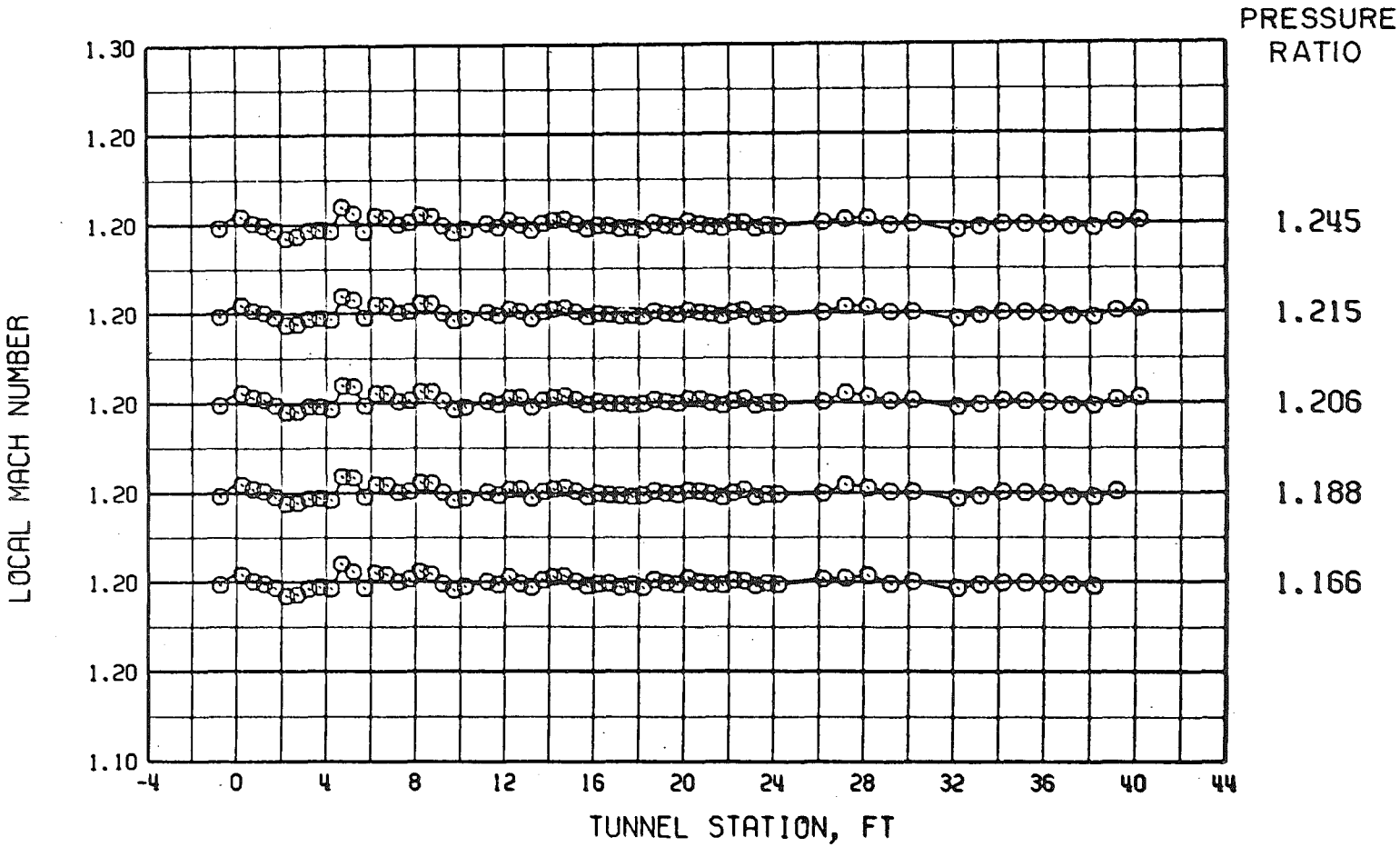

e. M = 1.2, θ_w = 0, and τ = 6

Figure 10. Continued.

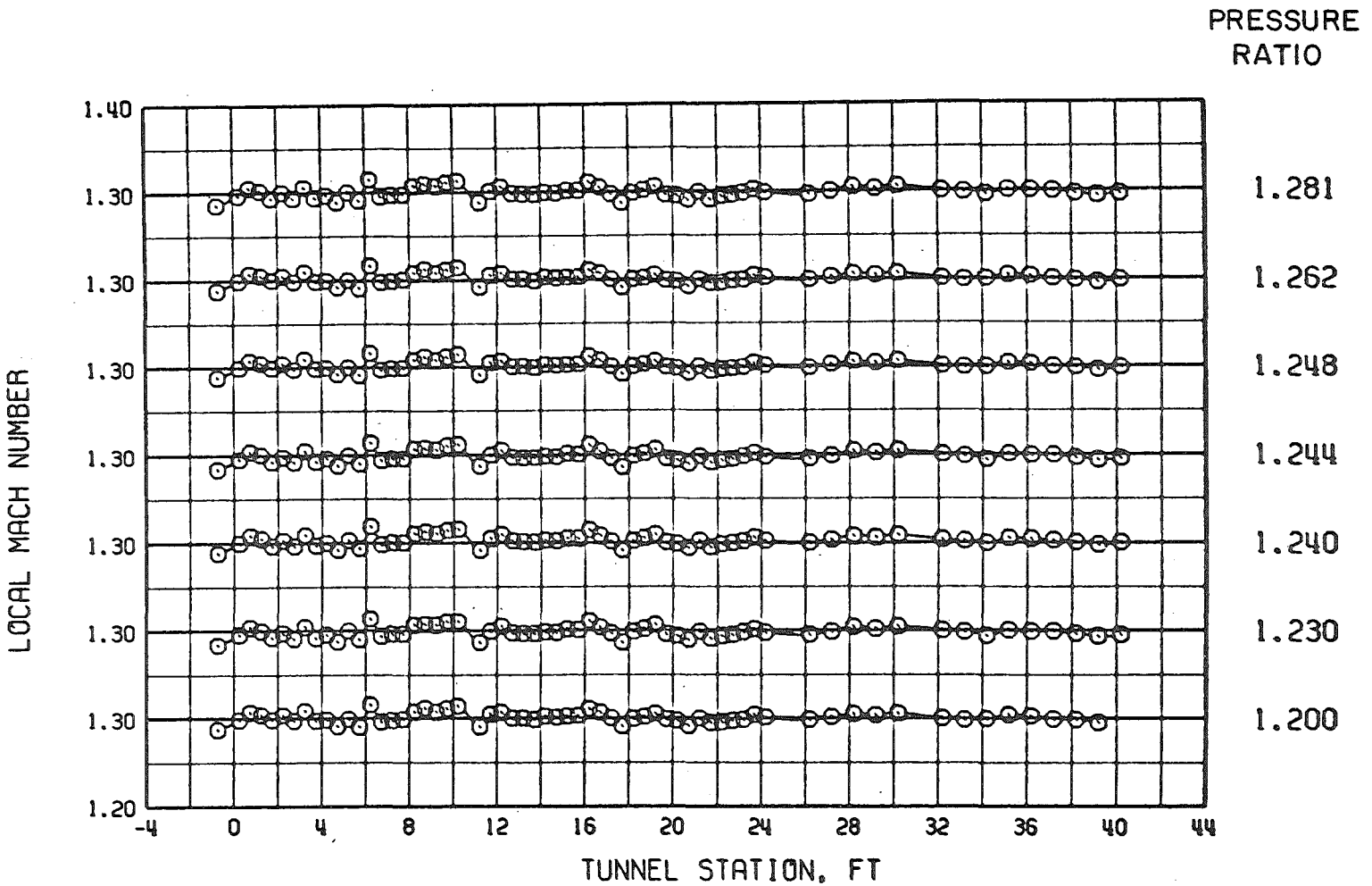

f. M = 1.3, θ_w = 0, and τ = 6

Figure 10. Continued.

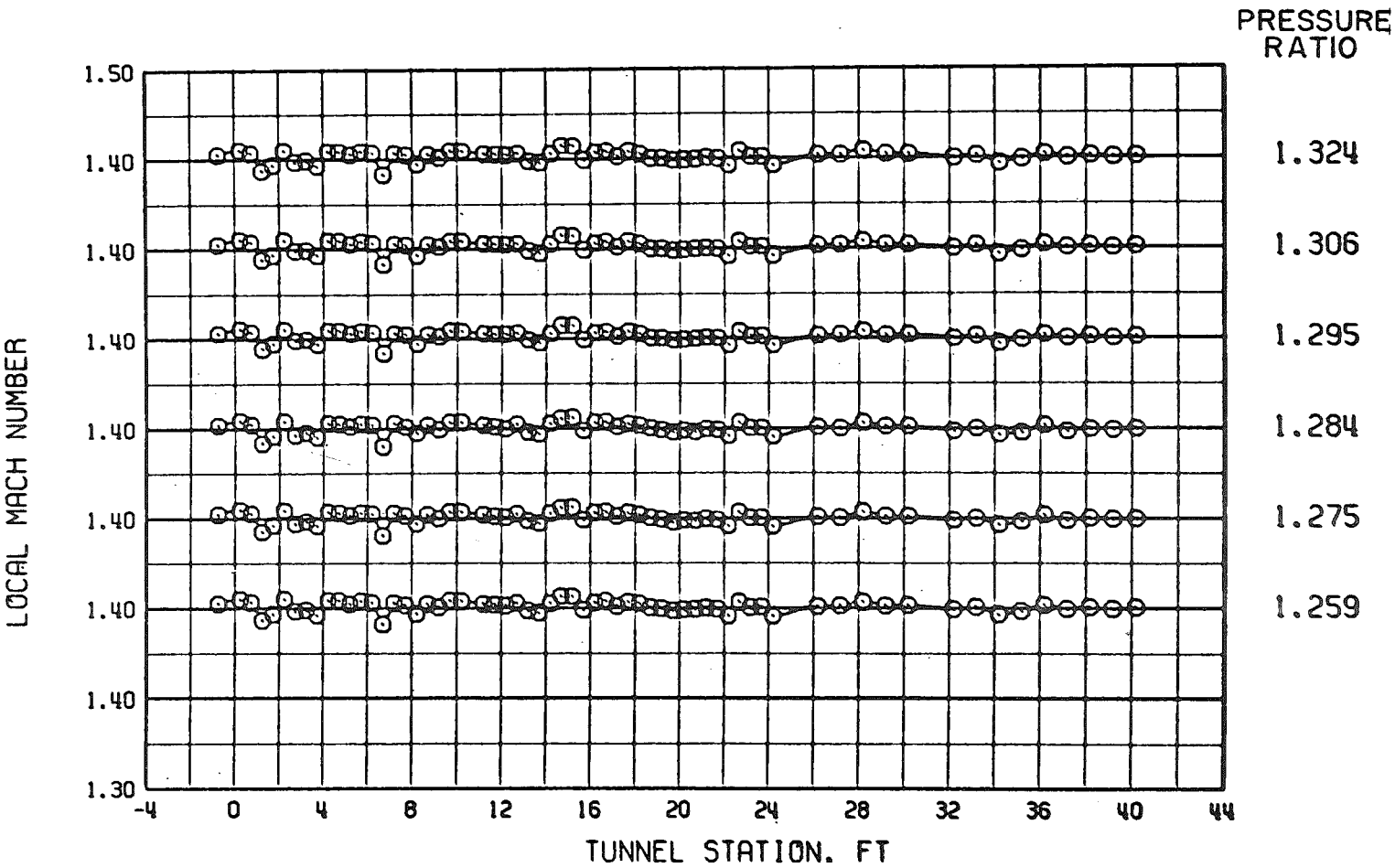

g. M = 1.4, θ_w = 0, and τ = 6

Figure 10. Continued.

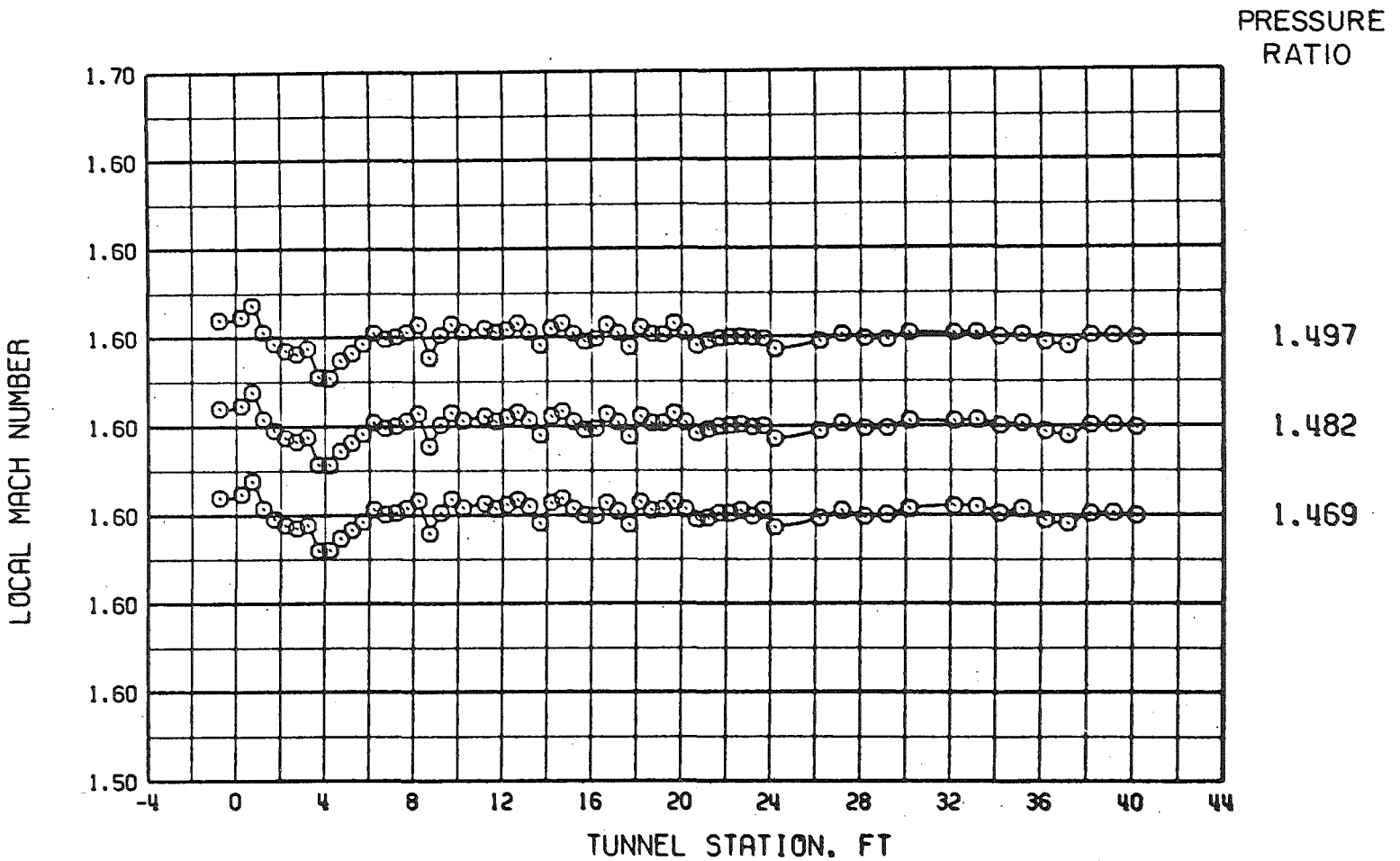

h. M = 1.6, θ_w = 0, and τ = 6

Figure 10. Concluded.

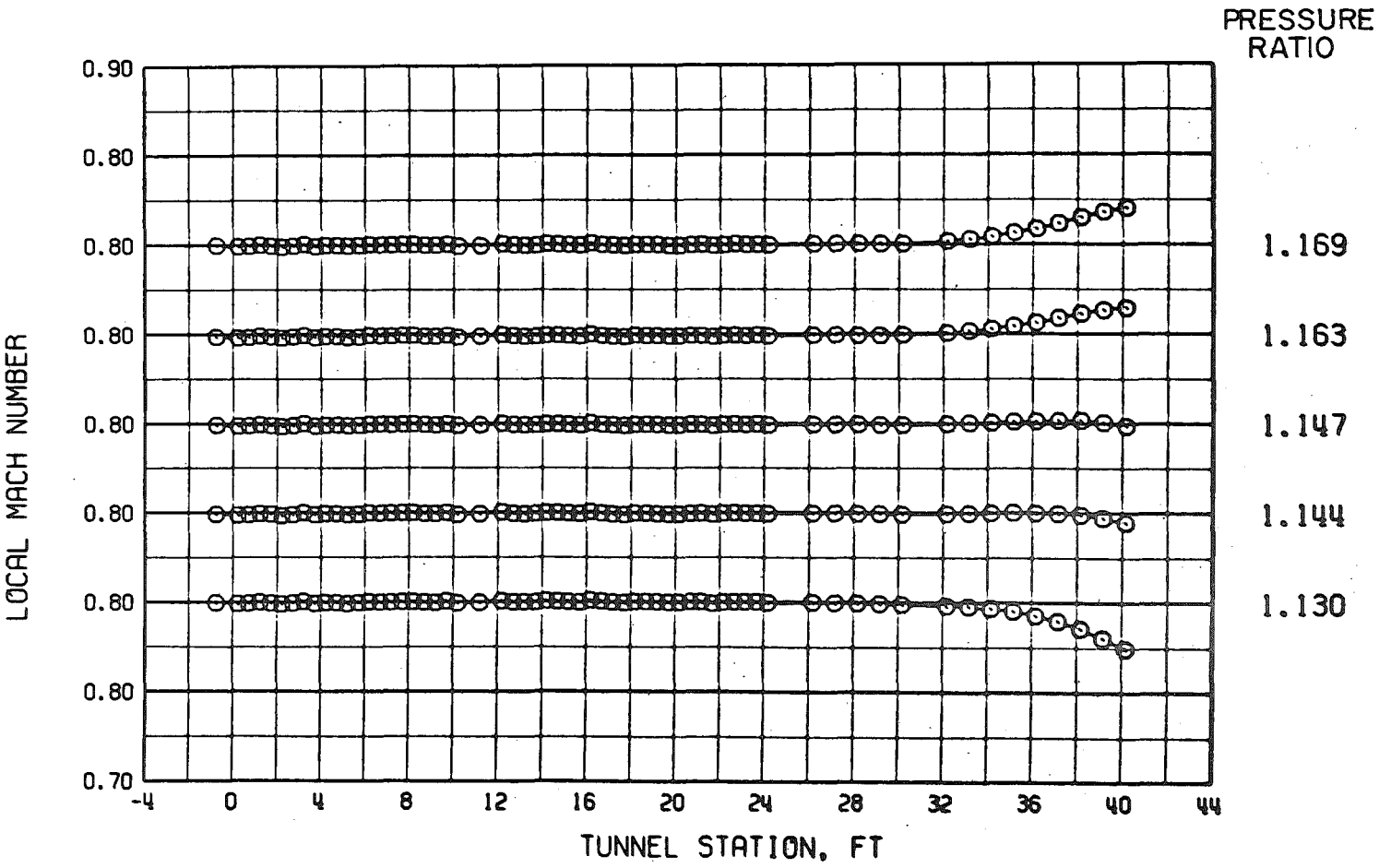

a. M = 0.8, θ_w = 0, and τ = 4

Figure 11. Tunnel 16T centerline Mach number distributions for various tunnel pressure ratios with four-percent porosity walls and θ_w = 0.

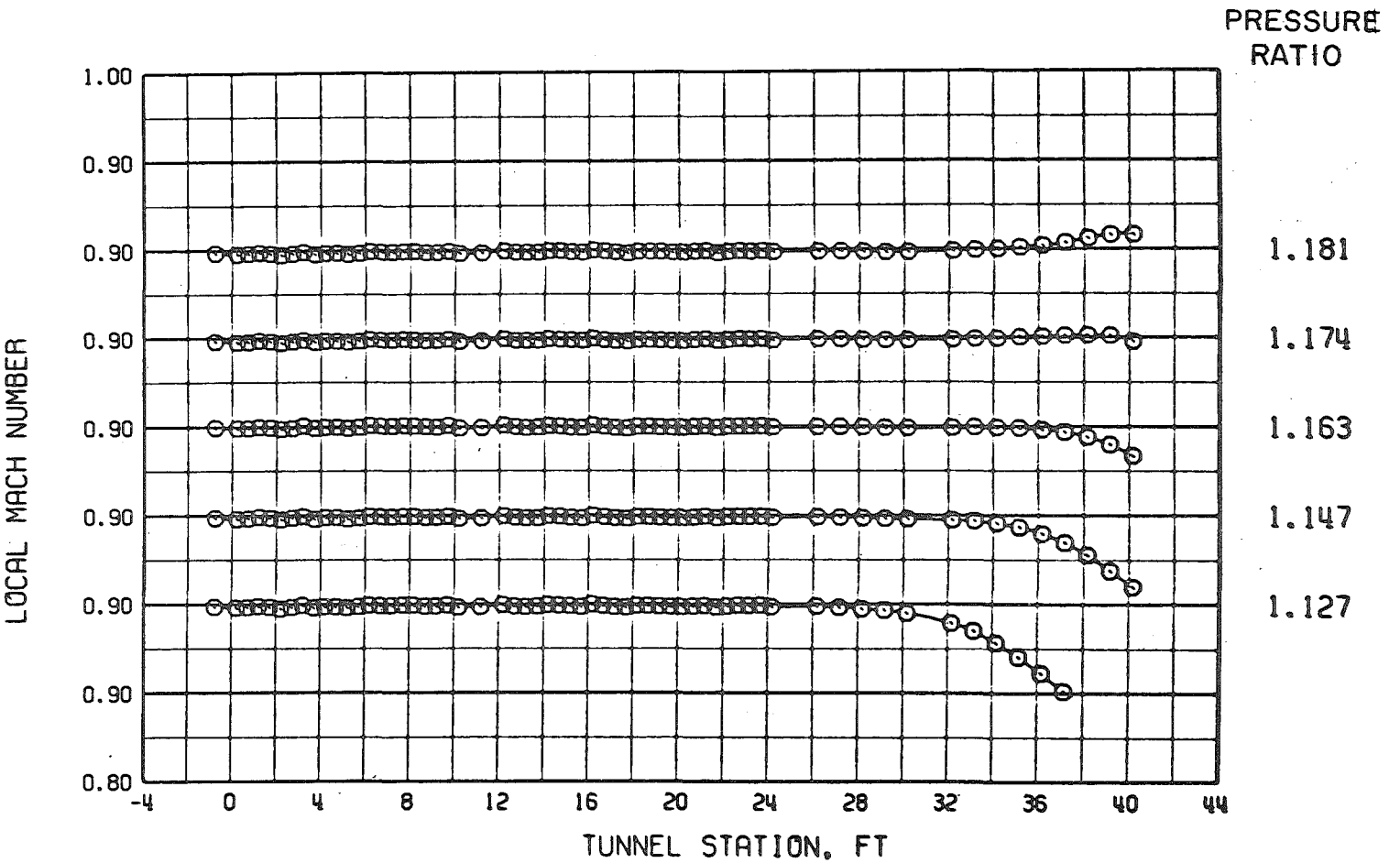

b. M = 0.9, θ_w = 0, and τ = 4

Figure 11. Continued.

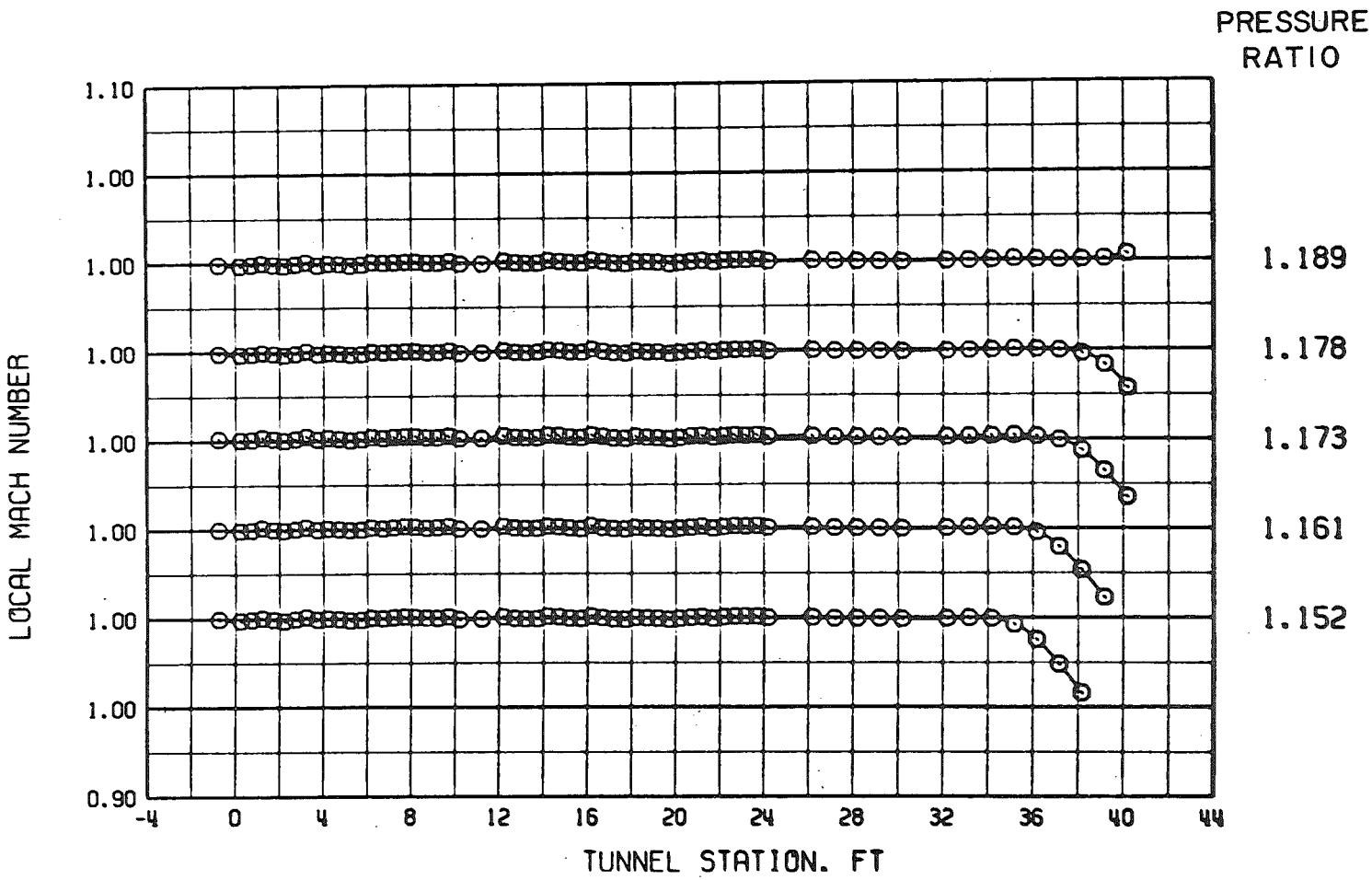

c. M = 1.0, θ_w = 0, and τ = 4
Figure 11. Continued.

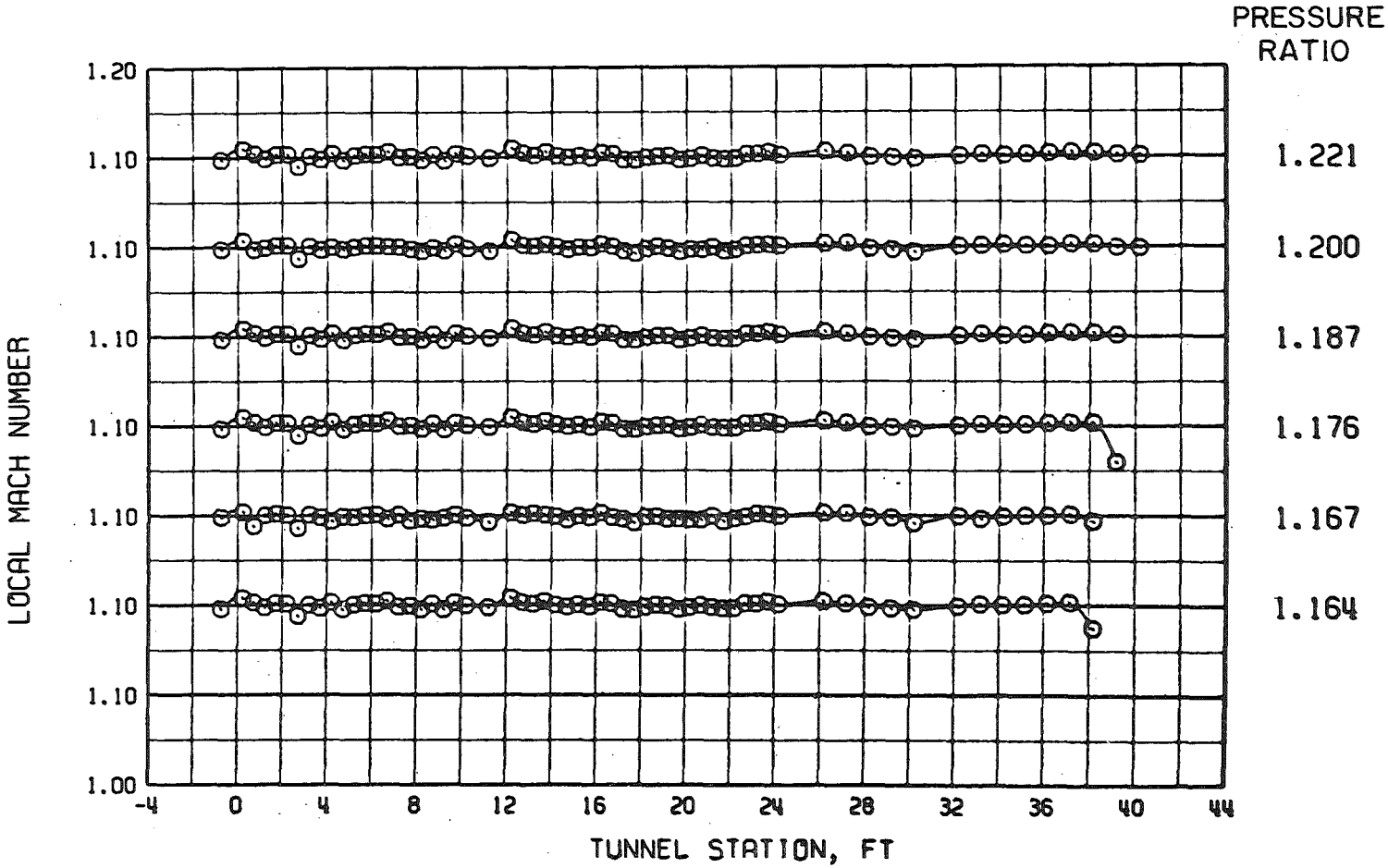

d. M = 1.1, θ_w = 0, and τ = 4

Figure 11. Continued.

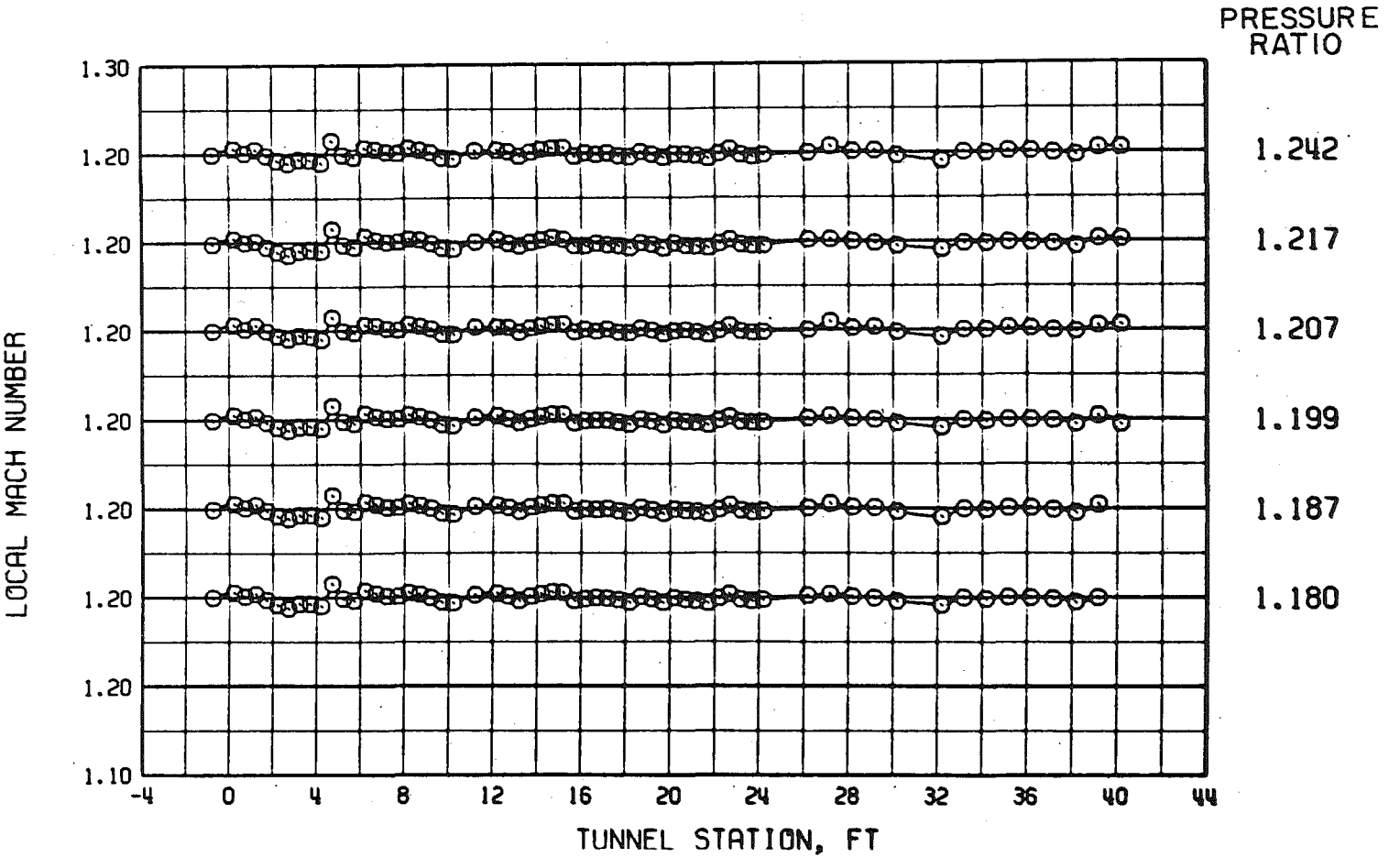

e. M = 1.2, θ_w = 0, and τ = 4

Figure 11. Continued.

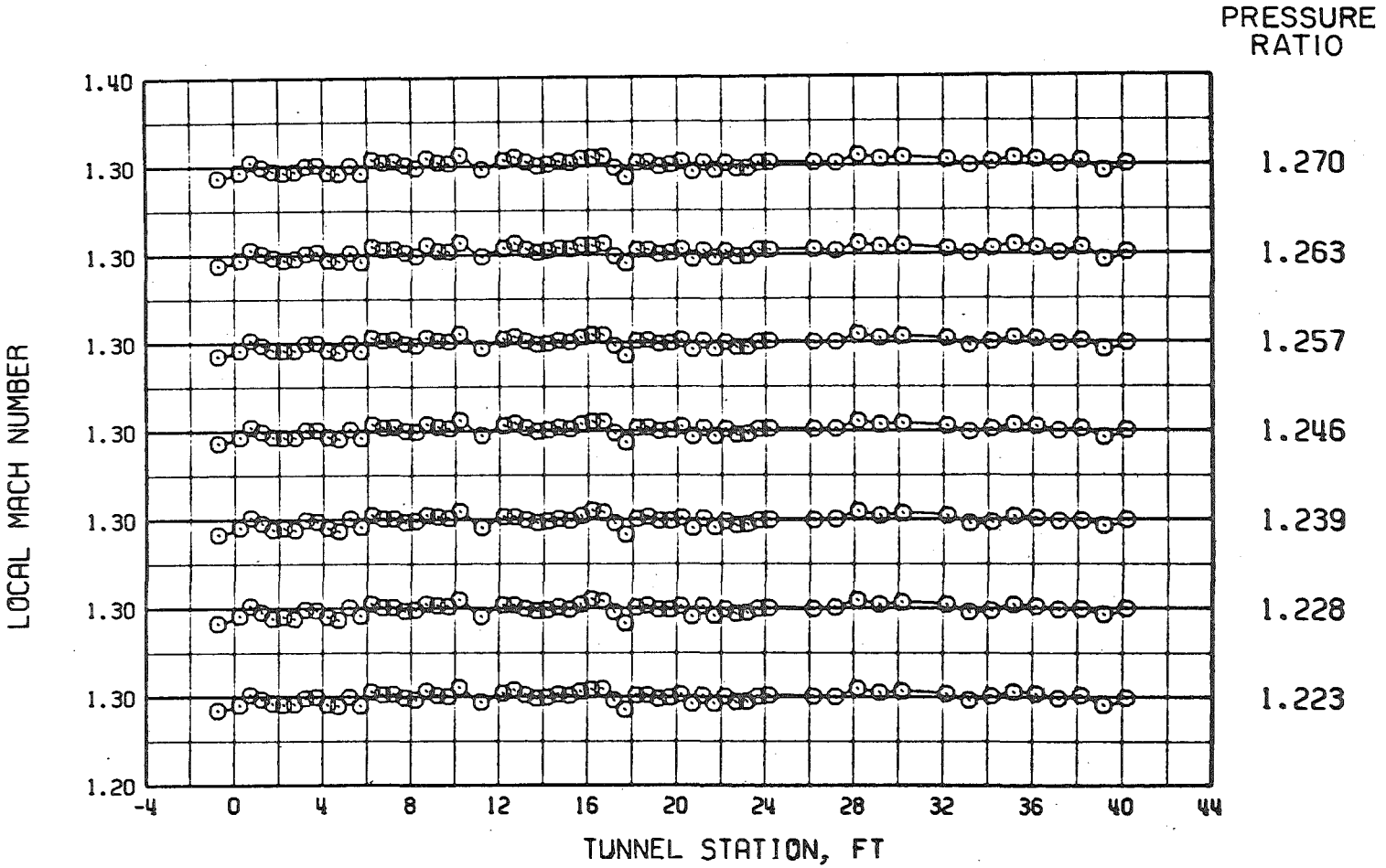

f. M = 1.3, θ_w = 0, and τ = 4

Figure 11. Continued.

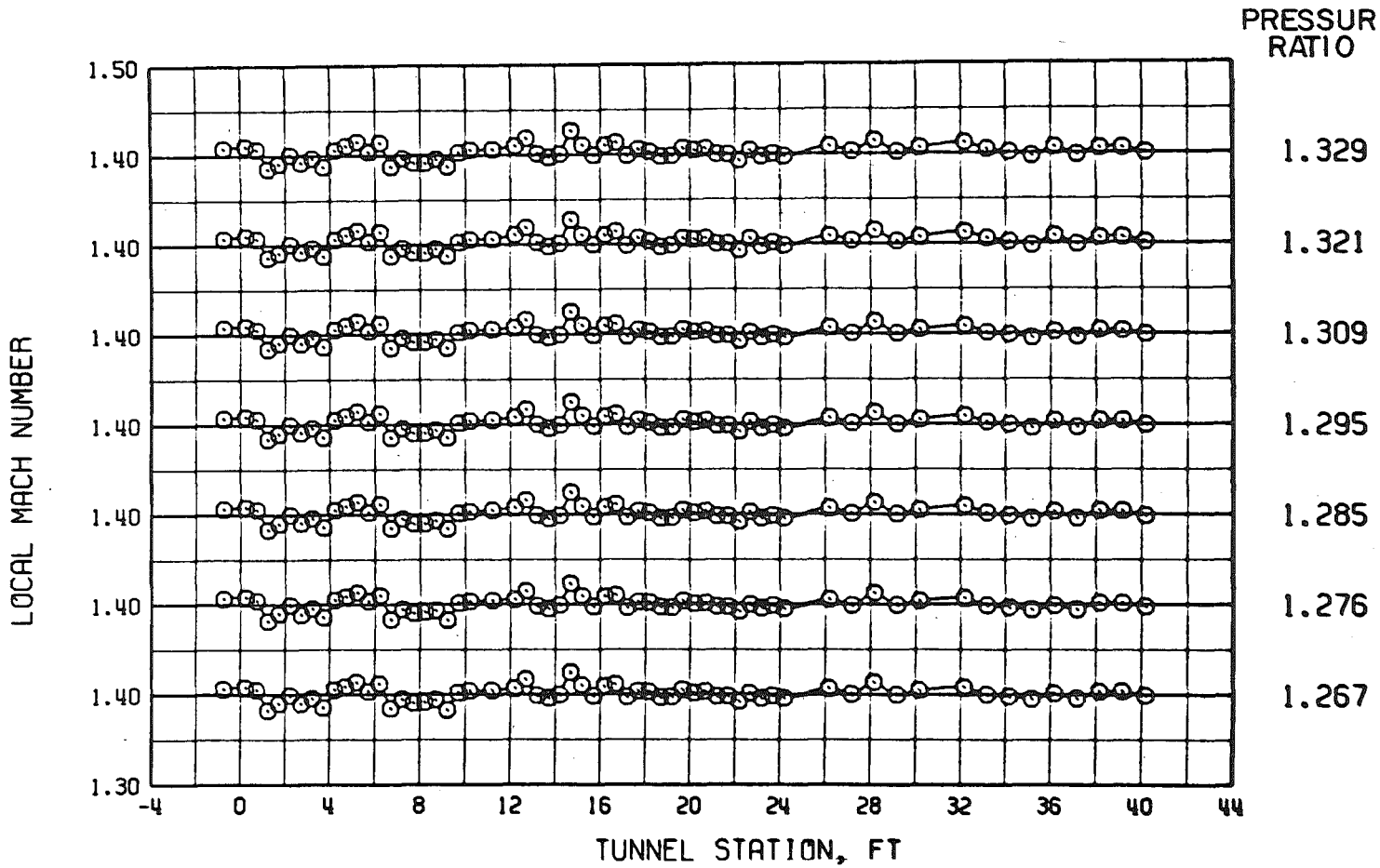

g. M = 1.4, θ_w = 0, and τ = 4

Figure 11. Continued.

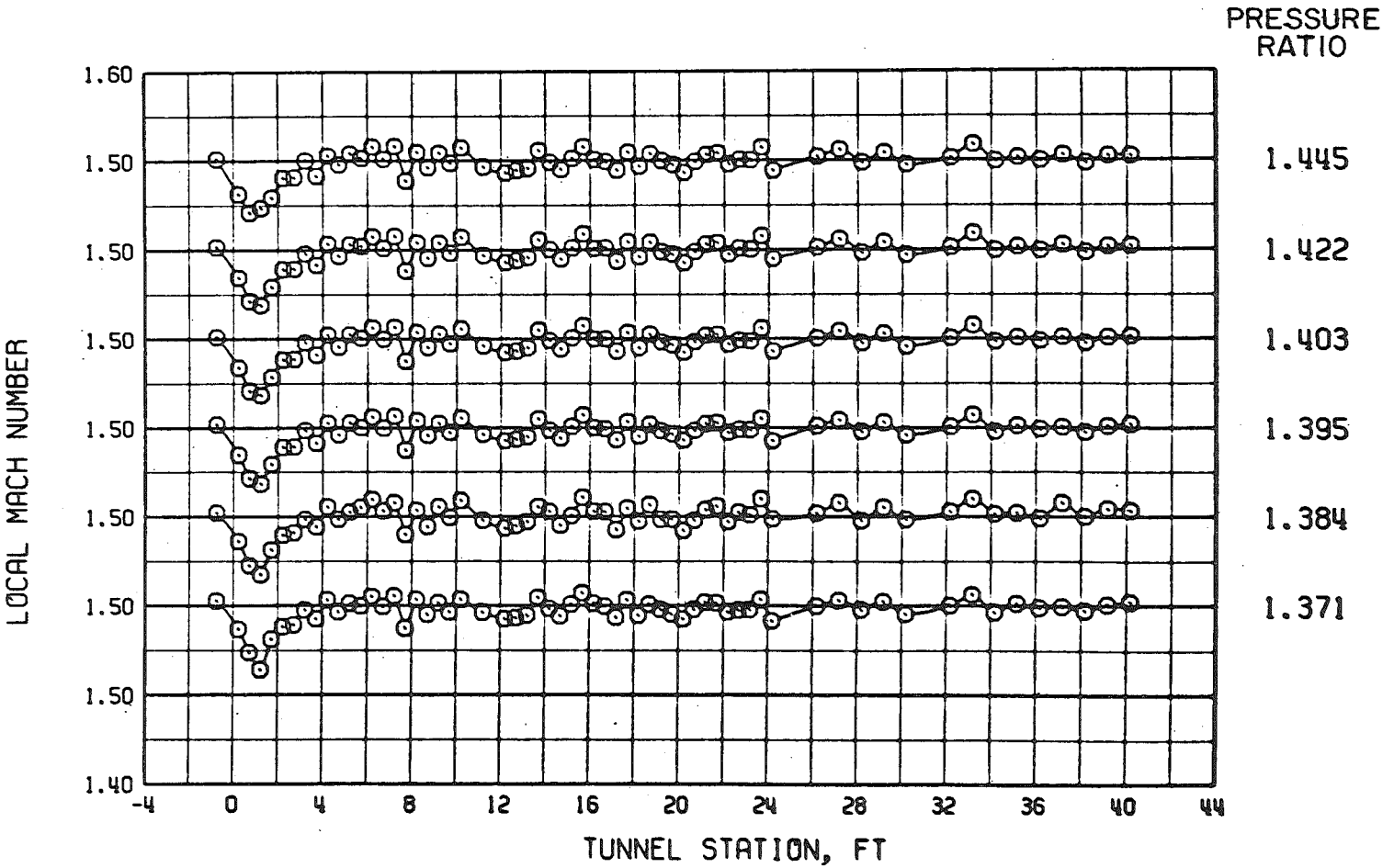

h. M = 1.5, θ_w = 0, and τ = 4

Figure 11. Continued.

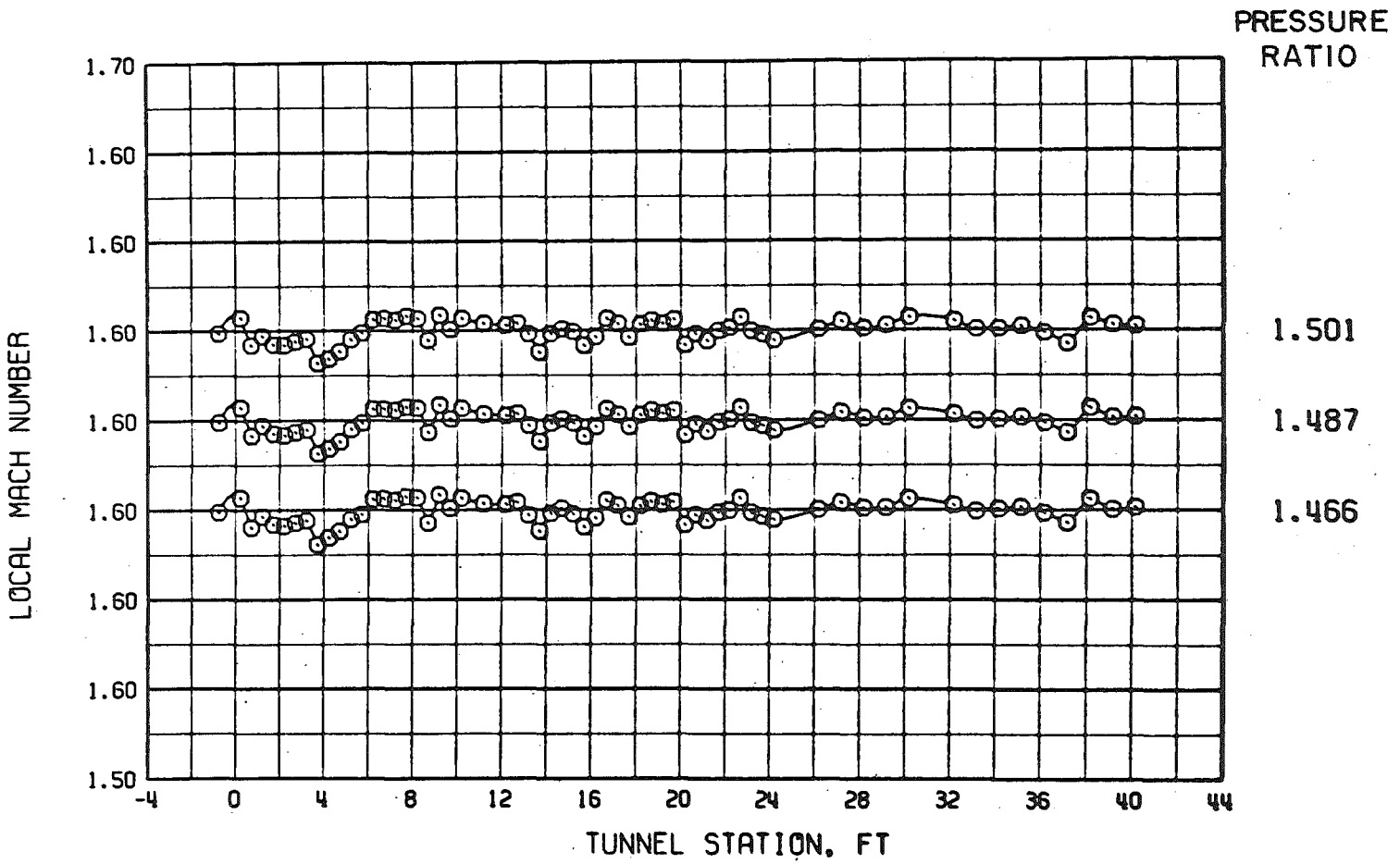

i. M = 1.6, θ_w = 0, and τ = 4

Figure 11. Concluded.

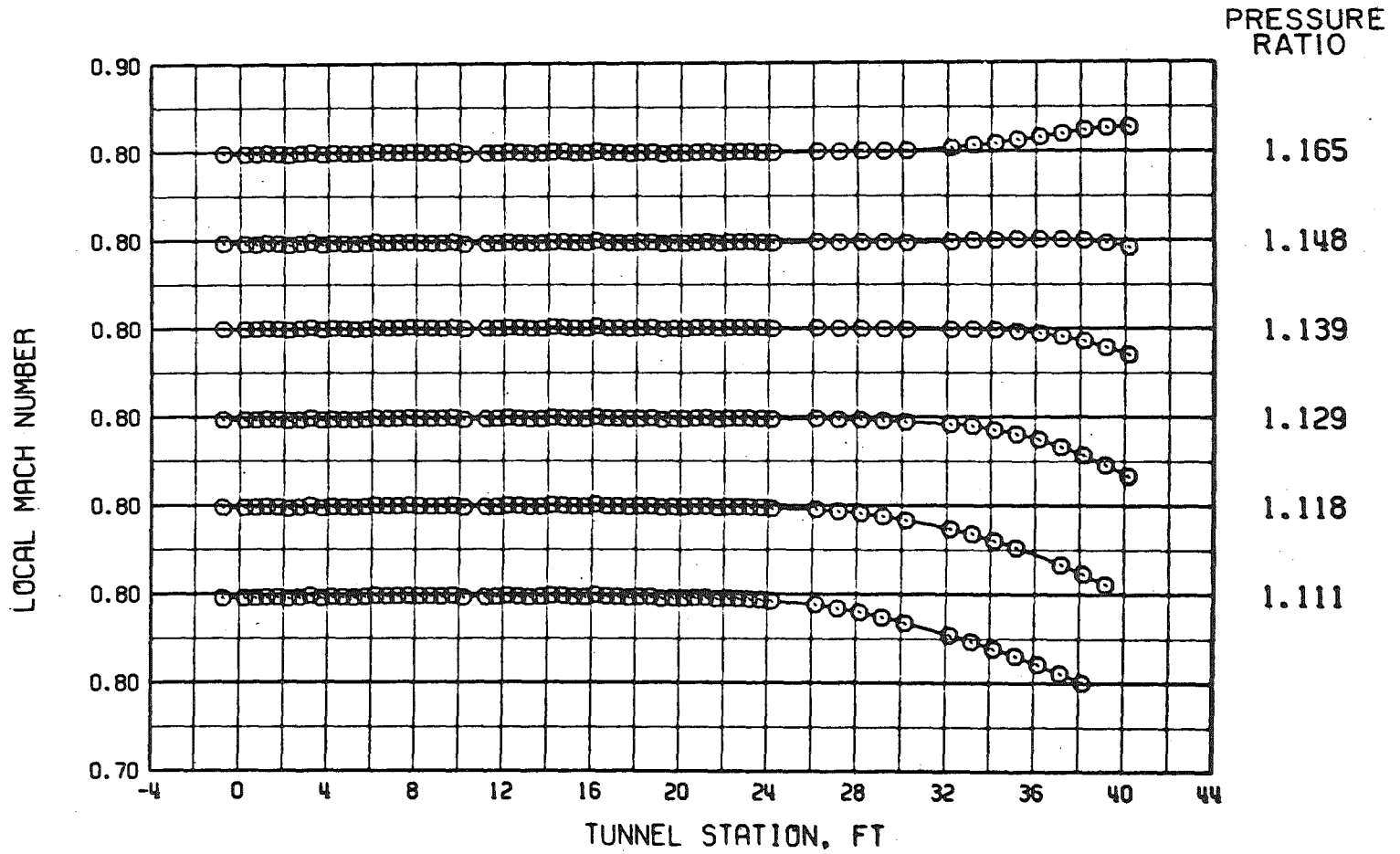

a. M = 0.8, θ_w = 0, and τ = 2

Figure 12. Tunnel 16T centerline Mach number distributions for various tunnel pressure ratios with two-percent porosity walls and θ_w = 0.

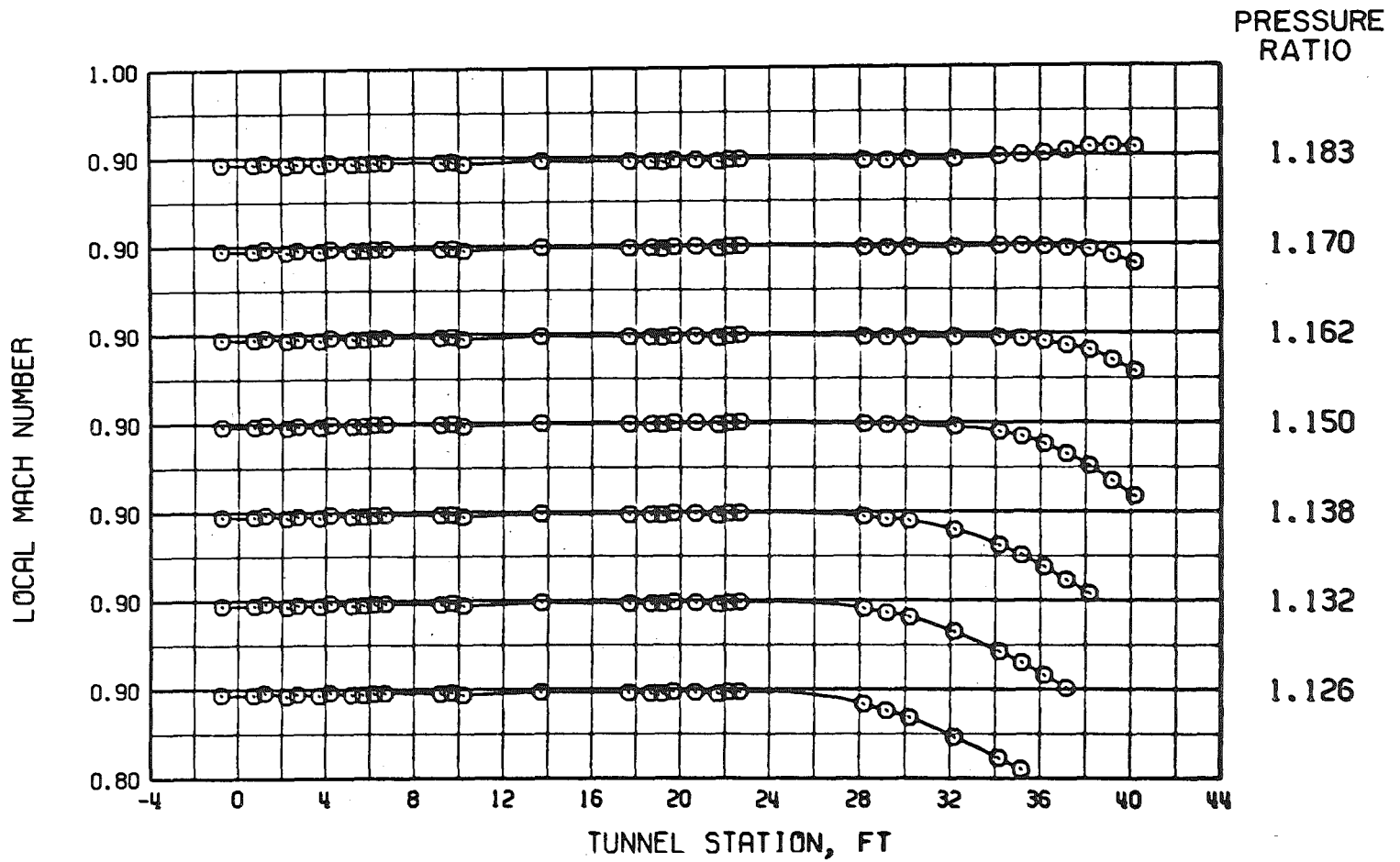

b. M = 0.9, θ_w = 0, and τ = 2
Figure 12. Continued.

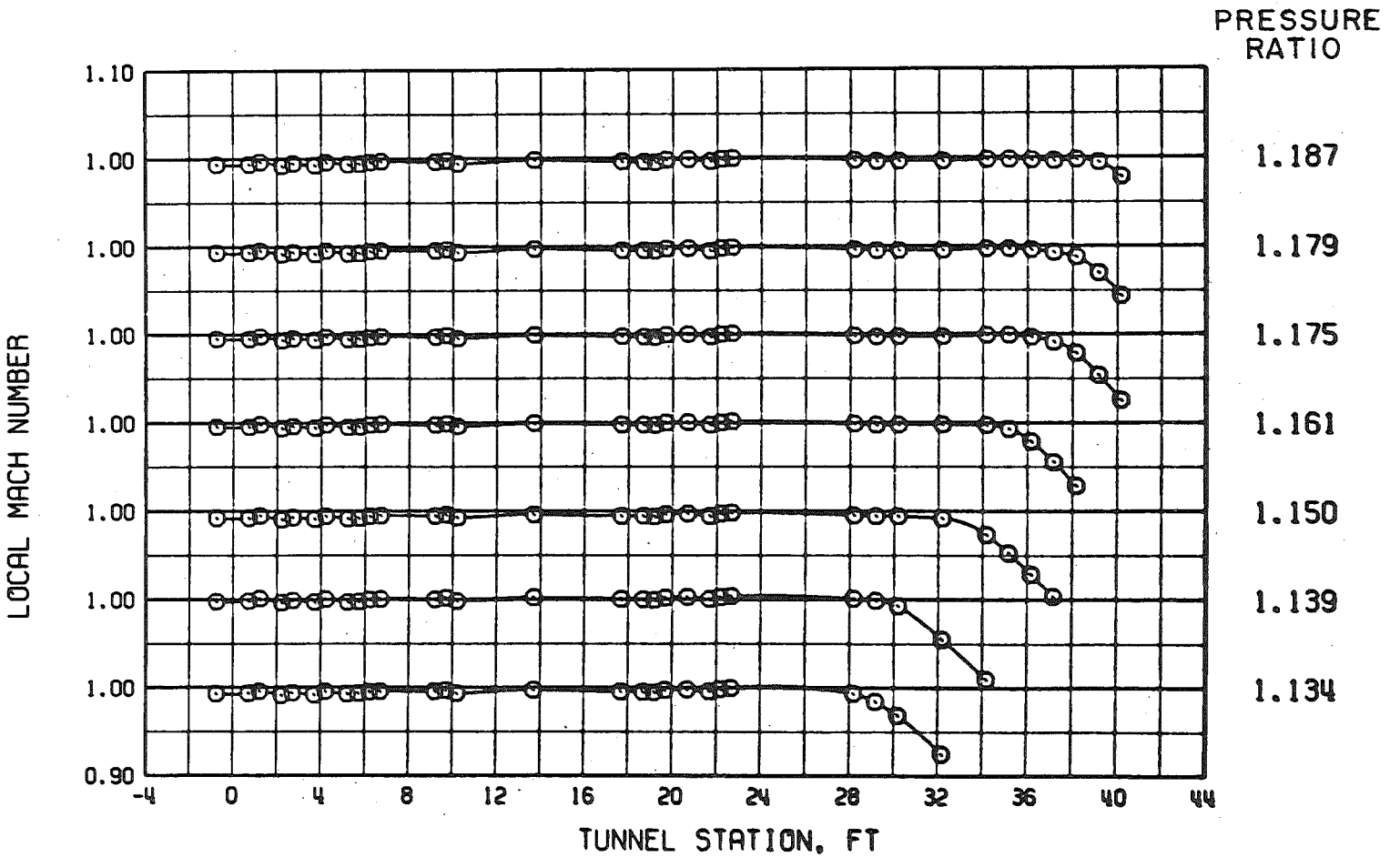

c. M = 1.0, θ_w = 0, and τ = 2

Figure 12. Continued.

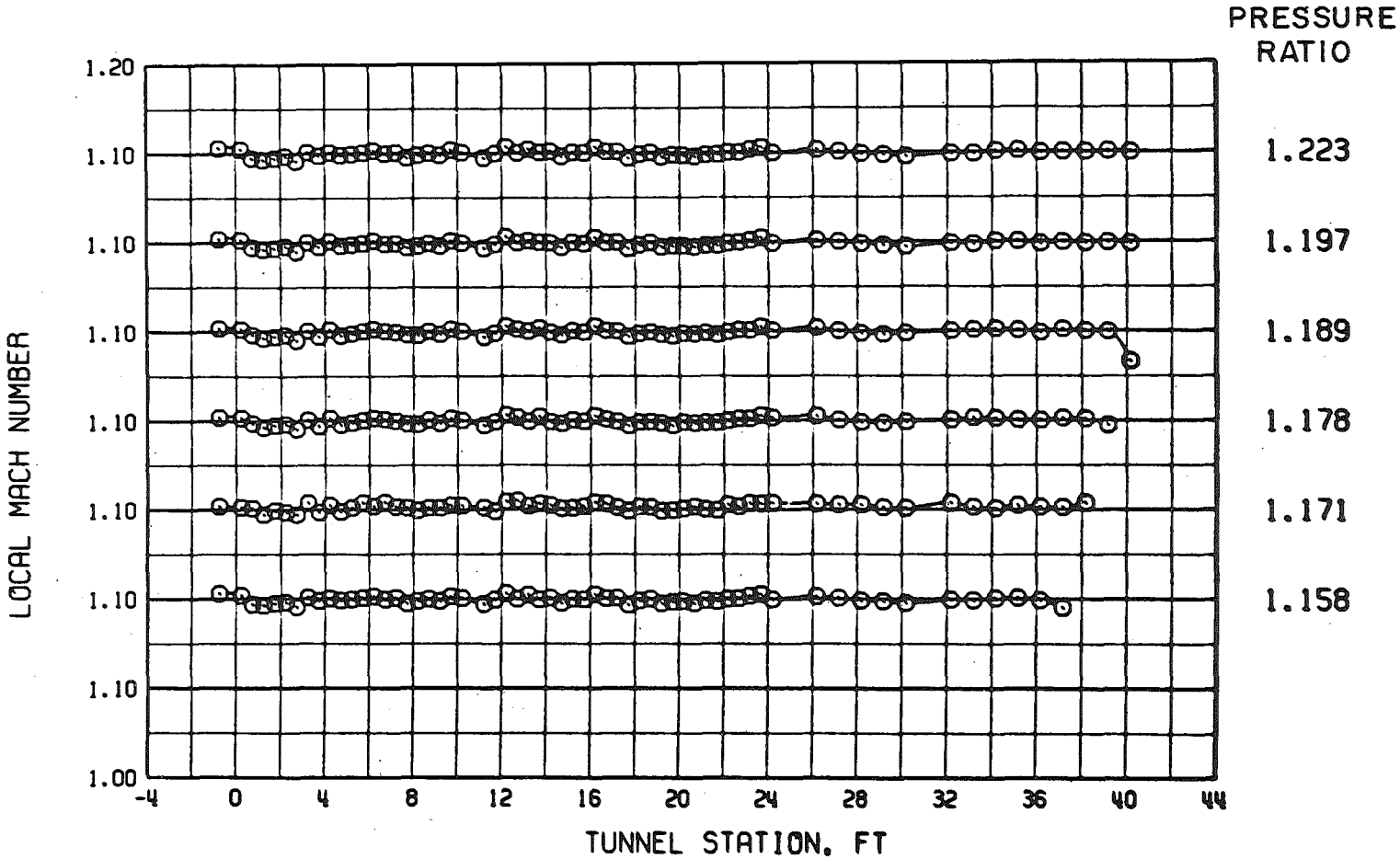

d. M = 1.1, θ_w = 0, and τ = 2

Figure 12. Continued.

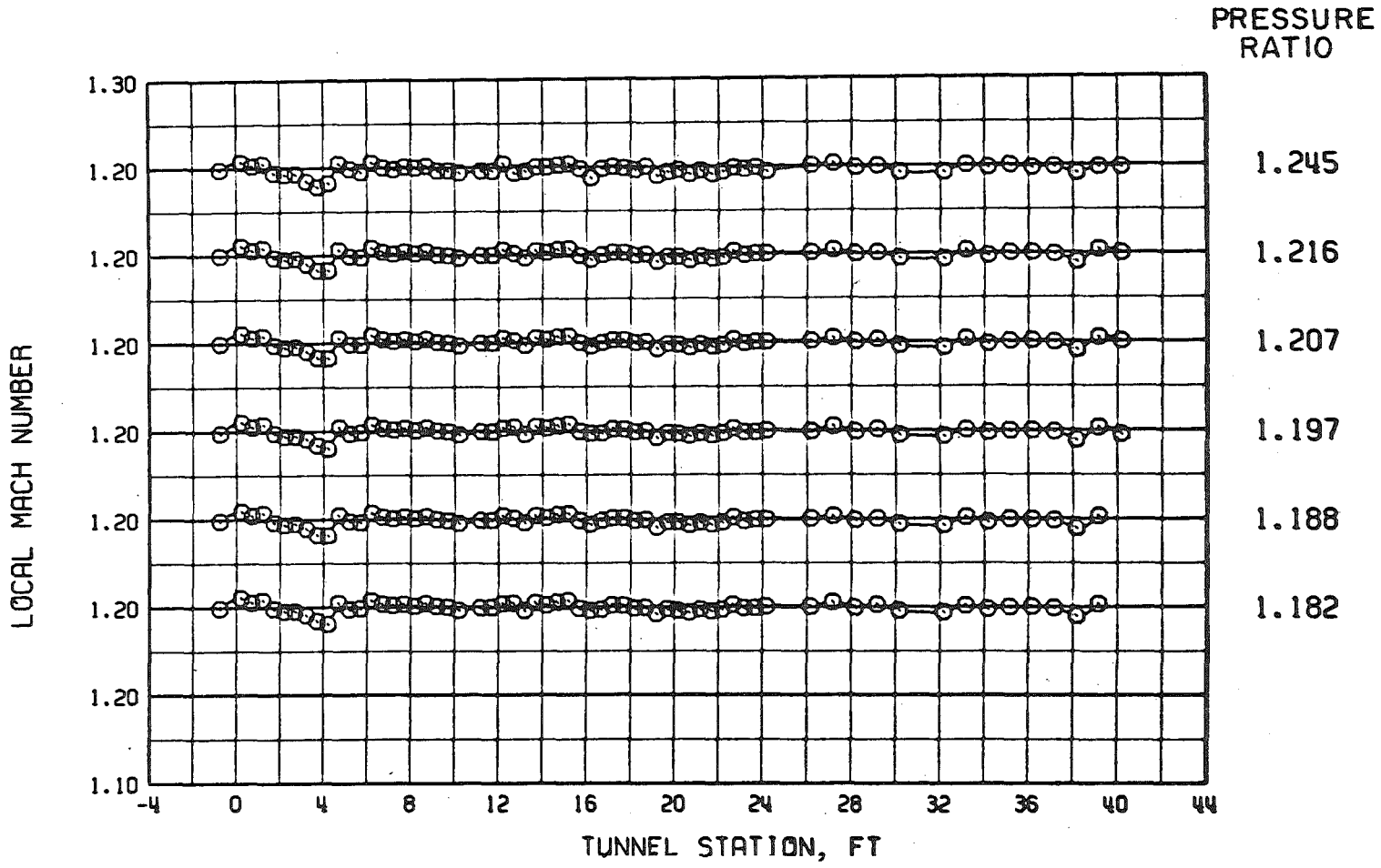

e. $\bar{M} = 1.2$, $\theta_w = 0$, and $\tau = 2$

Figure 12. Continued.

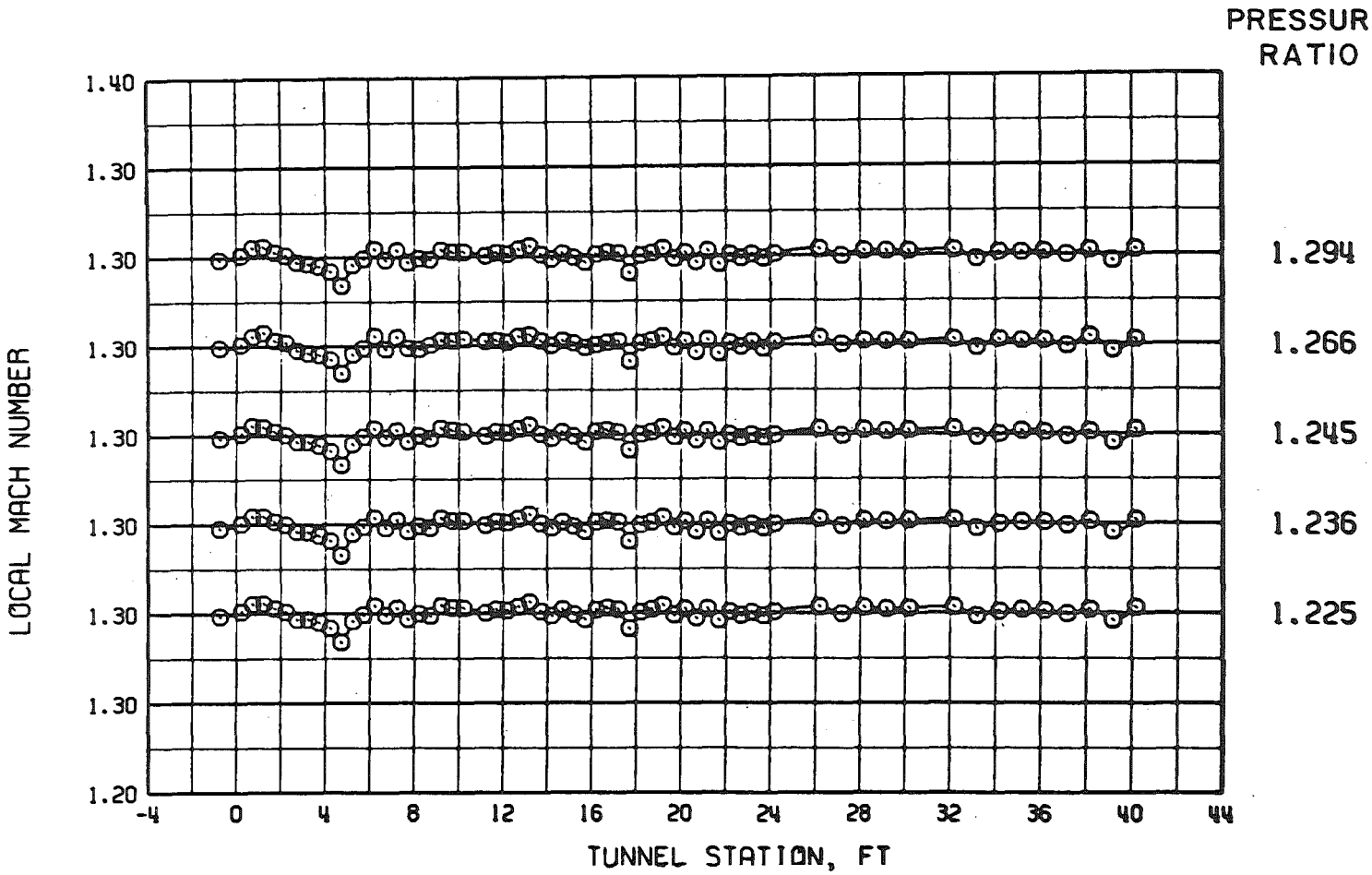

f. M = 1.3, θ_w = 0, and τ = 2

Figure 12. Continued.

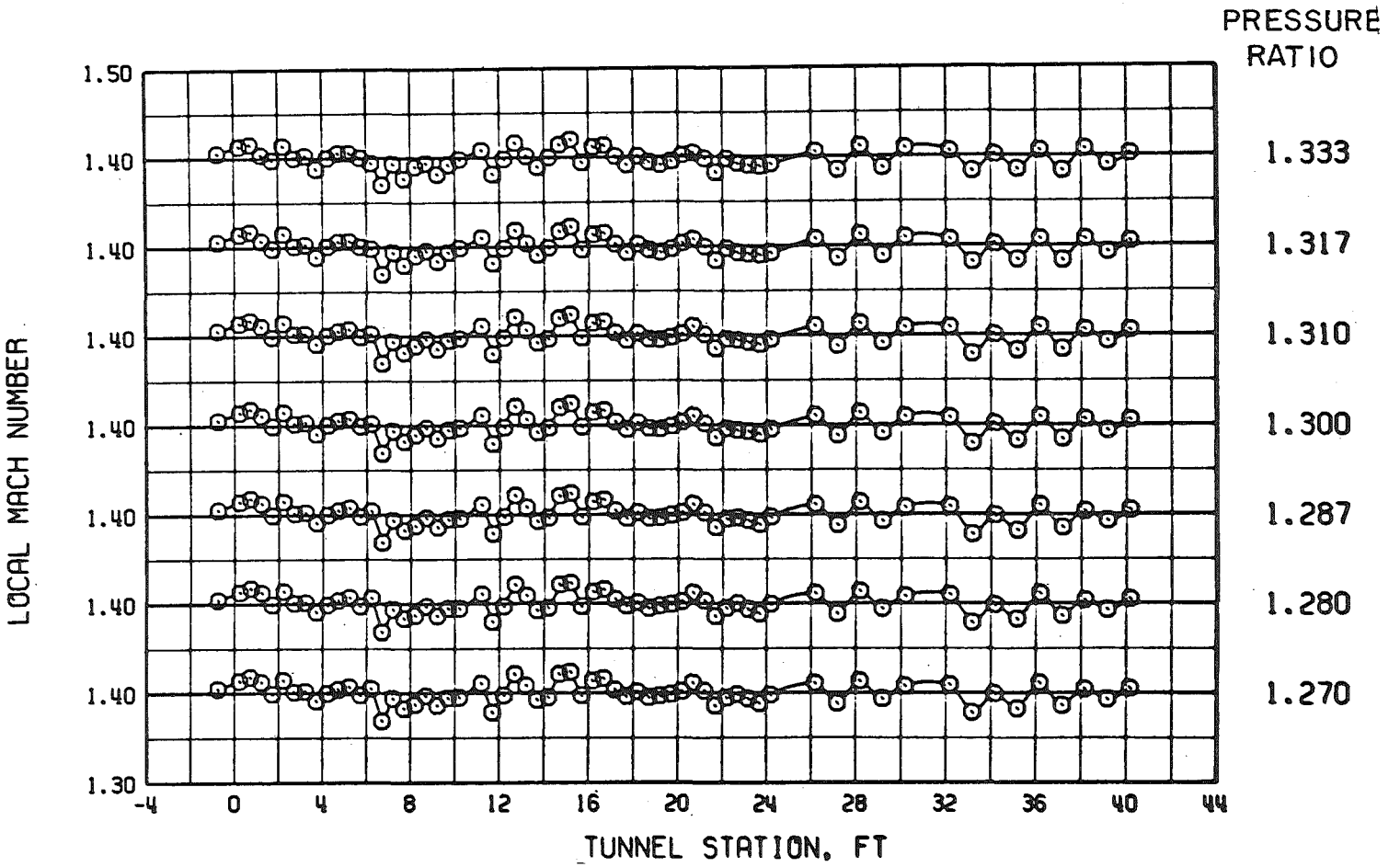

g. M = 1.4, θ_w = 0, and τ = 2
Figure 12. Continued.

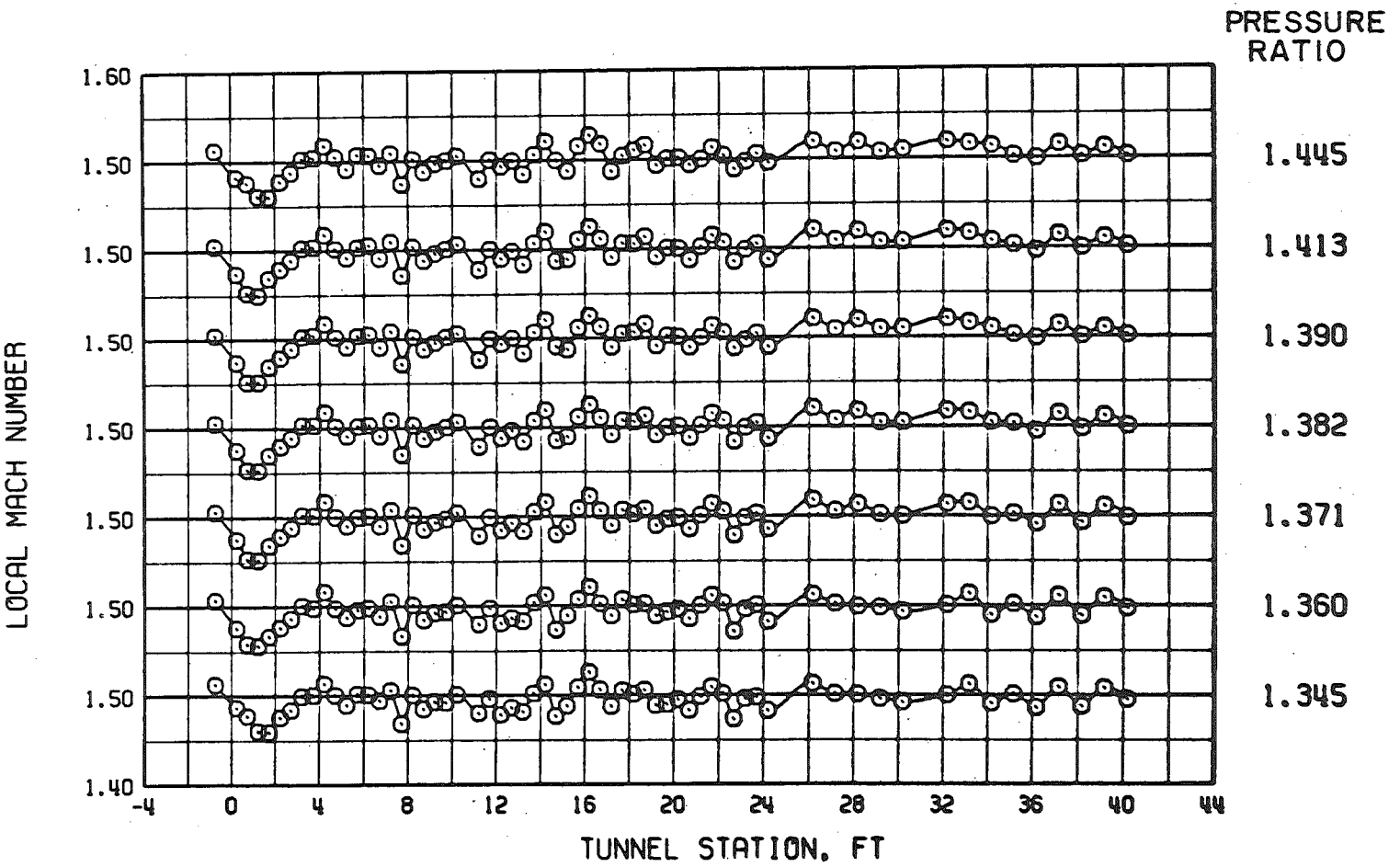

h. M = 1.5, θ_w = 0, and τ = 2

Figure 12. Continued.

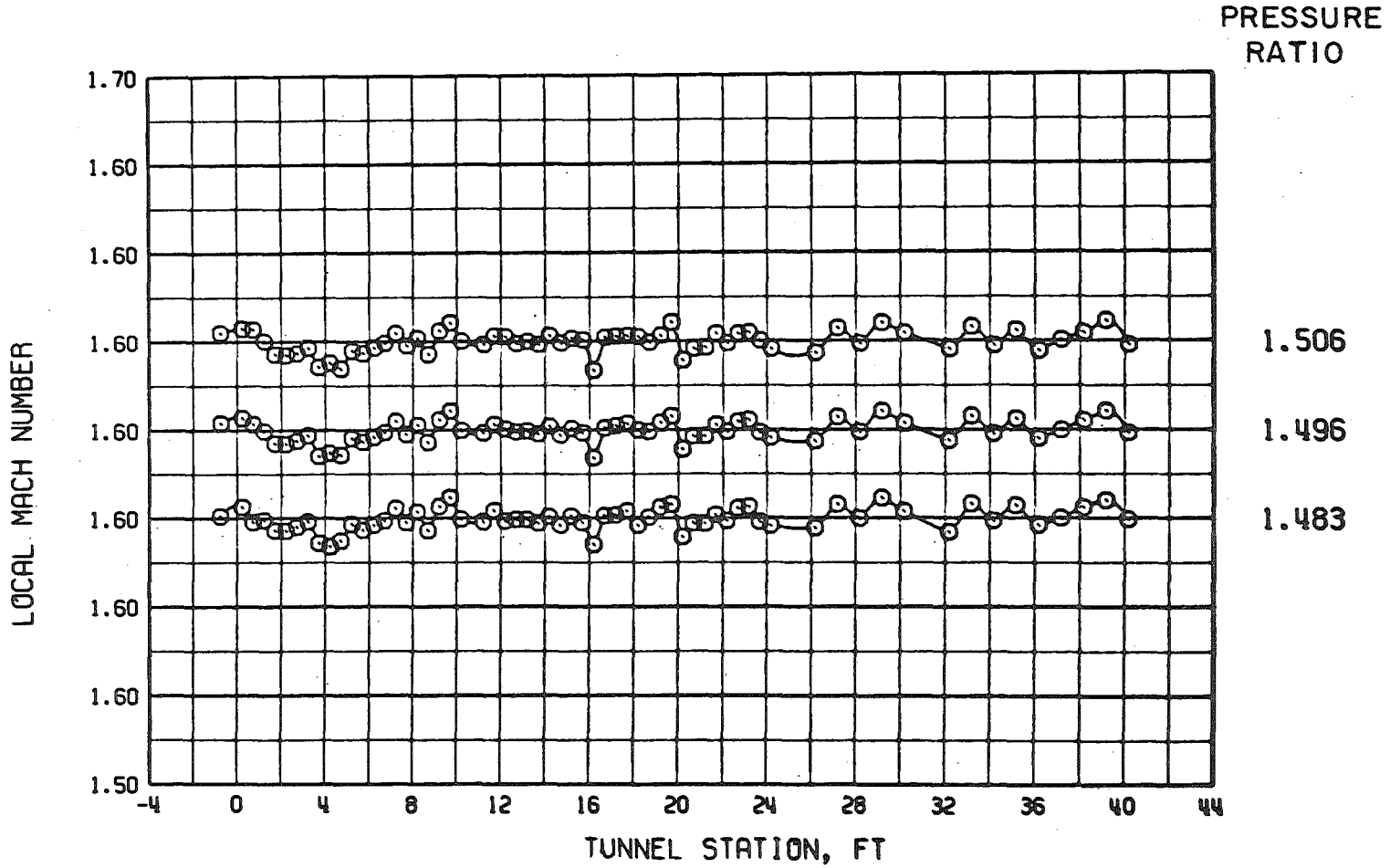

i. M = 1.6, θ_w = 0, and τ = 2

Figure 12. Concluded.

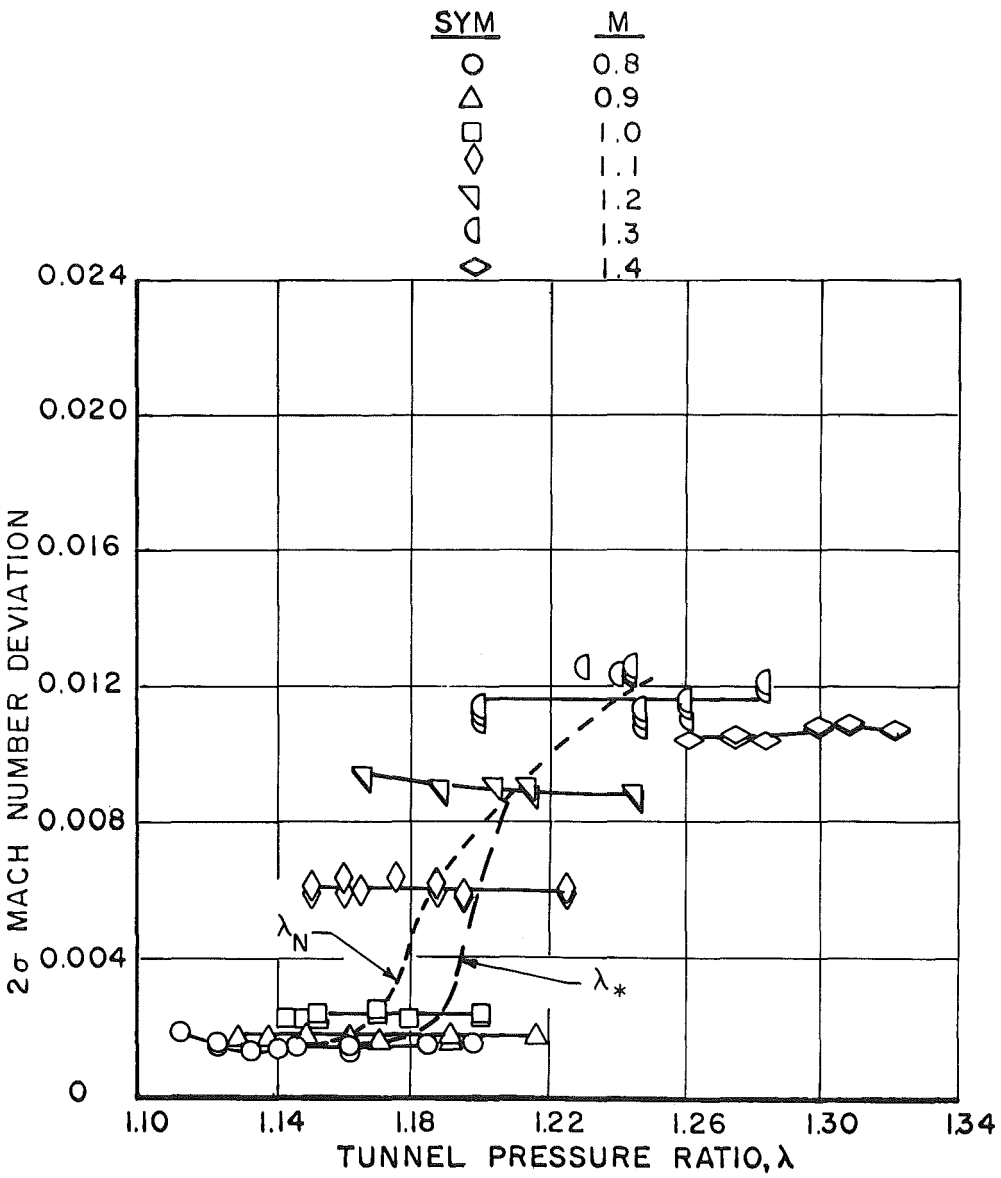

a. $\tau = 6$

Figure 13. Effect of tunnel pressure ratio variation upon the 2σ Mach number deviations for tunnel stations 8.2 to 28.2 at $\theta_w = 0$.

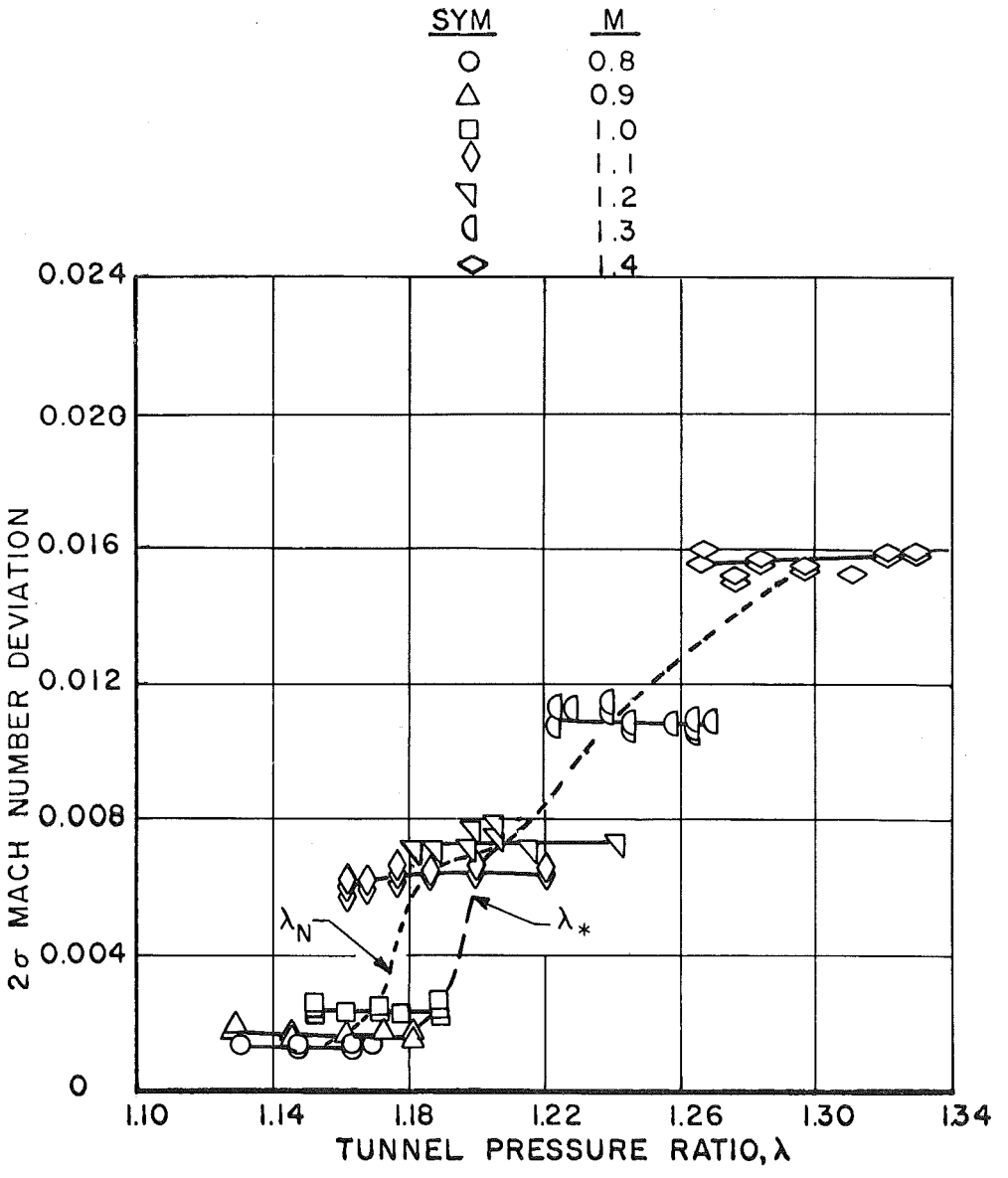

b. $\tau = 4$

Figure 13. Continued.

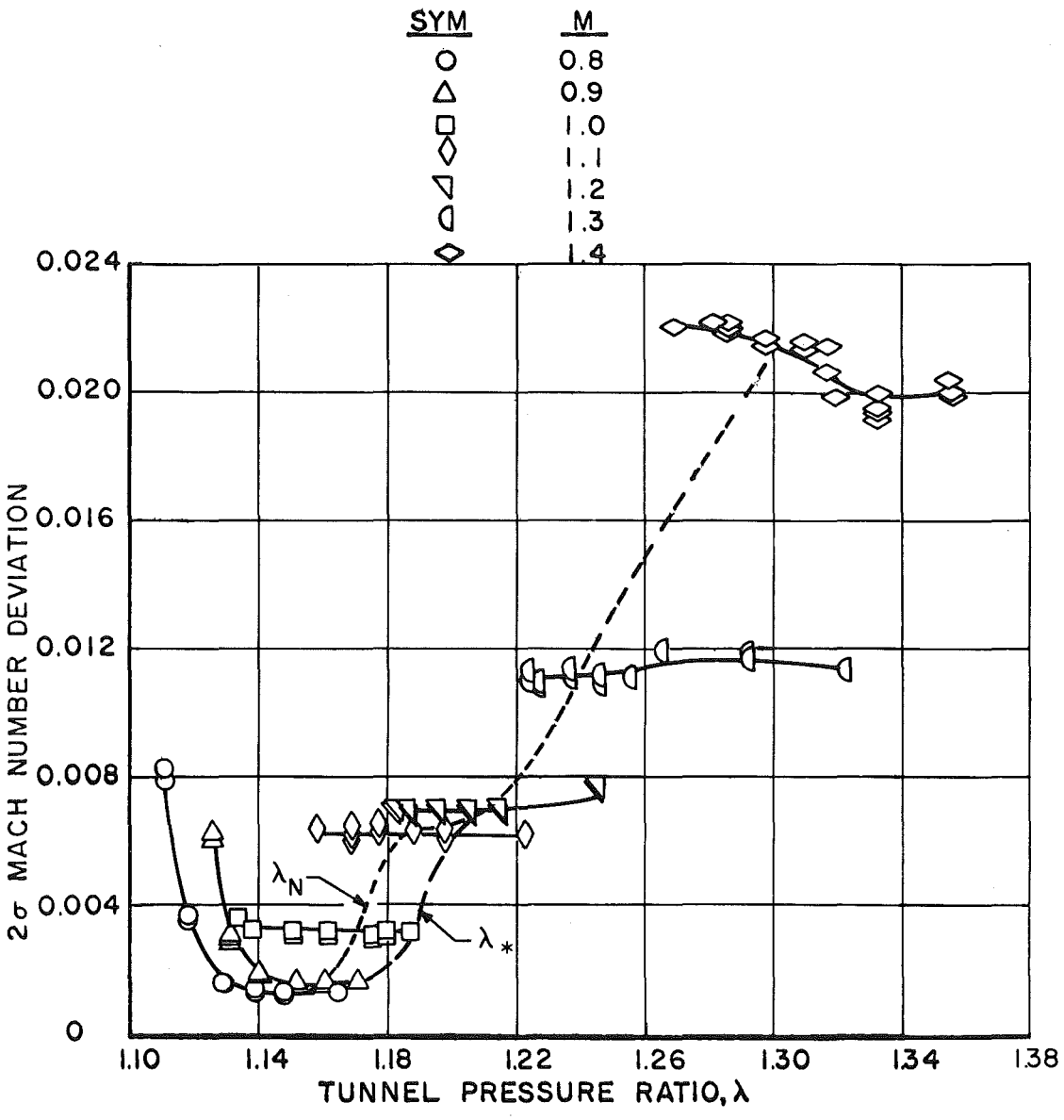

c. $\tau = 2$

Figure 13. Concluded.

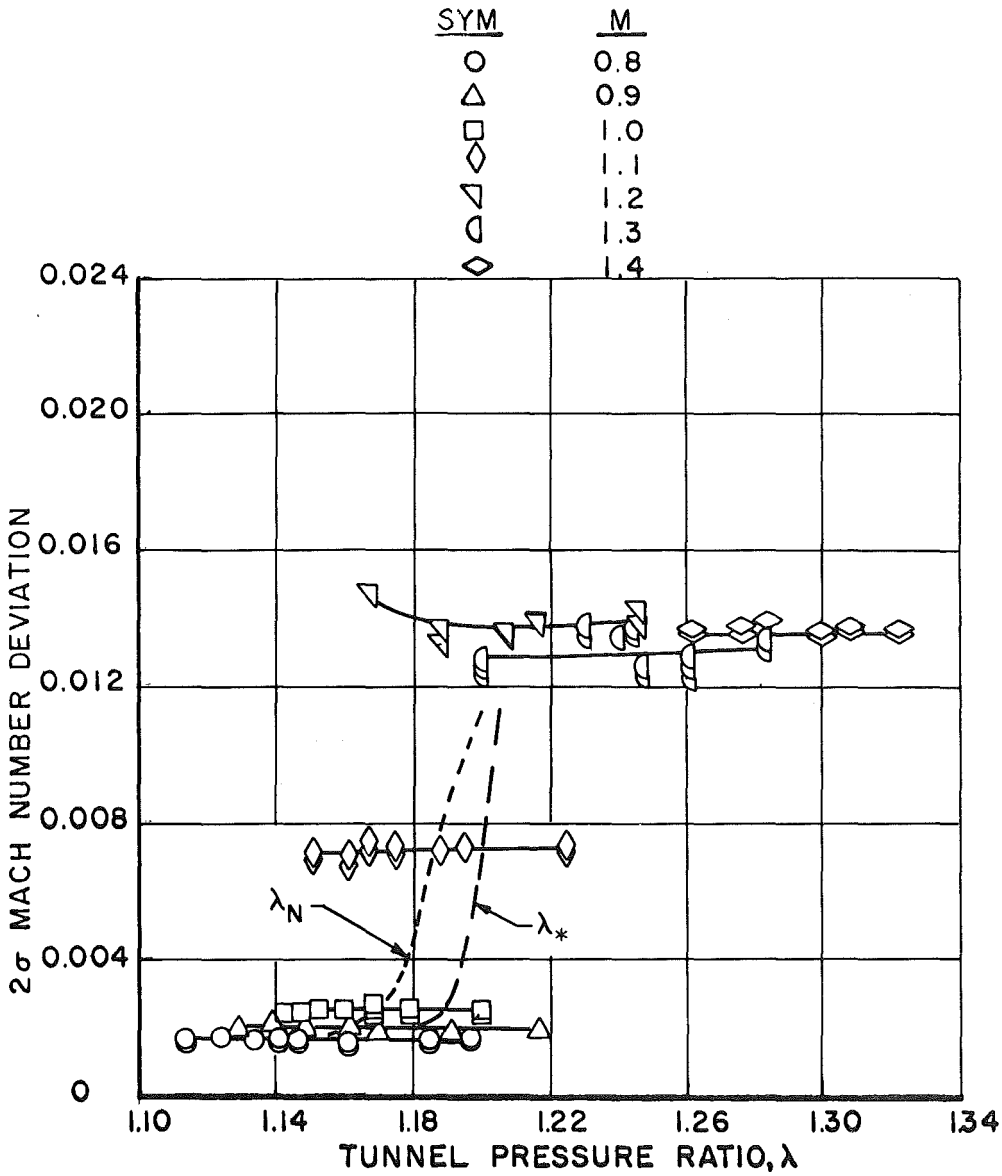

a. $\tau = 6$

Figure 14. Effect of tunnel pressure ratio variation upon the 2σ Mach number deviation for tunnel stations 1.2 to 20.2 at $\theta_w = 0$.

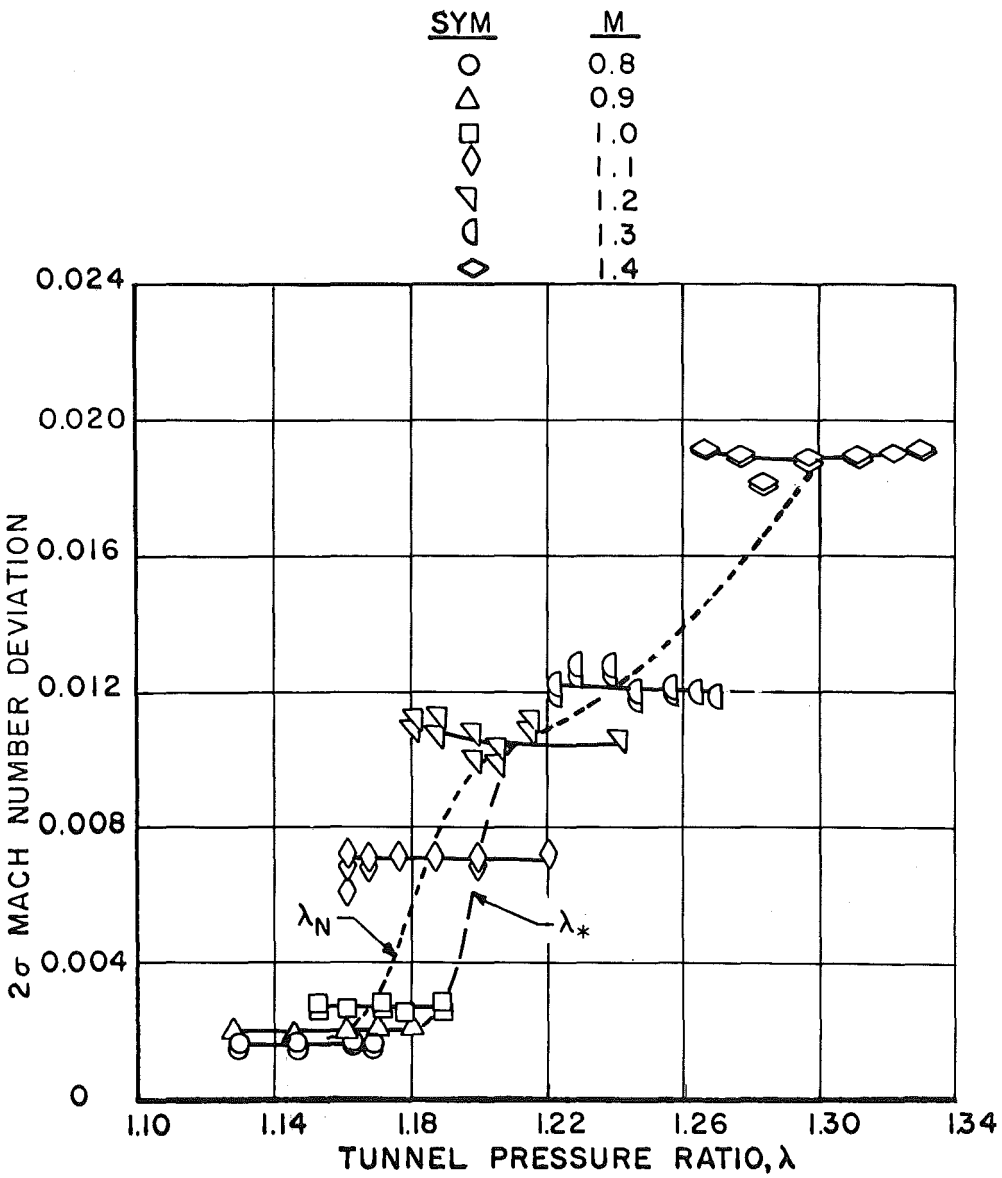

b. $\tau = 4$

Figure 14. Continued.

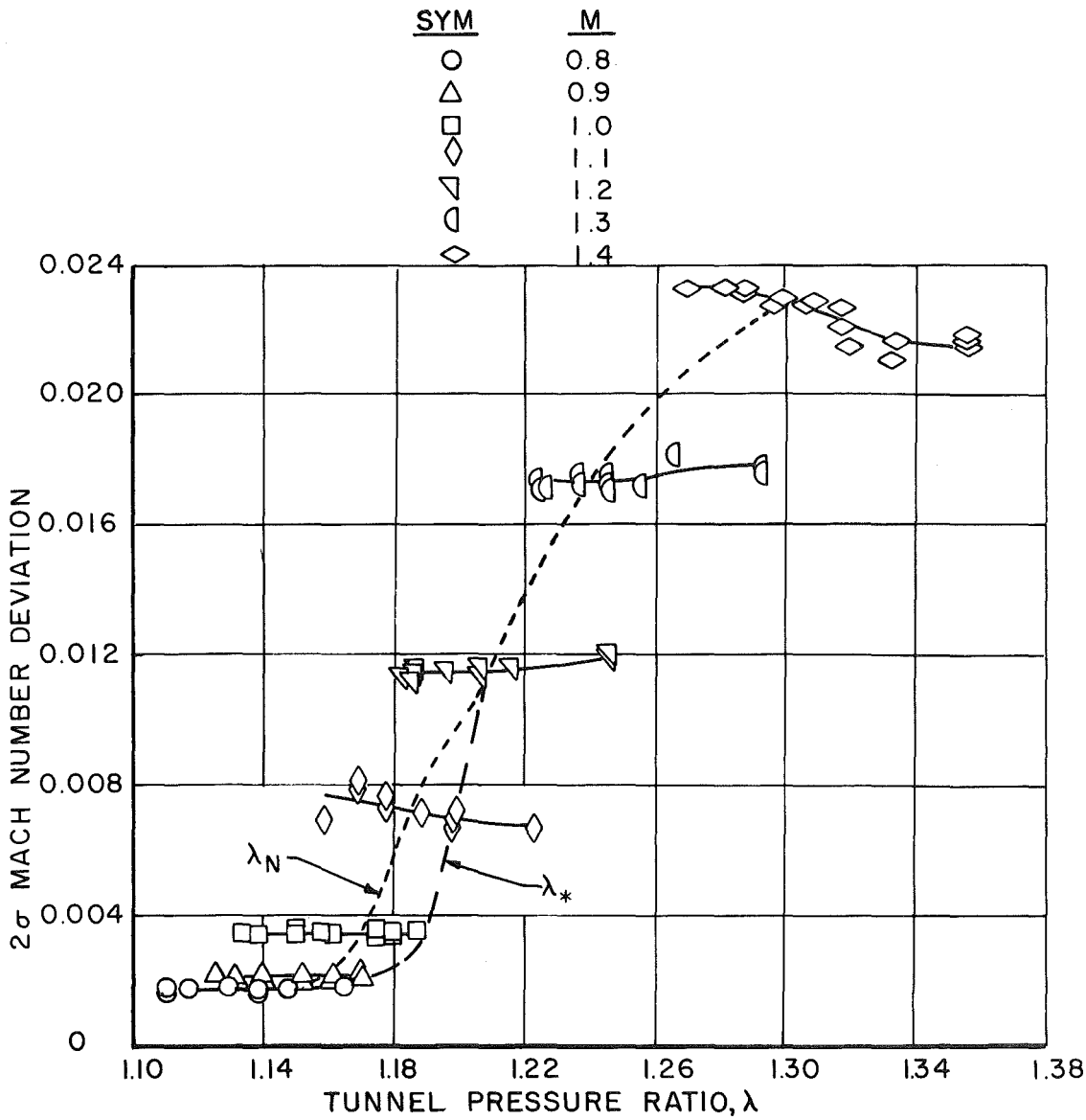

c. $\tau = 2$

Figure 14. Concluded.

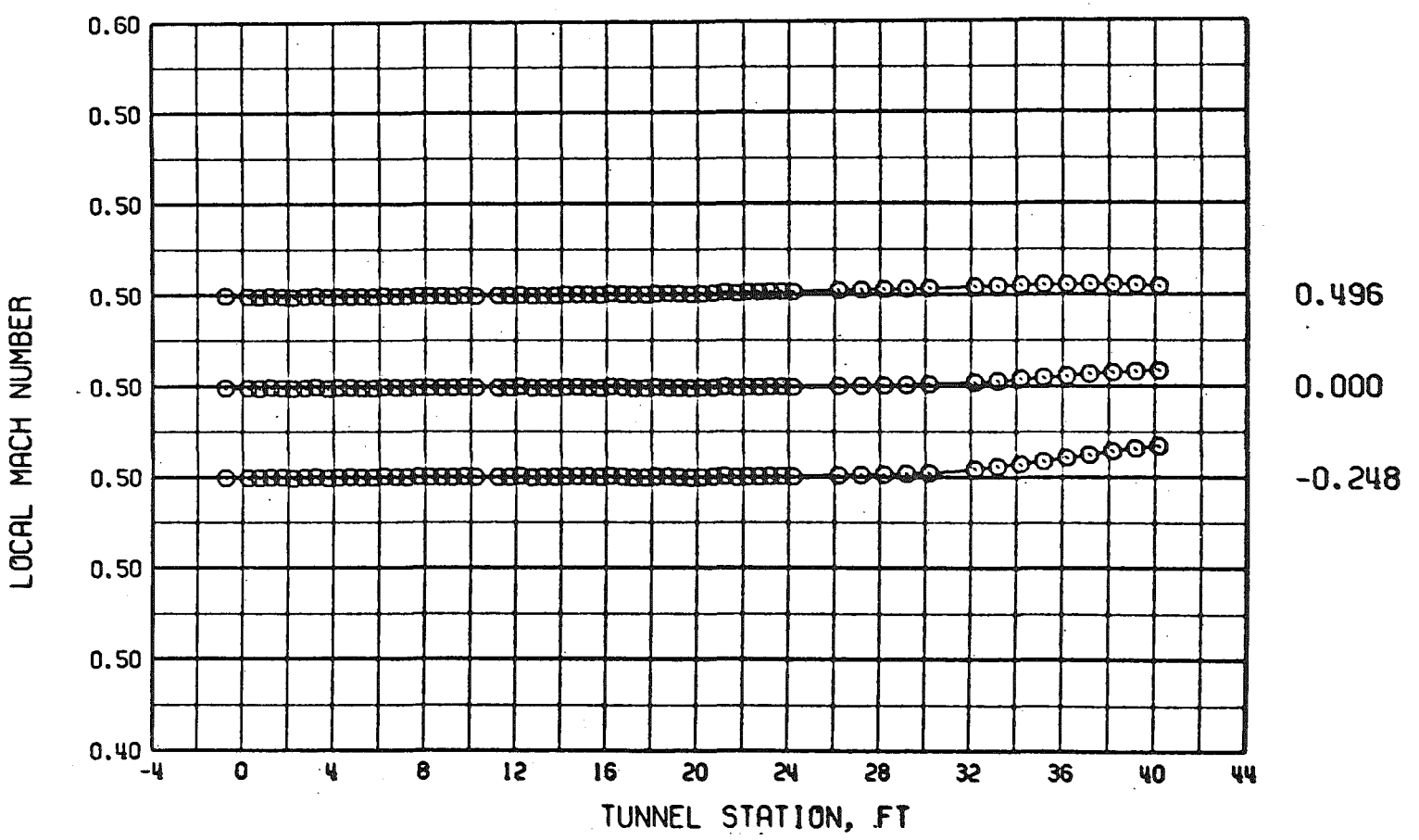

a. M = 0.5, $\lambda \cong 1.07$, and $\tau = 6$

Figure 15. Tunnel 16T centerline Mach number distributions for various test section wall angles with six-percent porosity walls and $\lambda \cong \lambda_N$.

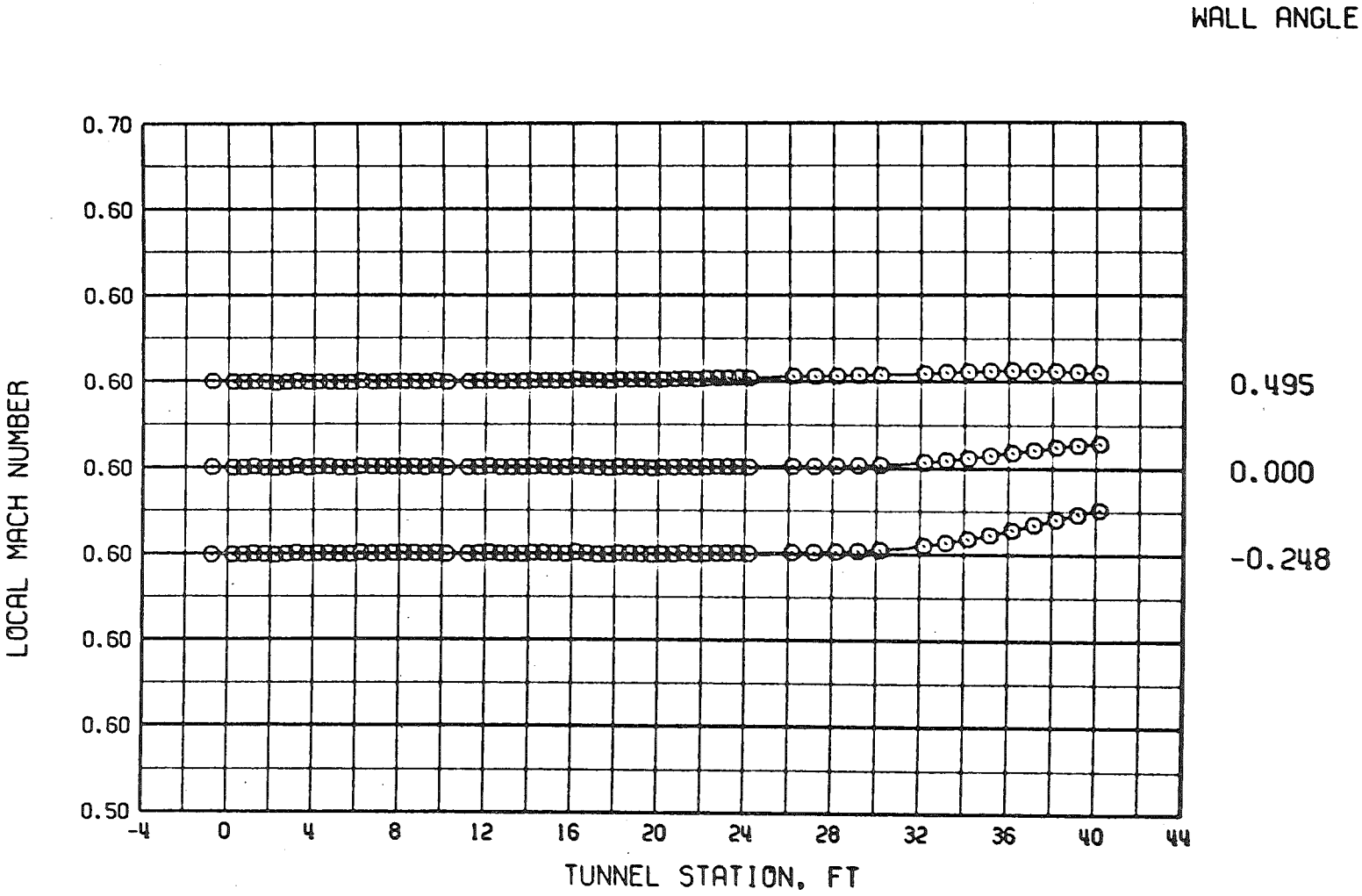

b. M = 0.6, $\lambda \cong$ = 1.10, and τ = 6

Figure 15. Continued.

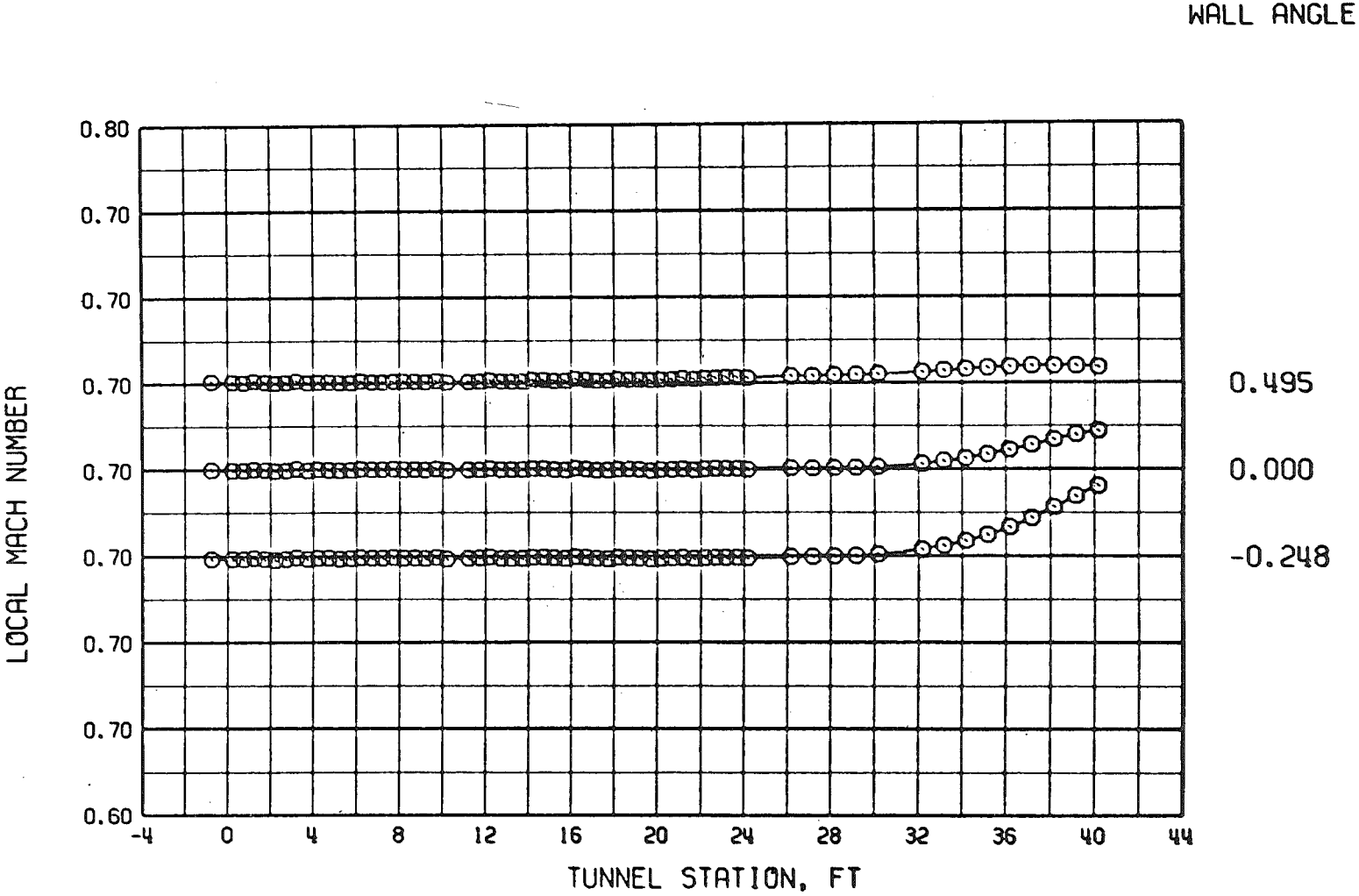

c. M = 0.7, $\lambda \cong 1.15$, and $\tau = 6$

Figure 15. Continued.

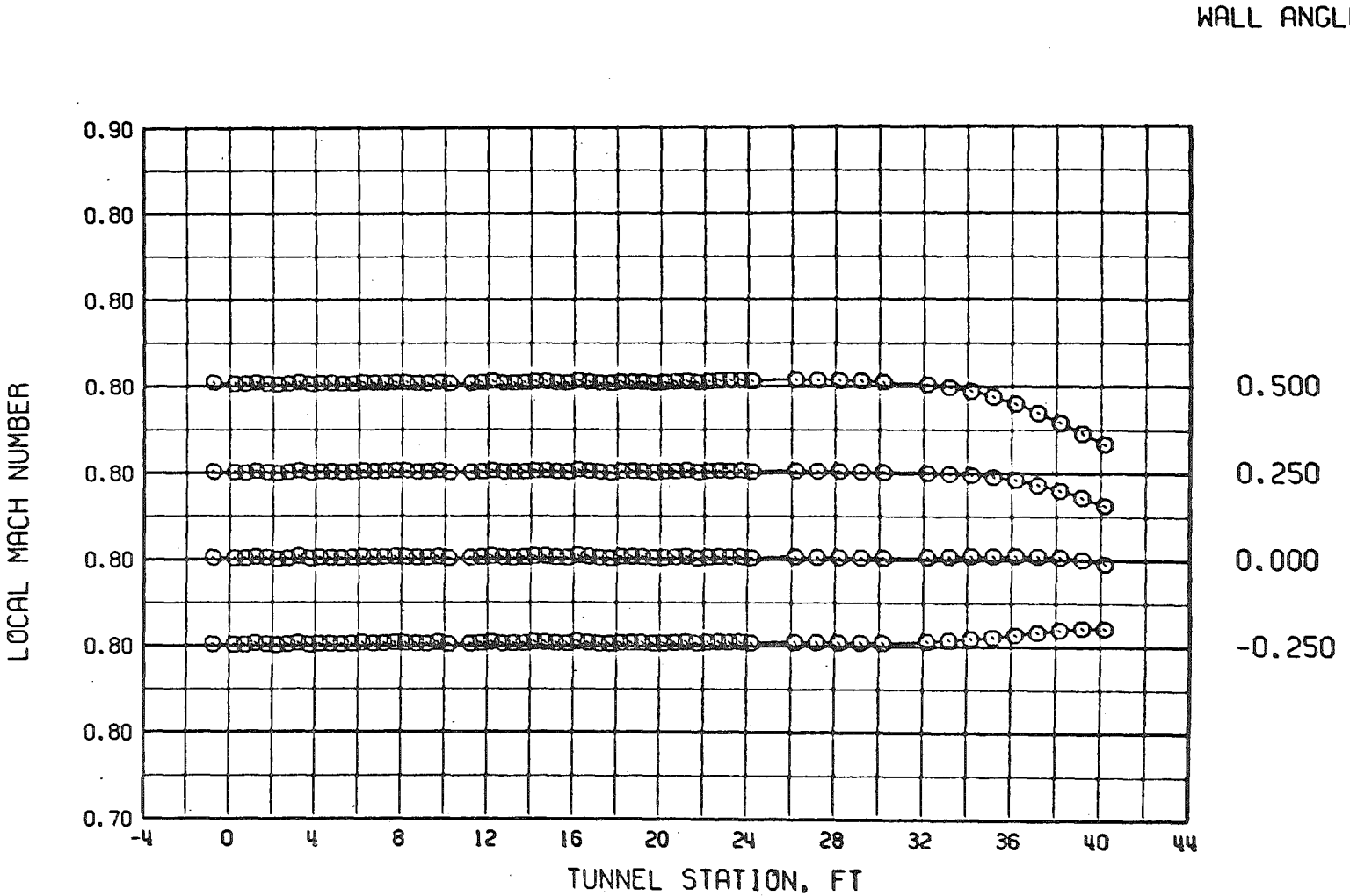

d. M = 0.8, λ = 1.15, and τ = 6

Figure 15. Continued.

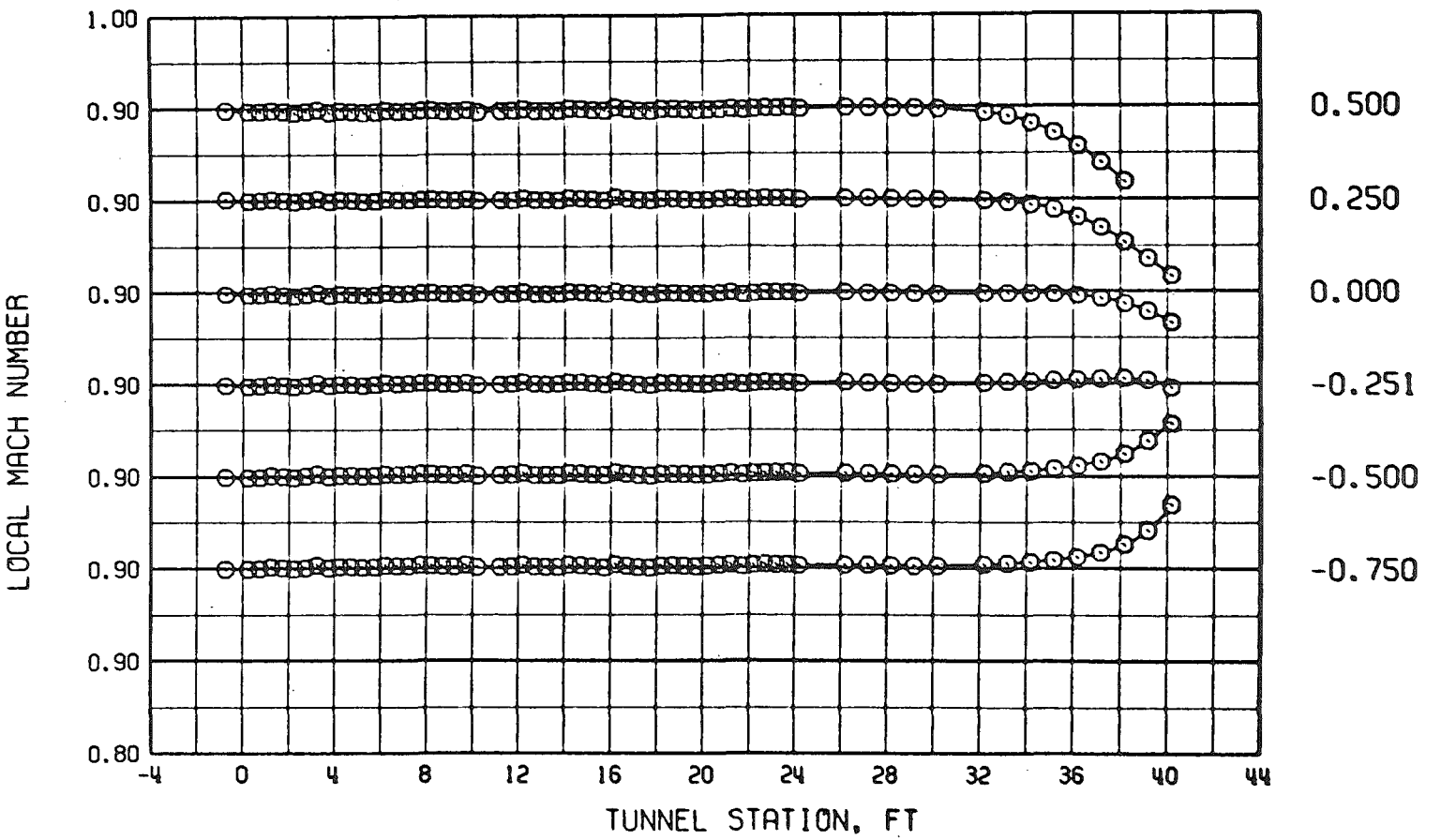

e. M = 0.9, λ = 1.16, and τ = 6

Figure 15. Continued.

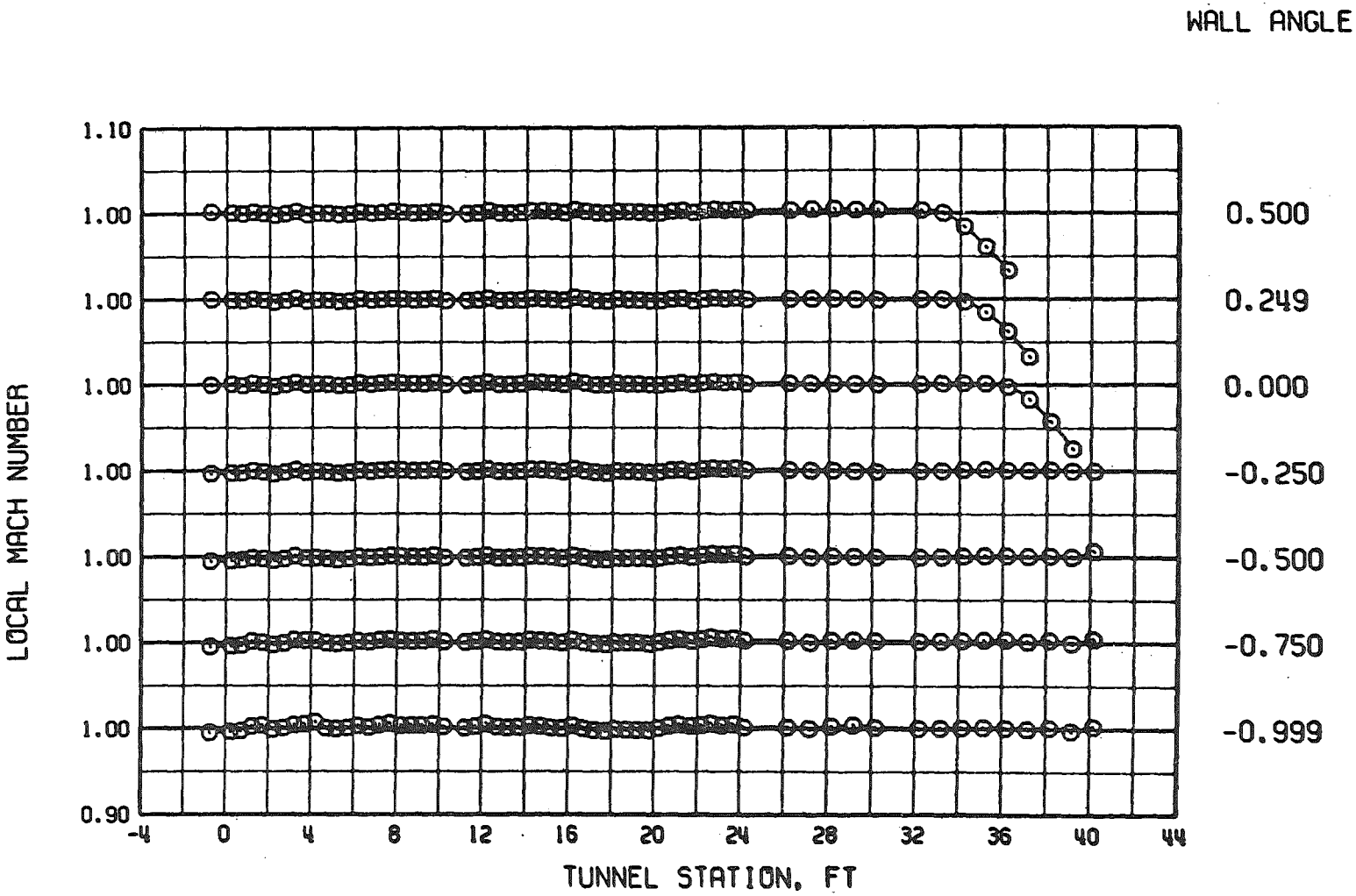

f. M = 1.0, λ = 1.17, and τ = 6

Figure 15. Continued.

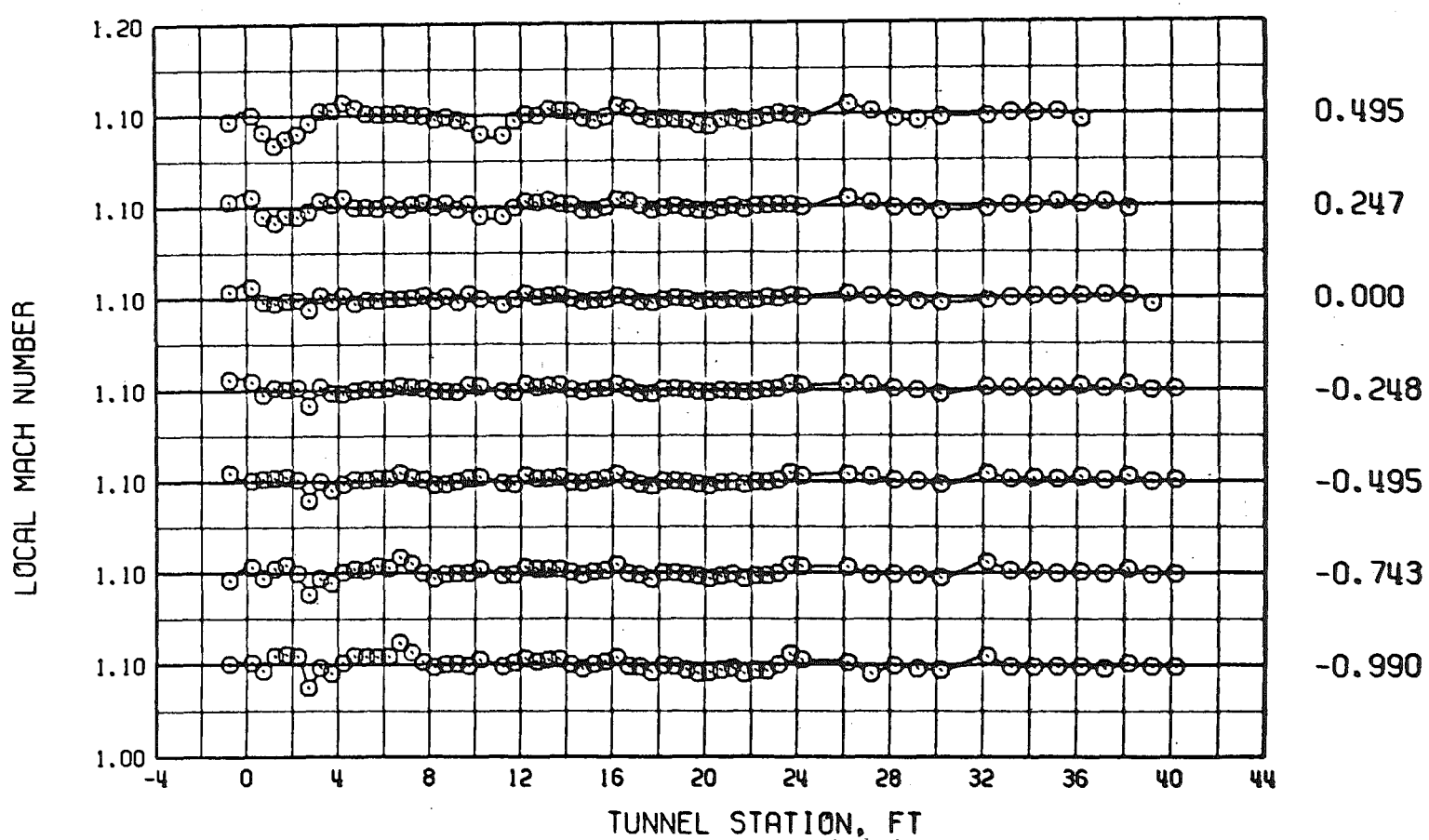

g. M = 1.1, λ = 1.19, and τ = 6

Figure 15. Continued.

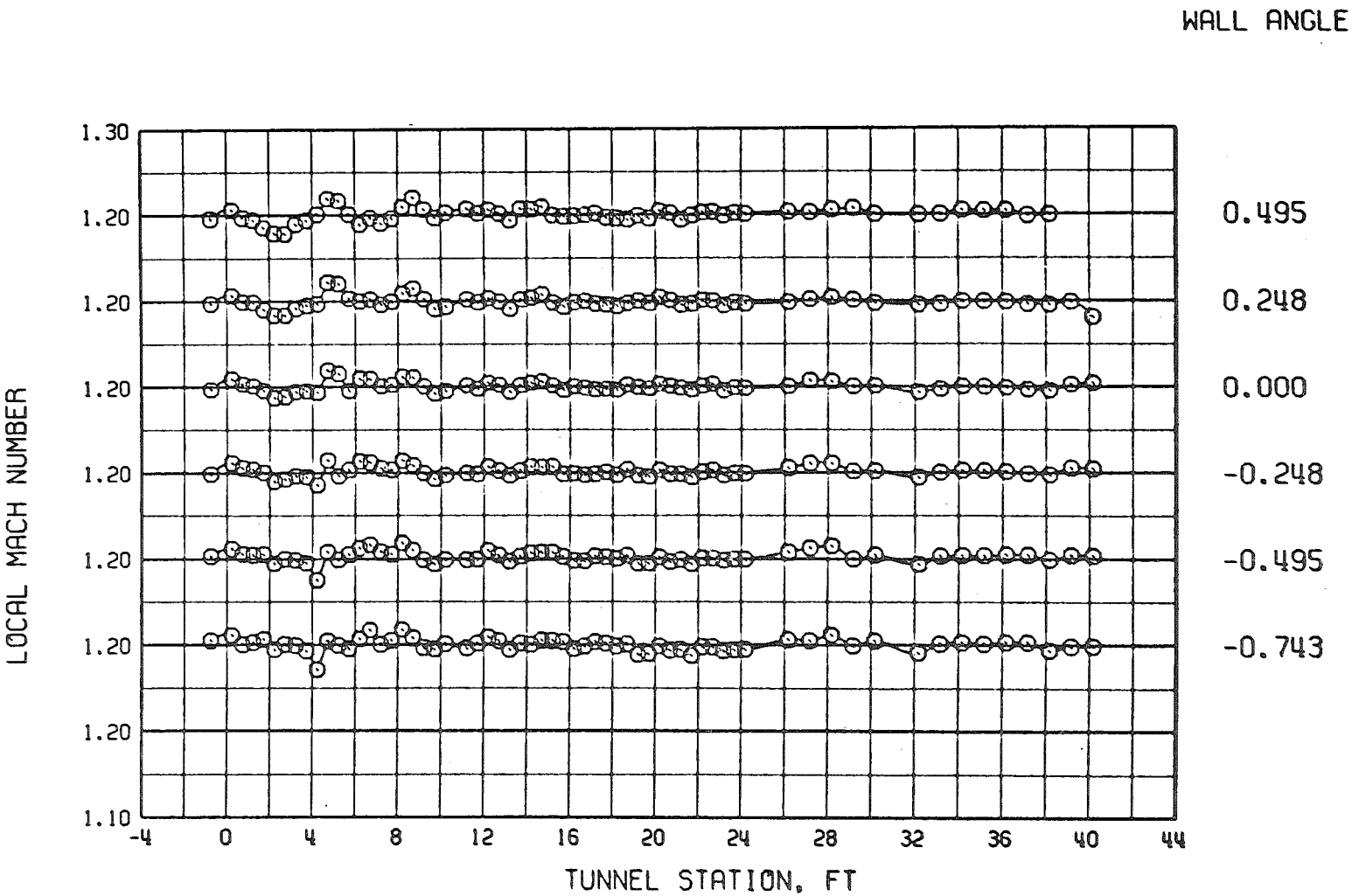

h. M = 1.2, λ = 1.22, and τ = 6

Figure 15. Continued.

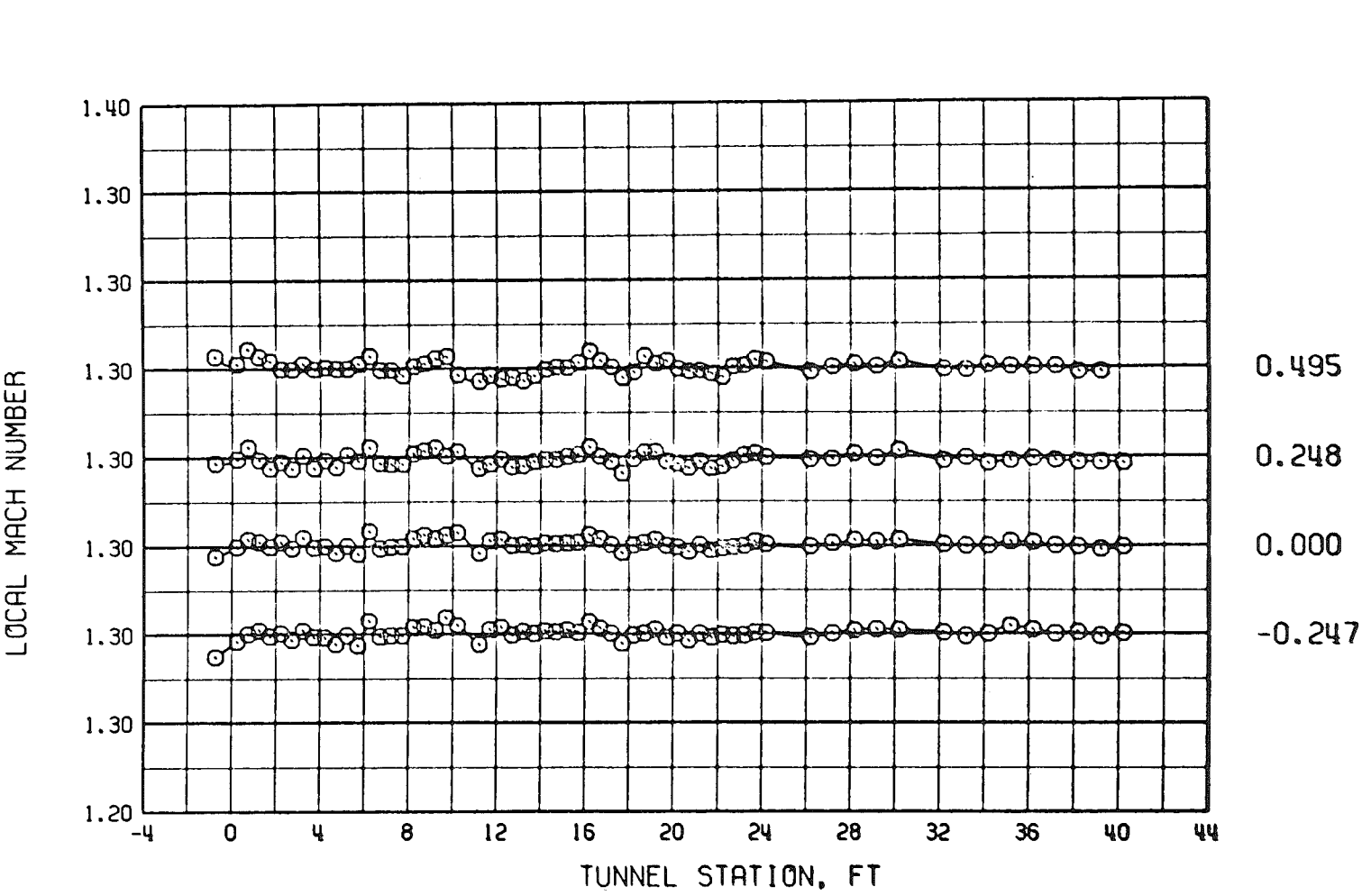

i. M = 1.3, λ = 1.25, and τ = 6

Figure 15. Continued.

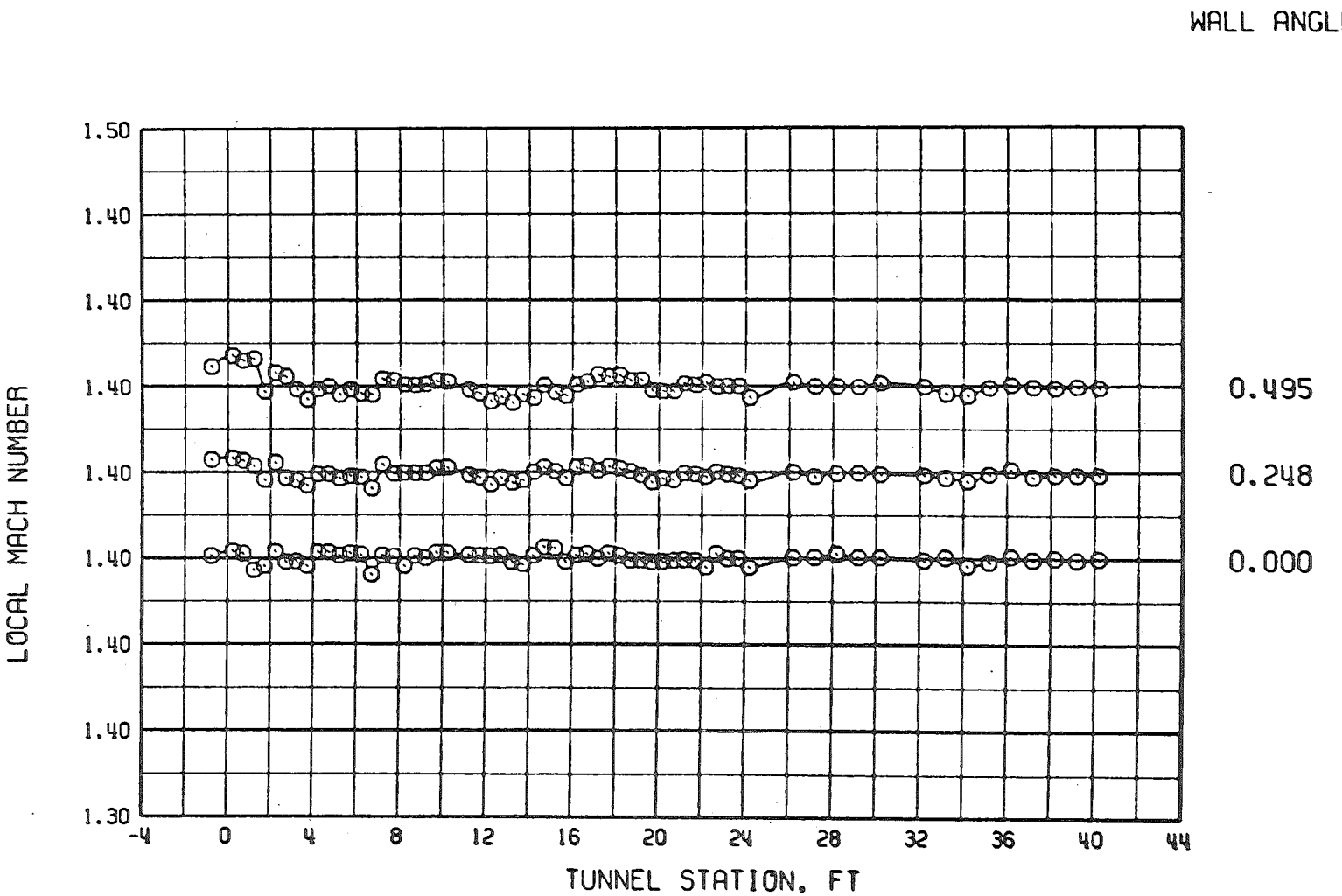

j. M = 1.40, λ = 1.30, and τ = 6

Figure 15. Continued.

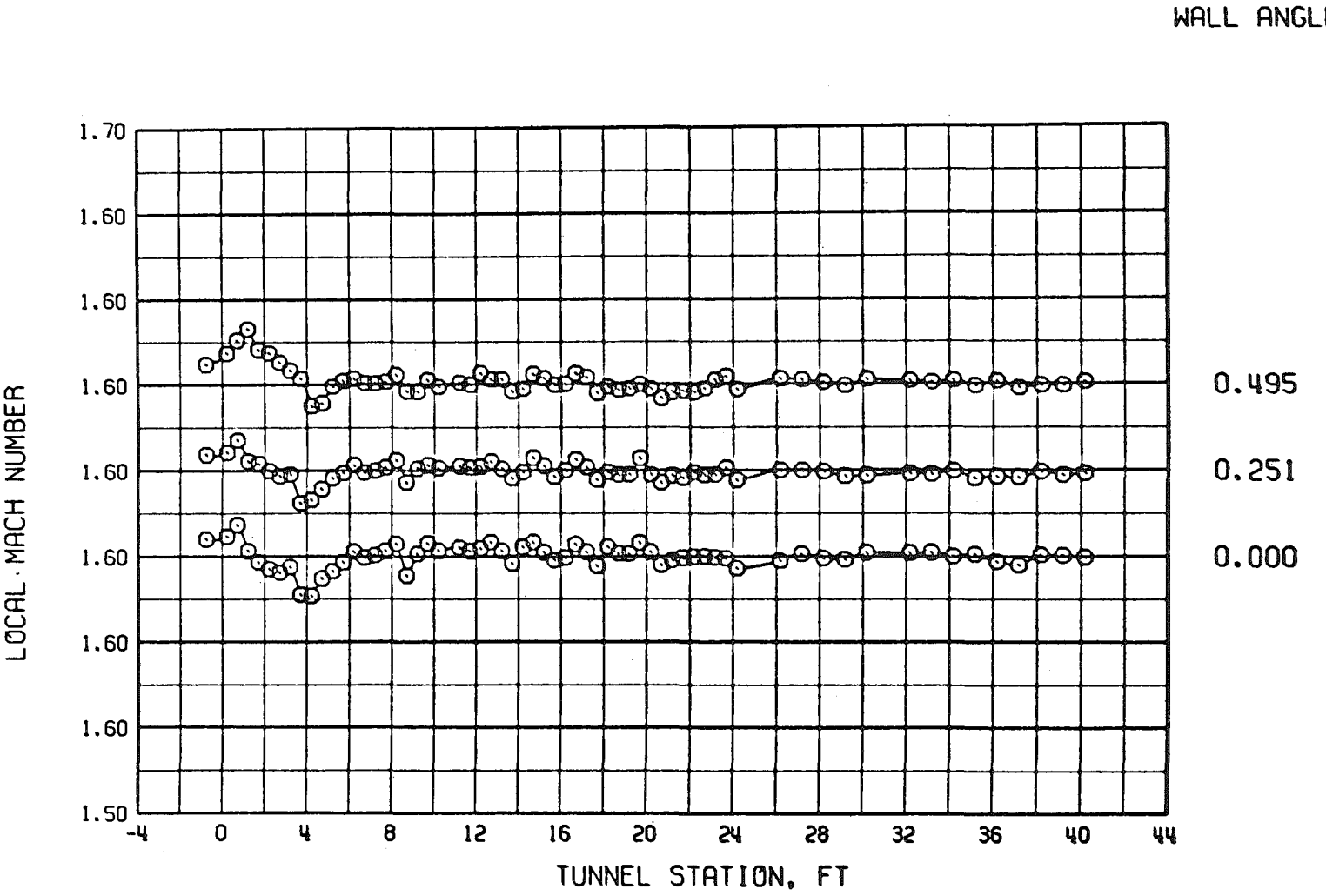

k. M = 1.6, λ = 1.50, and τ = 6

Figure 15. Concluded.

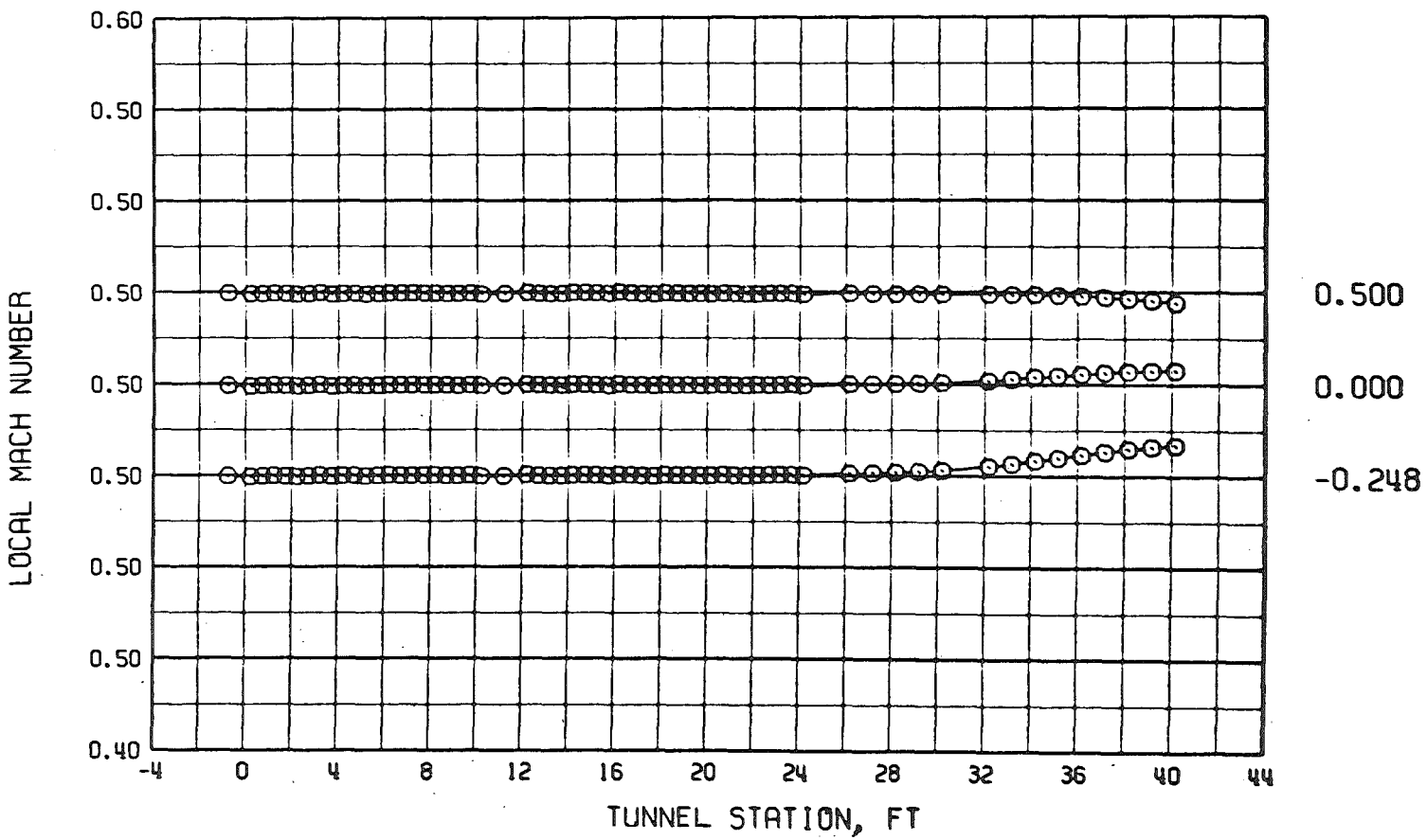

a. M = 0.5, $\lambda \cong 1.07$, and $\tau = 4$

Figure 16. Tunnel 16T centerline Mach number distributions for various test section wall angles with four-percent porosity walls and $\lambda \cong \lambda_N$.

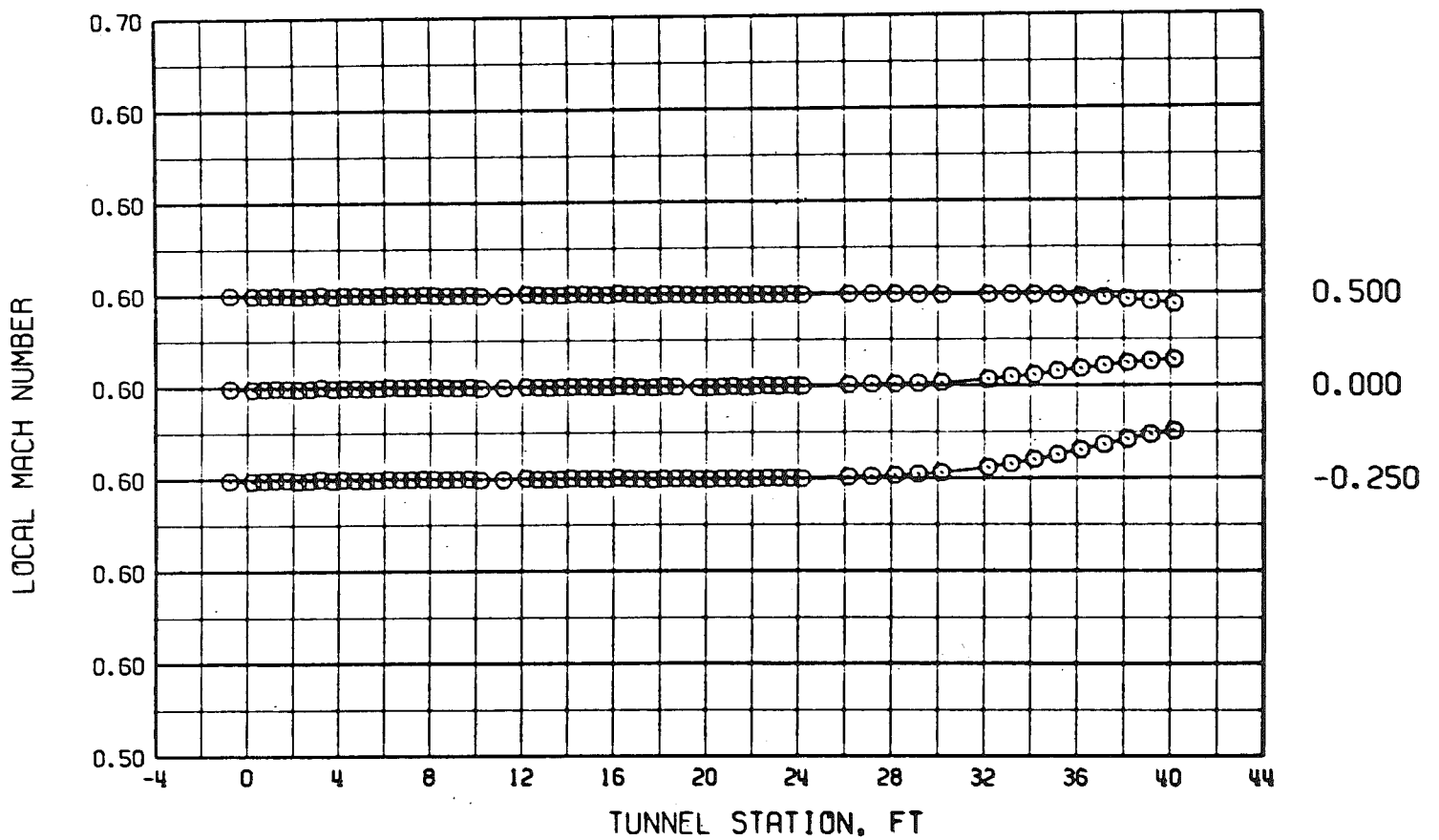

b. M = 0.6, $\lambda \cong 1.11$, and $\tau = 4$

Figure 16. Continued.

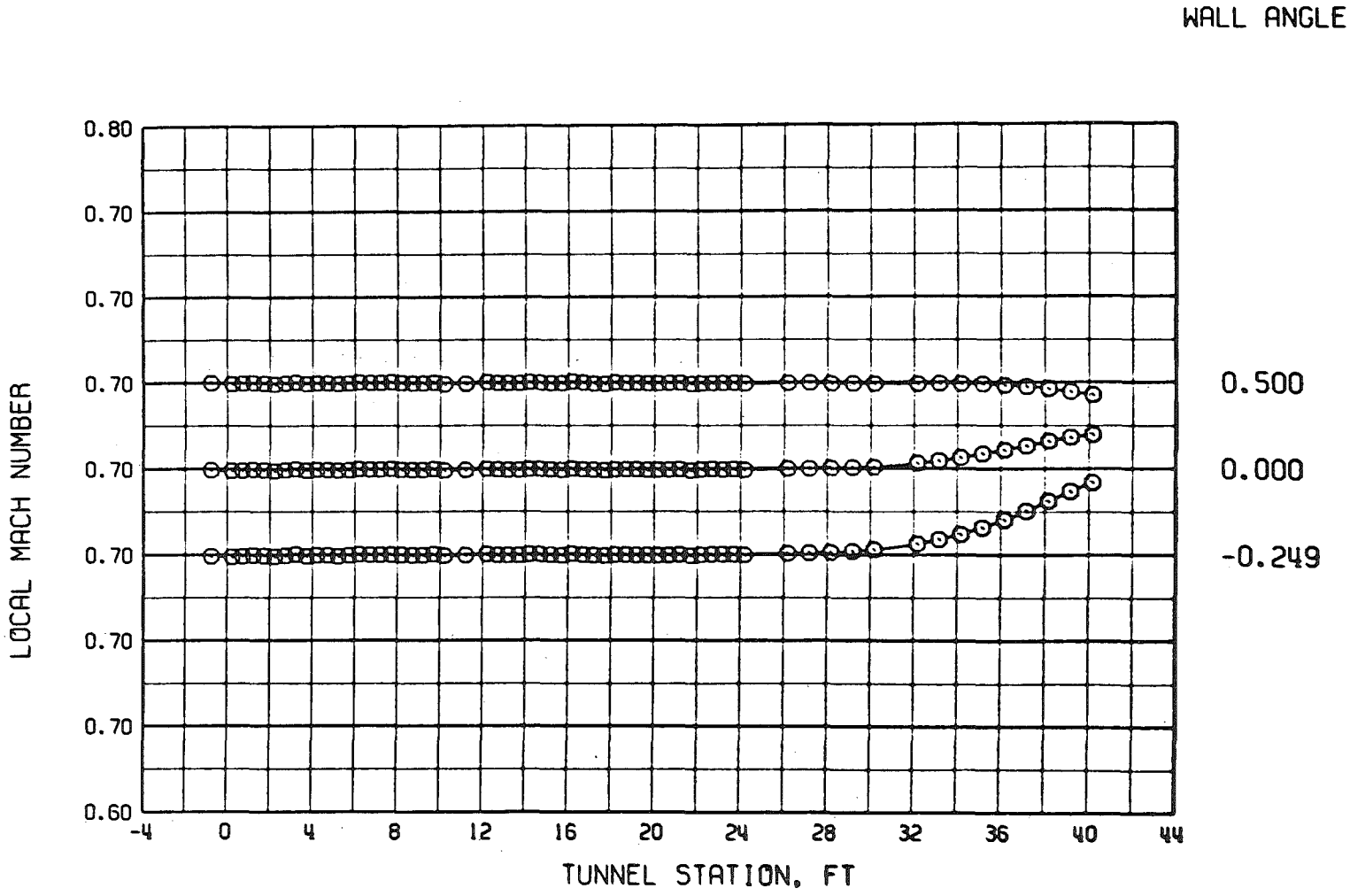

c. M = 0.7, $\lambda \cong 1.14$, and $\tau = 4$

Figure 16. Continued.

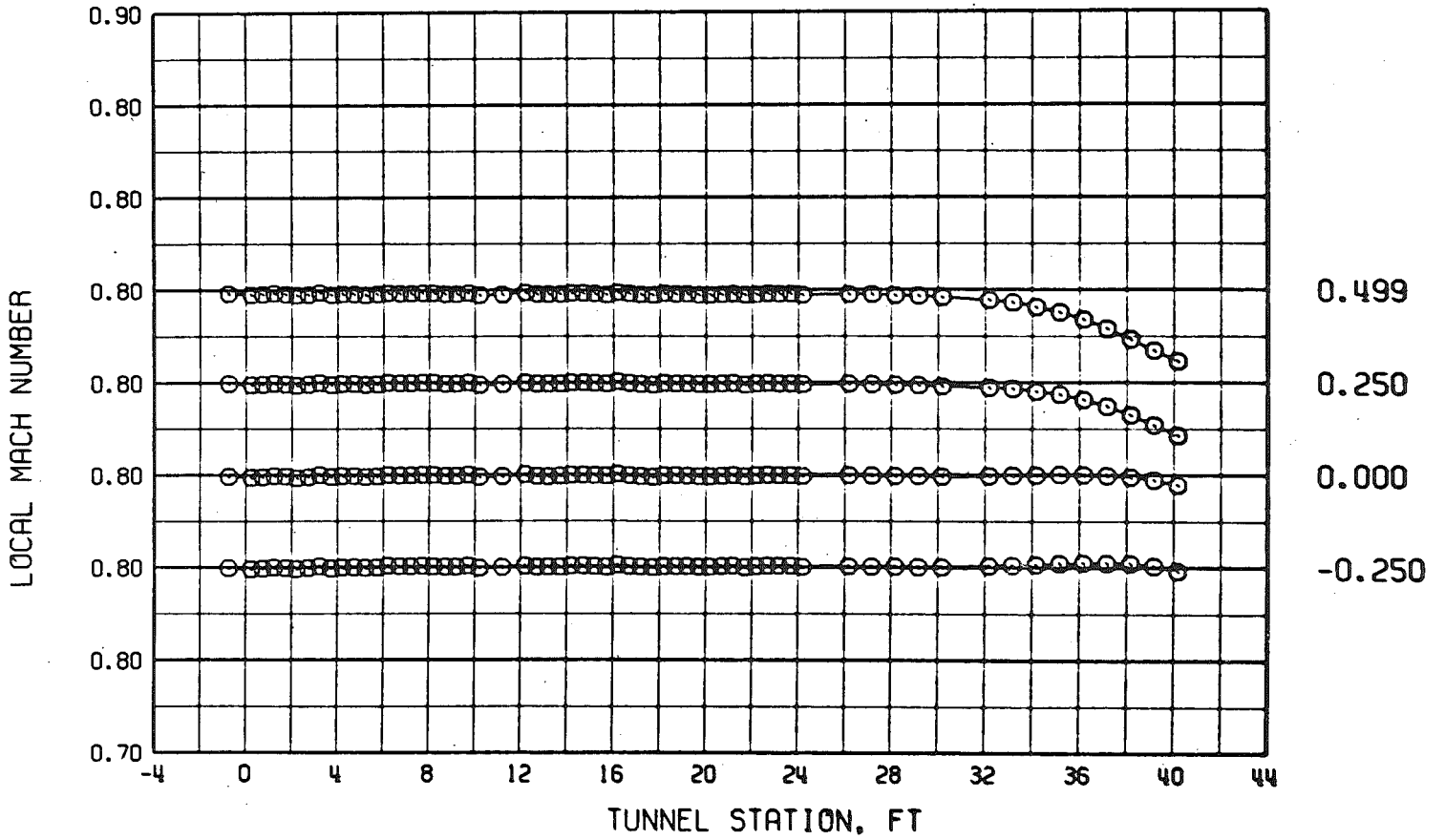

d. M = 0.8, λ = 1.14, and τ = 4

Figure 16. Continued.

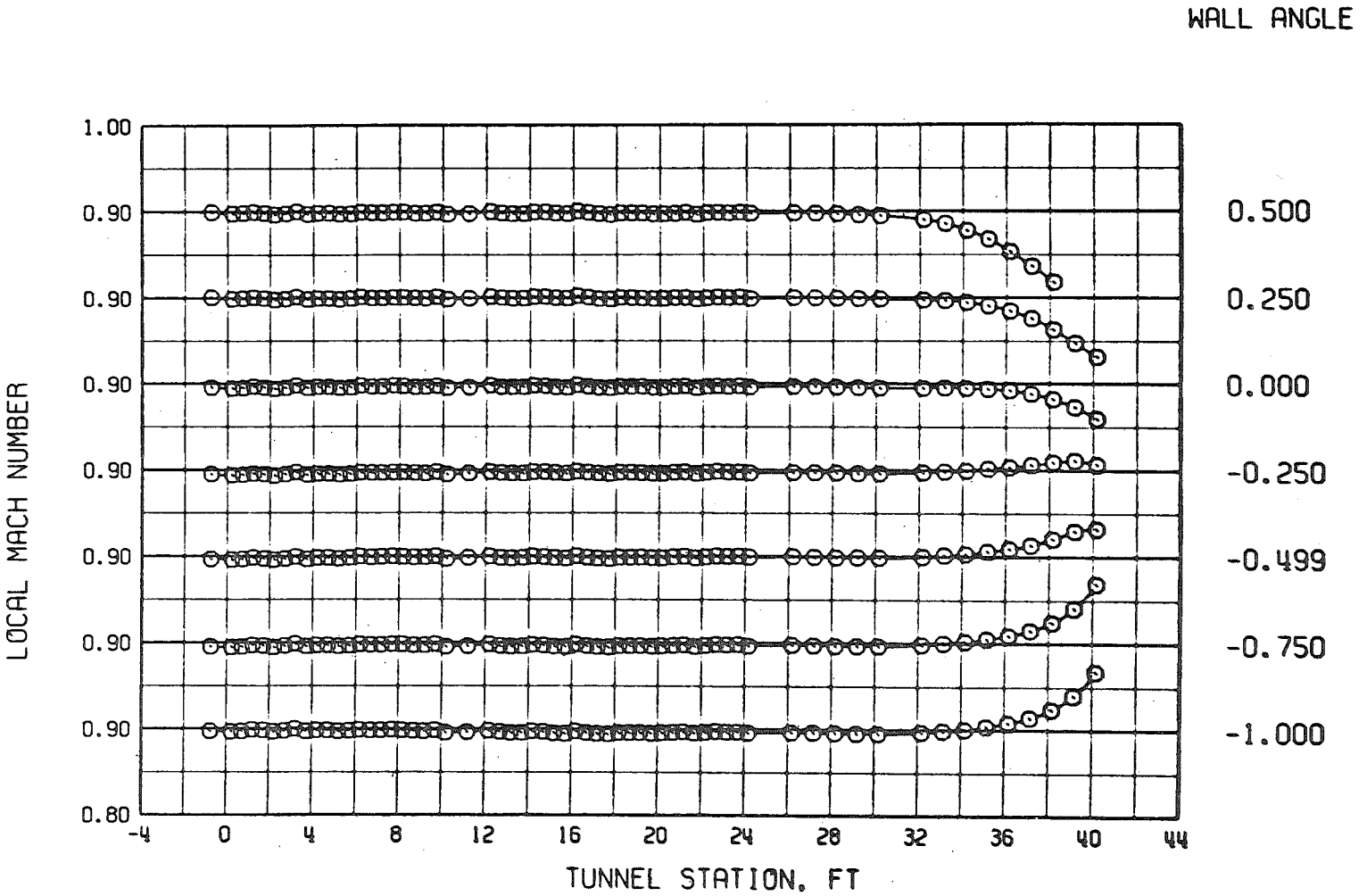

e. M = 0.9, λ = 1.16, and τ = 4

Figure 16. Continued.

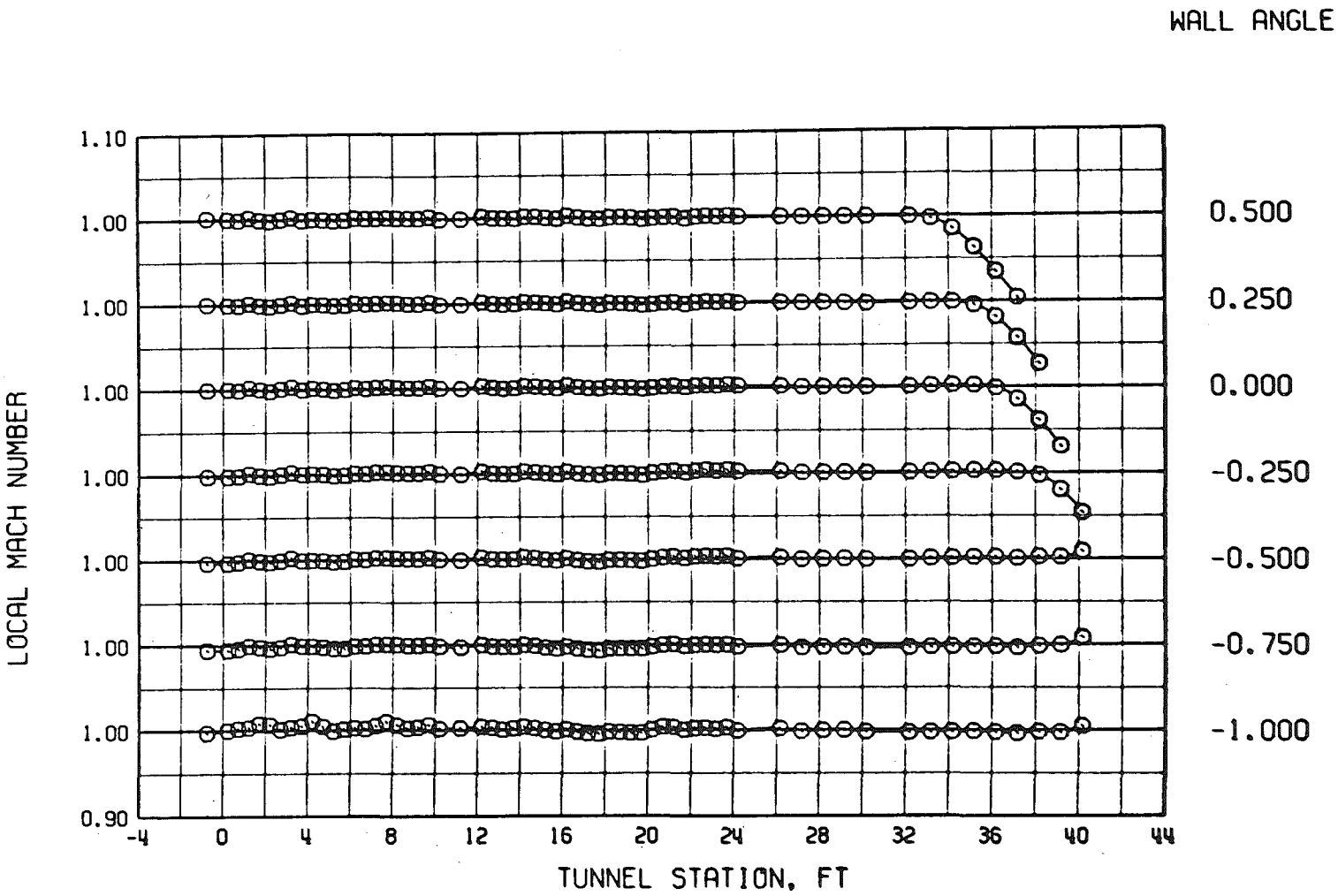

f. M = 1.0, λ = 1.17, and τ = 4

Figure 16. Continued.

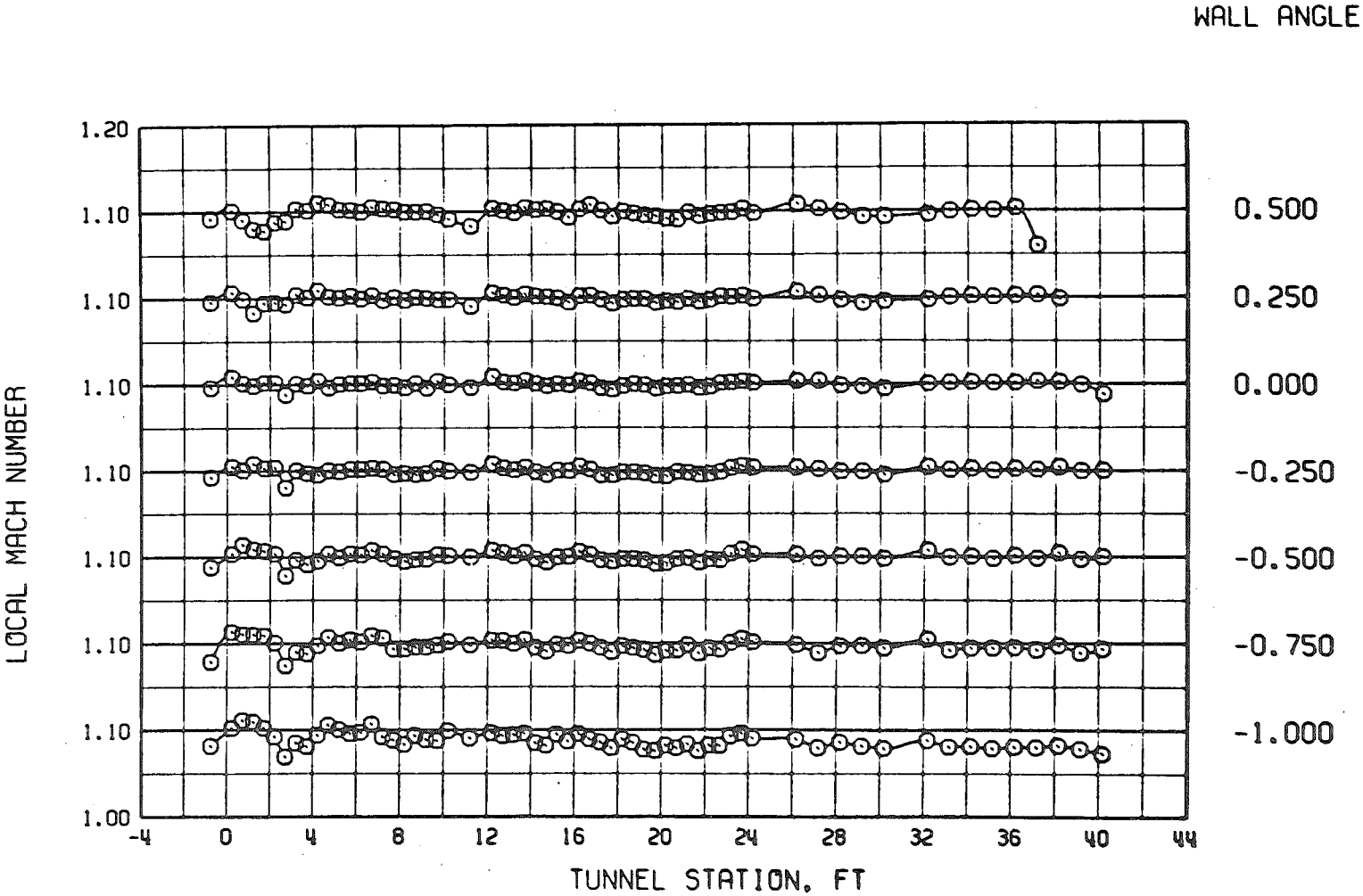

g. M = 1.1, λ = 1.19, and τ = 4

Figure 16. Continued.

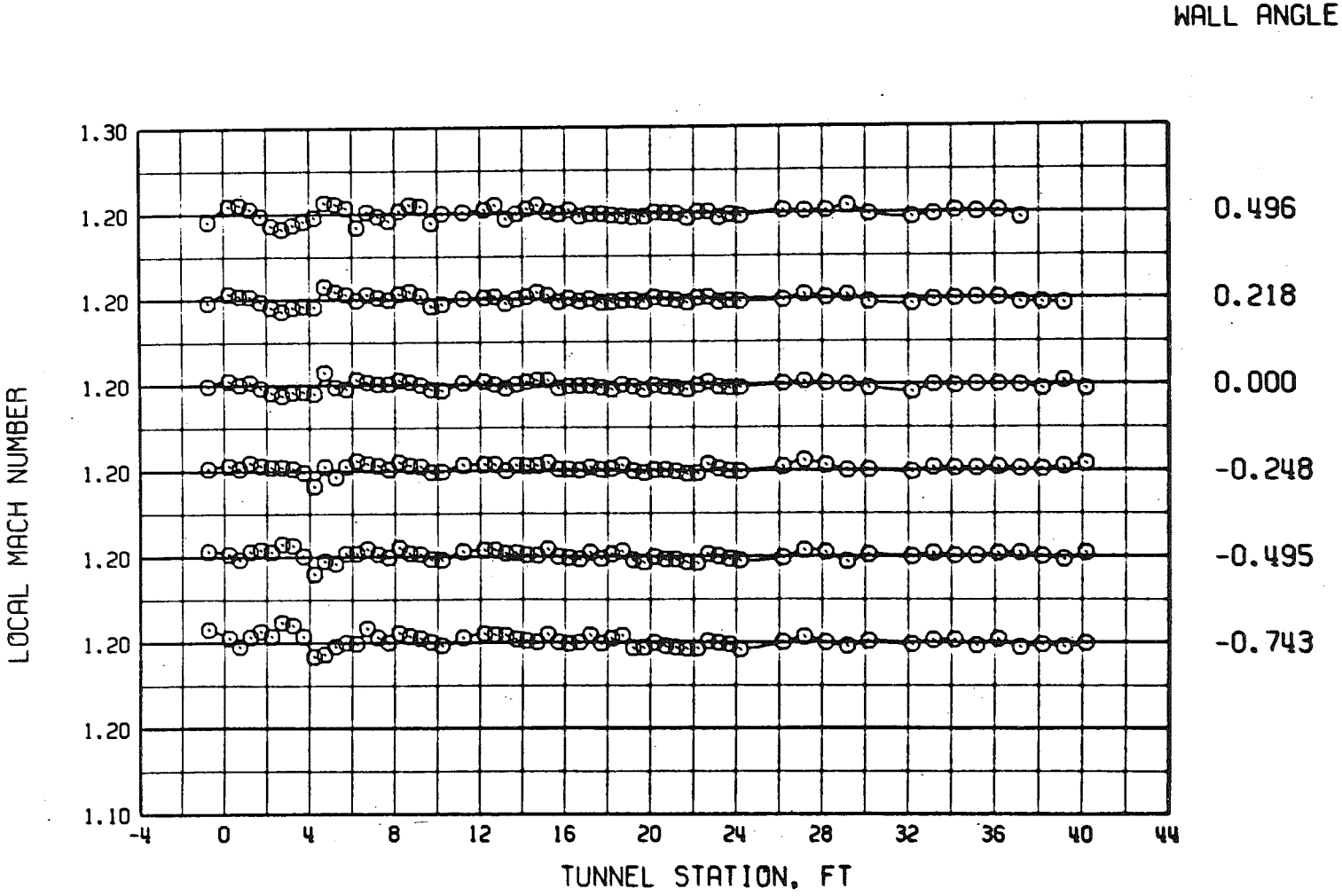

h. M = 1.2, λ = 1.20, and τ = 4

Figure 16. Continued.

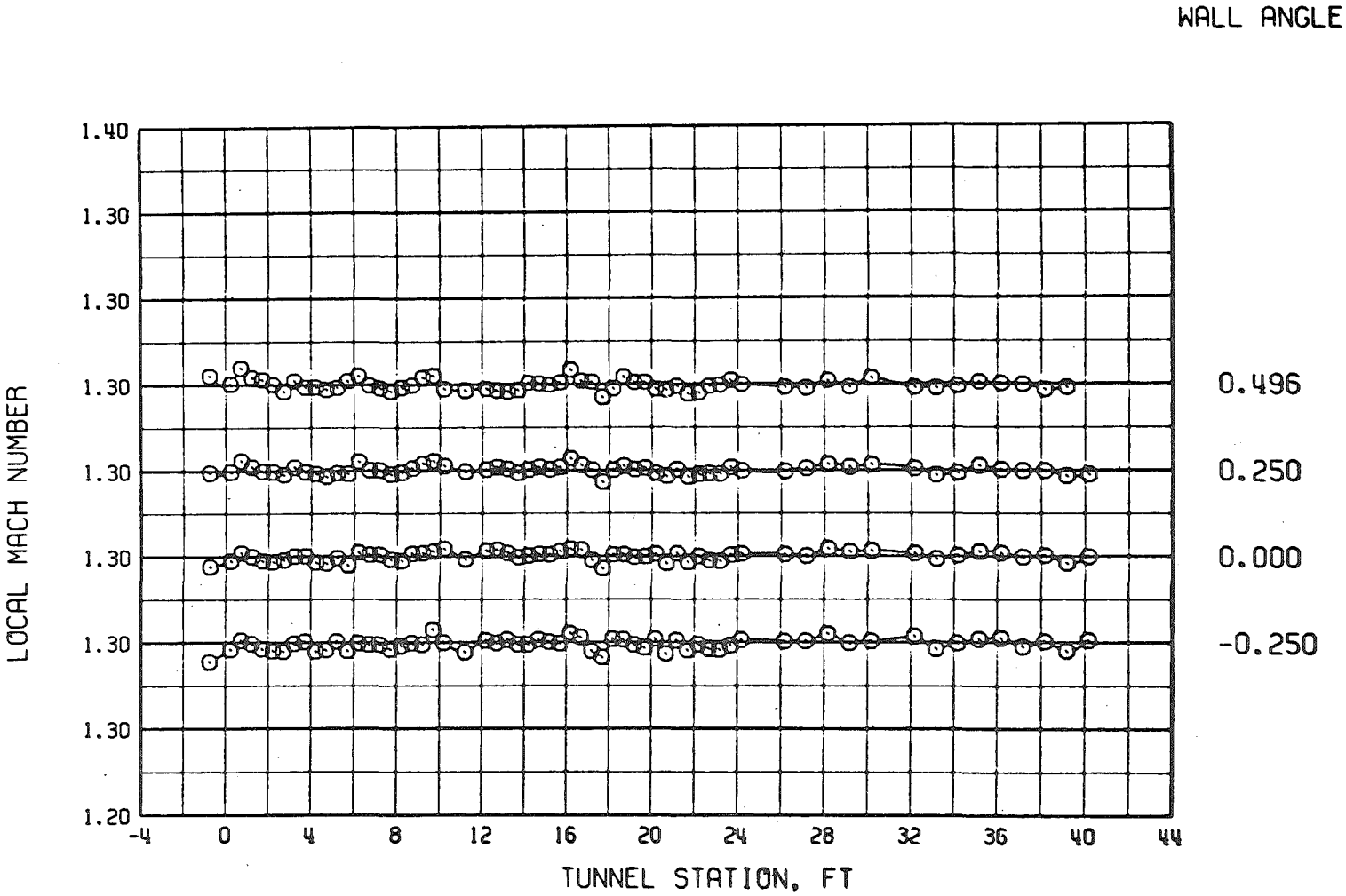

i. M = 1.3, λ = 1.24, and τ = 4

Figure 16. Continued.

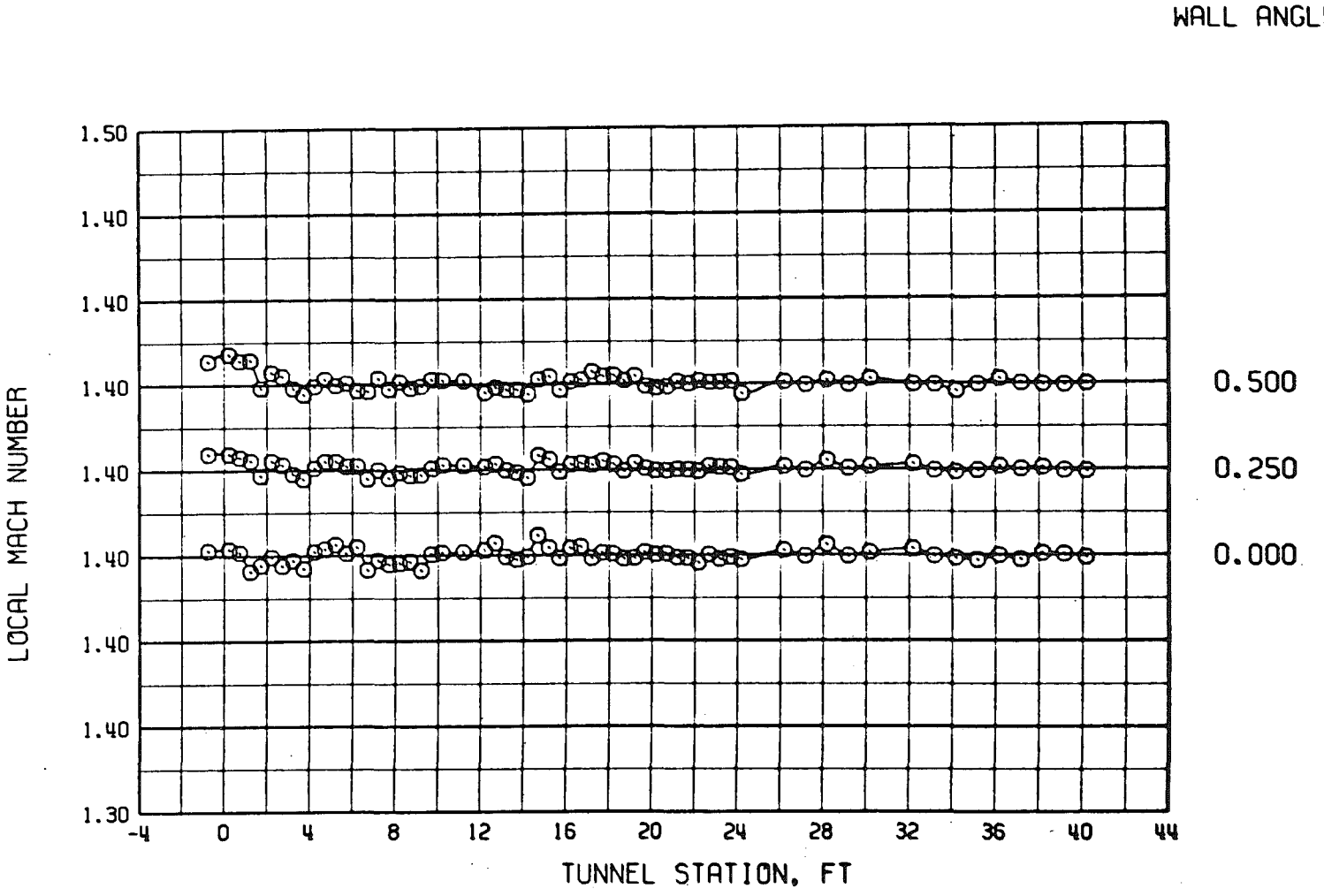

j. M = 1.40, λ = 1.30, and τ = 4

Figure 16. Continued.

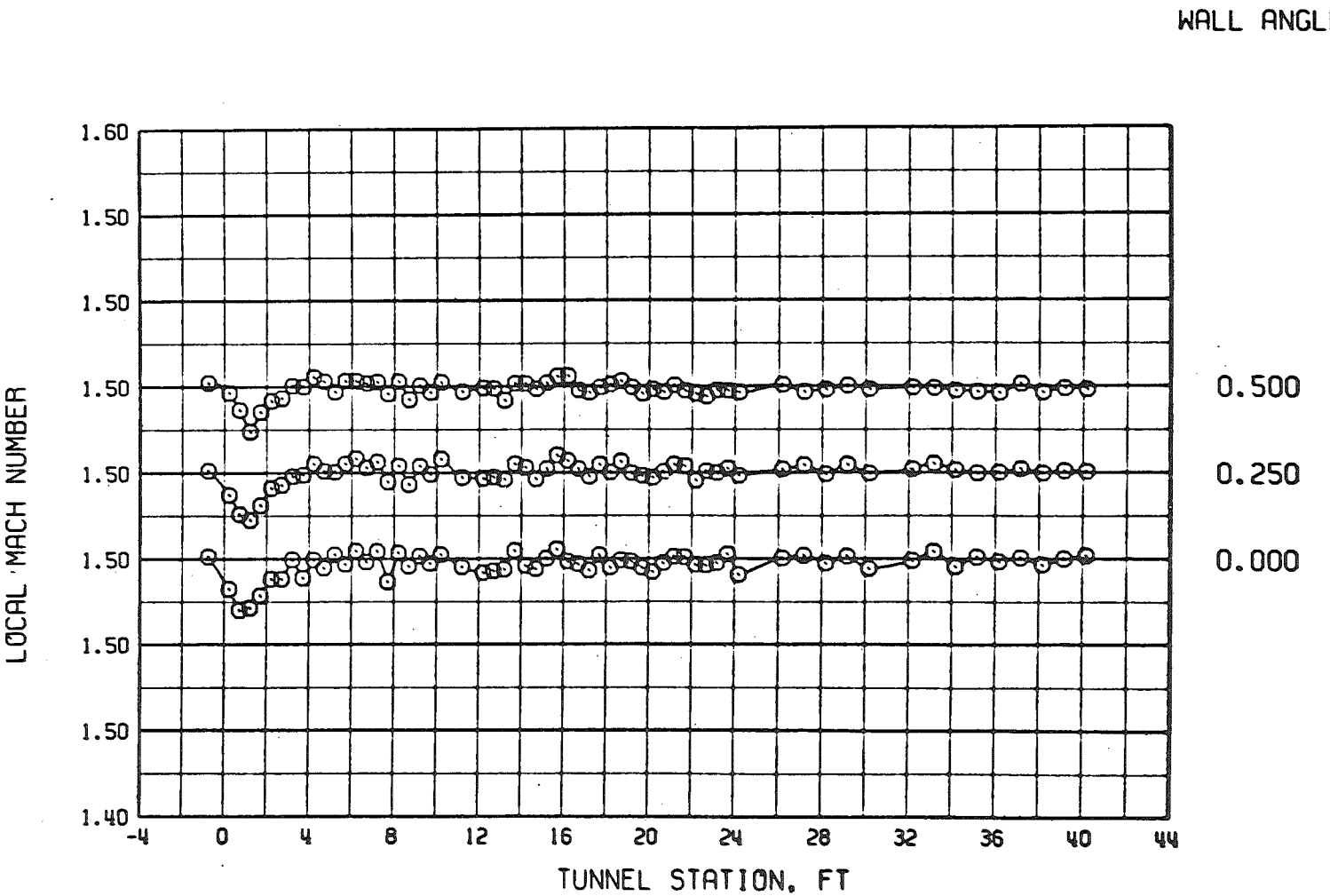

k. M = 1.5, λ = 1.40, and τ = 4

Figure 16. Continued.

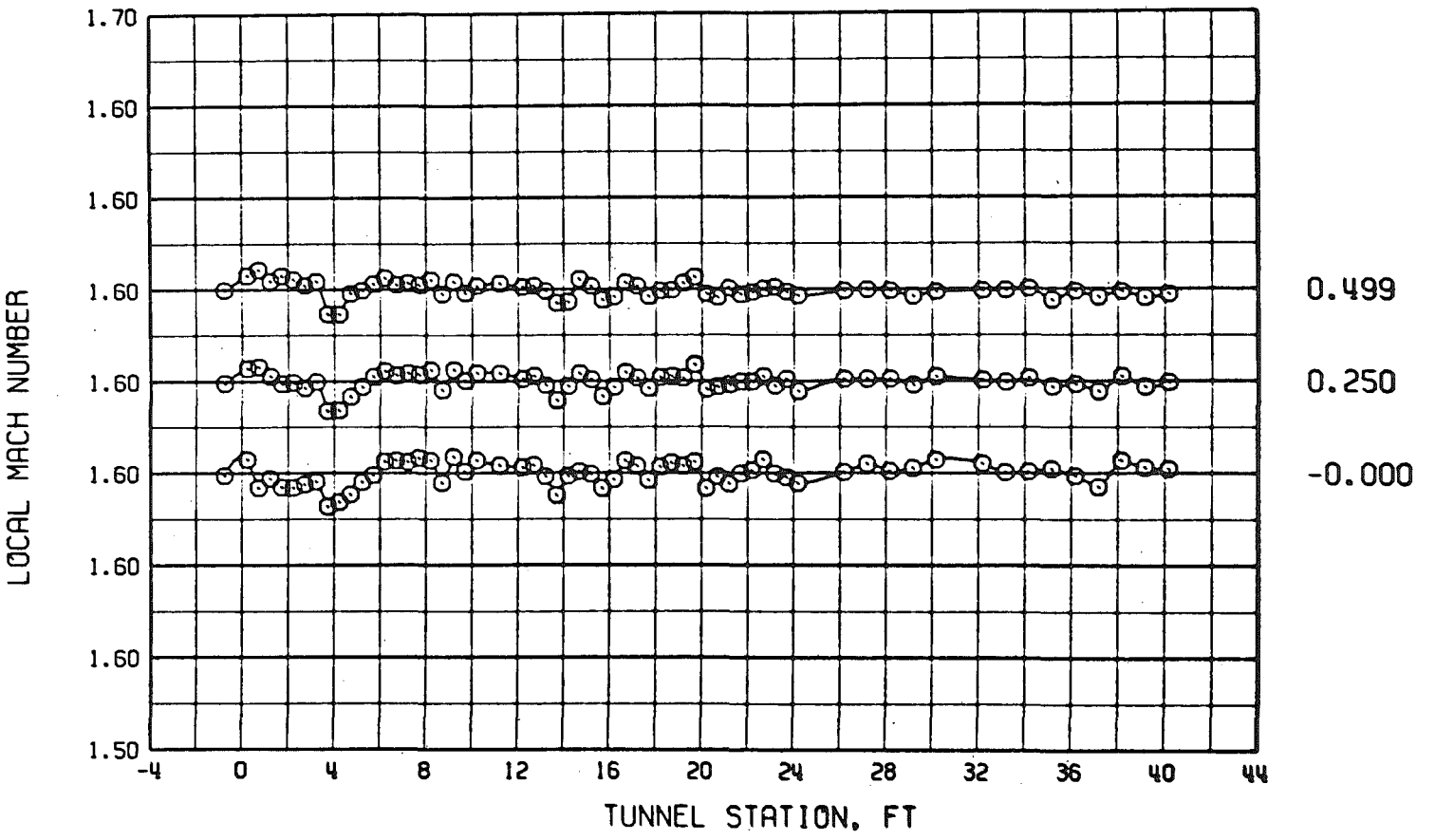

l. M = 1.6, λ = 1.50, and τ = 4

Figure 16. Concluded.

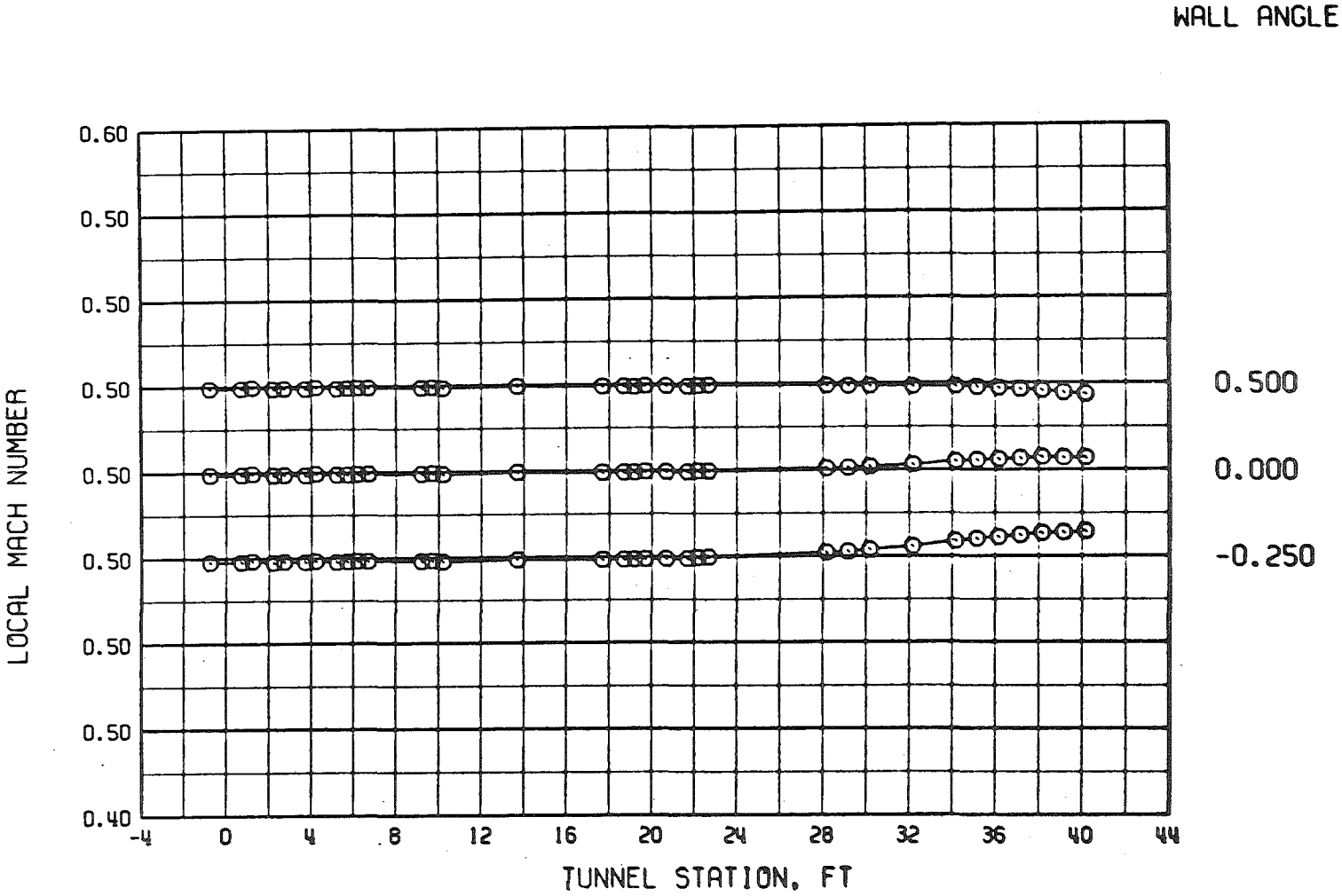

a. M = 0.5, $\lambda \cong 1.07$, and $\tau = 2$

Figure 17. Tunnel 16T centerline Mach number distributions for various test section wall angles with two-percent porosity walls and $\lambda \cong \lambda_N$.

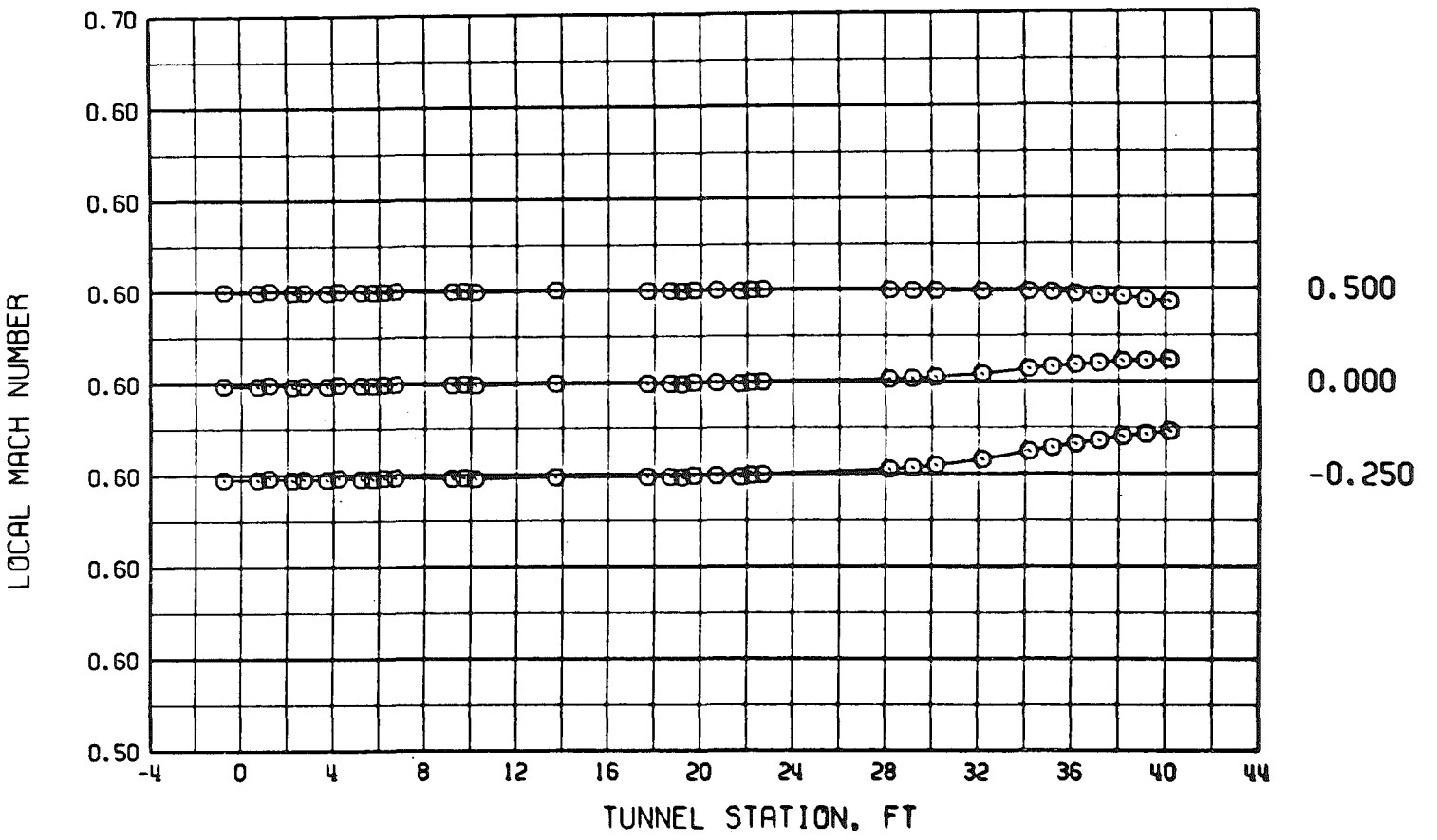

b. M = 0.6, $\lambda \cong 1.10$, and $\tau = 2$

Figure 17. Continued.

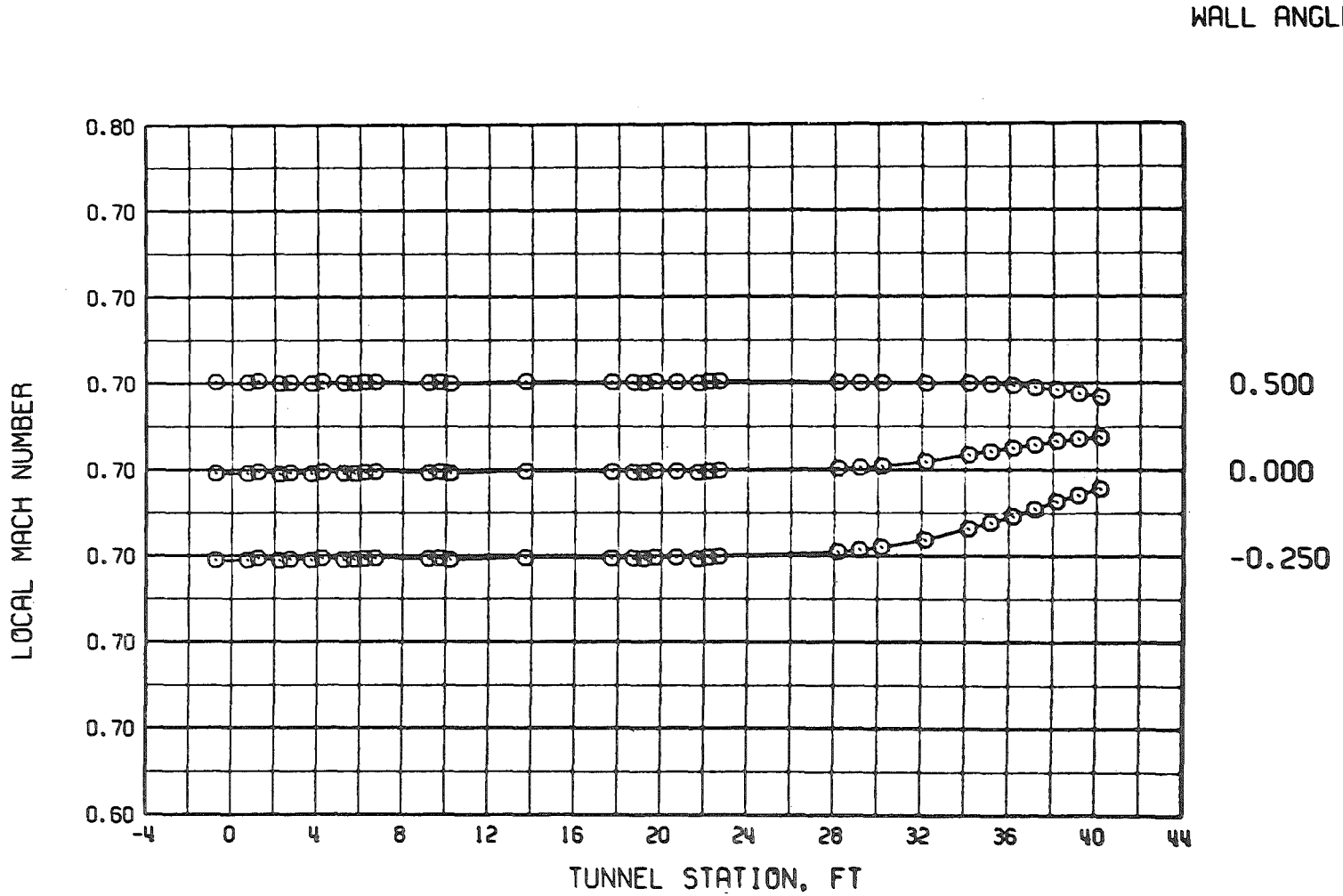

c. M = 0.7, $\lambda \cong 1.14$, and $\tau = 2$

Figure 17. Continued.

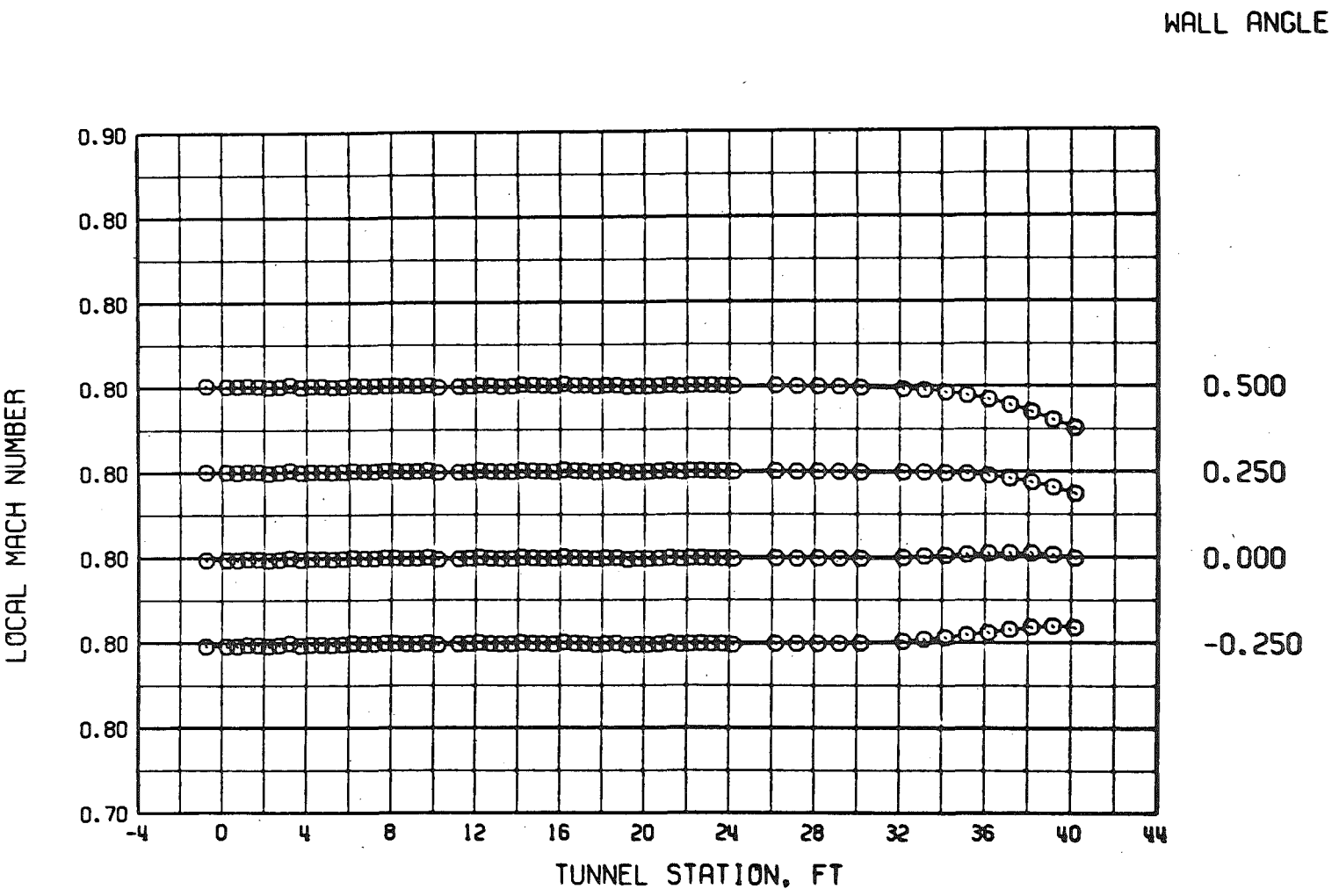

d. M = 0.8, λ = 1.15, and τ = 2

Figure 17. Continued.

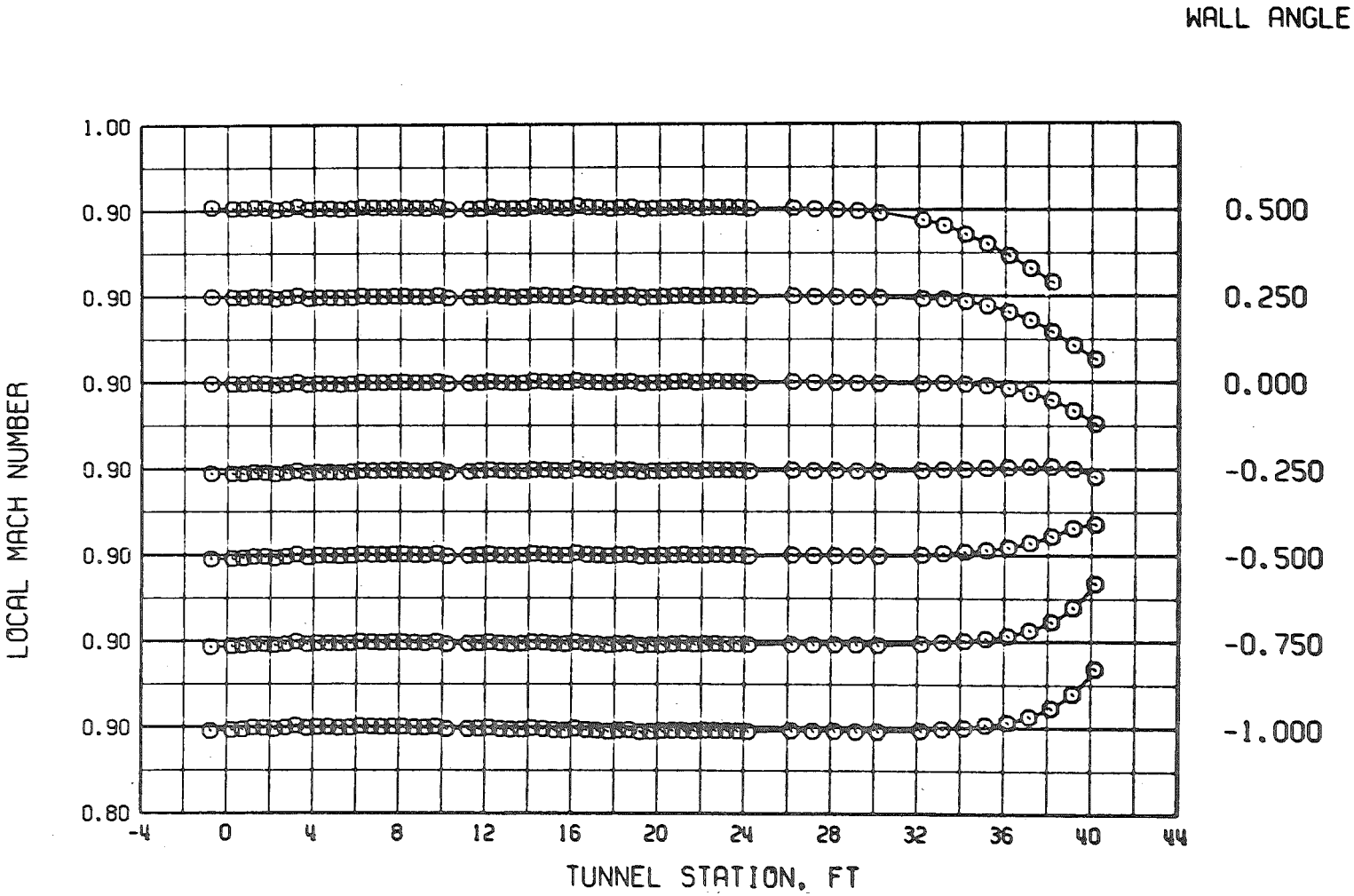

e. M = 0.9, λ = 1.16, and τ = 2

Figure 17. Continued.

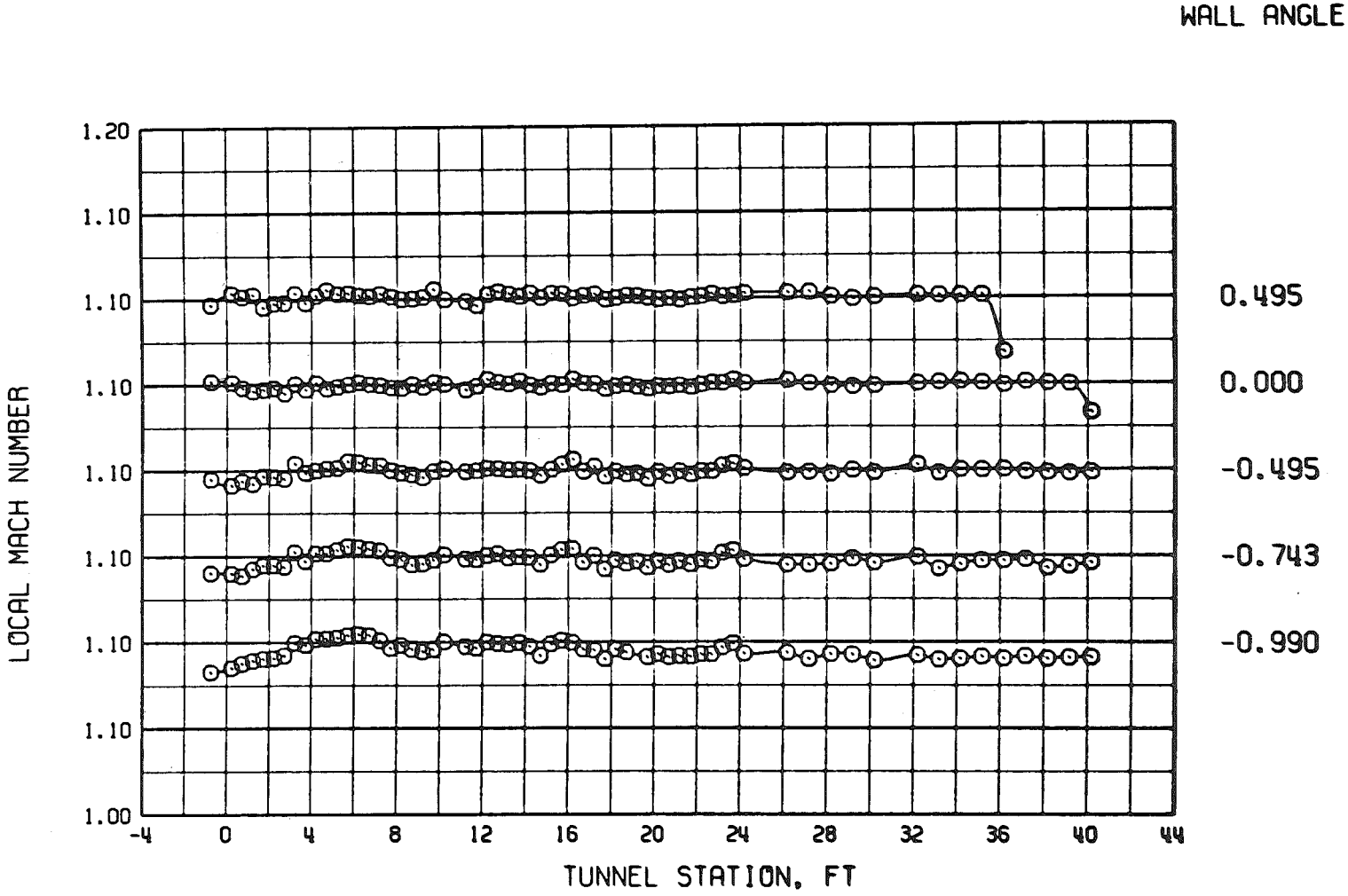

f. M = 1.1, λ = 1.19, and τ = 2

Figure 17. Continued.

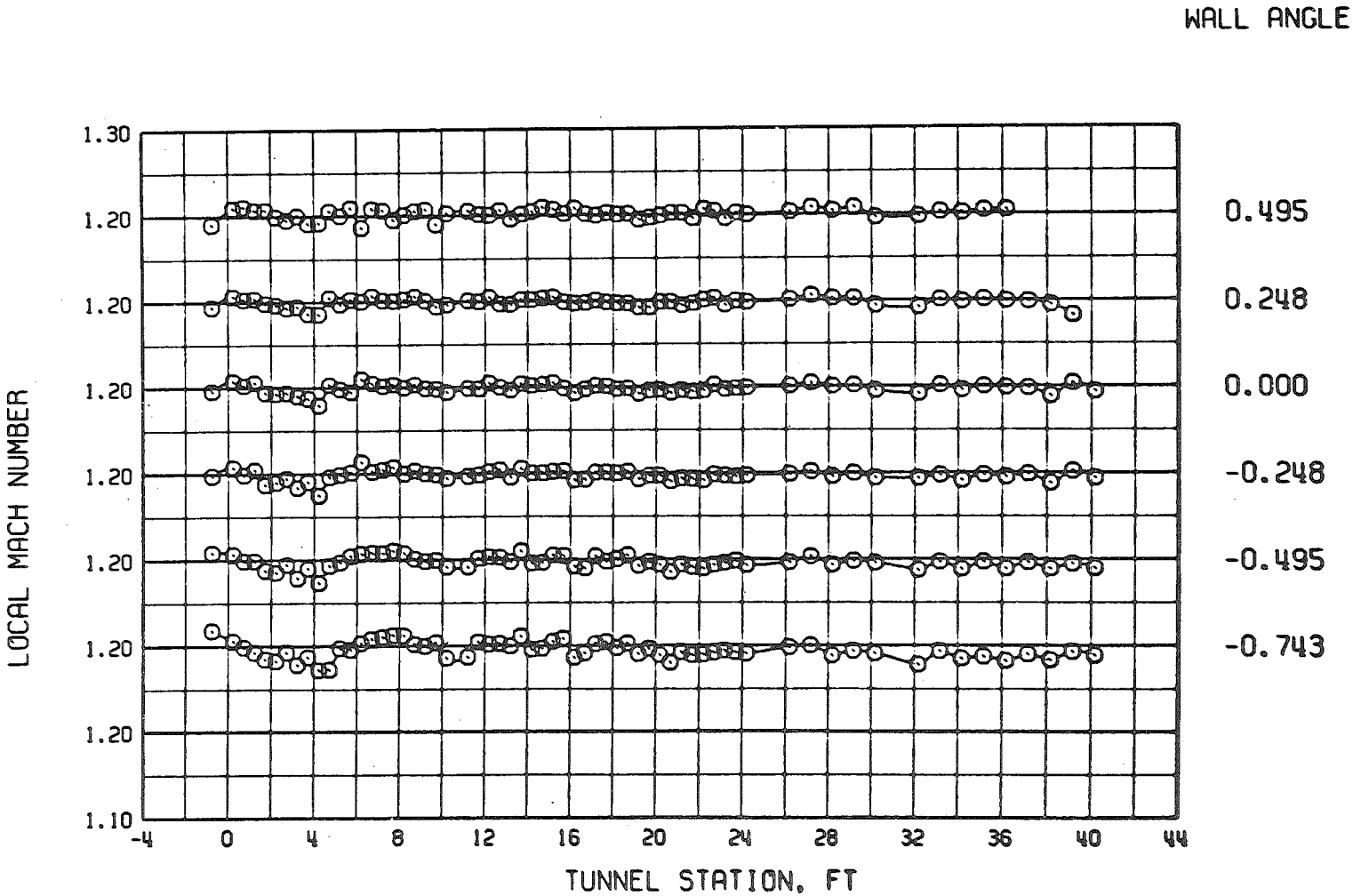

g. M = 1.2, λ = 1.20, and τ = 2

Figure 17. Continued.

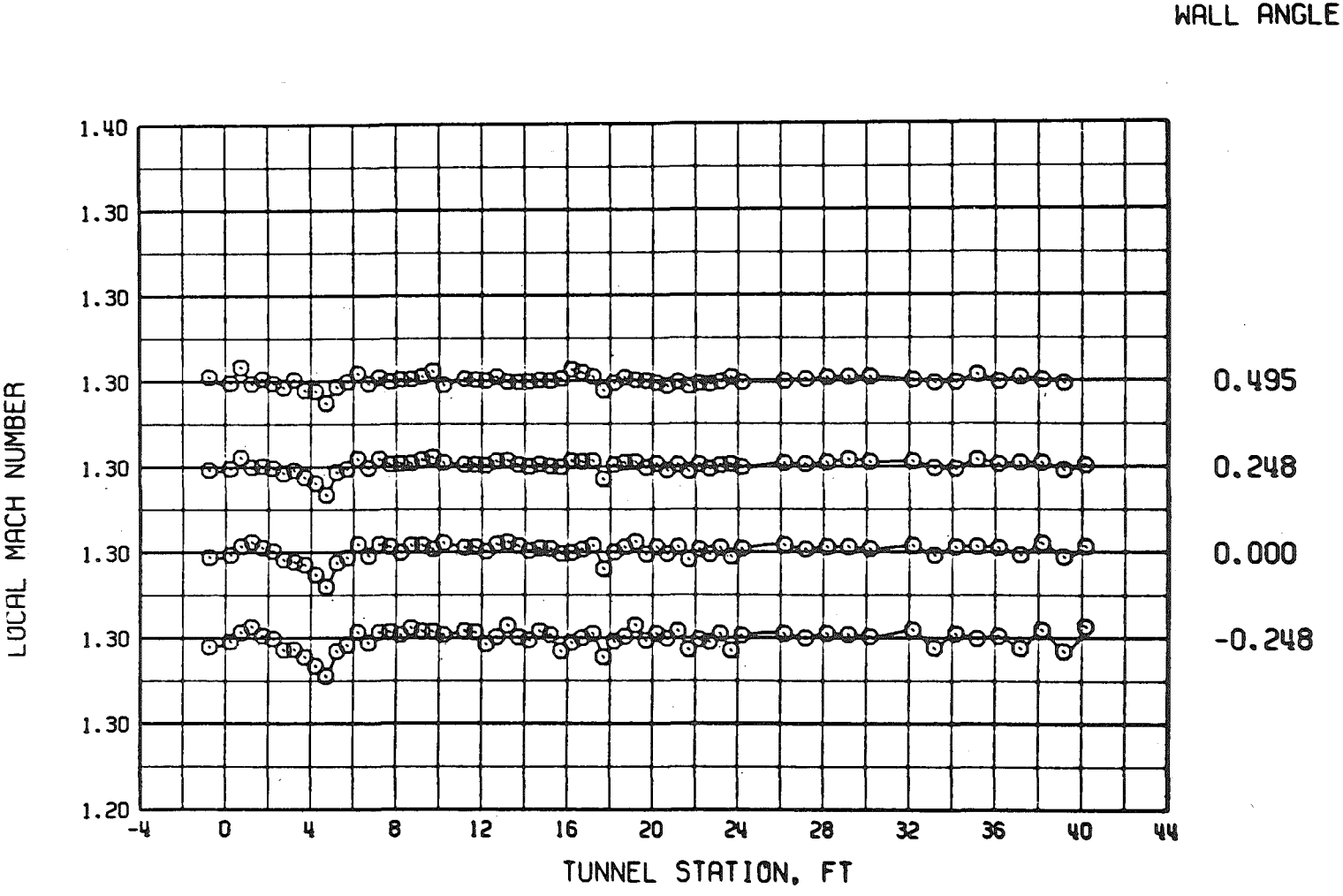

h. M = 1.3, λ = 1.25, and τ = 2

Figure 17. Continued.

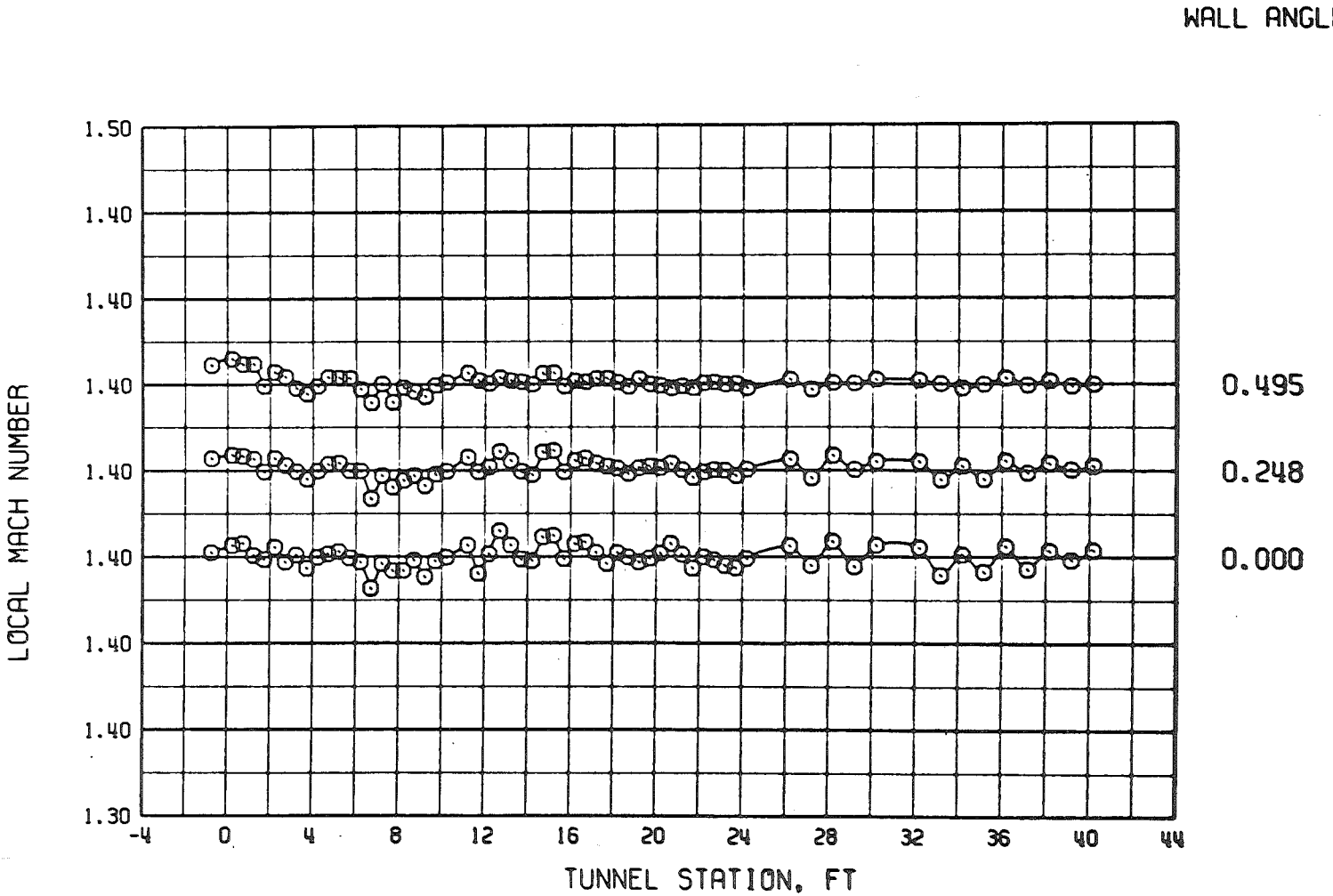

i. M = 1.4, λ = 1.30, and τ = 2

Figure 17. Continued.

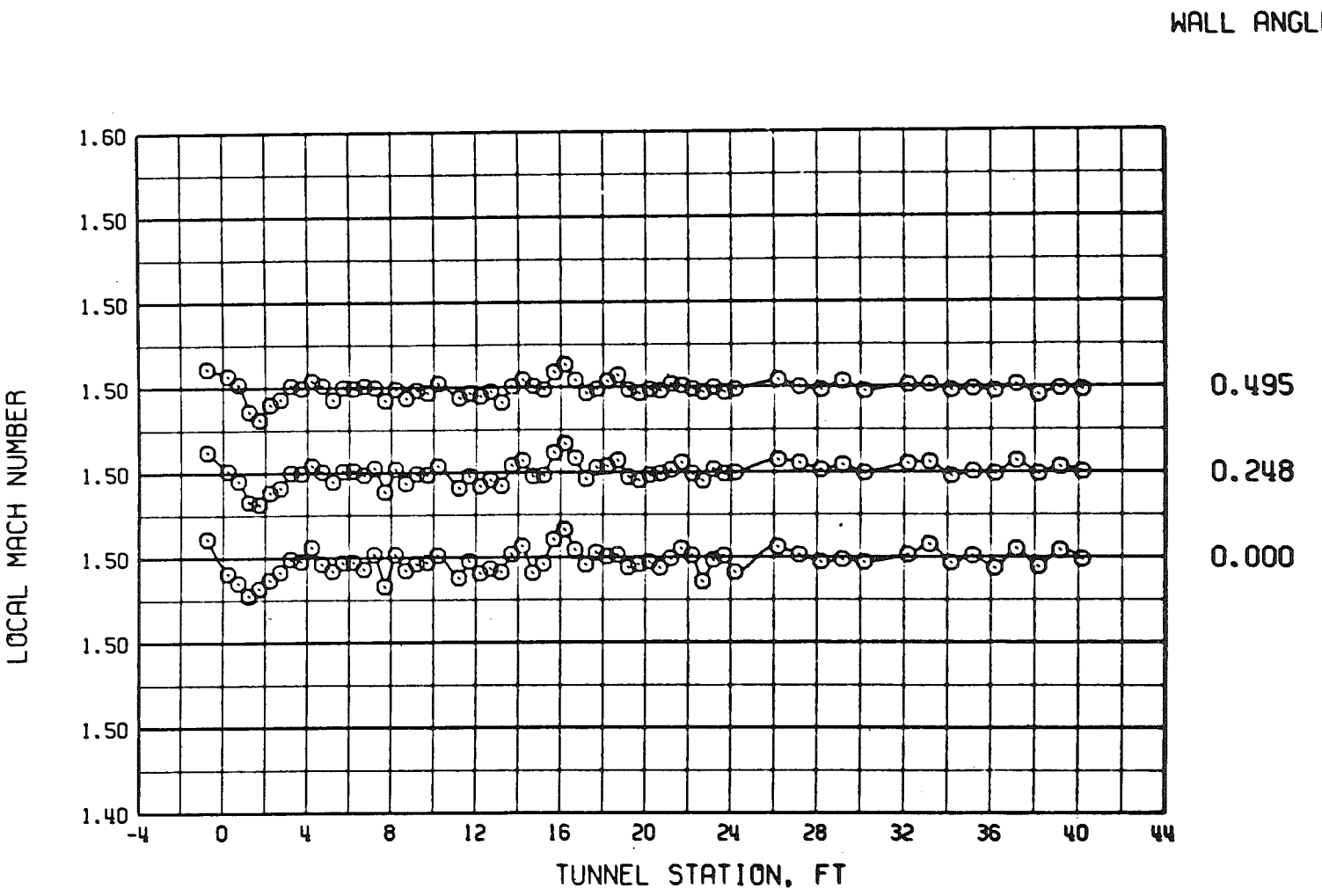

j. M = 1.5, λ = 1.39, and τ = 2

Figure 17. Continued.

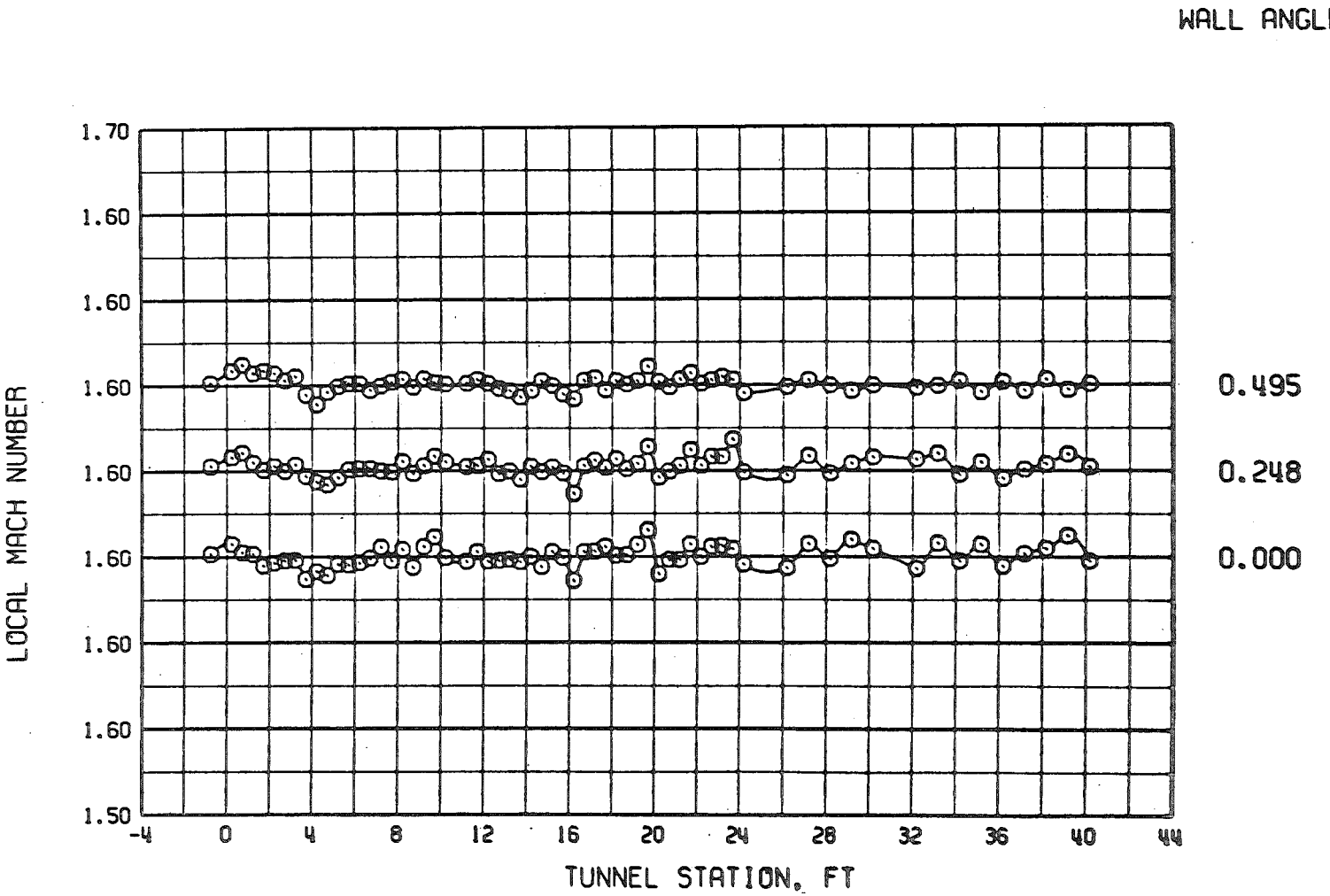

k. M = 1.6, λ = 1.50, and τ = 2

Figure 17. Concluded.

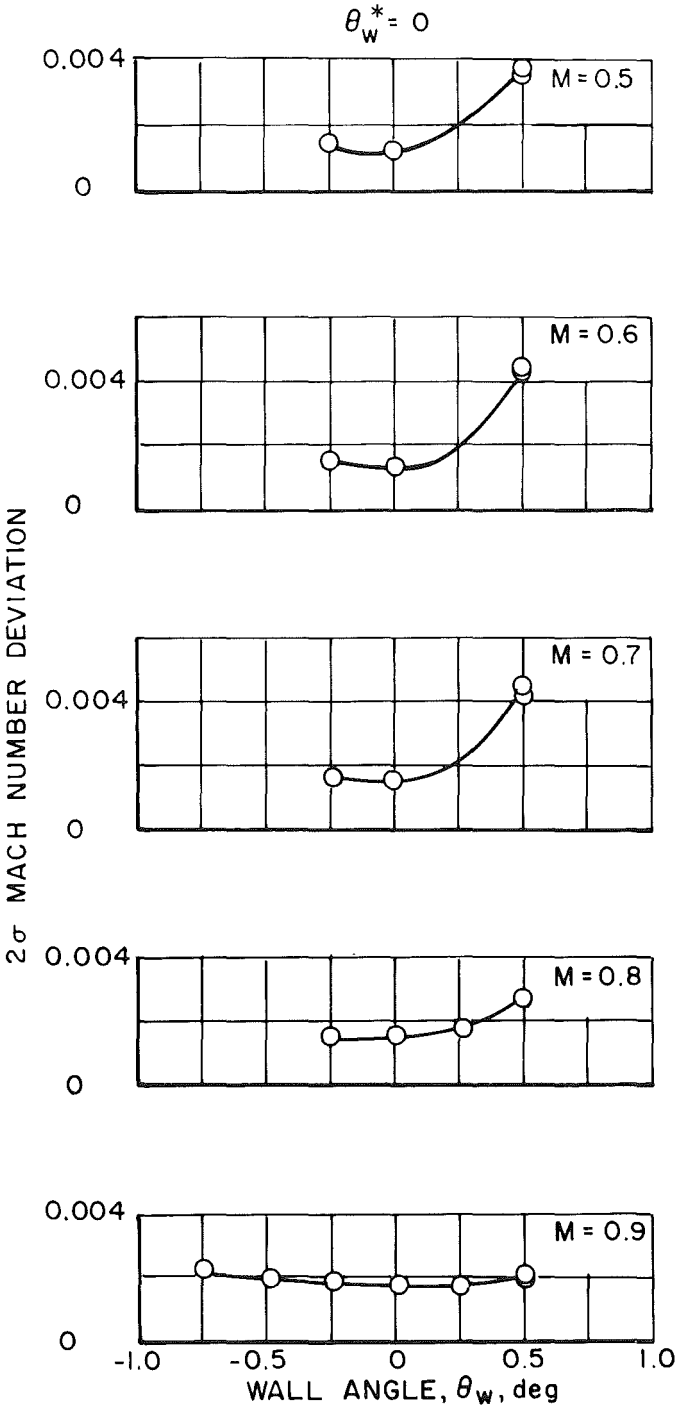

a. $\tau = 6$

Figure 18. Effect of test section wall angle variation upon the 2σ Mach number deviations for tunnel station 8.2 to 28.2 at $\lambda = \lambda_N$ and M = 0.5 to 0.9.

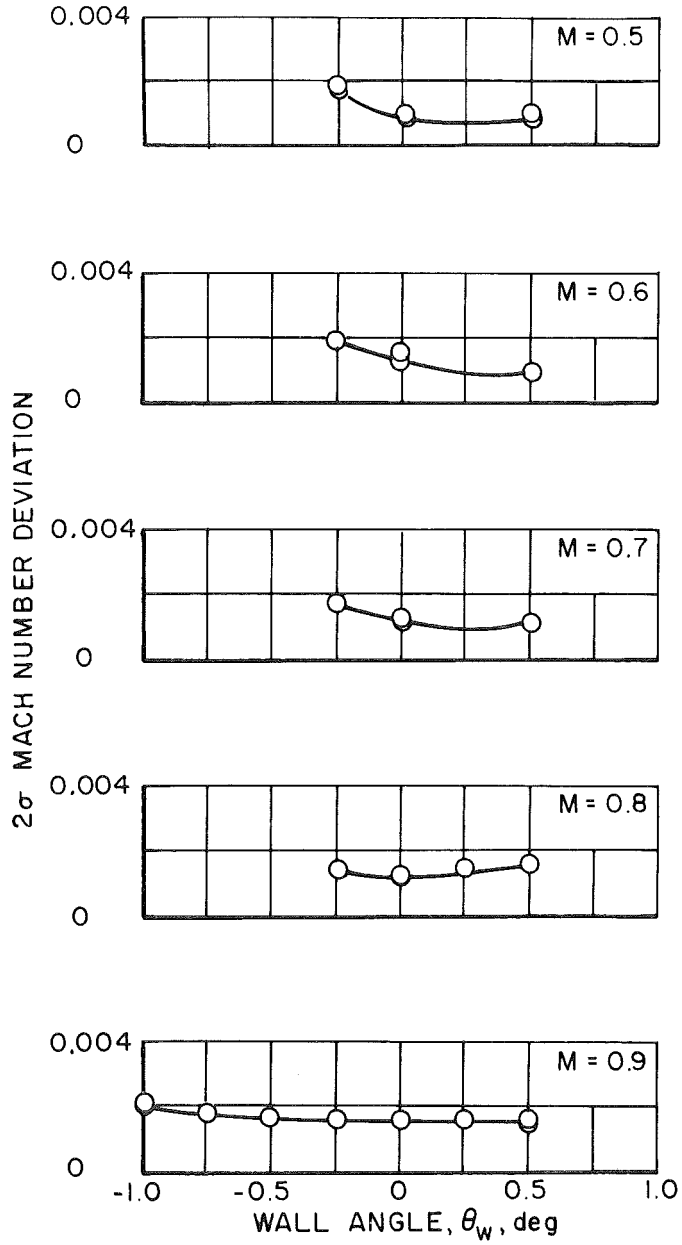

b. $\tau = 4$

Figure 18. Continued.

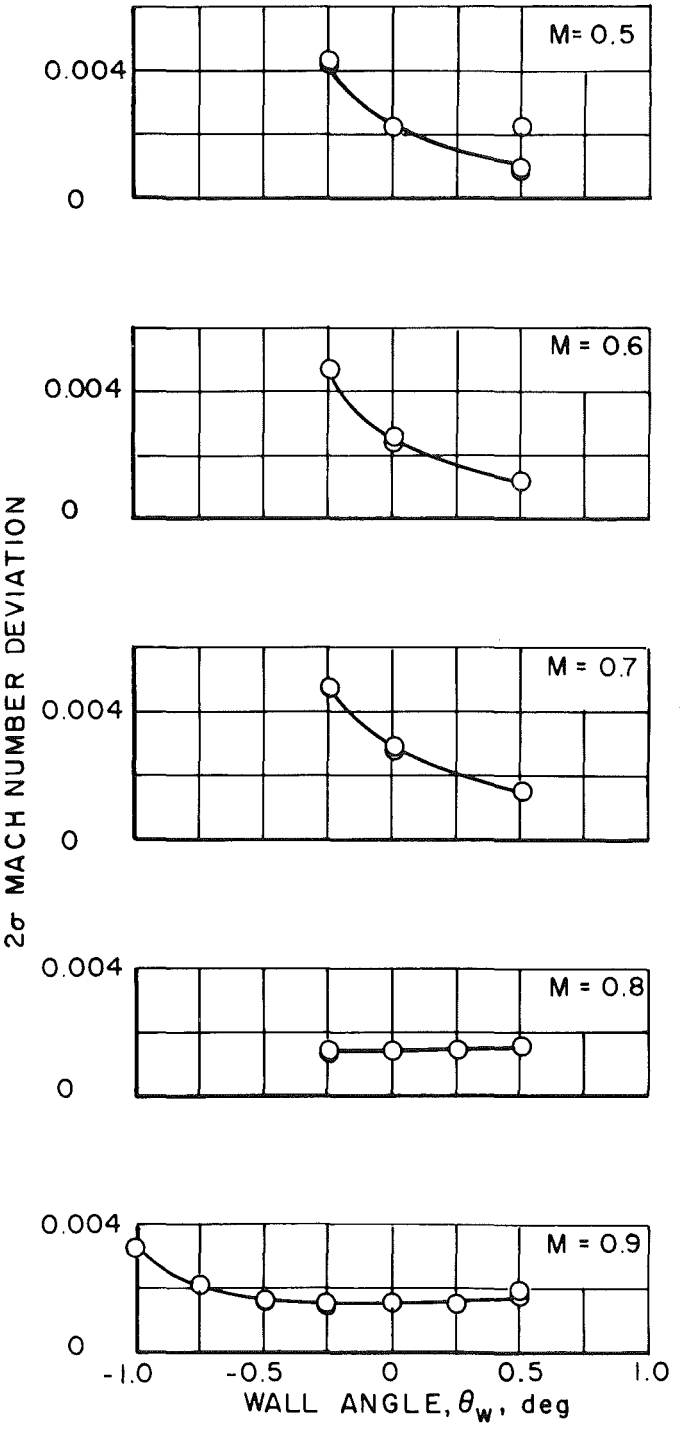

c. $\tau = 2$

Figure 18. Concluded.

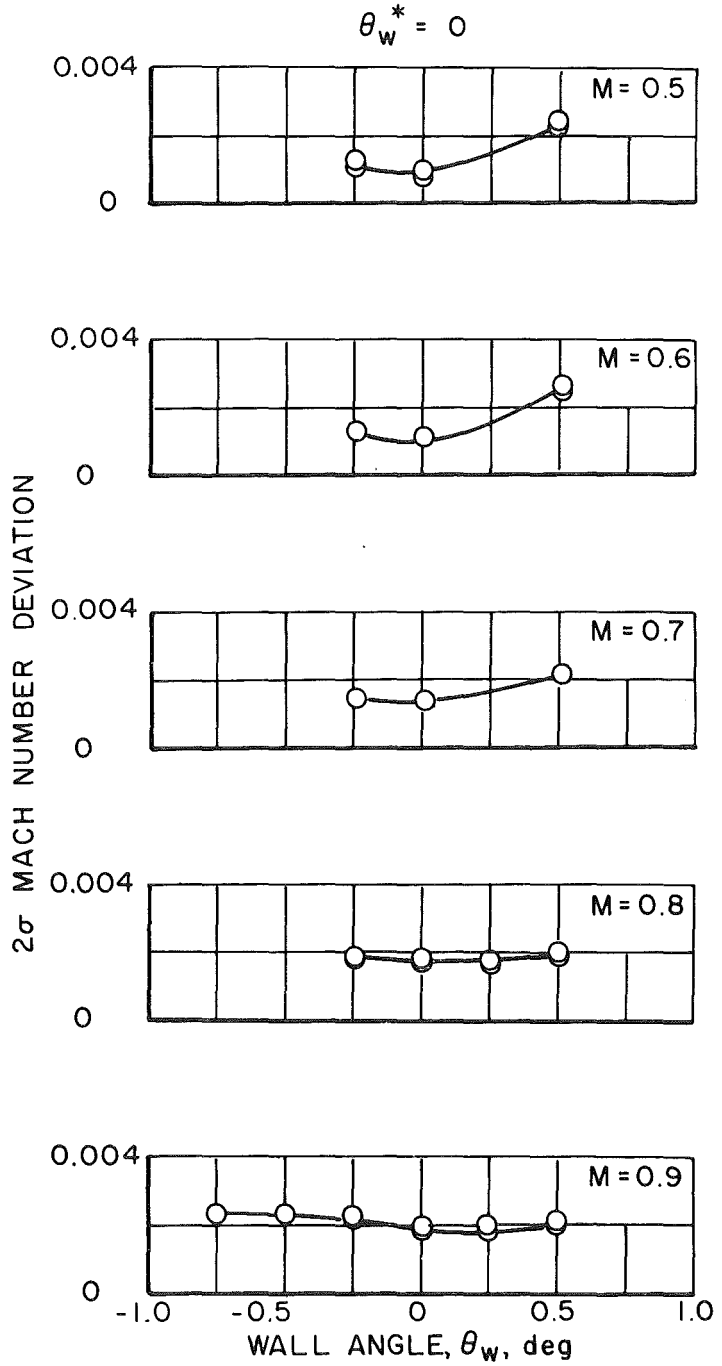

a. $\tau = 6$

Figure 19. Effect of test section wall angle variation upon the 2σ Mach number deviations for tunnel station 1.2 to 20.2 at $\lambda = \lambda_N$ and M = 0.5 to 0.9.

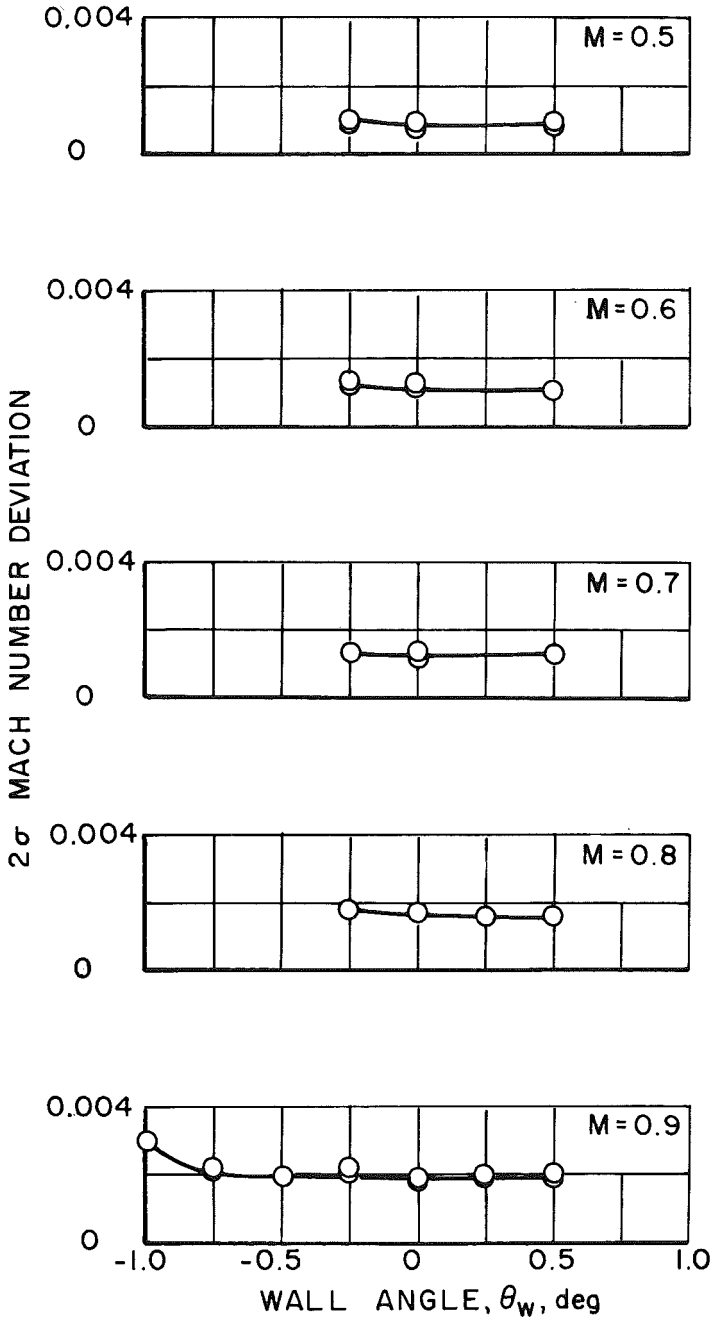

b. $\tau = 4$

Figure 19. Continued.

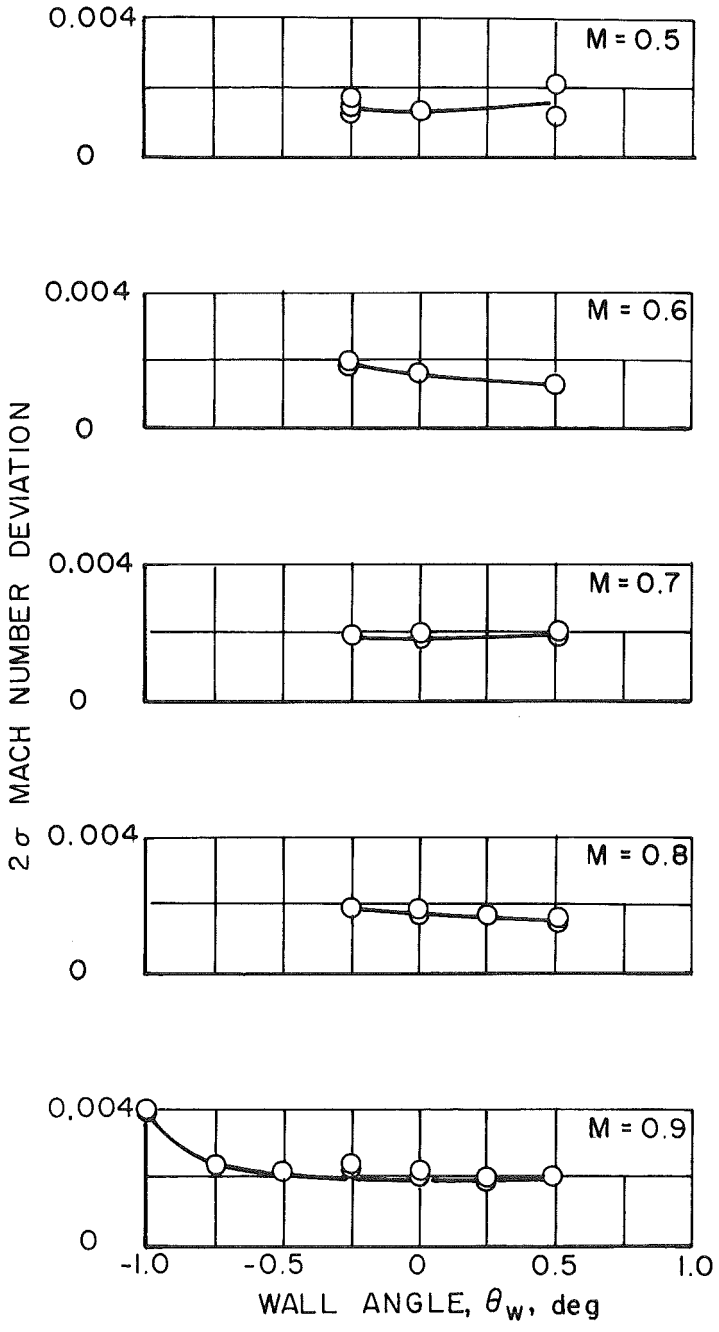

c. $\tau = 2$

Figure 19. Concluded.

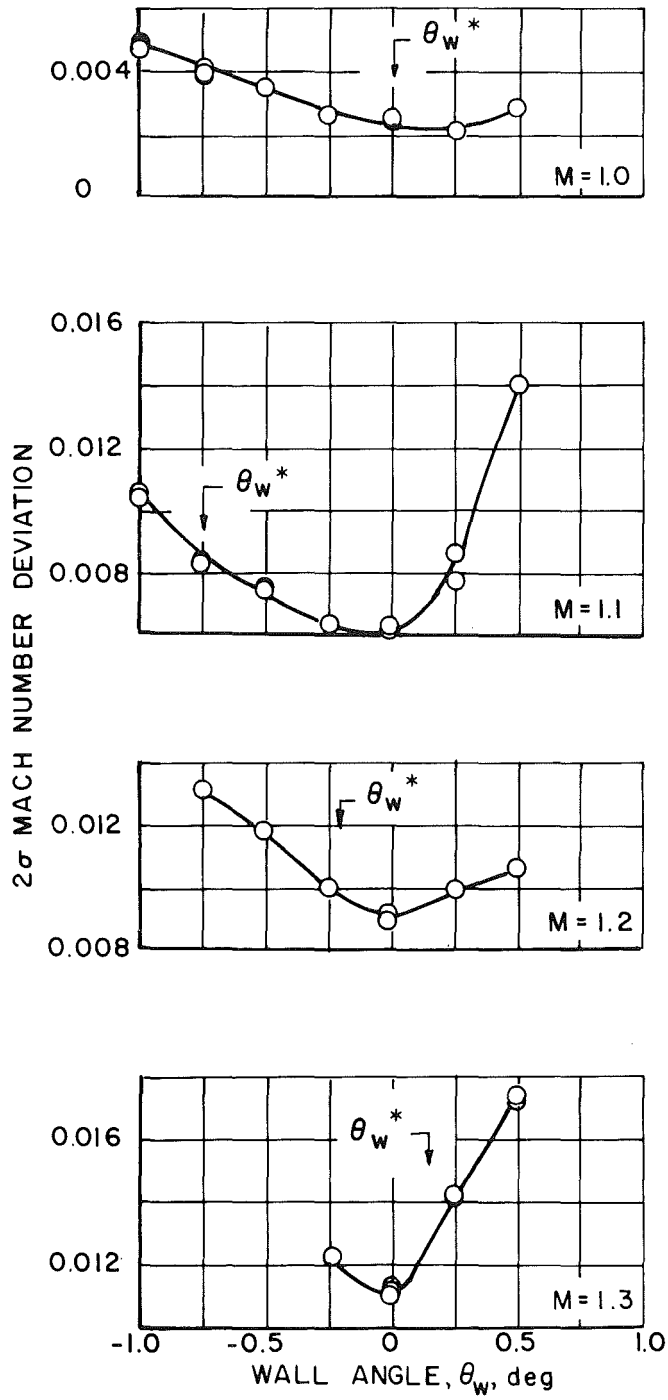

a. τ = 6

Figure 20. Effect of test section wall angle variation upon the 2σ Mach number deviations for tunnel station 8.2 to 28.2 at $\lambda = \lambda_N$ and M = 1.0 to 1.3.

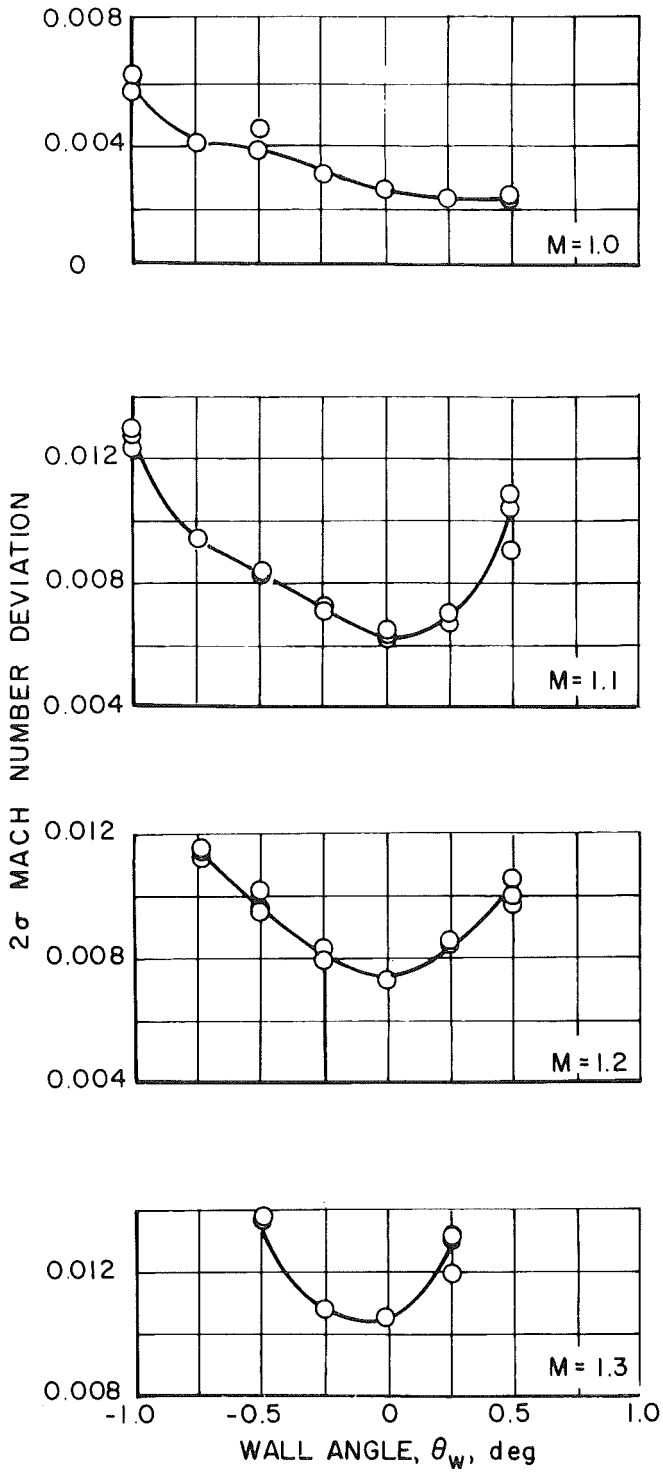

b. $\tau = 4$

Figure 20. Continued.

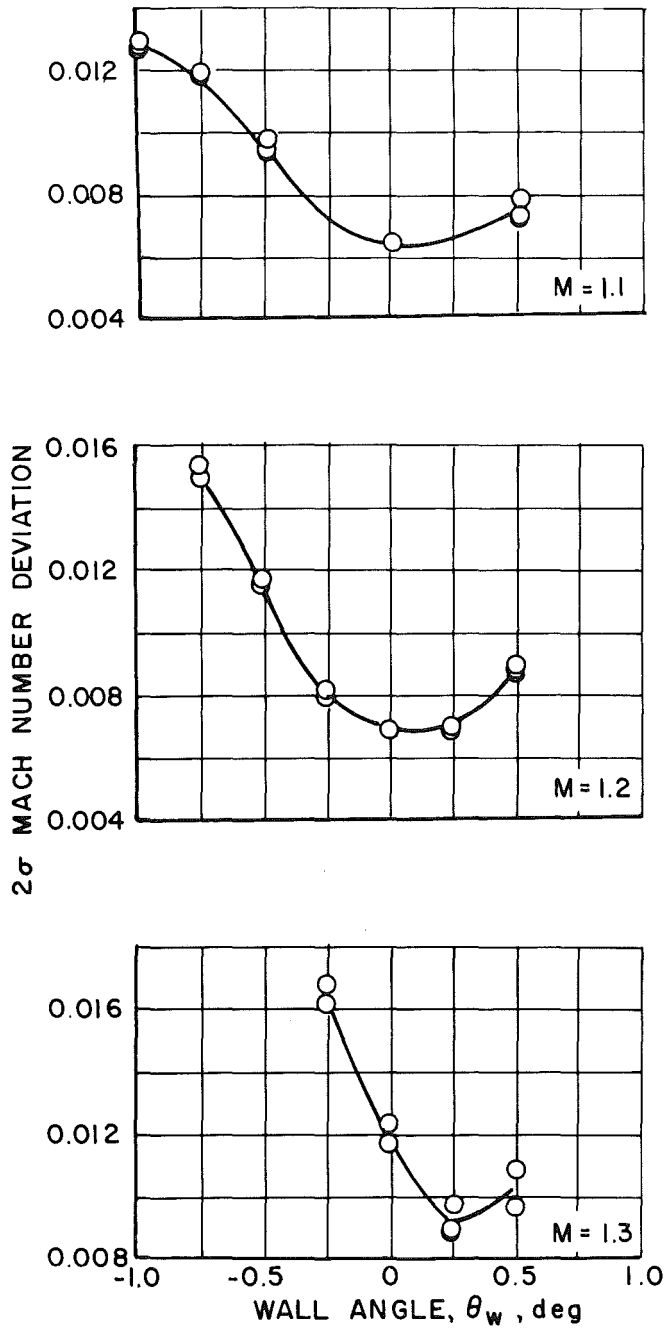

c. $\tau = 2$

Figure 20. Concluded.

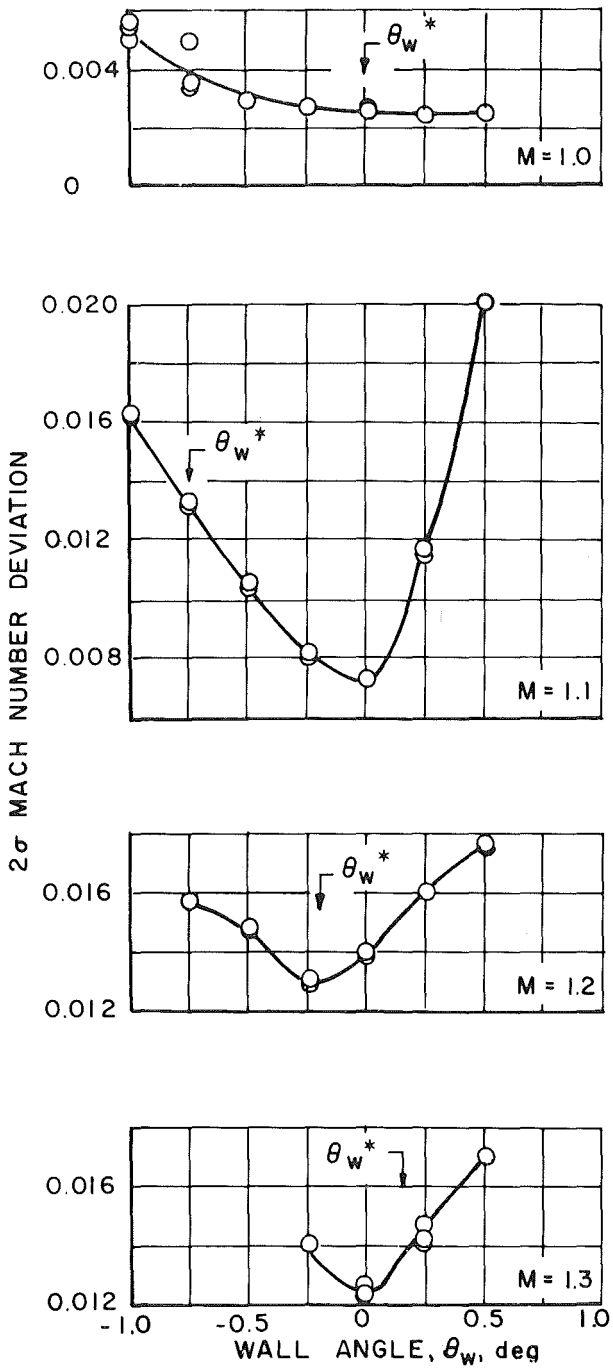

a. $\tau = 6$

Figure 21. Effect of test section wall angle variation upon the 2σ Mach number deviations for tunnel station 1.2 to 20.2 at $\lambda = \lambda_N$ and M = 1.0 to 1.3.

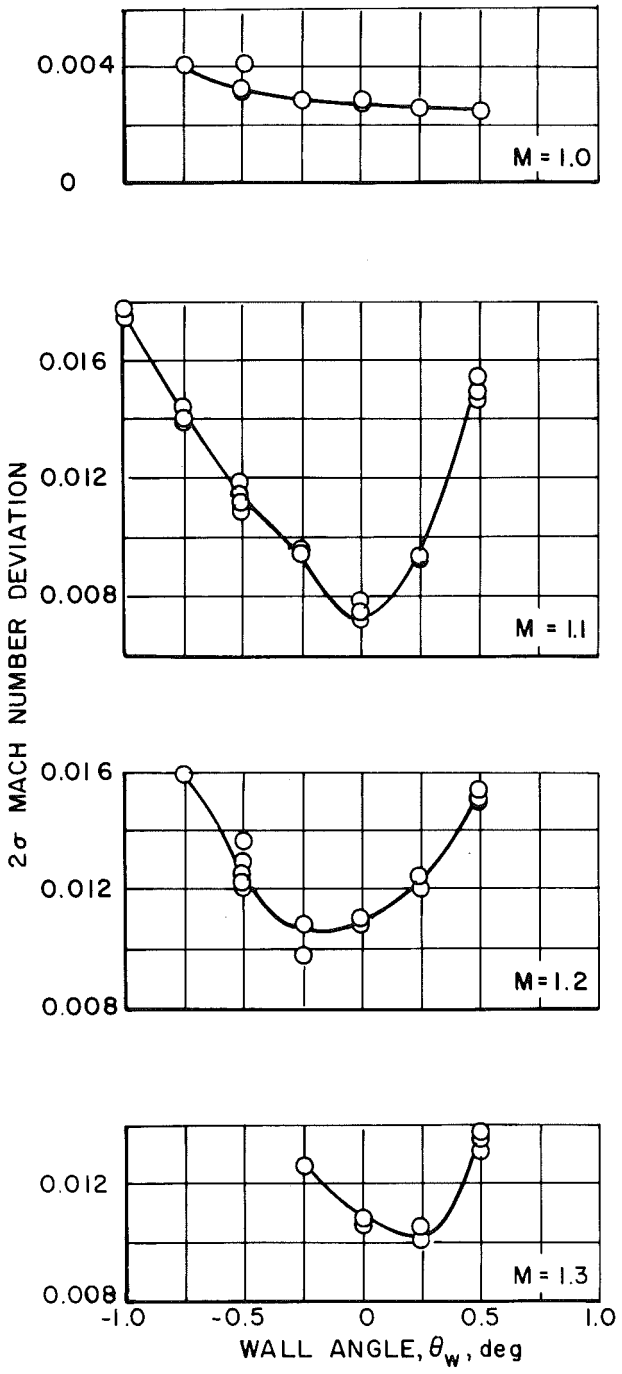

b. $\tau = 4$

Figure 21. Continued.

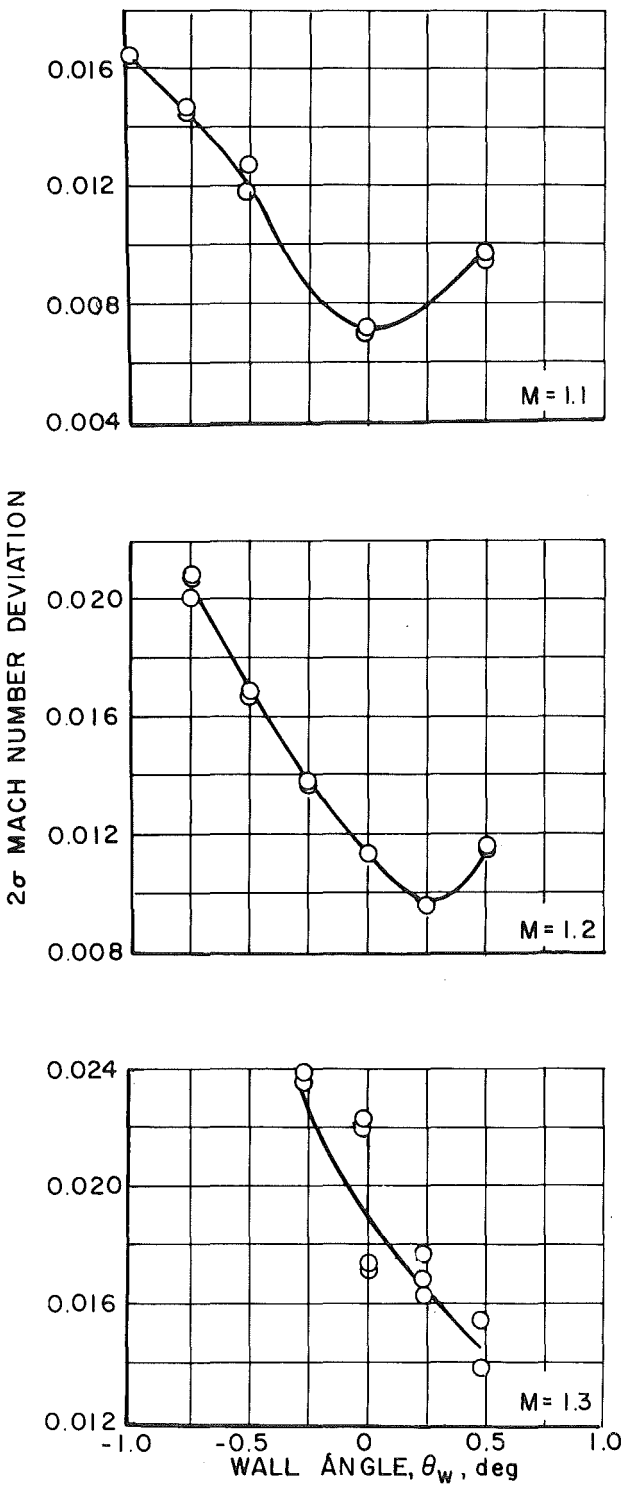

c. $\tau = 2$

Figure 21. Concluded.

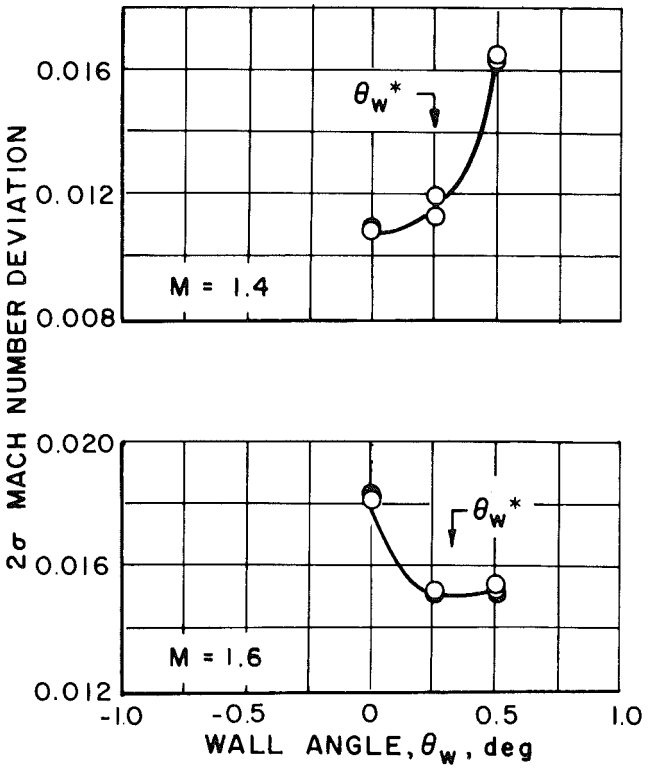

a. $\tau = 6$

Figure 22. Effect of test section wall angle variation upon the 2σ Mach number deviations for tunnel station 8.2 to 28.2 at $\lambda = \lambda_N$ and M = 1.4 to 1.6.

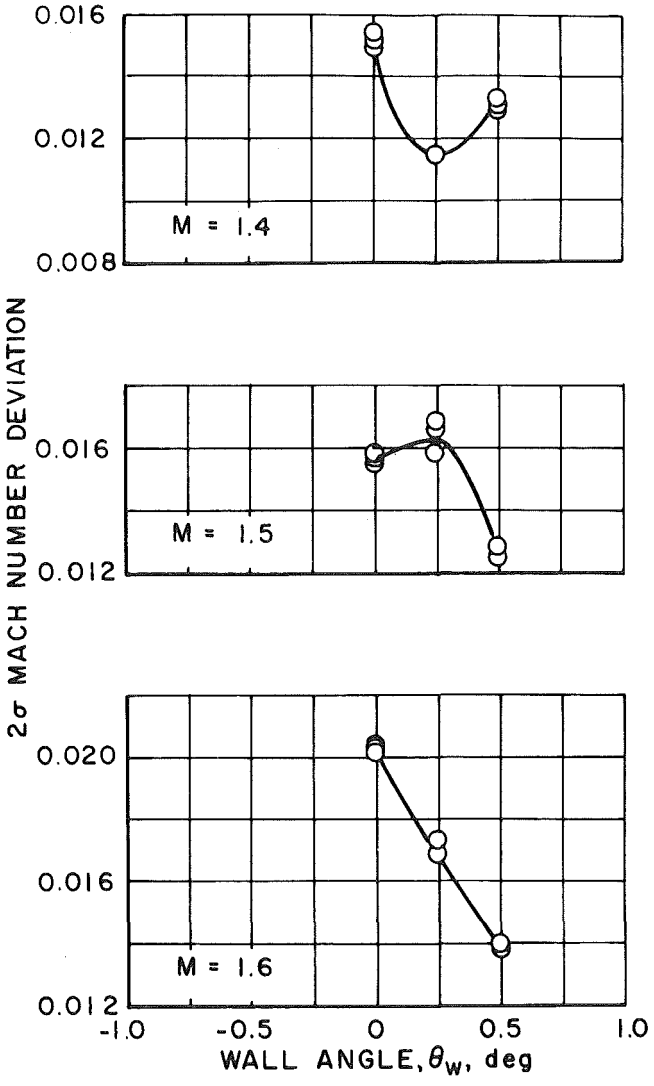

b. $\tau = 4$

Figure 22. Continued.

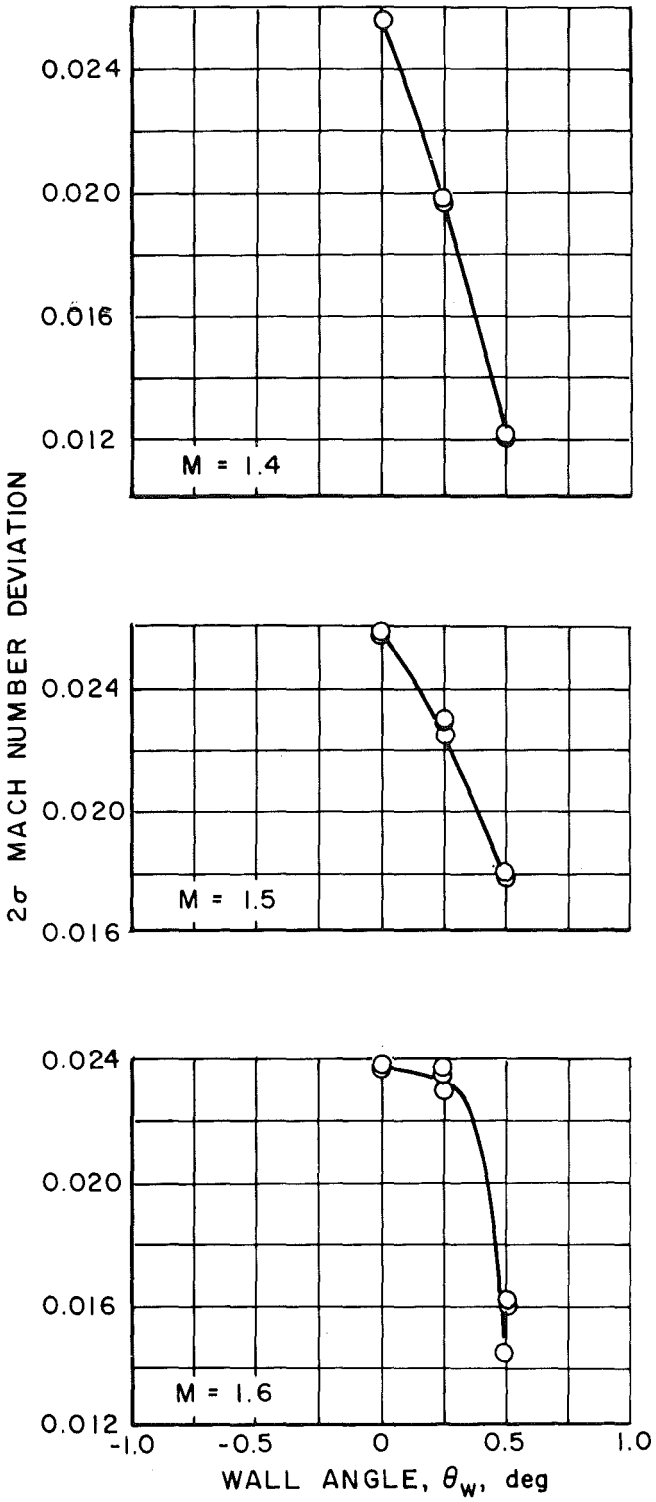

c. $\tau = 2$

Figure 22. Concluded.

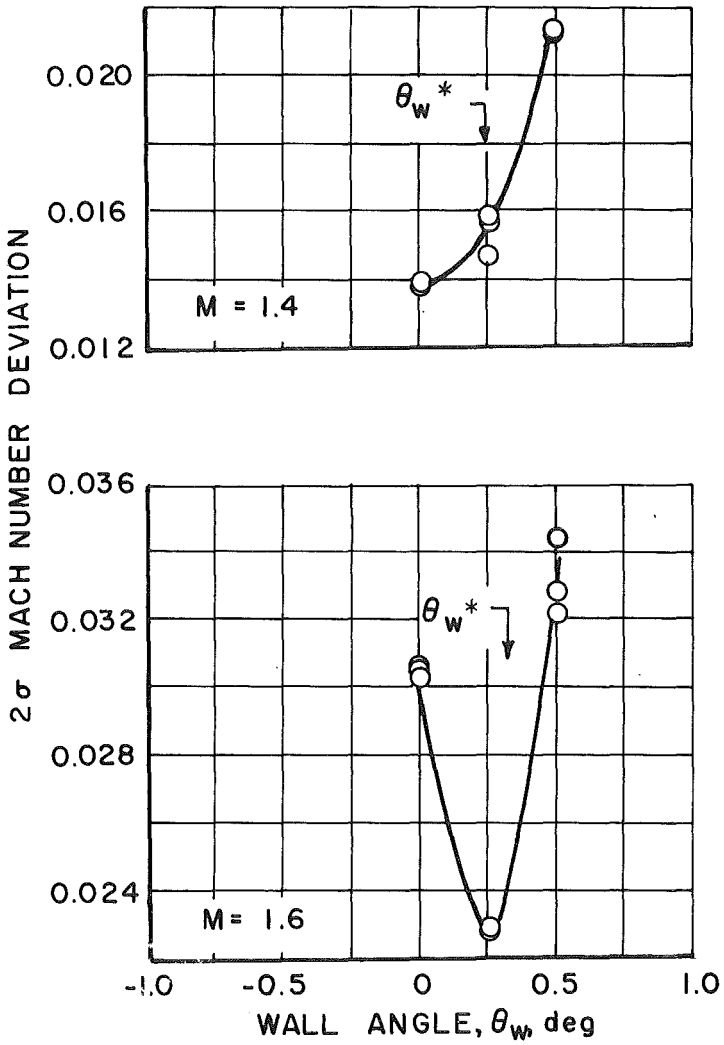

a. $\tau = 6$

Figure 23. Effect of test section wall angle variation upon the 2σ Mach number deviations for tunnel station 1.2 to 20.2 at $\lambda = \lambda_N$ and M = 1.4 to 1.6.

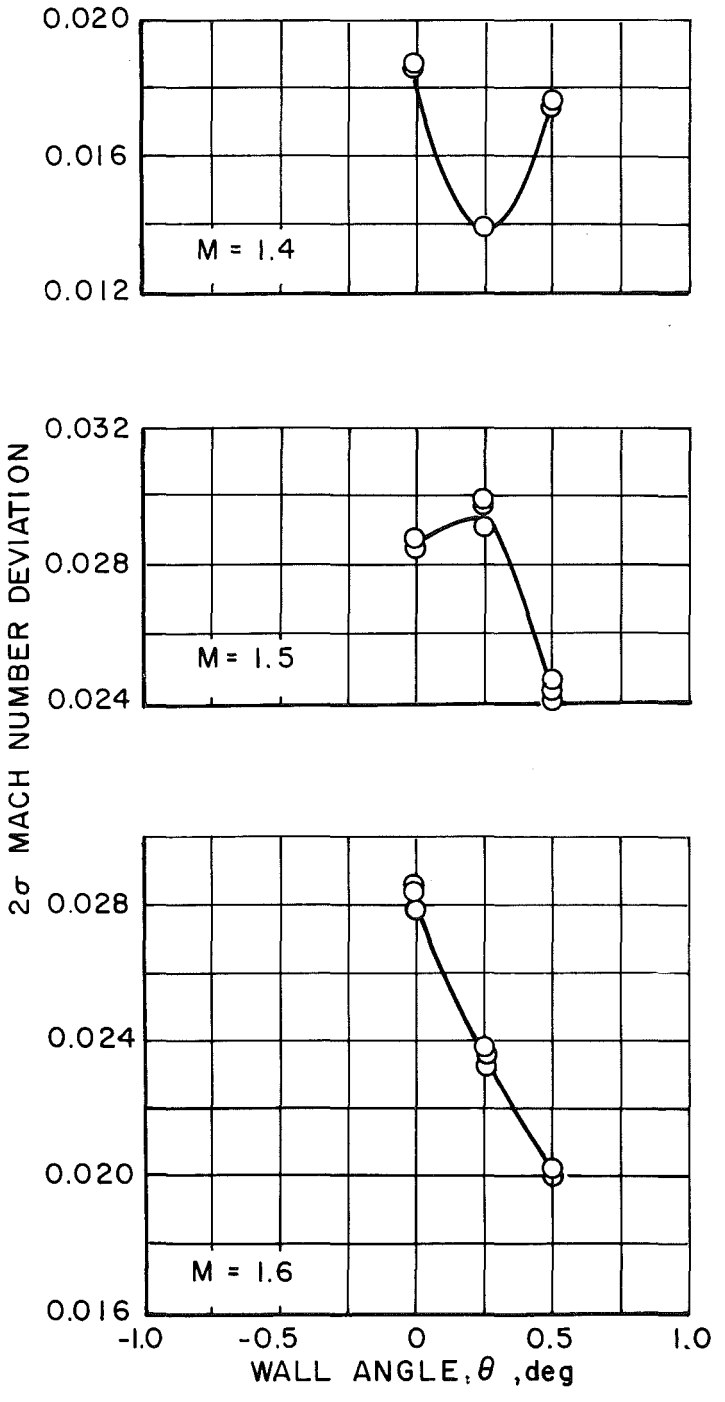

b. $\tau = 4$

Figure 23. Continued.

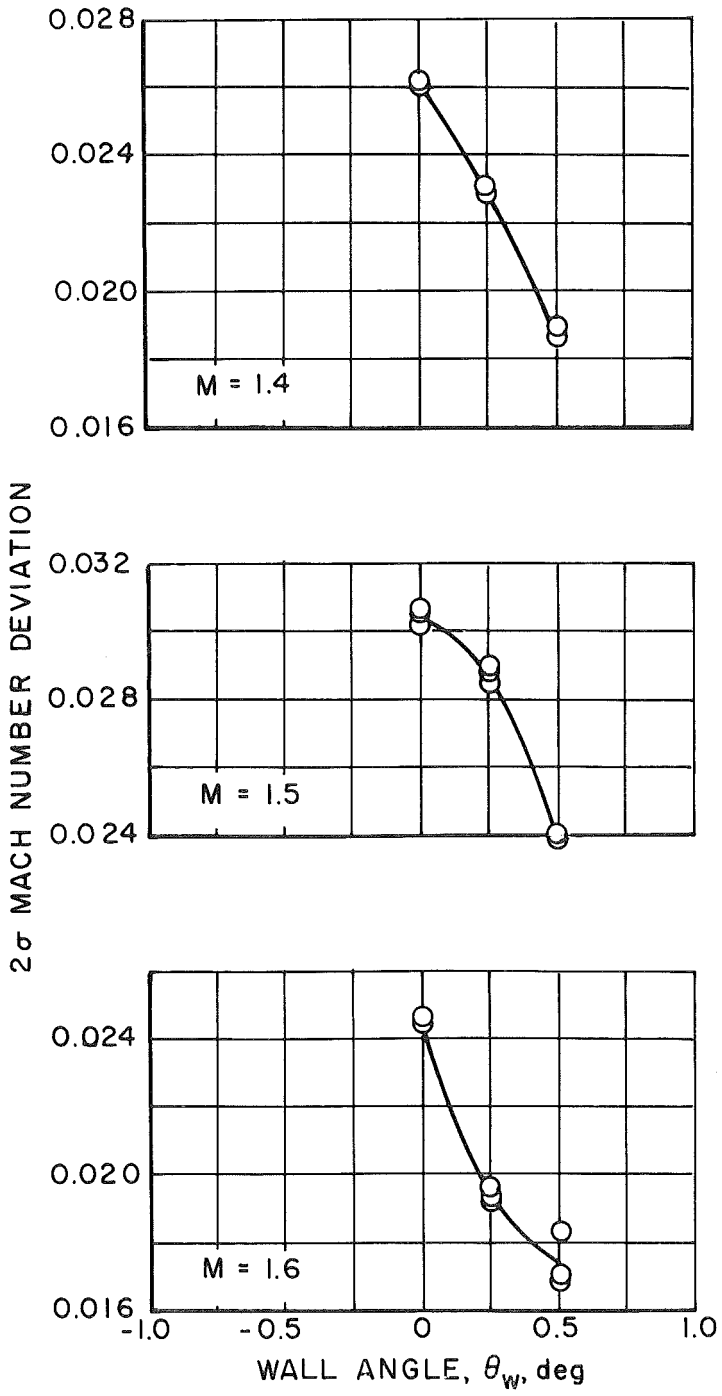

c. $\tau = 2$

Figure 23. Concluded.

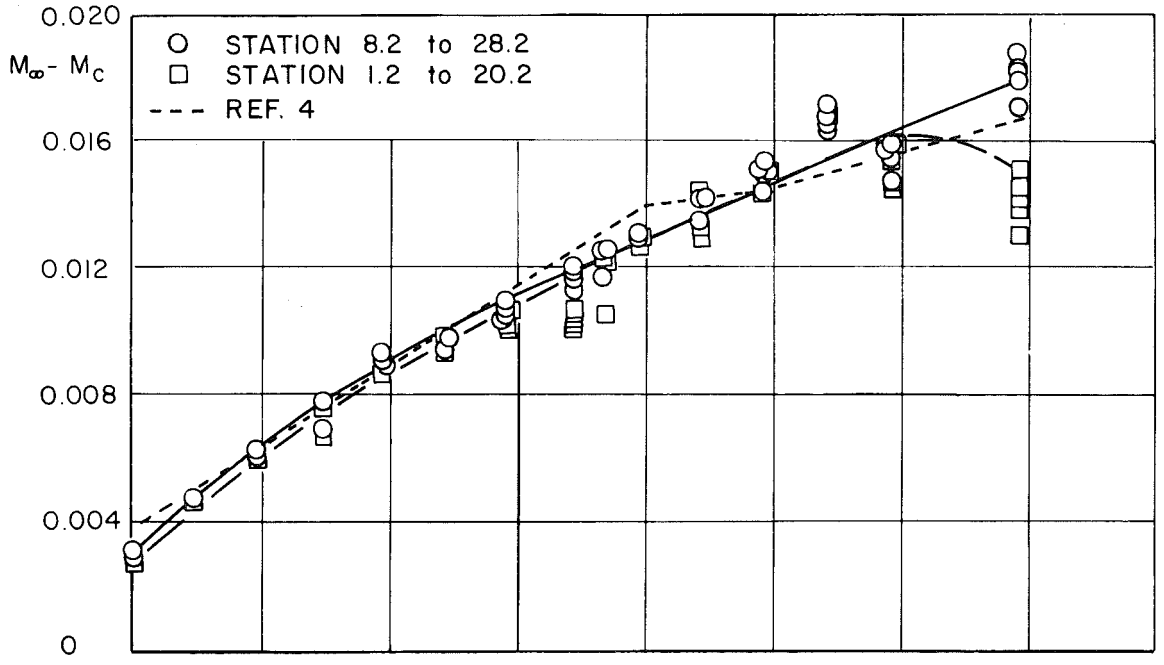

a. $\tau = 6$

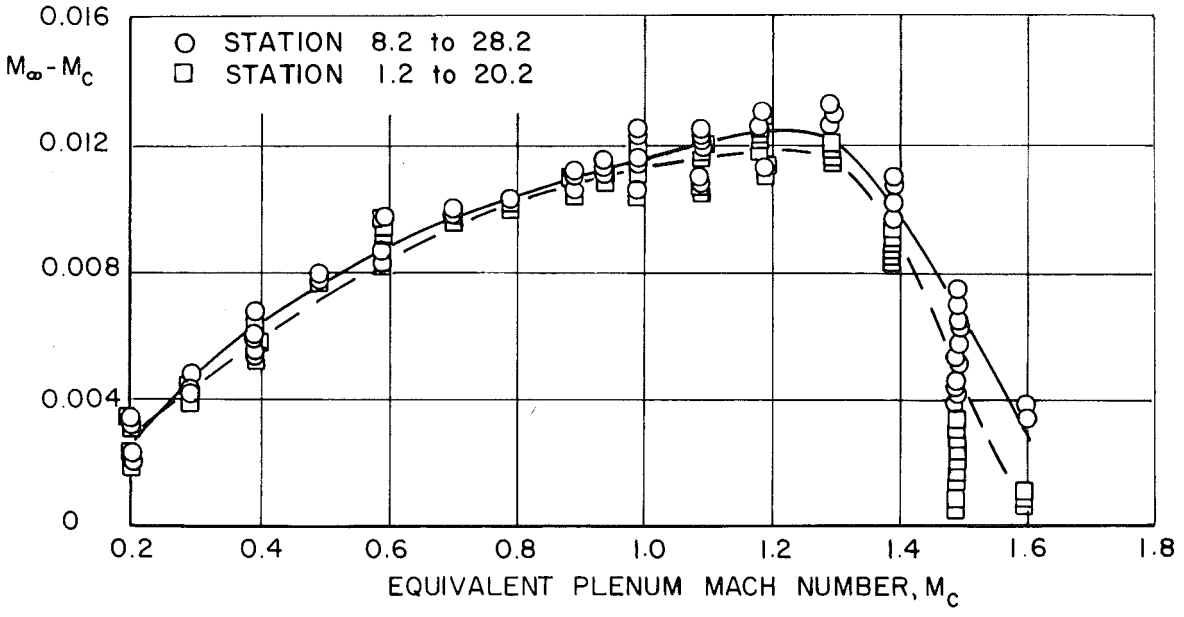

b. $\tau = 4$

Figure 24. Effect of test section region upon the tunnel 16T Mach number calibration at $\theta_w = 0$.

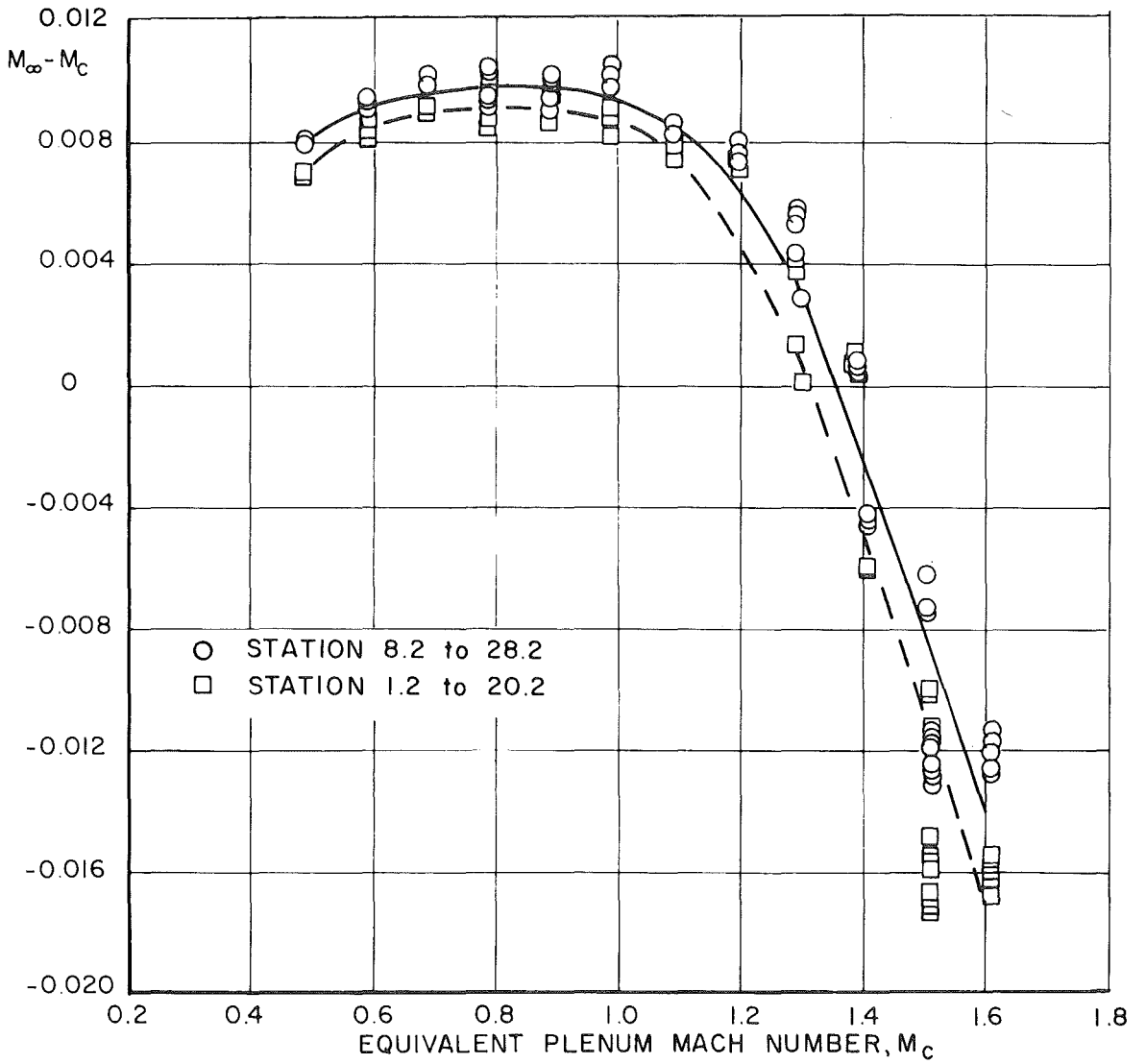

c. $\tau = 2$

Figure 24. Concluded.

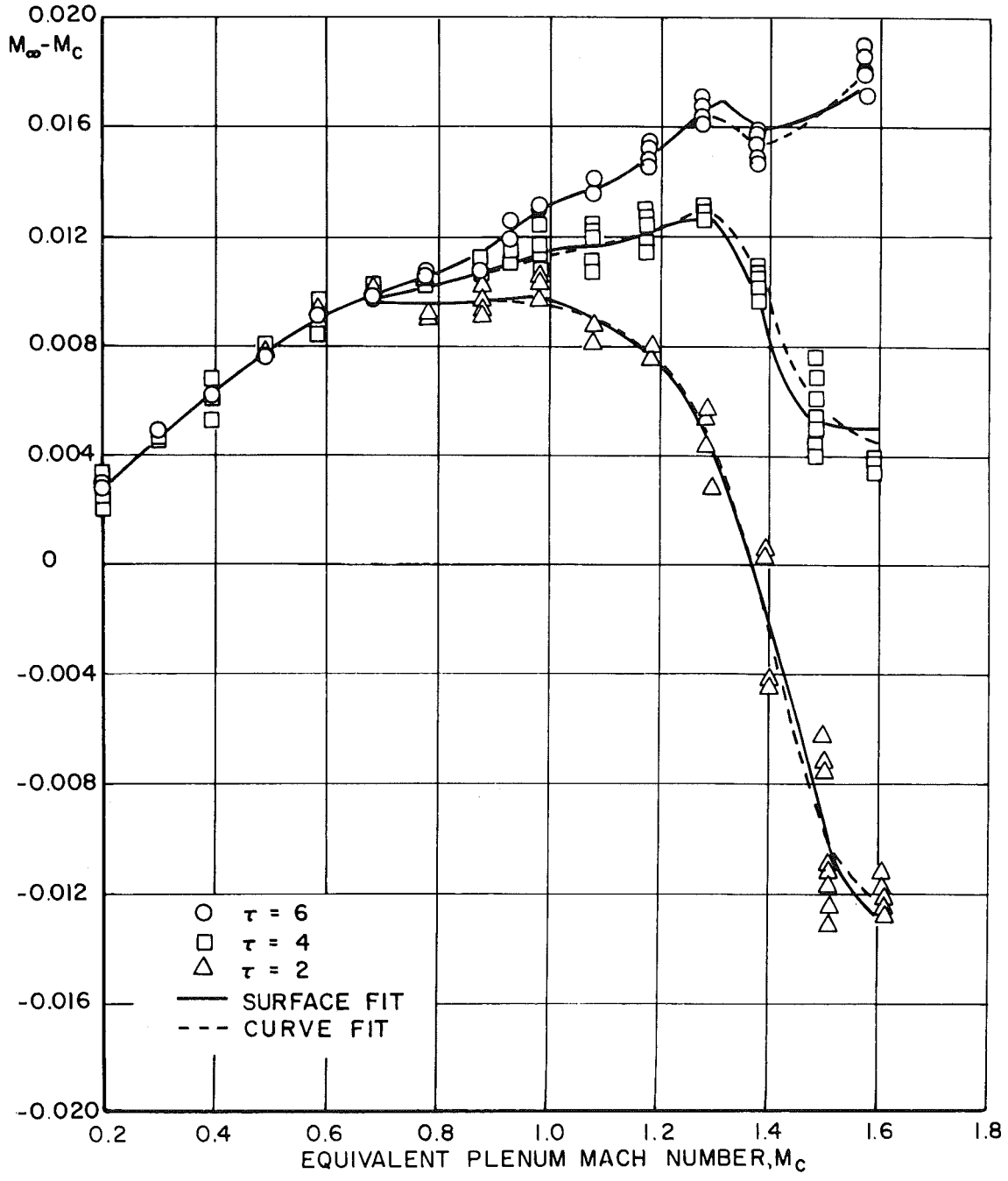

Figure 25. Tunnel 16T Mach number calibration at various test section porosities for θ_w = 0.

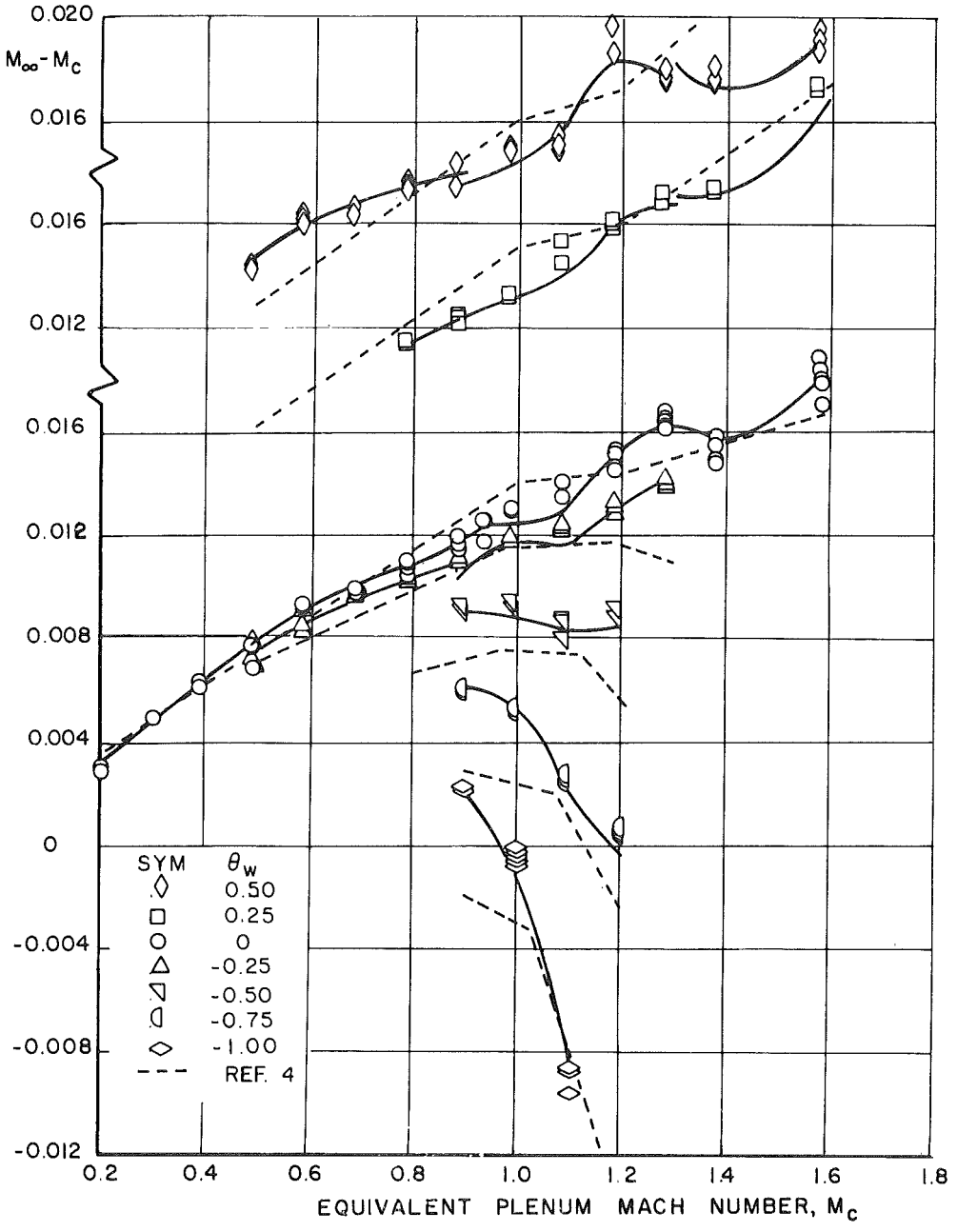

a. $\tau = 6$

Figure 26. Tunnel 16T Mach number calibration for various test section wall angles at wall porosities of two, four, and six percent.

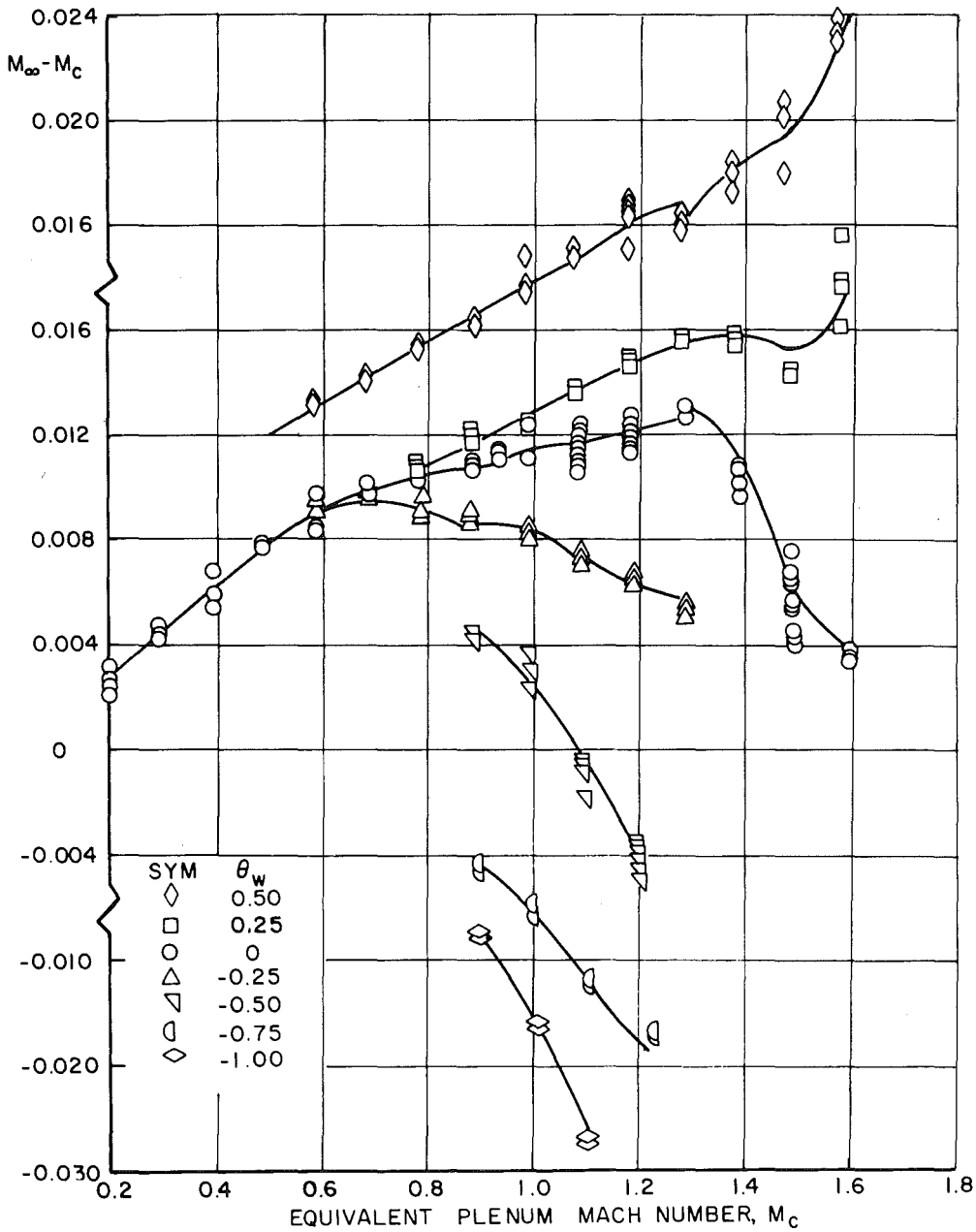

b. $\tau = 4$

Figure 26. Continued.

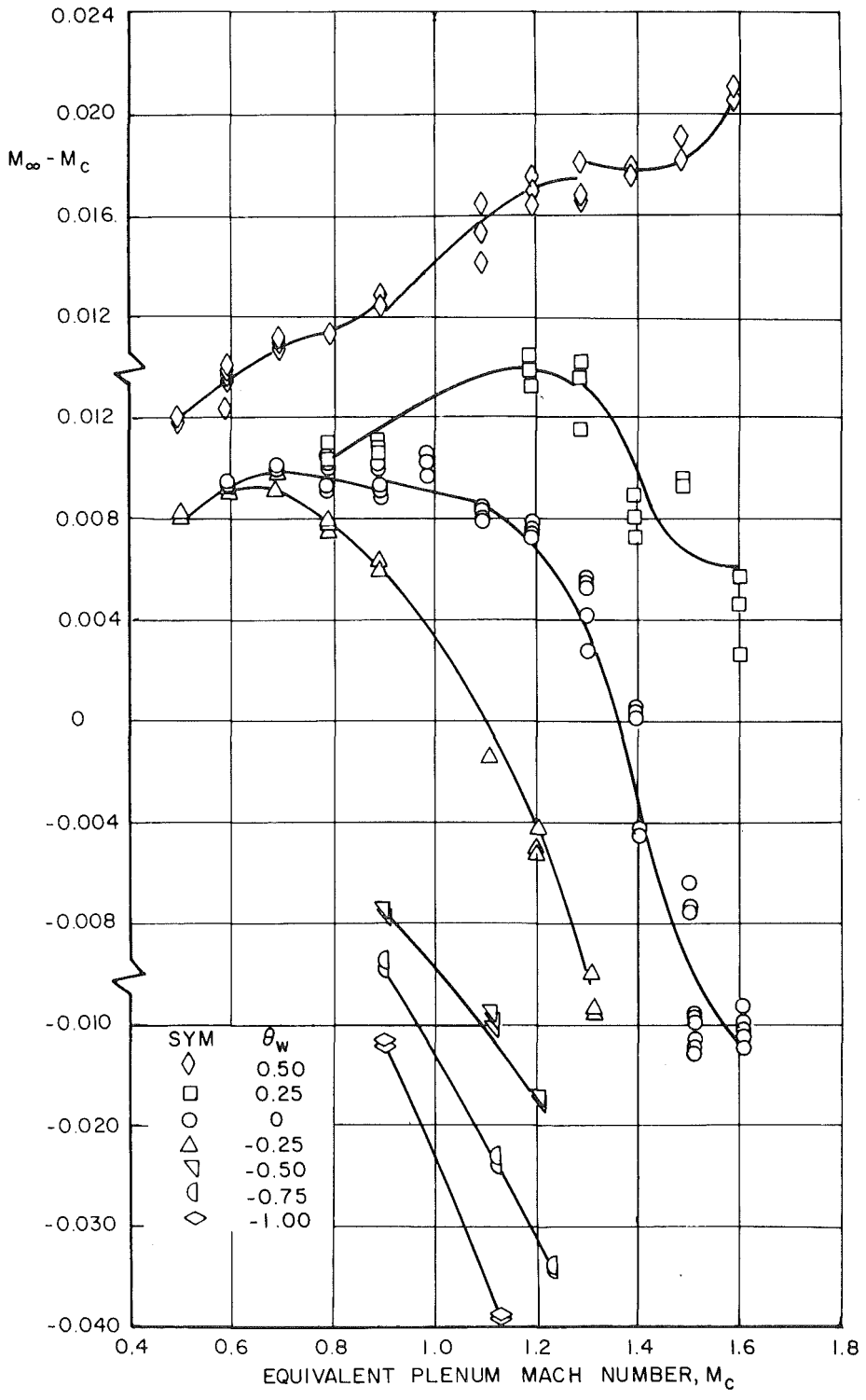

c. $\tau = 2$

Figure 26. Concluded.

Table 1. Coefficients of the 16T Calibration Surface Fit for θ_w = 0 and Variable Test Section Porosity

		$0.2 \leq M_\infty \leq 1.6$	$M_\infty \leq 1.0$	$1.0 < M_\infty \leq 1.3$	$M_\infty > 1.3$
i	j	a_{ij}	a_{ij}	a_{ij}	a_{ij}
0	0	2.5290-02	3.6764-03	-1.3284+00	-1.6341+00
1	0	-4.2743-02	-2.0041-02	4.9172+00	3.6295+00
0	1	-1.4922-02	-6.8558-04	1.4516-02	7.2060-03
2	0	5.1295-02	1.3317-01	-6.7641+00	-2.6381+00
1	1	2.6473-02	2.0234-03	-2.4875-02	-1.0285-02
0	2	2.8818-03	-2.5546-05	-1.7390-03	-1.0595-03
3	0	-3.0826-02	-1.9999-01	4.1586+00	6.2022-01
2	1	-1.1525-02	3.4030-03	-1.4460-02	1.0023-02
1	2	-4.3454-03	-1.1750-03	9.0391-03	-3.5331-04
0	3	-1.6302-04	7.7757-05	-4.8959-04	8.6126-05
4	0	-9.9312-04	8.7029-02	-9.7097-01	
3	1	5.4472-03	3.9565-04	2.0182-02	
2	2	4.1975-04	-1.3296-04	-4.8381-03	
1	3	2.5249-04	9.6462-05	3.2785-05	
0	4	-2.7028-06	-8.3686-06	2.9807-05	
Maximum Residual		0.0051	0.0008	0.0015	0.0032
Max. Residual for 95% Data		0.0029	0.0007	0.0008	0.0023

where the surface is of the form

$$M_\infty - M_c = \sum_{i,j=0}^{i,j=\max} a_{ij} M_c^i \tau^j$$

Table 2. Coefficients of the 16T Calibration Curve Fit for τ = 6 and θ_w = 0

	$0.2 \leq M_\infty \leq 1.6$	$M_\infty \leq 1.0$	$M_\infty > 1.0$
i	a_i	a_i	a_i
0	-6.7469-03	-5.4591-05	2.1562+00
1	7.8593-02	1.7627-02	-7.0423+00
2	-1.9132-01	-4.7721-03	8.5780+00
3	2.4950-01		-4.5903+00
4	-1.5031-01		9.1139-01
5	3.3588-02		
Maximum Residual	0.0015	0.0006	0.0010
Max. Residual for 95% Data	0.0009	0.0005	0.0009

where the curve is of the form

$$M_\infty - M_c = \sum_{i=0}^{i=\max} a_i \, M_c^i$$

Table 3. Coefficients of the 16T Calibration Curve Fit for τ = 6 and θ_w = 0

	$0.2 \leq M_\infty \leq 1.6$	$M_\infty \leq 1.2$	$M_\infty > 1.2$
i	a_i	a_i	a_i
0	-8.8447-03	-5.8453-04	-1.2907+00
1	8.8361-02	1.3874-02	2.8160+00
2	-2.0237-01	2.0340-02	-2.0024+00
3	2.4110-01	-3.7981-02	4.6745-01
4	-1.3069-01	1.5782-02	
5	2.4477-02		
Maximum Residual	0.0025	0.0011	0.0017
Max. Residual for 95% Data	0.0016	0.0009	0.0013

where the curve is of the form

$$M_\infty - M_c = \sum_{i=0}^{i=\max} a_i \, M_c^i$$

Table 4. Coefficients of the 16T Calibration Curve for $\tau = 2$ and $\theta_w = 0$

	$0.5 \leq M_\infty \leq 1.6$	$M_\infty \leq 1.0$	$1.0 < M_\infty \leq 1.3$	$M_\infty > 1.3$
i	a_i	a_i	a_i	a_i
0	-3.4379-01	1.0742-02	5.3280-02	-2.1250+00
1	2.0216+00	-9.8713-02	-1.5713-01	4.7224+00
2	-4.4596+00	3.7405-01	1.8510-01	-3.4380+00
3	4.7387+00	-4.7514-01	-7.1682-02	8.1978-01
4	-2.4210+00	1.9953-01		
5	4.7394-01			
Maximum Residual	0.0035	0.0008	0.0015	0.0040
Max. Residual for 95% Data	0.0030	0.0007	0.0012	0.0031

where the curve is of the form

$$M_\infty - M_c = \sum_{i=0}^{i=\max} a_i M_c^i$$

Table 5. Coefficients of the 16T Calibration Surface Fit for τ = 6 and Variable Test Section Wall Angle

		$0.2 \leq M_\infty \leq 1.6$	$M_\infty < 0.9$	$0.9 \leq M_\infty \leq 1.3$	$M_\infty > 1.3$
i	j	a_{ij}	a_{ij}	a_{ij}	a_{ij}
0	0	-1.8330-03	2.4004-03	-2.4945+00	-9.8018-01
1	0	3.1212-02	-8.8627-03	9.4038+00	2.1985+00
0	1	6.2866-03	-1.4840-02	7.3816-01	9.2375-02
2	0	-3.5239-02	8.5624-02	-1.3162+01	-1.6116+00
1	1	-5.7494-03	6.7658-02	-2.0808+00	-1.6346-01
0	2	-5.2767-03	-5.4025-03	-6.0025-02	1.3137-01
3	0	2.5762-02	-1.1911-01	8.1407+00	3.9239-01
2	1	-4.5889-03	-9.3334-02	1.9439+00	7.5299-02
1	2	3.5172-02	3.2066-02	1.2445-01	-1.1388-01
0	3	-1.1333-02	8.6576-03	-3.5545-02	2.0998-02
4	0	-6.9180-03	5.3149-02	-1.8753+00	
3	1	6.8420-03	4.3122-02	-5.9910-01	
2	2	-3.3240-02	-3.1870-02	-6.7429-02	
1	3	2.3636-02	3.2359-03	4.6085-02	
0	4	3.7633-03	6.0674-03	1.9858-03	
Maximum Residual		0.0029	0.0008	0.0015	0.0010
Max. Residual for 95% Data		0.0015	0.0004	0.0009	0.0009

where the surface is of the form

$$M_\infty - M_C = \sum_{\substack{i,j = 0 \\ i,j = \max}} a_{ij} M_C^i \theta_w^j$$

Table 6. Coefficients of the 16T Calibration Surface Fit for τ = 4 and Variable Test Section Wall Angle

		$0.2 \leq M_\infty \leq 1.6$	$M_\infty < 0.9$	$0.9 \leq M_\infty \leq 1.3$	$M_\infty > 1.3$
i	j	a_{ij}	a_{ij}	a_{ij}	a_{ij}
0	0	-8.0431-03	3.6742-03	-8.9590-01	7.2531+00
1	0	7.8542-02	-2.6221-02	3.3614+00	-2.2048+01
0	1	7.9867-02	3.1203-02	3.5878-01	2.0586+00
2	0	-1.6521-01	1.4381-01	-4.6515+00	2.5022+01
1	1	-4.3887-01	-1.4508-01	-1.0482+00	-4.1310+00
0	2	-1.2718-02	-4.7052-04	-3.0848-02	-5.5101-01
3	0	1.8455-01	-1.8890-01	2.8473+00	-1.2534+01
2	1	7.9489-01	1.9826-01	1.0067+00	2.6558+00
1	2	3.0836-02	1.0522-02	7.5004-02	9.4181-01
0	3	1.9017-02	-4.7097-03	1.9809-03	-1.3315-01
4	0	-9.3718-02	7.9251-02	-6.4979-01	2.3362+00
3	1	-5.9336-01	-7.6298-02	-3.0879-01	-5.2708-01
2	2	-4.2384-02	-2.5252-02	-5.9316-02	-4.2498-01
1	3	-3.3038-03	1.6812-02	8.9277-03	1.2781-01
0	4	5.0198-02	9.2183-03	8.4702-03	2.7552-02
5	0	1.5817-02			
4	1	1.6596-01			
3	2	5.0270-03			
2	3	-3.8033-03			
1	4	-2.9506-02			
0	5	8.1814-03			
Maximum Residual		0.0032	0.0010	0.0019	0.0018
Max. Residual for 95% Data		0.0015	0.0009	0.0010	0.0016

where the surface is of the form

$$M_\infty - M_c = \sum_{\substack{i,j = 0 \\ i,j = \max}} a_{ij} M_c^i \theta_w^j$$

Table 7. Coefficients of the 16T Calibration Surface Fit for τ = 2 and Variable Test Section Wall Angle

		$0.5 \leq M_\infty \leq 1.6$	$M_\infty < 0.9$	$0.9 \leq M_\infty \leq 1.3$	$M_\infty > 1.3$
i	j	a_{ij}	a_{ij}	a_{ij}	a_{ij}
0	0	-2.0346-01	3.8717-02	1.3786-01	-1.2149+00
1	0	1.2399+00	-2.6792-01	-3.8742-01	2.7460+00
0	1	-1.5675-02	8.8096-03	-1.3294-02	6.2626-03
2	0	-2.7981+00	7.4939-01	3.9209-01	-2.0177+00
1	1	1.2132-01	-5.1752-02	-7.0527-03	-3.9569-02
0	2	-1.3973-01	-3.1560-03	3.2872-02	-6.7671-02
3	0	3.0473+00	-8.3681-01	-1.3338-01	4.8188-01
2	1	-3.1609-01	6.1005-02	3.9002-02	5.4039-02
1	2	5.5445-01	1.2598-02	-4.9479-02	3.0713-02
0	3	-5.5350-02	2.1277-02	-3.2946-03	-1.1299-02
4	0	-1.5930+00	3.2720-01		
3	1	3.2159-01	-2.0311-03		
2	2	-6.8835-01	-2.1112-02		
1	3	1.2907-01	-1.8910-02		
0	4	1.9404-02	2.6310-03		
5	0	3.1740-01			
4	1	-9.3659-02			
3	2	2.5102-01			
2	3	-7.6780-02			
1	4	-6.5337-03			
0	5	9.7374-03			
Maximum Residual		0.0034	0.0011	0.0020	0.0035
Max. Residual for 95% Data		0.0026	0.0007	0.0014	0.0030

where the surface is of the form

$$M_\infty - M_c = \sum_{\substack{i,j = 0 \\ i,j = \max}} a_{ij} M_c^i \theta_w^j$$

APPENDIX A
PROCEDURES FOR OBTAINING VARIABLE WALL POROSITY IN 16T

The calibration utilized the PWT test Cart 1; however, corks were utilized to obtain two- and four-percent wall porosity. The porous wall working setup is illustrated in Fig. 2 of the body of this report. The following general comments apply to the corking procedure:

1. The initial setup was for two-percent porosity. Corks were removed to obtain four- and six-percent porosity during the conduct of the test. The four-percent porosity setup was expedited by painting the corks which were to be removed.

2. Solid plates, such as those used for Schlieren viewing, were replaced with porous plates so that a smooth porosity distribution was obtained throughout the cart. (TV coverage at Sta 25, however, was a requirement.)

3. The holes were corked moving in a counterclockwise direction, i.e., for east wall, move bottom to top; for bottom wall, move west to east; for top wall, move east to west; for west wall, move top to bottom.

4. Special tools to aid installation and removal of the corks were fabricated.

The specific procedures relative to obtaining two-percent porosity are as follows:

1. For the test cart, Sta 0.5 to 40:
   a. The rows of holes which are at 17 deg to the tunnel longitudinal centerline were corked (see Fig. 2a).

   b. Corking started at Sta 0.5 with plate 1 on the cart wall. With this starting point, the first row of holes (nearest the corner) was designated Row 3. In addition, the hole which is at the leading edge of the cart (Sta 0.5) and 7 in. from the corner is in Row 5 (see Fig. 2a).

   c. Proceeding as indicated in general comment 3, Rows 4, 5, 7, 8, 10, 11, 13, 14, ... etc., on each wall were corked; i.e., leaving one row open, corking two rows, one open, two corked, etc., until two-percent porosity was obtained for Sta 0.5 to 40.

2. For the flexure, Sta -0.5 to 0.5:

   a. The rows of holes which are at 17 deg to the tunnel longitudinal centerline were corked (see Fig. 2a).

   b. Corking started at Sta -0.5. With this starting point, the first row of holes (nearest the corner) was designated Row 1. In addition, the hole which is on the plate centerline at Sta -0.5 is on Row 5 (see Fig. 2a).

   c. Proceeding as indicated in general comment 3, Rows 1, 2, 4, 5, 7, 8, 10, 11, 13, 14, ... etc., on each wall were corked until two-percent porosity pattern was obtained.

3. For the taper strip region, Sta -8.5 to -0.5:

   a. The columns of holes which are at 73 deg to the tunnel longitudinal centerline were corked (see Fig. 2b). All stabilizer plates (2-ft-wide plates) were corked the same.

   b. Corking started at Sta -0.5. With this starting point for each plate, the column which contains the hole on the plate centerline at Sta -0.5 was designated Column 1 (see Fig. 2b).

   c. To obtain a smooth transition from 0- to 2-percent porosity: Columns 0, 2, 4, 5, 8, 10, 14, and 16 were corked. Columns 12 and 22 (except holes 1 and 3 from top) were corked. Columns 18, 20, and 24 (except hole 3 from top) were corked. Holes 2 and 5 (from top) on columns 5, 7, 9, and 15 were corked. Hole 2 on Column 29 was corked.

The specific procedures relative to obtaining four-percent percent porosity are as follows:

1. For Sta -0.5 to 40, Rows 2, 5, 8, 11, 14, 17, 20, ... etc., on each wall were uncorked to obtain a pattern whereby one row was corked, two open, one corked, etc.

2. For the taper strip region, Sta -8.5 to -0.5 were uncorked.
   a. Columns 2, 6, 8, 10, 12, 14, and 16 were uncorked.
   b. Column 4 (except holes 1, 4, and 7 from top) were uncorked.
   c. All holes between Sta -8.5 and -3.5 were uncorked.

APPENDIX B
EFFECT OF REYNOLDS NUMBER

INTRODUCTION

Early calibration experience in Tunnel 16T indicated that Reynolds number did not have a significant effect upon the tunnel calibration. As a consequence, stagnation pressure is usually not selected as a variable during tunnel calibration. Many calibrations, including Ref. 4, have been conducted at 1,000 psfa. The Ref. 3 calibration was conducted at a constant Reynolds number of 3.0 x 10^6/ft which corresponded to a stagnation pressure variation from about 1,500 to 2,000 psf. According to Ref. 3, the differences between that tunnel calibration and Ref. 4 were considered negligible. Considering the typical test operating conditions in Tunnel 16T, a stagnation pressure level of 1,600 psf was selected for the tunnel calibrations at wall porosities of two, four, and six percent.

During the conduct of this calibration, some data anomalies were discovered in some previous test data for which Reynolds number had been a variable. It was also noted that an objective of the AEDC NAB program was to evaluate the effect of Reynolds number on nozzle afterbody pressure drag. Considering these factors, the calibration program was modified and limited data were obtained to provide an indication of the effect of Reynolds number upon the calibration.

DISCUSSION

The calibration data acquired at stagnation pressures other than 1,600 psf consisted of Mach number distributions at 800 and 3,200 psf for M_∞ = 0.6 and 0.8 and a test section wall porosity of six percent. The test section wall angle was varied from -0.25 to 0.50 deg. In addition, the tunnel pressure ratio was varied from 1.12 to 1.18 at M_∞ = 0.8.

The centerline Mach number distributions for various test section wall angles and stagnation pressures are illustrated in Figs. B-1 and B-2 for M_∞ = 0.6 and 0.8, respectively. The effect of pressure ratio variation upon the distributions at M_∞ = 0.8 is illustrated in Fig. B-3.

The data presented in Figs. B-1 through B-3 indicate that the effects of stagnation pressure upon the Mach number distributions are small and confined to the rear end of the distributions. The data presented in Fig. B-3 also indicate that pressure ratio variation has an insignificant effect upon the distributions forward of tunnel station 28 at p_{t_∞} = 800 and 3,200 psf as well as p_{t_∞} = 1,600 psf.

The effect of Reynolds number variation upon the 2σ Mach number deviations at various test section wall angles is presented in Fig. B-4. The data presented in Fig. B-4 indicate that Reynolds number variation over the range investigated has an insignificant effect upon the deviations at $M_\infty = 0.6$ and 0.8.

The effect of Reynolds number on the tunnel calibration at M = 0.6 and 0.8 for $\theta_W = 0$ is illustrated in Fig. B-5. The data in Fig. B-5 indicate that the free-stream Mach number increases slightly with increasing Reynolds number. With the exception of data at $Re > 4.5 \times 10^6$ for $M_\infty = 0.6$ the Reynolds number calibration agrees with Ref. 4 within ±0.002. Such agreement is considered satisfactory, especially in view of the fact that the decrement is about the same order of magnitude as the Tunnel 16T Mach number precision. Based on the data presented herein, it was concluded that the effects of Reynolds number upon the 16T calibration at $M_\infty = 0.6$ and 0.8 were not significant.

SEQUEL

Considering the small effects of Reynolds number and in lieu of a complete calibration with Reynolds number, the Ref. 4 calibration was used to conduct the AEDC NAB test program. Following the conduct of the AEDC NAB tests, data analysis revealed that some trends in model afterbody drag with Reynolds number could be attributed to the tunnel calibration. The errors in stream parameters attributed to use of the Ref. 4 calibration and neglecting the effects of Reynolds number were less than 0.4, 0.2, and 0.6 percent for M_∞, static pressure, and dynamic pressure respectively. Such small errors are about the same order of magnitude as errors associated with Tunnel 16T instrumentation precision. For most test programs in the AEDC/PWT wind tunnels, such errors are not significant. For testing of half bodies, however, such as that used for the AEDC NAB program, the error in static pressure can induce significant error in afterbody drag. For example, at M = 0.6 and $Re = 5.0 \times 10^6$, the error in afterbody drag was found to be about 70 drag counts.

As a consequence of these results, a Tunnel 16T calibration was conducted with Reynolds number as a primary variable. The results of that calibration will be presented and discussed in a forthcoming AEDC report. It is sufficient to note herein that the magnitude of the effect of Reynolds number upon the 16T calibration at all Mach numbers was about the same or less than that shown in Fig. B-5. In addition, the data trends were definable such that Reynolds number effects could be taken into consideration.

The results of the Tunnel 16T Reynolds number calibration were utilized to correct AEDC nozzle afterbody test data. It is of interest to note that the corrections were considered significant at $M_\infty = 0.6$, marginally significant at $M_\infty = 0.8$, but insignificant at $M_\infty \geqslant 0.9$.

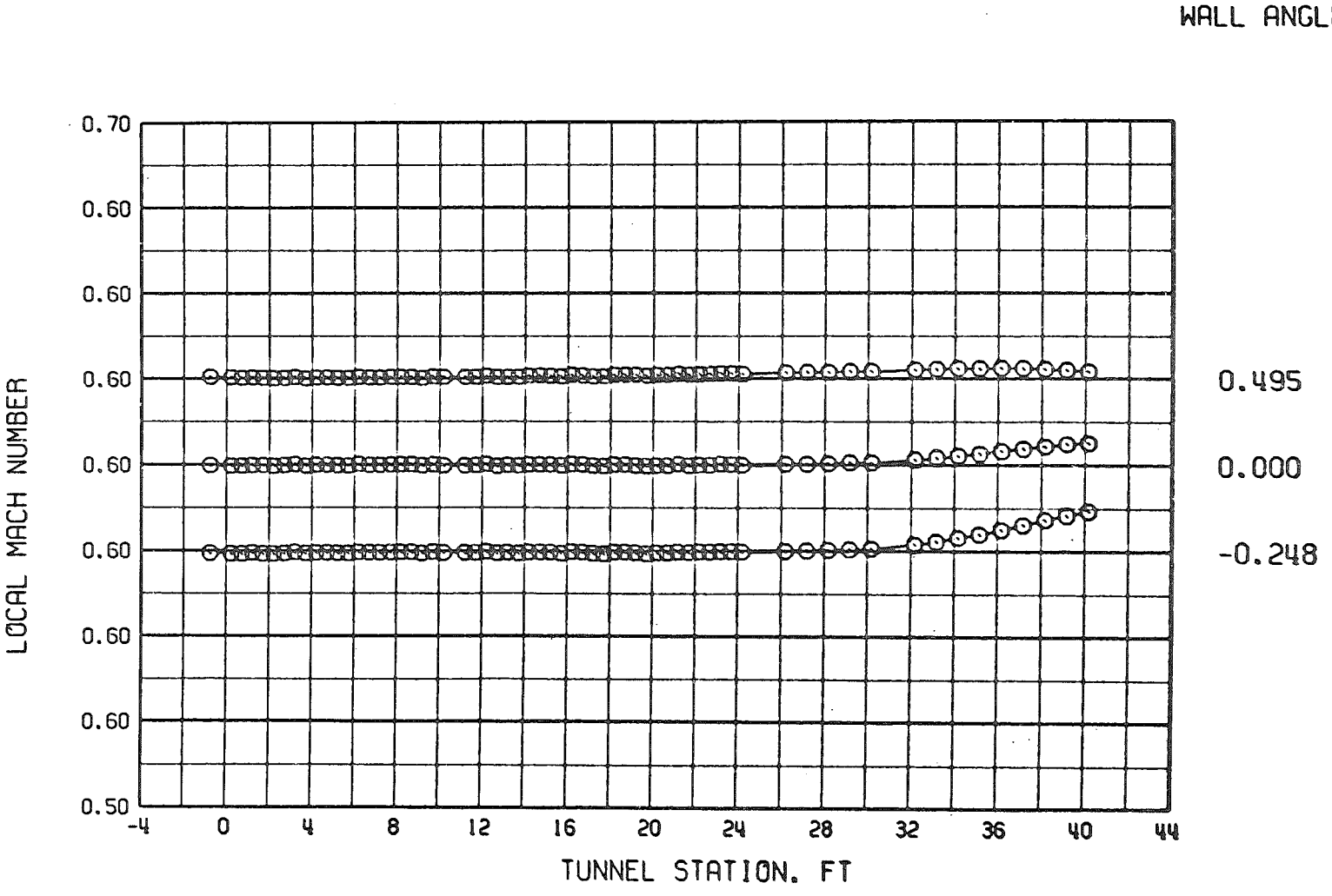

a. p_{t_∞} = 800

Figure B-1. 16T centerline Mach number distributions for various stagnation pressures and test section wall angles at M_∞ = 0.6, λ = 1.1, and τ = 6.

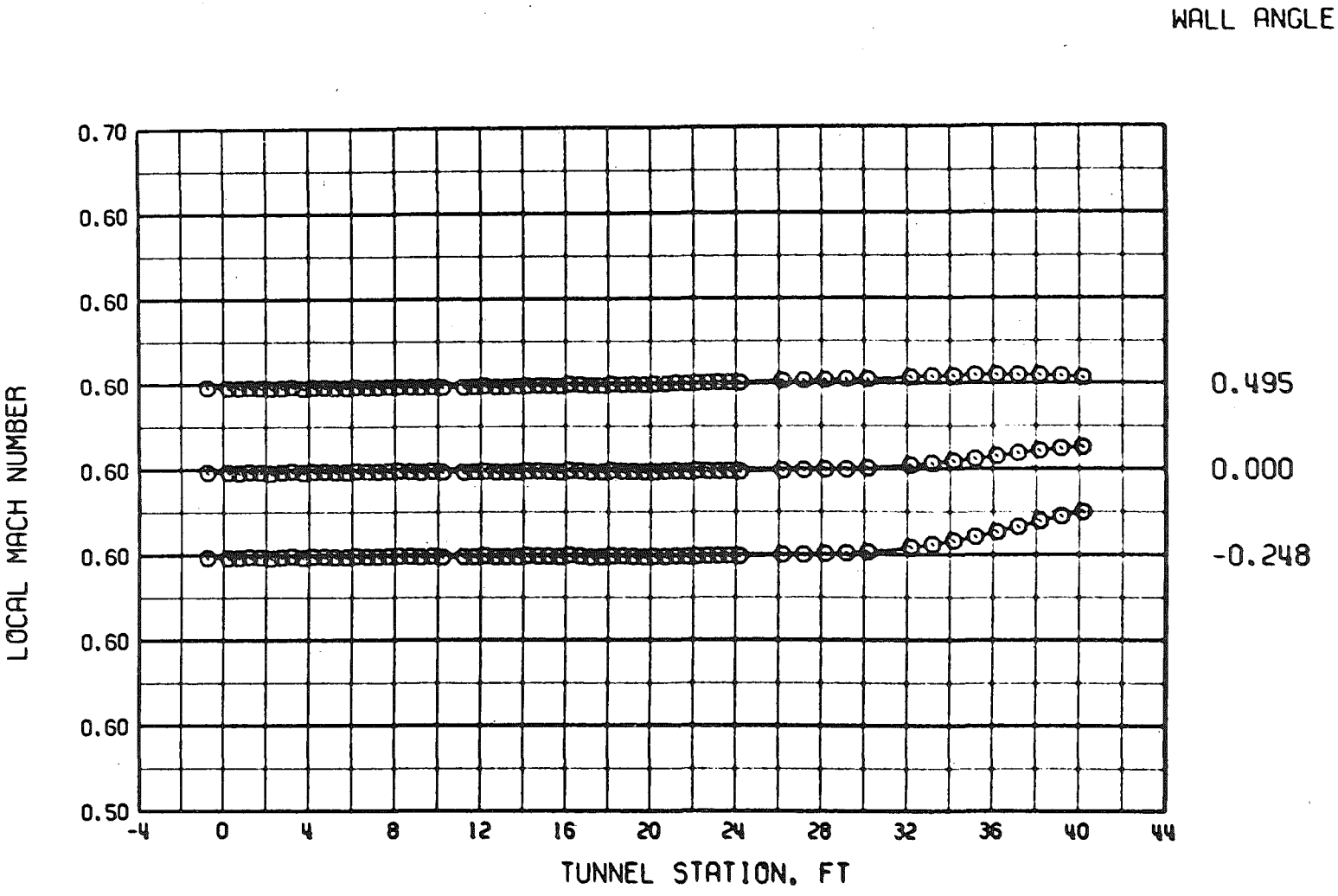

b. p_{t_∞} = 1,600

Figure B-1. Continued.

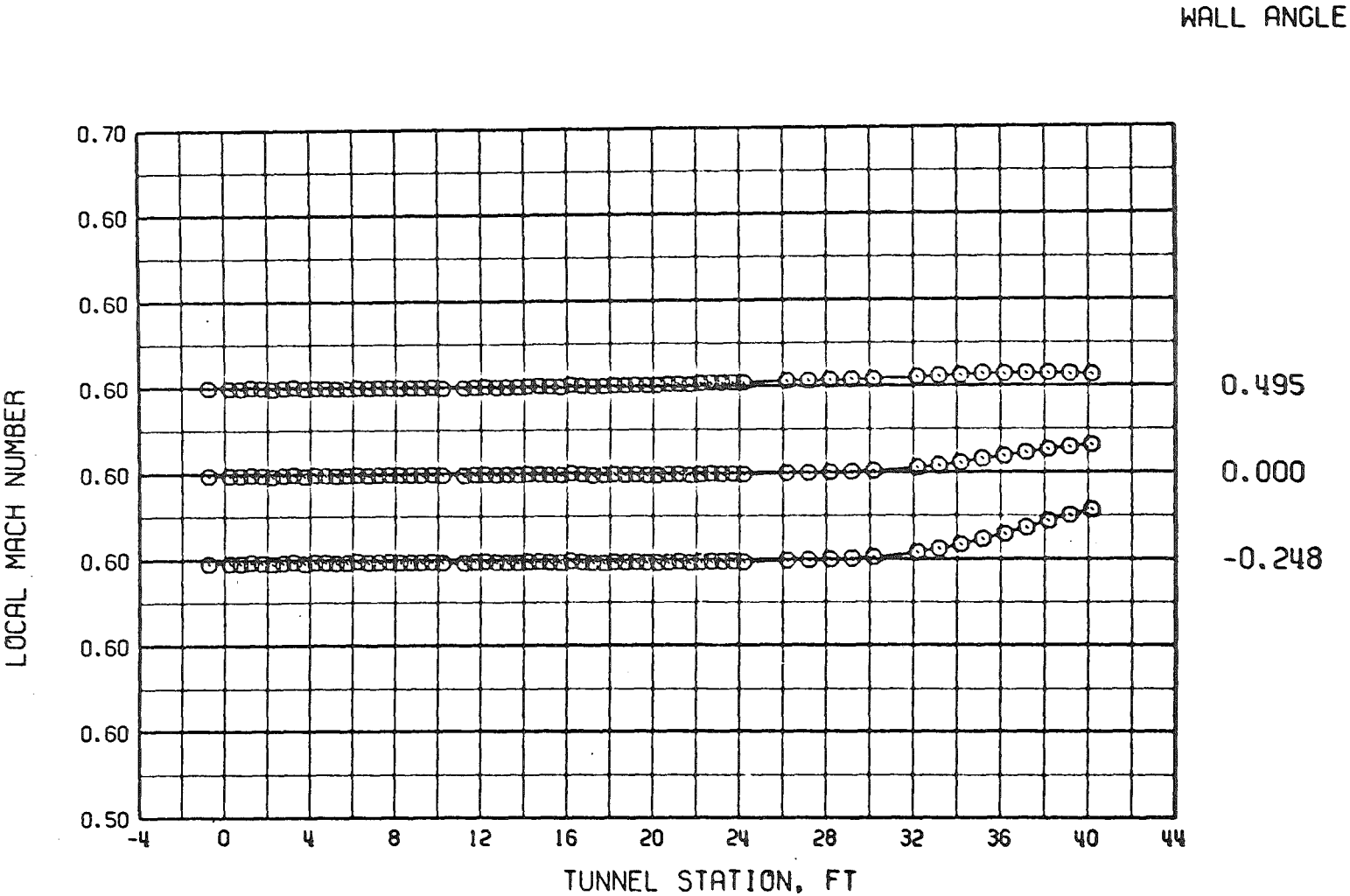

c. p_{t_∞} = 3,200

Figure B-1. Concluded.

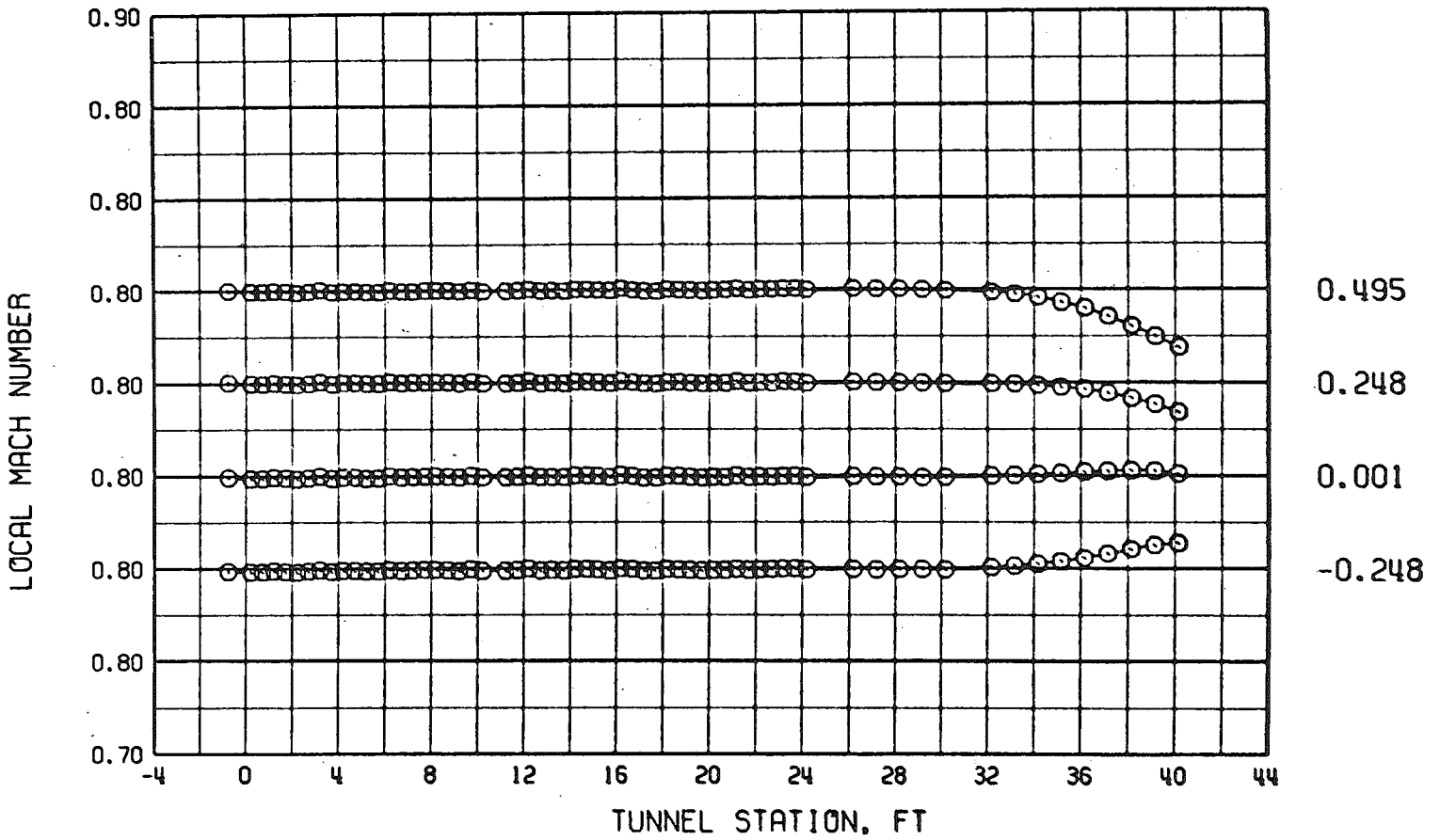

a. p_{t_∞} = 800

Figure B-2. 16T centerline Mach number distributions for various stagnation pressures and test section wall angles at M_∞ = 0.8, λ = 1.15, and τ = 6.

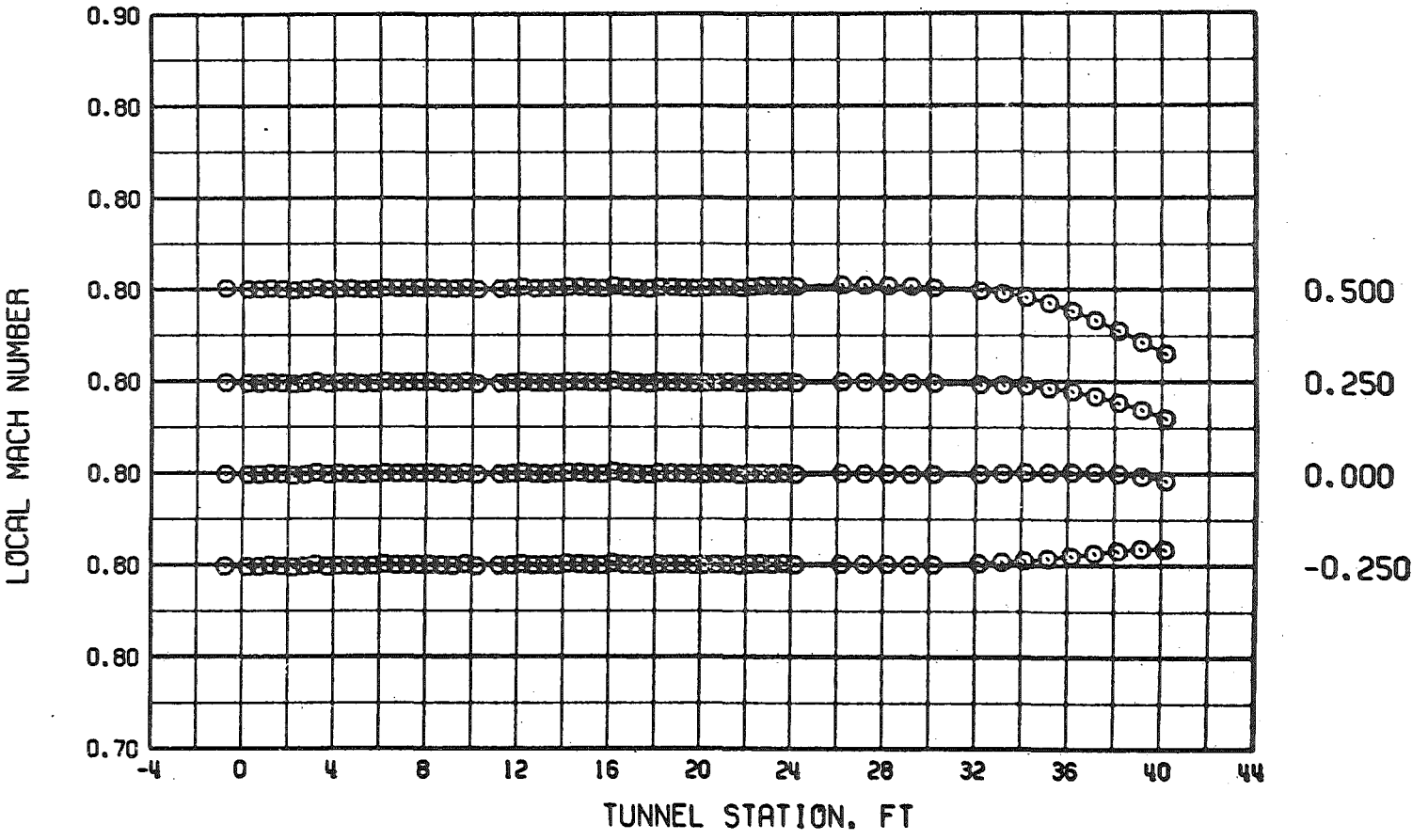

b. p_{t_∞} = 1,600

Figure B-2. Continued.

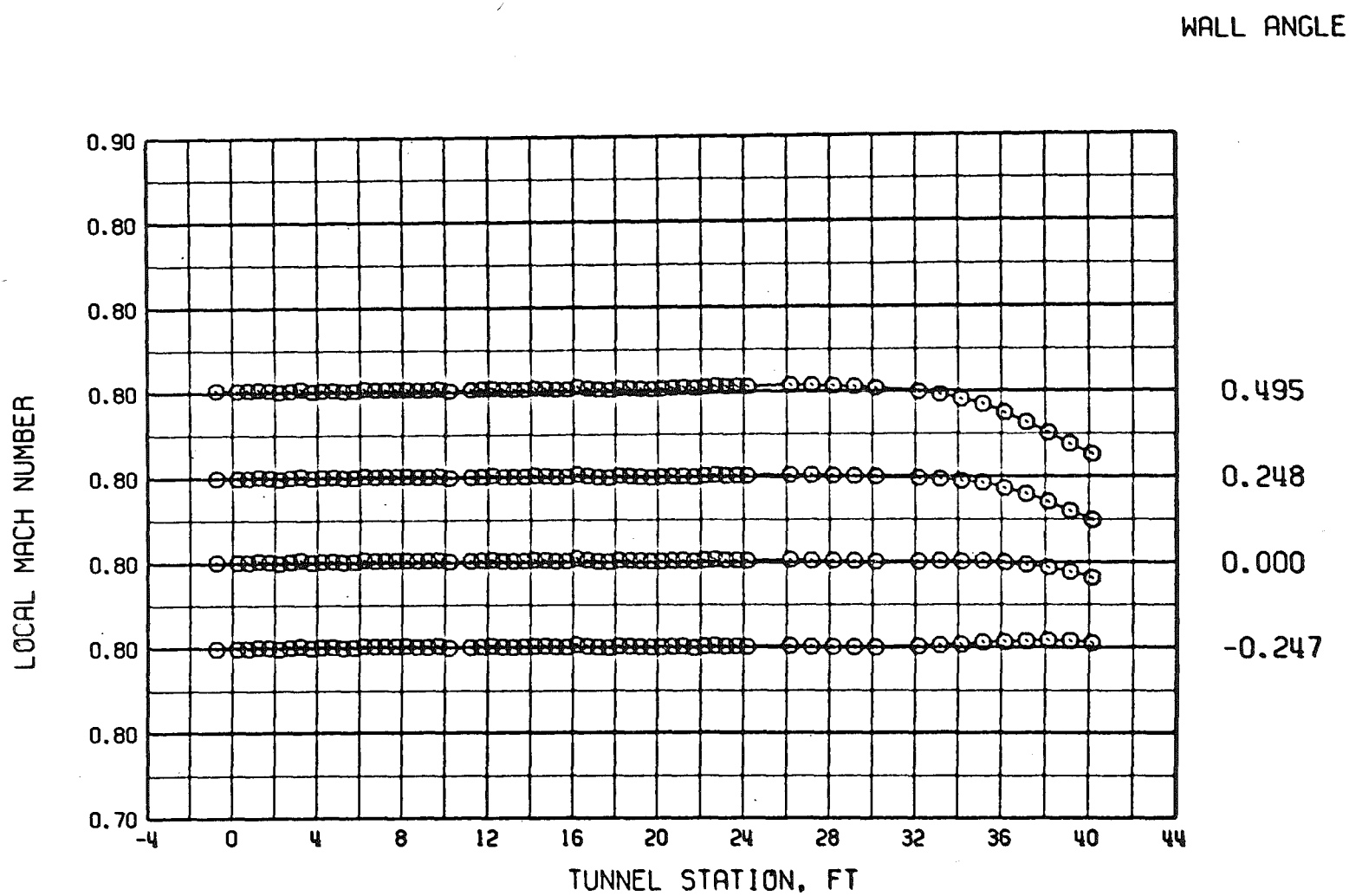

c. p_{t_∞} = 3,200

Figure B-2. Concluded.

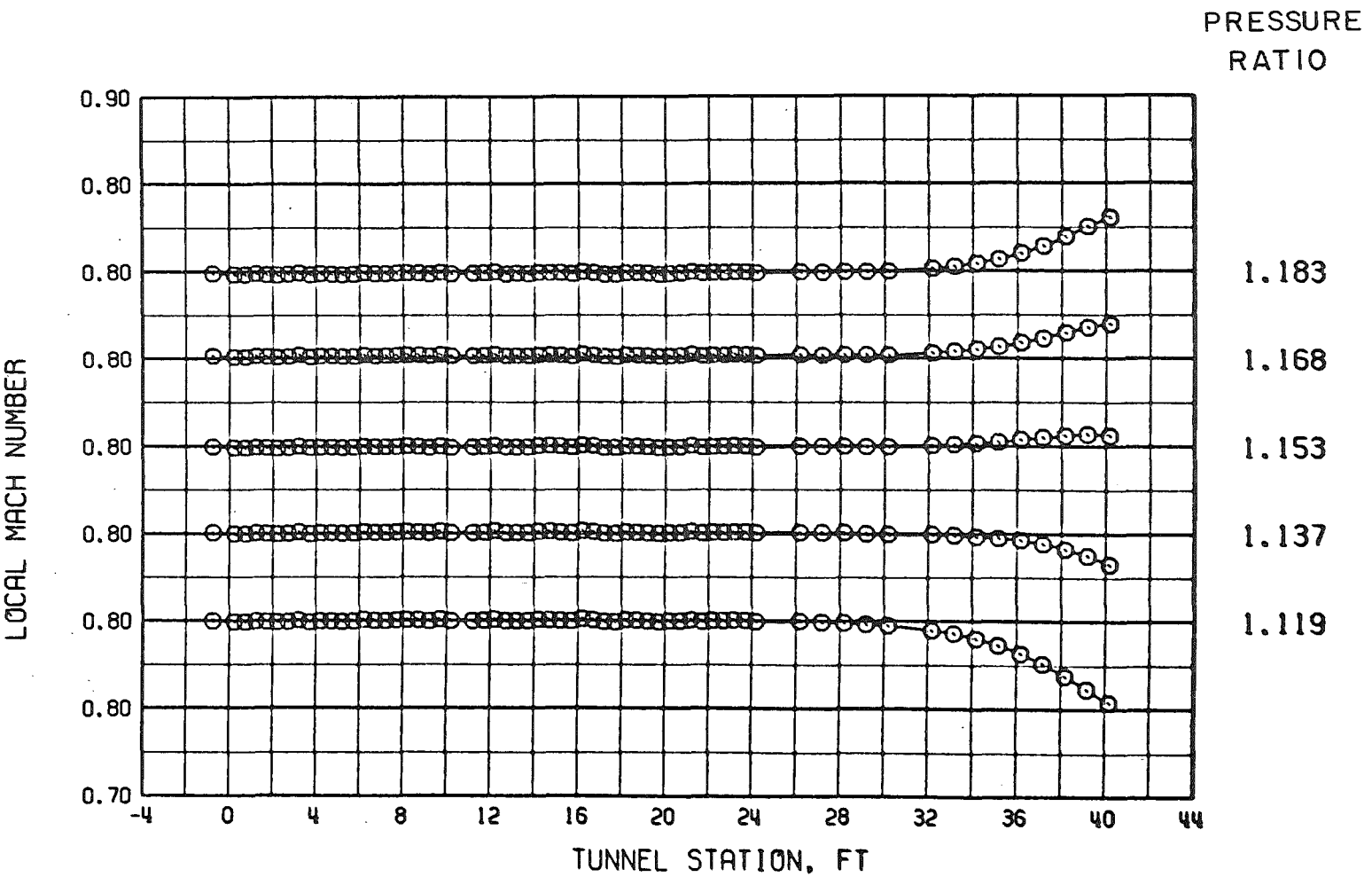

a. p_{t_∞} = 800

Figure B-3. 16T centerline Mach number distributions for various stagnation pressures and tunnel pressure ratios at M_∞ = 0.8, θ_w = 0, and τ = 6.

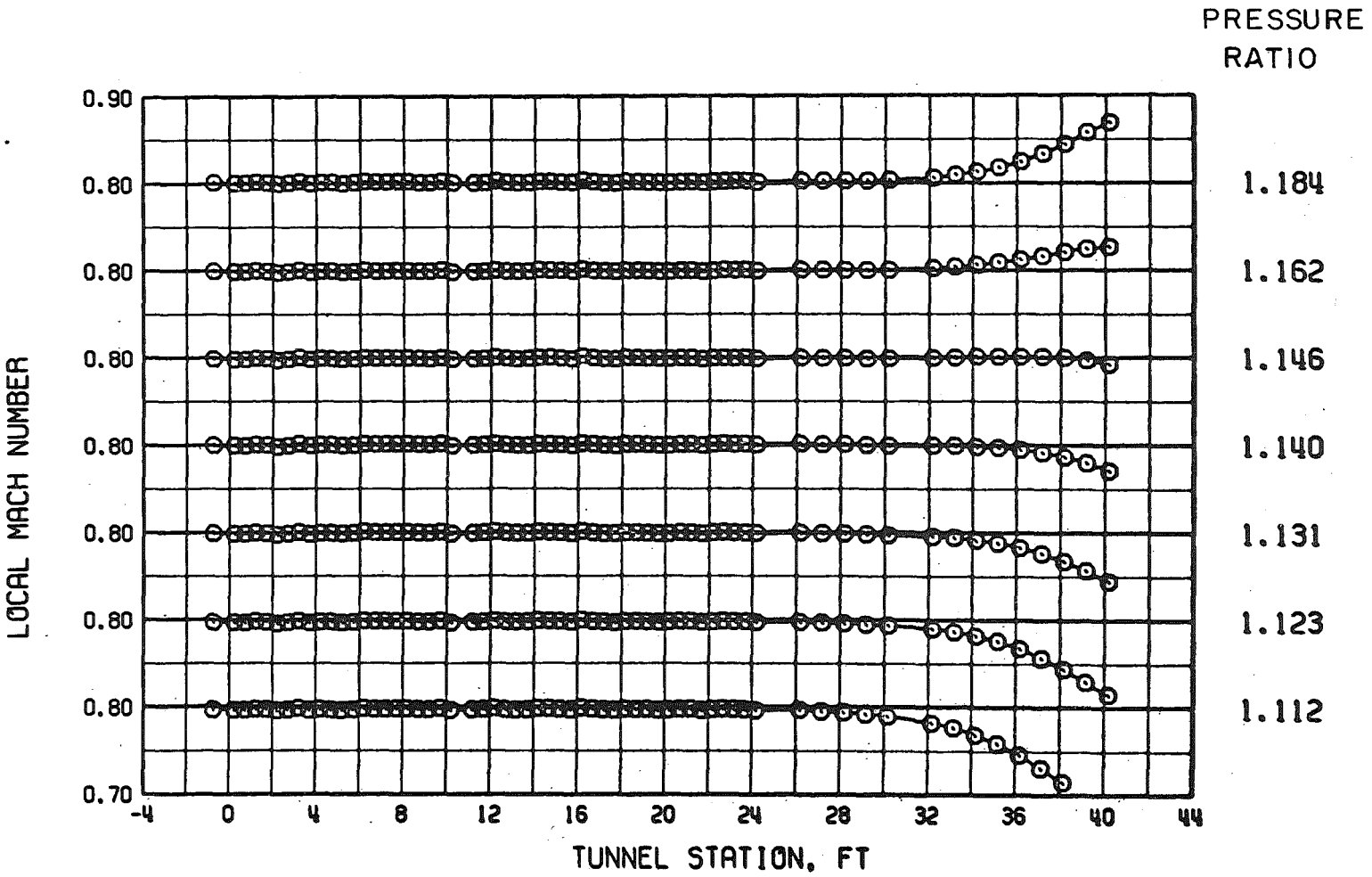

b. p_{t_∞} = 1,600

Figure B-3. Continued.

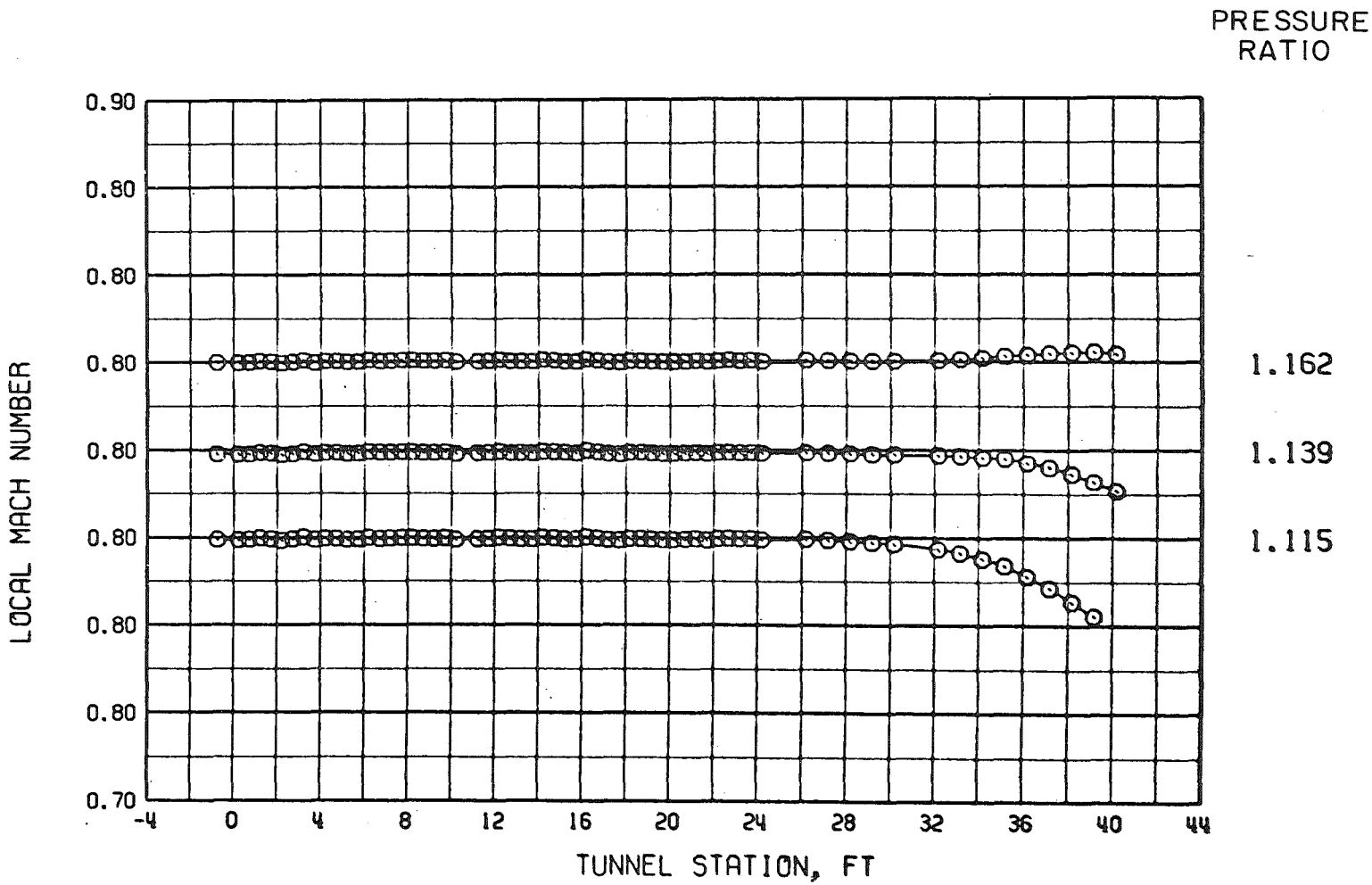

c. p_{t_∞} = 3,200

Figure B-3. Concluded.

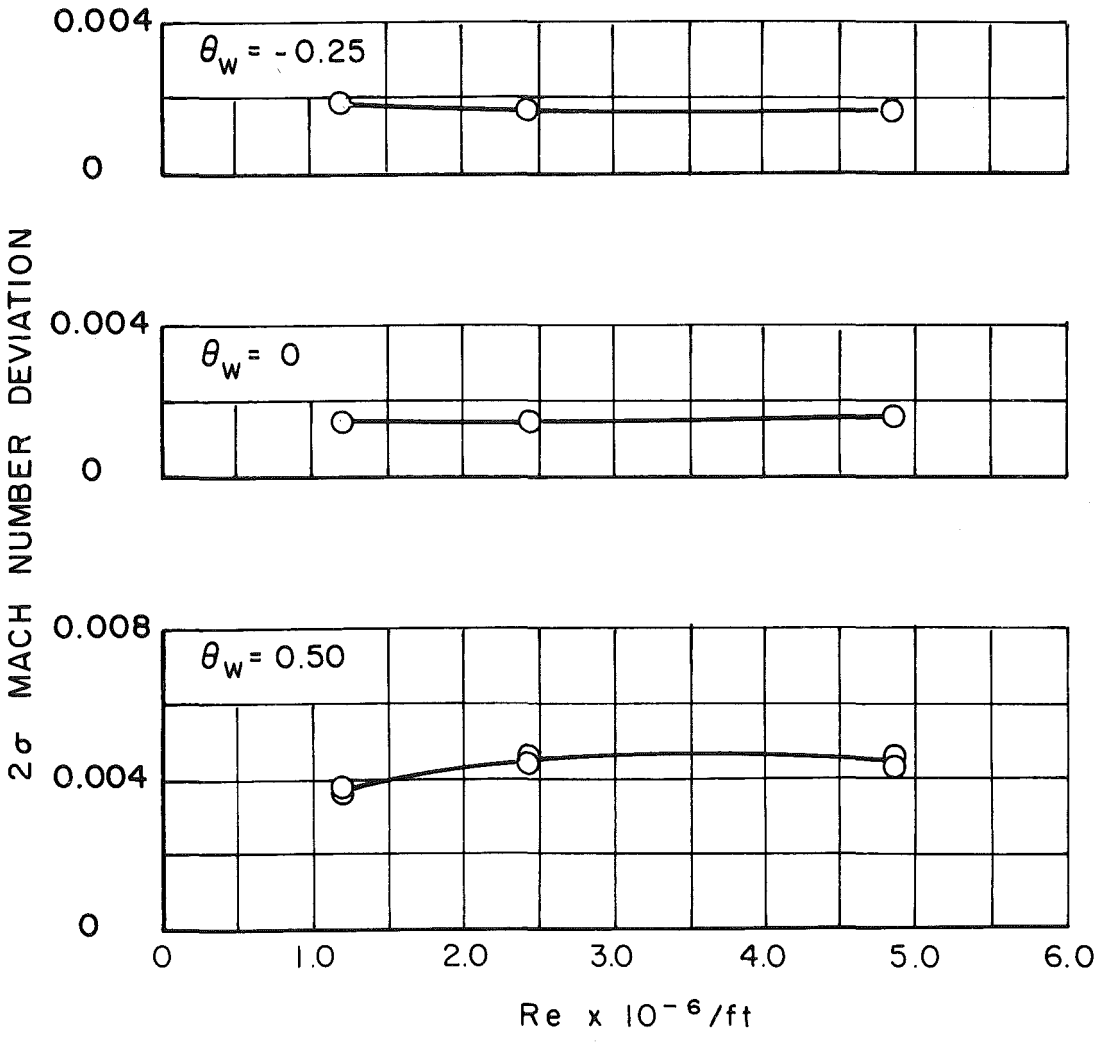

a. M_∞ = 0.6

Figure B-4. Effect of Reynolds number variation upon the 2σ Mach number deviation for tunnel station 8.2 to 28.2 at various wall angles for $\lambda = \lambda_N$ and τ = 6.

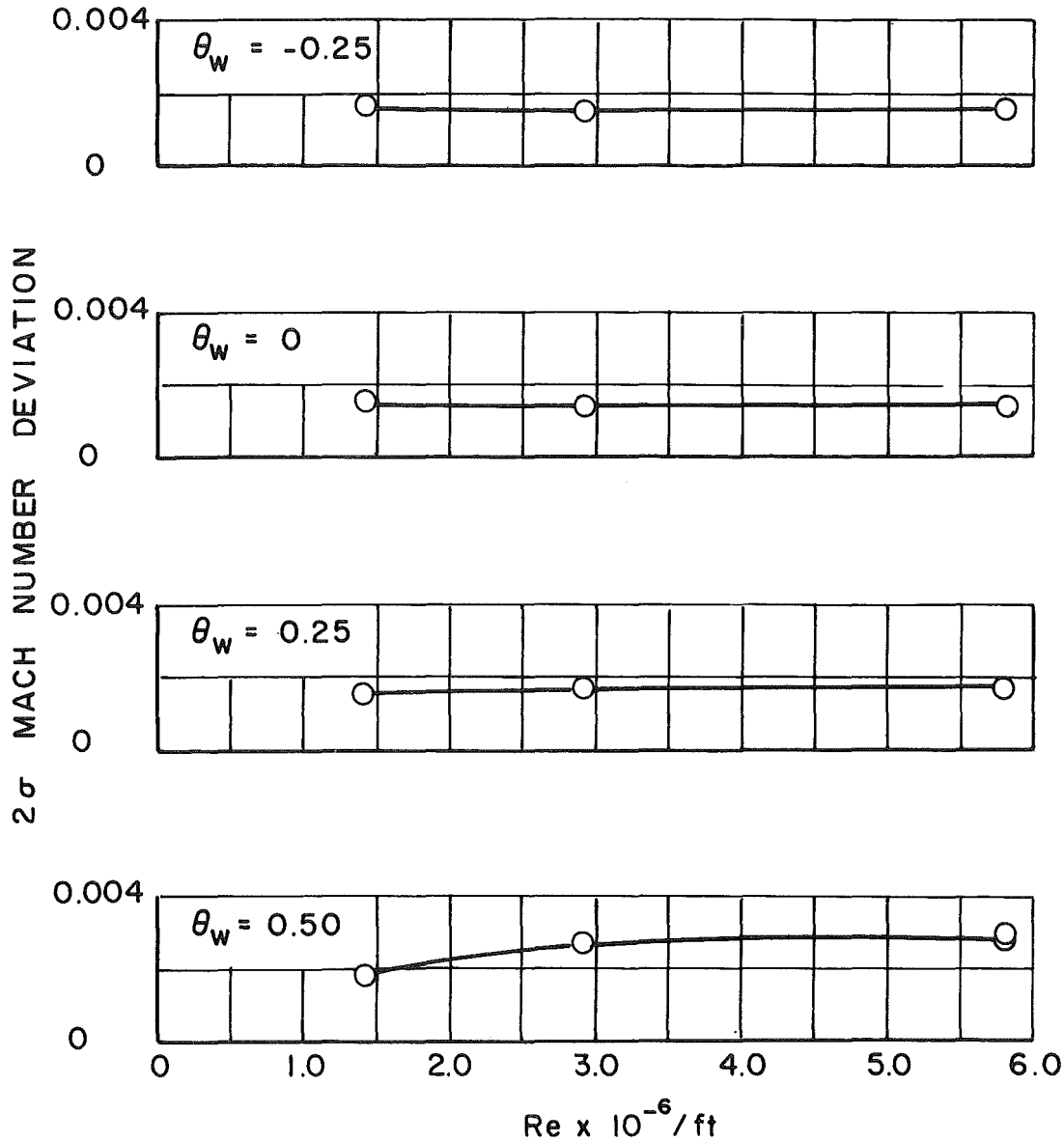

b. M_∞ = 0.8
Figure B-4. Concluded.

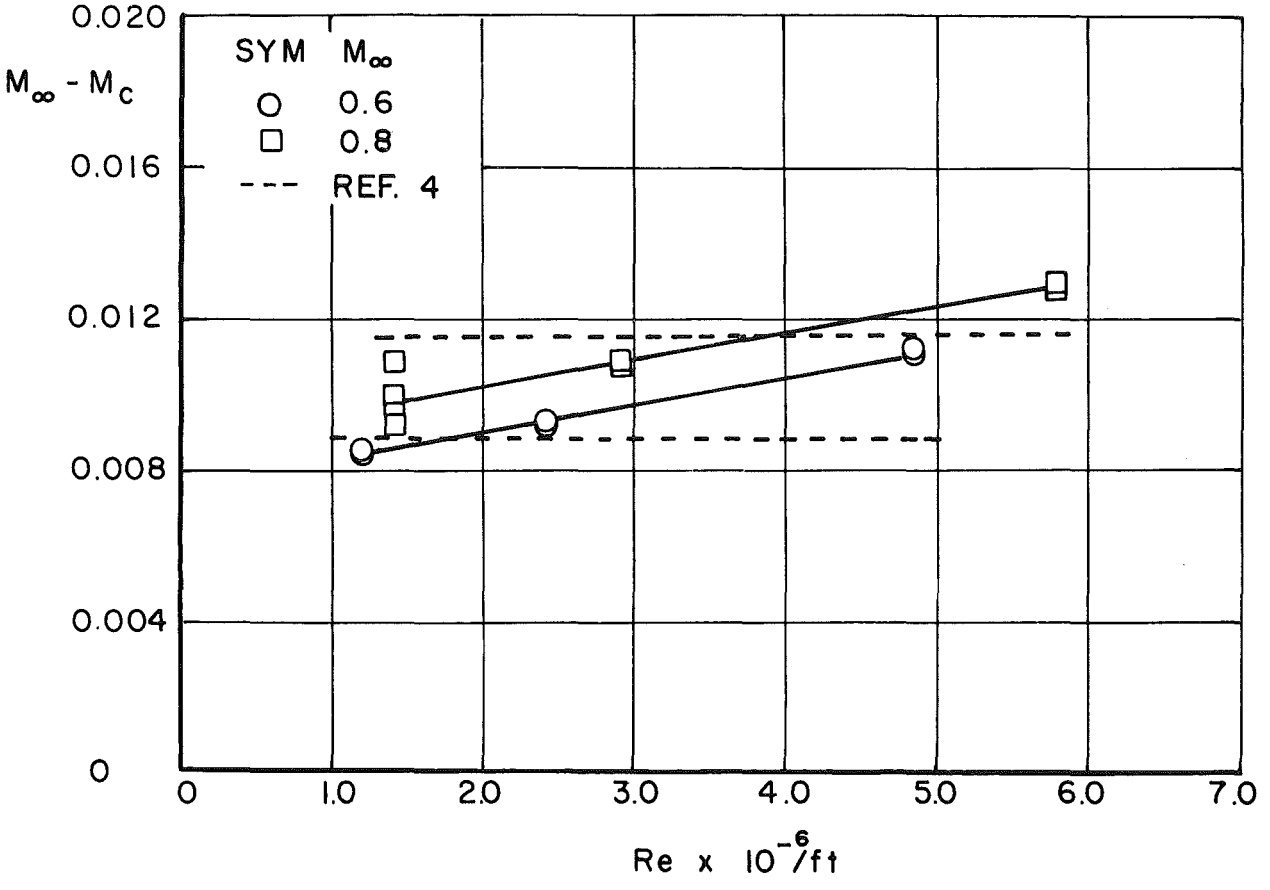

Figure B-5. Effects of Reynolds number upon the tunnel 16T calibration at M_∞ = 0.6 and 0.8 for θ_w = 0 and τ = 6.

NOMENCLATURE

M	Nominal Mach number for a selected set of data
M_c	Equivalent plenum Mach number
M_∞	Free-stream Mach number, determined from the average of local Mach numbers from tunnel station 8.2 to 28.2
p_{t_∞}	Tunnel stagnation pressure, psfa
Re	Unit Reynolds number, 10^{-6}/ft
θ_W	Test section wall angle, deg (positive when walls are diverged)
λ	Tunnel pressure ratio, ratio of p_{t_∞} to the compressor inlet pressure
λ_N	Nominal tunnel pressure ratio for data acquisition
λ_*	Tunnel pressure ratio associated with a flat Mach number distribution to tunnel station 40
σ	Standard deviation (conventional statistical parameter)
τ	Test section wall porosity, percent